EVALUATION OF AN INDUCED GRADIENT TRACER TEST IN AN ALLUVIAL AQUIFER

by

G.C. Bohling

Kansas Geological Survey
Open-file Report 99-6

EVALUATION OF AN INDUCED GRADIENT TRACER TEST IN AN ALLUVIAL AQUIFER

by

Geoffrey C. Bohling

KGS Open-File Report 99-6

Prepared as a Doctoral Dissertation
submitted to the Department of Geology
of the University of Kansas
January, 1999

Research reported in this document has been supported in part by grant number AFOSR-91-0298 from the U.S. Department of Defense and grant number 14-08-0001-G2093 from the U.S. Geological Survey, Department of the Interior. The views and conclusions contained in this document are those of the author and should not be interpreted as necessarily representing official policies, either expressed or implied, of the U.S. Government.

ABSTRACT

An induced-gradient tracer test was performed in the alluvial aquifer at an extensively studied research site in the Kansas River Valley northeast of Lawrence, Kansas. The movement of bromide tracer from an injection well to a discharge well was tracked using a network of multilevel samplers installed between the two wells. The tracer moved through the 14.2-meter length of the network under the influence of steady pumping at the discharge well. The test lasted 32 days and almost 6000 samples were collected and analyzed for bromide concentration during that time. Exploratory analysis of the tracer concentrations and analysis of the tracer breakthrough curves using a radially-convergent transport model reveal that much of the tracer mass moved rapidly through a few narrow, high-conductivity zones. This result emphasizes the importance of identifying such zones in order to have any chance of predicting contaminant transport at a site. A vertical profile of hydraulic conductivity developed from the results of the tracer test is used to assess the results of various well tests at the site. This comparison shows that multilevel slug tests and single-well dipole flow tests both show promise as methods for characterizing the distribution of hydraulic conductivity in the subsurface. A new method, hydraulic tomography, also shows considerable promise as a means for characterizing the conductivity distribution in great detail.

TABLE OF CONTENTS

LIST OF FIGURES

LIST OF TABLES

CHAPTER 1: INTRODUCTION

I. MOTIVATION

It has long been recognized that aquifer heterogeneity, or spatial variation in hydraulic conductivity and other flow and transport parameters, exerts an important influence on contaminant transport in groundwater. Although various investigators have proposed different conceptual models for aquifer heterogeneity, none of these models removes the need to collect site-specific data. A number of natural- and induced-gradient tracer tests at various sites have shown that site-specific features of the conductivity distribution and other aspects of the hydrogeologic setting must be taken into account in order to accurately predict contaminant transport.

A decade ago, researchers from the Kansas Geological Survey established the Geohydrologic Experimental and Monitoring Site (GEMS) in the Kansas River valley northeast of Lawrence, Kansas. Since its establishment in 1988, GEMS has been the subject of considerable research aimed at the development of well testing methodologies for delineating the aquifer heterogeneities controlling contaminant transport in groundwater (McElwee and Butler, 1995; Butler and McElwee, 1996). The goal of this work has been to develop economically viable and logistically feasible methods for characterizing the distribution of flow and transport parameters at a site, particularly the distribution of hydraulic conductivity. Ideally, every contamination site would be characterized on the basis of controlled natural-gradient tracer tests. However, such an approach is not feasible considering the large amount of resources and time required for such a test. Even induced-gradient tracer tests, which can be carried out over shorter time frames, are usually not an option at most sites. Accordingly, research at GEMS has focused on enhancing traditional hydraulic well testing methodologies in order to be able to derive more detailed information from them than has been possible in the past.

Aquifer characterization techniques employed at GEMS have included pumping tests, multilevel slug tests, permeameter analysis of core samples, single-well electrical tracer tests, wireline logging of natural gamma ray activity, and assessment of the aqueous geochemistry at the site. Chapter 2 presents a more detailed discussion of the site characterization efforts to date along with a description of the alluvial aquifer at the site.

In the fall of 1994, an induced-gradient tracer test, dubbed GEMSTRAC1, was performed at the site. The test involved pulse injection of a conservative tracer in an approximately radial flow field established by pumping at a single discharge well. Tracer concentrations were measured in a network of multilevel samplers between the injection and discharge well as the test proceeded. Along with simply providing more information concerning the site, this test was intended to provide some ground truth for assessing the effectiveness of the other characterization efforts at the site: Which methods provided the most reliable information for predicting the outcome of the tracer test? In fact, none of the previous characterization efforts prepared us for the degree of heterogeneity revealed by the tracer test, in which much of the tracer mass was transported more rapidly than expected through narrow, high-permeability zones. Furthermore, complications affecting many of the earlier characterization efforts prevent us from making conclusive assessments of these efforts. Nevertheless, a comparison of the conductivity estimates provided by several of the site characterization techniques to a conductivity profile derived from the results of GEMSTRAC1 indicates that these methods might prove highly effective upon further refinement.

The comparative assessment of site characterization techniques shows that both single-well dipole flow tests and multilevel slug tests could prove to be reliable and economically feasible methods for routine site characterization studies. In addition, hydraulic

tomography, a new characterization technique under investigation at the site, shows considerable promise. This technique involves the simultaneous analysis of high-resolution drawdown data from multiple pumping tests, each stressing a different vertical interval of the aquifer. Numerical simulations show that the data provided by a tomographic testing format greatly reduce the nonuniqueness associated with aquifer parameter estimation, allowing for resolution of considerable detail in the conductivity distribution. At GEMS we are currently investigating methods for obtaining pressure measurements in the tubes of multilevel samplers, such as those used to collect water samples during GEMSTRAC1. Such measurements could provide vertical profiles of drawdown of the resolution necessary for the success of hydraulic tomography.

II. SCOPE OF DISSERTATION

The performance of GEMSTRAC1 was a collaborative effort involving a team of researchers from the Kansas Geological Survey and the Department of Geology of the University of Kansas. The particular contributions to this effort that constitute my dissertation work include:

- 1) the design modeling presented in Chapter 3, along with the analysis of pumping tests and other site characterization efforts carried out prior to GEMSTRAC1;

- 2) the exploratory analysis of the GEMSTRAC1 data, presented in Chapter 4, including development of an animation of tracer movement along the centerline of the sampling network;

- 3) the modification of an existing model for radially convergent tracer transport in order to make that model applicable to the analysis of GEMSTRAC1, discussed in Chapter 5;

- 4) the fitting of the transport model to tracer breakthrough curves from individual sampling ports and groups of sampling ports, as presented in Chapter 6, including the synthesis and assessment of the fitting results;

- 5) the comparative assessment of various well-testing methodologies employed to date at the site in light of the results of GEMSTRAC1, presented in Chapter 7, along with the development of a finite-difference radial flow model allowing for simulation and analysis of pumping tests in a tomographic format; and

- 6) preparation of the dissertation itself, which serves as a comprehensive report on GEMSTRAC1.

The remainder of this chapter is intended to place GEMSTRAC1 within the context of our current understanding of contaminant transport processes, much of which has been provided by a relatively small number of controlled, field-scale tracer tests. Section III covers various transport modeling paradigms, and particularly different approaches to modeling and characterizing aquifer heterogeneity. Section IV discusses the results of a number of well-known natural- and induced-gradient tracer tests which have provided ground truth for evaluating different theories and characterization techniques.

III. TRANSPORT MODELING PARADIGMS

The transport of a conservative (nonreactive) solute in groundwater is governed by the following advection-dispersion equation:

$$\nabla \cdot (\mathbf{D}\nabla C) - \nabla \cdot \mathbf{v}C = \frac{\partial C}{\partial t} \qquad (1.1)$$

where C [M/L^3] represents the concentration as solute mass per volume of solution, **D** [L^2/T] the dispersion coefficient matrix, and **v** [L/T] the average linear velocity of the groundwater. The above equation assumes that no sources or sinks of solute are present in the interior of the modeled domain. The advective velocity, v, is determined by Darcy's law

$$\mathbf{v} = -\frac{\mathbf{K}}{n}\nabla h \tag{1.2}$$

where **K** [L/T] is the hydraulic conductivity matrix, n [dimensionless] is the aquifer porosity, and ∇h [L/L] is the gradient of hydraulic head, determined from the solution of the groundwater flow equation:

$$\nabla \cdot (\mathbf{K}\nabla h) = S_s \frac{\partial h}{\partial t} \tag{1.3}$$

where S_s $[L]^{-1}$ is the specific storage. Equation 1.3 assumes that no sources or sinks of water are present in the modeled domain. Detailed derivations of the advection-dispersion equation can be found in Chapter 8 of Wang and Anderson (1982) and Appendix X of Freeze and Cherry (1979).

Although Equation 1.1 does not account for a number of mechanisms, including chemical reactions in solution, radioactive decay, dissolution and precipitation of minerals, sorption reactions with the solid phase, and mass transfer between mobile and immobile zones, it serves to illustrate the fundamental mechanisms of advective-dispersive transport. The solute undergoes an advective flux, n**Cv**, driven by the average linear velocity of the groundwater, and a Fickian style dispersive flux, $-n\mathbf{D}\nabla C$, driven by the concentration gradient. Equation 1.1 states that the time rate of change of concentration in a given volume is equal to the sum of the gradients of these two flux terms.

For at least two decades it has been commonly held that the distinction between the two flux terms actually depends on the scale of resolution of the modeled advective velocity. When modeling field-scale contaminant transport, the dispersive flux term actually accounts for fluctuations of the velocity field about the average linear velocity, v. The magnitude of these fluctuations is commonly considered to be a linear function of the magnitude of the average linear velocity, v, resulting in the following expressions for the longitudinal and transverse dispersion coefficients (Freeze and Cherry, 1979; Javandel *et al.*, 1984):

$$D_L = \alpha_L v + D_d \quad D_T = \alpha_T v + D_d. \tag{1.4}$$

D_d represents the coefficient associated with the molecular diffusion process, which is generally (but not always) quite small compared to the terms $\alpha_L v$ and $\alpha_T v$. The proportionality constants α_L and α_T, with units of length, are termed the longitudinal and transverse dispersivities. As the velocity field is modeled in greater detail, more of the solute flux is accounted for in the advective transport term and less is attributed to the dispersive transport term. This will lead to a decrease in the effective values of dispersivity as the resolution of the model increases. In the extreme limit, the dispersion coefficients will be dominated by the molecular diffusion coefficient.

Over the past 20 years many researchers have attempted to quantify the influence of aquifer heterogeneity on contaminant transport. Sudicky and Huyakorn (1991) summarize work in this area primarily during the 1980's. Various researchers have proposed theories relating field-scale "macrodispersivities" (effective values of α_L and α_T) to parameters characterizing the spatial variability of the conductivity field. Variations in the hydraulic conductivity at scales smaller than the explicitly modeled scale induce the fluctuations in advective velocity that contribute to the macrodispersive term in the

advection-dispersion equation. Perhaps the most frequently cited results of stochastic-analytic transport theory are those developed by Gelhar and Axness (1983) for transport in a two-dimensional steady-state flow field (with unidirectional mean flow) in an isotropically autocorrelated log-conductivity field. In this case, the expressions for macroscopic longitudinal and transverse dispersivities are:

$$\alpha_L = \sigma_Y^2 \lambda \tag{1.5}$$

and

$$\alpha_T = \frac{\sigma_Y^2 \alpha_L^*}{8}\left(1 + 3\frac{\alpha_T^*}{\alpha_L^*}\right) \tag{1.6}$$

where σ_Y^2 is the variance of the log-conductivity field, λ is the correlation length of the log-conductivity field, and α_L^* and α_T^* are "local-scale" dispersivities, associated with a scale much smaller than the dominant scale of heterogeneity.

Although Equations 1.5 and 1.6 apply to a particular flow configuration, they illustrate some of the general insights provided by stochastic transport theory. Equation 1.5 states that longitudinal dispersivity, describing solute spreading in the direction of mean flow, increases as the variability of the log-conductivity increases. Larger variations in conductivity induce larger fluctuations in the velocity field, resulting in greater solute spreading. Longitudinal dispersivity also increases with increasing correlation length, or increasing size of typical features in the conductivity field. Greater spatial persistence of regions of higher or lower conductivity leads to larger differences in the overall rate of movement of portions of a solute plume encountering those regions. One might imagine that greater spatial persistence could result in reduced spreading, since most of the plume could be contained in a region of relatively homogeneous conductivity. However, Equations 1.5 and 1.6 represent asymptotic results; they are valid only after the plume has traversed a number of correlation

lengths, averaging out the effects of specific, local features of the conductivity field. Equation 1.6 shows that transverse macrodispersivity, describing solute spreading perpendicular to the mean flow direction, is proportional to the local-scale longitudinal dispersivity and is thus quite small in comparison to the longitudinal macrodispersivity.

Dagan (1988) argues that a plume needs to be transported over tens of correlation lengths before it displays the asymptotic characteristics described by Gelhar and Axness (1983). Typical conductivity fields are usually characterized by large correlation lengths in the horizontal direction, displaying an imperfectly layered character. This implies that exceptionally large transport distances may be required for asymptotic theory to be applicable. Dagan (1988) develops expressions describing pre-asymptotic, time-dependent macrodispersivities, but even these describe average behavior over an ensemble of possible realizations of the log-conductivity field, not the particular behavior of an actual plume. In many cases transport will in fact be predominantly controlled by a few specific features of the conductivity field, such as persistent zones of high or low conductivity. The inability of stochastic transport theory to account for such dependence has led a number of investigators to pursue other means of characterizing aquifer heterogeneity and its influence on solute transport.

Molz and colleagues have voiced the strongest opposition to stochastic-analytic transport theory. They have focused on developing field methods for determining the vertical variation of horizontal hydraulic conductivity, asserting that this will be the most important factor controlling contaminant transport at many sites, at least under advectively-dominated conditions. Molz *et al.* (1986) demonstrate that the concentration history at a fully-penetrating pumping well in a dual-well tracer test can be adequately simulated using a purely advective stratified flow and transport model, based on a deterministic

representation of the conductivity field. The vertical distribution of conductivity used to simulate the dual-well tracer test was derived from analysis of a more limited single-well tracer test. They have investigated a number of methods for quantifying the vertical variation of conductivity, including multilevel slug tests (Melville *et al.*, 1989; Widdowson *et al.*, 1990), borehole flowmeter tests (Molz *et al.*, 1989), and single- and dual-well tracer tests (Molz *et al.*, 1986; Molz *et al.*, 1988). The utility of these techniques increases with increasing stratification of flow and transport, and thus with increasing horizontal persistence of the conductivity field or decreasing transport distance.

A number of investigators have contended that the hydraulic conductivity of unlithified deposits will be controlled by sedimentary processes, resulting in conductivity fields with more persistent features and greater contrasts across boundaries than those predicted by stochastic theory, but also with complicated geometries that defy a layered aquifer approach. Thus there has been increasing effort to develop more geologically based models of aquifer geometry. Koltermann and Gorelick (1996) review a number of methods for representing heterogeneity in sedimentary deposits. Much of their review focuses on methods for developing geologically based images of aquifer heterogeneity, many based on sedimentary process models. Although these investigations provide insight concerning typical geometries that might develop in different sedimentary environments, the results are somewhat limited in practical utility due to the impossibility of conditioning sedimentary-process models to site-specific data. Furthermore, these models are typically limited to generating images representing spatial variability of the grain size distribution, only one of a number of factors which could potentially influence the spatial distribution of hydraulic conductivity.

A promising field of investigation involves the use of stochastic simulation techniques that allow for the incorporation of various kinds of soft data, including geological and geophysical information. In

petroleum investigations, such an approach has been championed by researchers associated with the Stanford Center for Reservoir Forecasting (Journel and Zhu, 1990; Deutsch and Hewett, 1996). Recently other Stanford investigators have described the use of stochastic techniques and incorporation of auxiliary information in groundwater investigations (Copty and Rubin, 1995; Hyndman and Gorelick, 1996). Non-Gaussian stochastic techniques are particularly promising. These techniques focus more on delineating boundaries between regions of contrasting properties, rather than modeling parameters as smooth, continuous fields (Journel and Alabert, 1987). Typically this is accomplished using some form of indicator kriging or simulation, techniques that provide a measure of the probability of occurrence of each of a set of different classes (hydrogeologic facies, for example). Many non-Gaussian stochastic techniques can be conditioned on soft data, auxiliary information provided by geological knowledge or geophysical investigations, as well as on hard data, actual measurements of hydraulic properties. Thus, conditional stochastic models can be used to integrate all information about a site into a consistent, quantitative framework (Srivastava, 1994).

Many of the studies described above focus on the transport of conservative solutes through a steady-state flow field, in order to isolate the effects of conductivity variation on solute transport. Certainly the spatial variation of hydraulic conductivity is a first-order effect in most transport problems; however, the investigator must avoid the temptation to neglect the influence of other mechanisms affecting transport, both chemical and physical. Other important physical mechanisms affecting transport include local diffusion (Kitanidis, 1994), transfer of solute between mobile and immobile zones (Thorbjarnarson and Mackay, 1994), and temporal variation in the flow field (Rehfeldt and Gelhar, 1992). Chemical mechanisms include decay, sorption reactions, and biotransformation, among others. As described in Sudicky and Huyakorn (1991) the parameters controlling these additional physical and chemical mechanisms can

also vary in space, leading to unexpected and complex solute behavior in some cases.

The research to date at GEMS has been somewhat more in the deterministic school represented by Molz and colleagues. Activities at GEMS have been based on the premise that practitioners faced with predicting the behavior of real contaminant plumes need reliable and accessible methods for assessing the salient features of the hydraulic conductivity distribution at a particular site. Since logistical and financial considerations preclude the performance of even an induced-gradient tracer test at most sites, accessible methods primarily mean hydraulic well tests. The information on hydraulic conductivity provided by slug tests or pumping tests is all that many investigators will have available when attempting to predict contaminant behavior at a site. The work at GEMS has focused on modifying and enhancing traditional well testing methodologies in order to improve their reliability and their ability to delineate conductivity variations. Clearly, all available information, including auxiliary geophysical information and geologic knowledge, should be brought to bear when investigating a site. However, reliable characterization of a site will always be grounded in measurements of hydraulic and, if possible, transport processes at the site.

IV. MAJOR TRACER TESTS

Several large-scale natural-gradient experiments have been carried out, in part to test the applicability of stochastic theories of solute transport, but also, more fundamentally, to investigate the dominant mechanisms controlling transport. Major natural-gradient tracer tests have been conducted at the Borden site (Mackay *et al.*, 1986), the Twin Lake site (Killey and Moltyaner, 1988), the Cape Cod site (LeBlanc *et al.*, 1991), a site in Denmark (Jensen *et al.*, 1993), and the Columbus Air Force Base in Mississippi (Boggs *et al.*, 1992). All of these tests have been carried out in sandy, unconsolidated aquifers, thus

limiting the range of applicability of some of the results. Table 1.1 presents a summary of some of the characteristics of these sites.

In natural-gradient tests, tracers move with the ambient groundwater flow, resulting in tests lasting on the order of years. Induced-gradient tests can be performed over much shorter time periods and are therefore more attractive to many investigators. Some notable induced-gradient tests include those reported by Molz *et al.* (1988), Mackay *et al.* (1994), and Yeh *et al.* (1995). The test reported by Molz *et al.* (1988) was performed in an alluvial aquifer near Mobile, Alabama. That reported by Mackay *et al.* (1994) was performed adjacent to the site of the natural-gradient test at the Borden site, allowing a valuable comparison between the results of two different formats of test. The test reported by Yeh *et al.* (1995) was performed in a coastal plain aquifer in South Carolina. Information concerning these tests is also reported in Table 1.1. An important question concerning induced-gradient tracer tests is whether such tests provide reliable estimates of the parameters necessary to predict larger scale transport under natural-gradient conditions, given that parameter estimates depend to some extent on test configuration and scale. Induced-gradient tests are much more advectively dominated than natural-gradient tests and are also performed over a much shorter scale. In addition, induced-gradient tests are generally much more amenable to analysis based on a stratified flow assumption, as employed by Molz *et al.* (1988) and Mackay *et al.* (1994), especially if fully penetrating wells are employed, whereas effects of vertical flow for larger-scale transport may be significant.

Natural-gradient tracer tests

The large-scale natural-gradient tests at Borden (Mackay *et al.*, 1986) initially appeared to be a great success for stochastic transport theory. This test, which lasted three years and involved monitoring of transport over 150 meters in a glacial outwash aquifer, was

Table 1.1. Characteristics of GEMS and sites of other tracer tests mentioned in the text.

Reference, site name	Aquifer description	Test type	Conductivity (m/s)
McElwee *et al.* (1995), GEMS	alluvial sand & gravel, confined	radially convergent	$2.7X10^{-8}$ - $3.8X10^{-3}$ (core permeameter)
Boggs *et al.* (1992), Columbus, MS	alluvial sand & gravel, unconfined	natural-gradient	$3.1X10^{-7}$ - $1.0X10^{-2}$ (core permeameter) [Rehfeldt *et al.*, 1992]
Jensen *et al.* (1993), Jutland peninsula, Denmark	glaciofluvial sands, unconfined	natural-gradient	$0.8\text{-}22.5X10^{-4}$ (slug tests in short-screened wells)
Killey and Moltyaner (1988), Twin Lake, Ontario	fluvial and aeolian sands, unconfined	natural-gradient	$2.1\text{-}20.9X10^{-5}$ (slug tests)
LeBlanc *et al.* (1991), Cape Cod	glacial outwash sand & gravel, unconfined	natural-gradient	$1\text{-}37X10^{-4}$ (borehole flowmeter) $0.06\text{-}14X10^{-4}$ (core permeameter) [Hess *et al.*, 1992]
Mackay *et al.* (1986), Borden, Ontario	glaciofluvial sands, unconfined	natural-gradient	$5\text{-}10X10^{-5}$ (slug test) $0.05\text{-}20X10^{-5}$ (core permeameter) [Freyberg, 1996]
Mackay *et al.* (1994), Borden, Ontario	glaciofluvial sands, unconfined	two-well recirculating	same as above
Molz *et al.* (1988), Mobile, AL	alluvial sand, confined	single-well; dual-well	$2.3\text{-}27X10^{-4}$ (borehole flowmeter) [Molz *et al.*, 1989]
Yeh *et al.* (1995)	'coastal' sand, unconfined	dual-well	$0.7\text{-}7.6X10^{-5}$ (multilevel slug tests)

accompanied by extensive laboratory and field investigations of the aquifer properties. Sudicky (1986) presents estimates of the geostatistical parameters based on permeameter measurements of 1279 subsamples from 32 cores obtained along two perpendicular transects (Sudicky, 1986). These estimates agree remarkably well with those estimated by Freyberg (1986) based on analysis of the spatial moments of the vertically averaged tracer concentrations. Sudicky (1986) concludes that "The generally good agreement between the rates of macrodispersion observed during the long-term tracer test and those rates computed independently from theory using the statistical description of the Borden aquifer as input has demonstrated that workable results are presently at hand." However, this apparent success was tempered by a later paper showing that even the extensive and carefully controlled data sets obtained at Borden could be subjected to a wide range of interpretations (Woodbury and Sudicky, 1991) and also by some controversy surrounding the vertical splitting of the plume into a higher, faster-moving portion and a lower, trailing portion. This behavior, caused by site-specific large-scale heterogeneities in the velocity field, led Molz and Güven (1988) to question the applicability of macrodispersive parameters derived from stochastic theory, which would predict the development of a smooth Gaussian plume.

LeBlanc *et al.* (1991) present an overview of a large-scale tracer test at a site on Cape Cod, which lasted three years and involved transport over a distance of 280 meters. The aquifer at the site consists of stratified sand and gravel deposited as glacial outwash. The Cape Cod test was also accompanied by an extensive program of conductivity measurements, using permeameter analysis of core samples and flowmeter surveys in 16 long-screened wells. In this case, there was somewhat less agreement between the observed characteristics of the tracer plume (Garabedian *et al.*, 1991) and those based on geostatistical modeling of the log-conductivity values (Hess *et al.*, 1992). Although the longitudinal macrodispersivity predicted by stochastic theory is of

the same order of magnitude as the value estimated from the observed plume moments, the predicted transverse dispersivities are orders of magnitude smaller than those producing the best match to the plume moments. Hess *et al.* (1992) attribute the enhanced horizontal transverse dispersion observed in the test to time variation in the gradient direction, a mechanism explored in detail by Rehfeldt and Gelhar (1992). The enhanced vertical dispersion is probably attributable to the significant vertical components of transport velocity resulting from the density- and recharge-induced sinking of the plume. Furthermore, the Cape Cod plume also exhibited a vertical splitting, very similar to that of the Borden plume. Although it is probably coincidental that both the Borden and Cape Cod plumes displayed similar bimodal structures, it is probably generally true that most contaminant plumes will display some characteristic deviation from the smooth, Gaussian behavior predicted by stochastic theory. Such features will depend on the larger-scale structure of the conductivity field, the timing and configuration of contaminant sources, and the particularities of the hydrogeologic setting.

Both the Borden and Cape Cod tracer tests employed extensive networks of multilevel samplers. The multilevel samplers employed at GEMS, consisting of color-coded polyethylene sampling tubes threaded through PVC casing, are very similar in design to those employed at Cape Cod.

Killey and Moltyaner (1988) and Moltyaner and Killey (1988a, 1988b) present the results of two natural-gradient tracer tests in the fluvial and aeolian sand aquifer at the Twin Lake site on the grounds of the Chalk River Nuclear Laboratories in Ontario. These tests employed a novel sampling technique: The movement of a radioactive tracer (^{131}I) was monitored using a scintillation detector trolled through dry access tubes installed in the aquifer, allowing vertically continuous profiles of the tracer concentration to be obtained. In the earlier test, conducted in 1982, tracer movement was monitored

over 20 meters of travel, while the second test, in 1984, was carried out over a forty-meter travel distance. In both tests, hydraulic conductivities were estimated based on estimated travel times between lines of samplers and estimated hydraulic gradients. Killey and Moltyaner (1988) found that the conductivities could be adequately grouped into six different regions of approximately constant conductivity. They claim that the tracer transport can be adequately modeled using the six-zone conductivity distribution and small longitudinal dispersivity values, comparable to those measured in laboratory column experiments (on the order of a few centimeters). That is, they oppose the macrodispersivity approach advocated by the investigators involved with the tracer tests described above, arguing instead for the use of more deterministic flow and transport models employing detailed descriptions of the conductivity field in conjunction with local dispersivity values.

Jensen *et al.* (1993) discuss two natural-gradient tracer tests performed in an unconfined glacial outwash aquifer located on the Jutland peninsula in western Denmark. Tritium was used as the tracer in the first test and chloride in the second. The sampling network (about 200 m long and 40 m wide in its final configuration) consisted of a large number of nests of short-screened piezometers (each with a screen length of 0.25 meters). A number of slug tests in these piezometers provided 334 estimates of hydraulic conductivity, which Jensen *et al.* (1993) grouped into three layers characterized by somewhat different mean conductivities, variances and horizontal correlation lengths.

Jensen *et al.* (1983) analyzed the tritium tracer test using a three-dimensional numerical transport model, first employing a three-layered conductivity structure, and then employing a fully three-dimensional heterogeneous conductivity field. The three-dimensional field was synthetically generated using statistical parameters estimated from the slug test results. They were able to successfully calibrate both

models by adjusting the dispersivity values. As expected, the calibration of the three-layered model yielded much larger dispersivity values than the calibration of the fully three-dimensional model, graphically demonstrating the trade-off between the level of resolution in the modeled velocity field and the magnitude of the effective dispersivity. Using the parameters estimated from calibration of the layered-conductivity model against the observed tritium plume, Jensen *et al.* (1993) were able to predict the observed chloride transport with reasonable success. The modeling process in this case represents a mixture of deterministic and stochastic philosophies, since the overall heterogeneity of the conductivity field is represented deterministically by the layered structure, while the within-layer heterogeneity is represented by the macrodispersivity assigned to each layer.

Boggs *et al.* (1992) present an overview of the natural-gradient tracer test performed in an alluvial aquifer at the Columbus Air Force Base near Columbus, Mississippi. This aquifer is considerably more heterogeneous than those at the sites described above, as can be seen in Table 1.1. The bromide tracer plume was monitored using an expanding network of multilevel samplers, which eventually reached 250 meters in length. The sampling efforts were focused on the collection of eight synoptic snapshots over the 20-month duration of the test. However, the leading edge of the plume was beyond the leading edge of the developing sampling network at each sampling time. The resulting failure to sample the leading portion of the plume was one of several factors complicating the analysis of this test, including a strongly nonuniform flow field due to large-scale heterogeneities in the conductivity field and possible mass loss to the vadose zone due to fluctuations in the water table elevation.

Rehfeldt *et al.* (1992) present a geostatistical analysis of the conductivity field at the Columbus Air Force Base site, focusing primarily on the analysis of 2483 borehole flowmeter measurements acquired in 58 wells. The dispersivity estimates resulting from this

analysis are notably lower than those estimated by Adams and Gelhar (1992) based on analysis of plume moments. However, both analyses involved ad-hoc procedures intended to compensate for the site-specific "complications" associated with this test. In particular, Rehfeldt *et al.* (1992) account for the large-scale heterogeneity at the site by fitting a third-order trend model to the log-conductivity data and then analyzing the residuals from the trend. Their choice of a third-order trend (as opposed to a trend of lower or higher order) was based largely on external evidence regarding the conductivity field, particularly that provided by the tracer test itself. They also point out the large uncertainty associated with their correlation length estimates, despite the large number of high-quality data obtained at the site. Such results do not bode well for the predictive capability of stochastic models at sites with more than mild heterogeneity.

Although the natural-gradient tracer tests discussed above can certainly be subjected to a range of interpretations, it is clear that they point out some of the shortcomings of stochastic transport theory. Transport processes will almost always be influenced by significant heterogeneities in the conductivity which cannot be adequately represented by the "homogeneously heterogeneous" autocorrelated random function model employed in stochastic theory. It is important to point out that the Borden tracer test, the greatest success so far for the stochastically-based macrodispersivity approach, is as homogeneous an aquifer as one could ever hope to find (Table 1.1). The Columbus tracer test, the one influenced by the most significant heterogeneity, in fact represents a failure for stochastic transport theory, despite attempts by the investigators to interpret the results in a positive light. Furthermore, very large numbers of conductivity measurements are required to obtain reliable estimates of the parameters describing the autocorrelation of the conductivity field. It seems as if measurement efforts would be better spent identifying the important large-scale heterogeneities in the conductivity field, along with other important physical and chemical processes influencing transport, rather than

attempting to estimate effective macrodispersivities from fine-scale variations in the conductivity.

Induced-gradient tracer tests

An induced-gradient tracer test at the Borden site provided an opportunity for a comparative assessment of induced-gradient and natural-gradient tests. Mackay *et al.* (1994) provide an overview of the induced-gradient test, which involved the injection of one conservative tracer, iodide, and four organic solutes. This test was carried out in a dipole format, with the injection and discharge wells separated by 8.5 meters. The tracers were introduced into the injection well over a period of 48 hours and their progress from the injection to the discharge well was then monitored in three multilevel samplers and one partially penetrating well. Thorbjarnarson and Mackay (1994) analyzed the iodide transport using a finite-difference advection-dispersion model assuming perfectly stratified flow and transport between the injection and discharge wells. The fitting parameters employed in their analysis are the injection rate per unit thickness for each 0.15-meter vertical interval centered on a sampling port elevation and the longitudinal dispersivity for that interval. They neglect the effects of horizontal and vertical transverse dispersion, due to the advectively-dominated nature of the test. The vertical distribution of fitted flow rate per unit thickness is taken to be indicative of the vertical distribution of relative hydraulic conductivity, because the stratified flow assumption implies that the total flow will be distributed in accordance with the vertical conductivity distribution. Essentially the same assumptions have been employed in the analysis of GEMSTRAC1.

Thorbjarnarson and Mackay (1994) convert the fitted injection rates per unit thickness into a profile of relative hydraulic conductivity. The dimensions of apparent "features" in this profile appear to be consistent with the correlation lengths determined by Sudicky's (1986)

geostatistical analysis of core permeameter data. In fact, the induced-gradient tracer test was conducted parallel to one of Sudicky's core transects, one meter away. Most of the estimated longitudinal dispersivities presented by Thorbjarnarson and Mackay (1994) are of the order of a few centimeters, indicative of "local" dispersion, and comparable to values obtained from analysis of individual breakthrough curves in earlier natural-gradient tests (Sudicky *et al.*, 1983; Goltz and Roberts, 1986). Analysis of breakthrough curves obtained during GEMSTRAC1 yielded dispersivity estimates of the same magnitude.

Molz and colleagues have perhaps been the strongest proponents of a deterministic approach to contaminant transport modeling, stating that the use of field-scale macrodispersivities "is both unrealistic and misleading physically" (Molz *et al.*, 1989). Instead, they have focused their research efforts on developing economically viable means for identifying the distribution of hydraulic conductivity, particularly the vertical distribution of horizontal hydraulic conductivity. They carried out much of this research in an alluvial aquifer at a field site near Mobile, Alabama. Methods for characterizing the vertical distribution of conductivity have included single-well tracer tests (Molz *et al.*, 1988), multilevel slug tests (Melville *et al.*, 1989), and borehole flowmeter tests (Molz *et al.*, 1989). Although they were not in complete agreement, these three methods revealed largely the same picture of the conductivity distribution at a given location.

Molz *et al.* (1986) and Molz *et al.* (1988) report surprising success in predicting the discharge well breakthrough curves resulting from two dual-well tracer tests (each carried out over 32 days, with a distance of about 40 meters between the injection and discharge wells) using the layered conductivity distribution derived from single-well tracer tests (carried out over four days, with a distance of about 5 meters between the injection/withdrawal well and the observation well). Two transport models were used, both assuming stratified, horizontal flow

in the aquifer, but one employing small (local) dispersivity values and the other assuming purely advective flow. Both models produced similar results. However, the models were less successful at reproducing the breakthrough curves obtained at different levels in observation wells between the injection and discharge wells, indicating that although the simple layered conductivity model may be adequate for predicting the vertically averaged transport behavior, pointwise concentrations are significantly influenced by heterogeneities unaccounted for in this model. Tests at various locations did indicate the presence of lateral heterogeneity over the site, leading to some ambiguity in the definition of the vertical distribution of horizontal conductivity.

Yeh *et al.* (1995) present the results of two dual-well tracer tests conducted in a "coastal sandy aquifer" at Georgetown, South Carolina. Both experiments employed a pair of wells five meters apart as injection and withdrawal wells. Thirty-two sampling wells were laid out between these two wells, in a regular grid with 1-meter spacings in each direction. In each well, packers were used to isolate five 15-cm sampling intervals throughout the saturated thickness of the aquifer. Yeh *et al.* (1995) used an extensive multilevel slug test survey of the sampling wells to generate a three-dimensional hydraulic conductivity field for the site. A finite element transport model employing this conductivity field was quite successful in matching the characteristics of the observed tracer plume. The transport model employed constant values for the dispersivities, namely 0.05 m for longitudinal dispersivity and 0.015 m for transverse dispersivity, values representative of local dispersivity. A simulation was also performed using a layered conductivity field and larger dispersivity values (macrodispersivities) for each layer. Although the layered model employing macrodispersivities was reasonably successful, it was notably less accurate than the fully three-dimensional approach employing local dispersivities. Yeh *et al.* (1995) conclude that the plume movement was controlled by a few "significant

heterogeneities", so that not all the detail of the conductivity field need be retained for successful modeling. However, they note that "a large number of hydraulic conductivity measurements were necessary in order to identify these 'significant' heterogeneities."

The results of these induced-gradient tracer tests seem to represent a triumph for the deterministic school of transport modeling. However, it is not surprising that models employing deterministic conductivity fields and small dispersivity values would be able to reproduce the results of advectively-dominated tests affecting relatively small aquifer volumes. One cannot assume that deterministic models would be equally successful at predicting transport under natural conditions, in which the cumulative affect of smaller-scale velocity variations could be much closer in magnitude to the larger-scale variations in mean flow velocity.

V. SUMMARY

The tracer tests described above have shown the clear need to identify significant, site-specific heterogeneities in the conductivity field in order to be able to model or predict contaminant transport. GEMSTRAC1, the induced-gradient tracer test performed at GEMS in 1994, also clearly demonstrated the importance of such site-specific features. During GEMSTRAC1 much of the tracer entered narrow high-conductivity zones and was rapidly transported to the discharge well. Although this dissertation demonstrates that some of the tracer breakthrough curves can be matched reasonably well using a model assuming vertically stratified, horizontal flow and transport, the data also reveal substantial deviations from this model. Some of those deviations are almost certainly caused by a lack of perfect stratification of the hydraulic conductivity. As discussed in Koltermann and Gorelick (1996), most real conductivity distributions defy both the layered aquifer model employed by Molz and colleagues and the autocorrelated random field model espoused by the proponents of

stochastic transport theory. Although sedimentary process models provide some insight concerning geometric patterns that might occur within certain depositional environments, they do not provide the information necessary to characterize the conductivity distribution at a specific site. A reliable characterization of the conductivity field will always require a program of hydraulic tests, perhaps augmented by geophysical surveys. The comparative assessment of well-testing methodologies presented in Chapter 7 shows that multilevel slug tests, single-well dipole flow tests, and hydraulic tomography are promising site characterization techniques, although all three require further investigation and refinement.

CHAPTER 2: SITE DESCRIPTION AND PAST WORK

I. INTRODUCTION

In 1988, researchers from the Kansas Geological Survey established the Geohydrologic Experimental and Monitoring Site (GEMS) on land owned by the University of Kansas Endowment Association. GEMS is located in the Kansas River Valley northeast of Lawrence, Kansas (Figure 2.1). Research at the site has focused on the development of well-testing methodologies for delineating aquifer heterogeneities controlling contaminant transport in groundwater. GEMSTRAC1, the induced gradient tracer test performed at GEMS in October 1994, was primarily intended to provide a means for evaluating the effectiveness of these various site characterization techniques. This chapter describes the geologic and hydrologic setting of GEMS and work to date at the site, along with discussing previous studies of the alluvial aquifer in this area.

The aquifer under study at the site consists of approximately 10.7 meters (35 feet) of alluvial sand and gravel which is overlain by approximately 10.7 meters of silt and clay. The aquifer rests on sandstone bedrock of Pennsylvanian age. A simplified representation of the stratigraphy at GEMS is shown in Figure 2.2, along with the natural gamma ray logs measured in two wells at the site. Figure 2.3 shows the locations of all wells and multilevel samplers at the site.

II. GEMS SITE DESCRIPTION

Geologic setting

GEMS is located in a portion of the Kansas River valley that is aligned roughly northwest-southeast, with the Kansas River flowing along the southwestern edge of the valley. GEMS is located near the northeastern edge of the valley, approximately 3.5 kilometers northeast

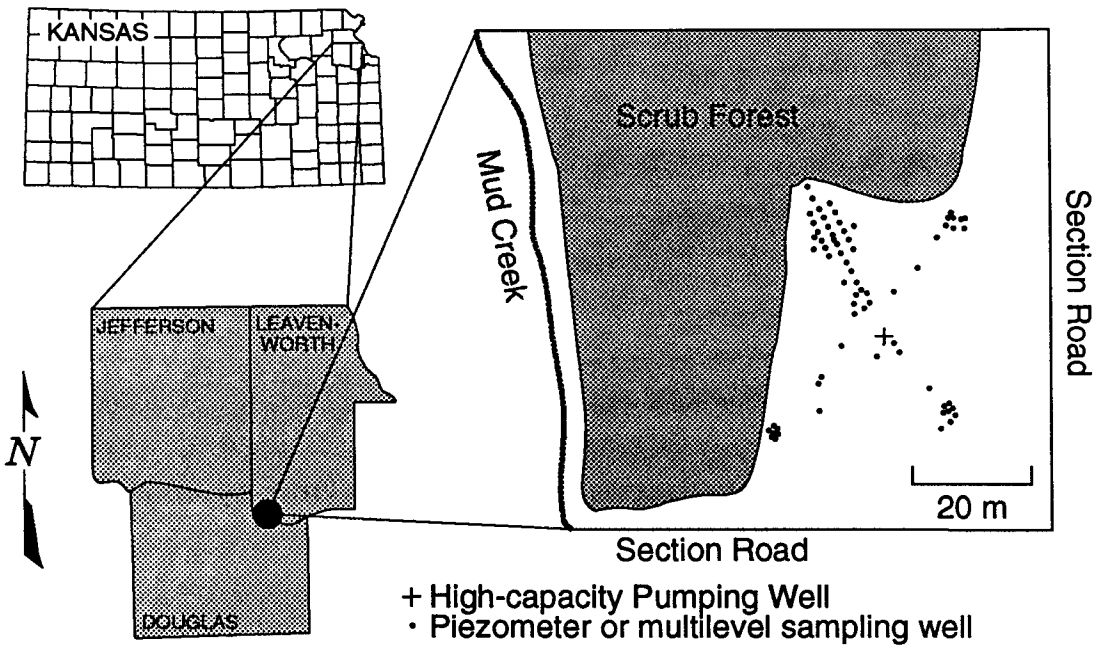

Figure 2.1. Location of GEMS.

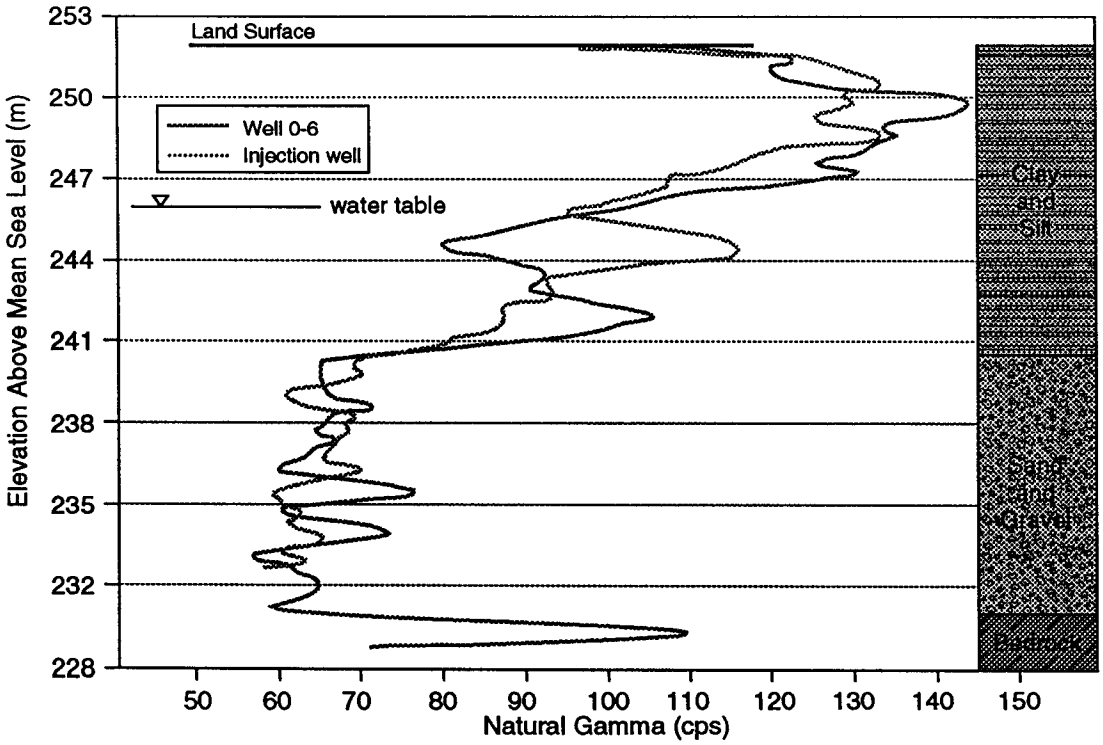

Figure 2.2. Gamma ray logs in two wells and GEMS stratigraphy.

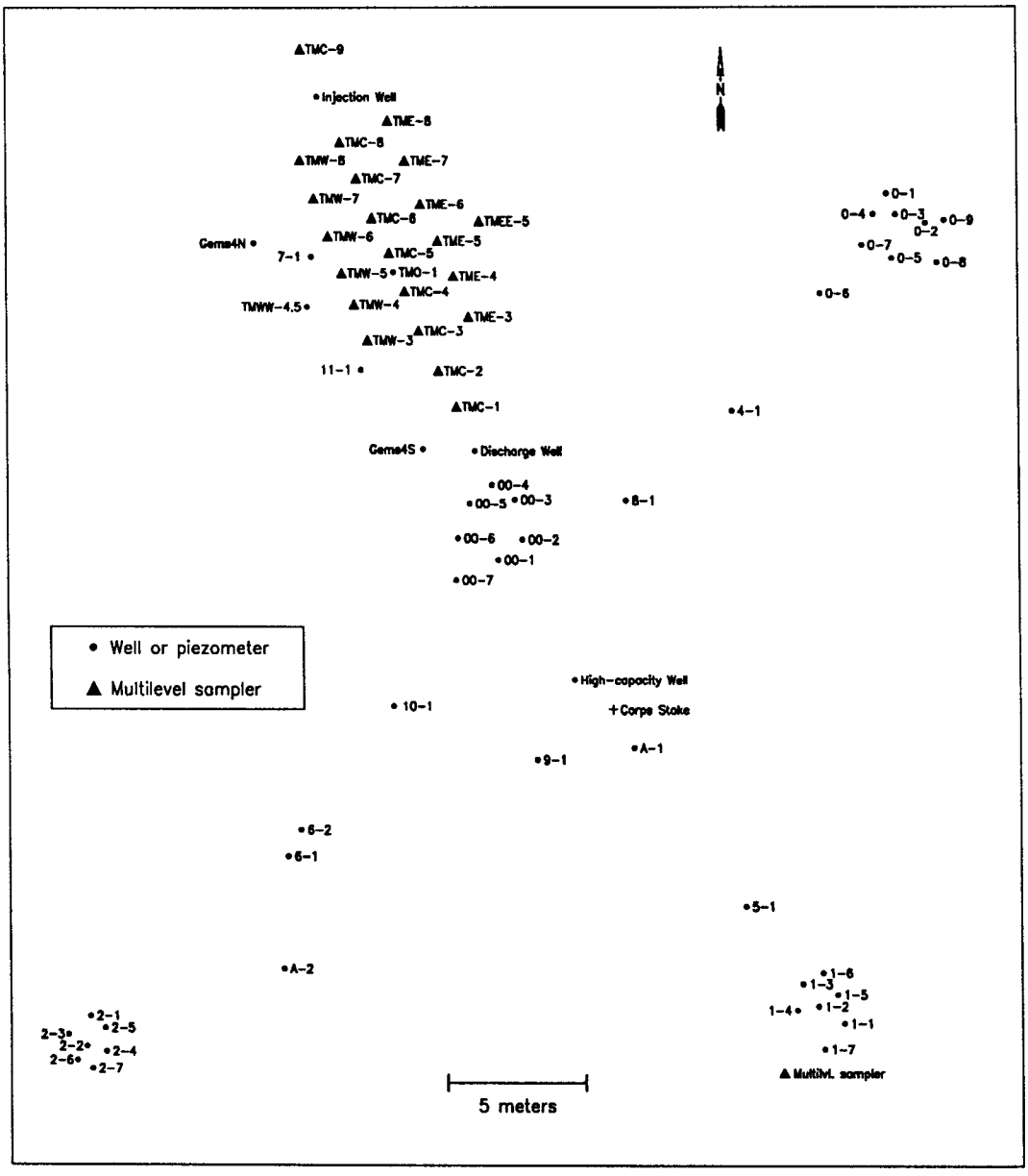

Figure 2.3. Wells and multilevel samplers at GEMS.

of the river. The sediments at the location of GEMS have been consistently mapped as Newman Terrace deposits for several decades (Dufford, 1958; Fader, 1974; O'Connor, 1992). Dufford (1958) states that the coarse basal portion of the alluvium underlying the Newman Terrace was probably deposited as outwash from retreating Wisconsinan glaciers. Denne *et al.* (1998) state that entrenchment of the valley occurred during the late Wisconsinan, perhaps around 13,000 years before the present, with the Newman Terrace being built up during the subsequent Early Holocene alluviation. More recent entrenchment has created a modern floodplain approximately 2.5 to 3 meters below the level of the Newman Terrace. Dufford (1958) states that the Newman Terrace has continued to aggrade, citing evidence of deposition on the Newman Terrace during the 1951 flood.

Core samples obtained at GEMS (McElwee and Butler, 1995) show the fining upward sequence expected in Newman Terrace deposits, similar to that seen in test holes penetrating Newman Terrace deposits described by Fader (1974) and Dufford (1958). Although the aquifer sediments are quite coarse overall, there appears to be a general trend from gravel and very coarse sand overlying the bedrock to coarse and medium sand at the top of the aquifer. In most holes drilled at the site, the contact between the sand and gravel aquifer and the overlying silt and clay is fairly sharp. However, core samples from a few holes seem to exhibit a more transitional contact, with significant silt and clay occurring in the upper portions of what is generally considered aquifer material. Most notably, the entirety of the uppermost core sample (1.5 meters) obtained from the hole drilled for TME-8 (2.7 meters from the injection well, IW) was too rich in clay to be analyzed in the core permeameter. In addition, some clay-rich segments of core were obtained from lower portions of the aquifer in a few holes, indicating that patchy lenses of silt and clay may be distributed throughout the aquifer. Fader (1974) describes a segment of clay encountered immediately above the basal gravel in a test hole

penetrating Newman Terrace deposits approximately 3 kilometers northwest of GEMS at Midland Junction.

The Kansas River valley alluvial aquifer is highly permeable. Denne *et al.* (1998) report hydraulic conductivity values of 530 to 1300 m/day estimated from pumping tests in Kansas River alluvium, although a few tests yielded estimates on the order of 10 m/day. A pumping test performed at GEMS in 1988 yielded a hydraulic conductivity estimate of approximately 190 m/day, a specific storage of $7.3X10^{-4}$, and a leakage coefficient of $9.0X10^{-4}$ m^{-1} (see Chapter 3).

Hydrologic setting

In certain respects, the hydrologic setting of GEMS is rather poorly characterized. We have little information about certain critical aspects of the flow system, including the direction and magnitude of the regional gradient, the extent of leakage to the aquifer from the overlying silt and clay and the underlying sandstone, and the influence, if any, of the nearby Mud Creek. Leakage could have a particularly important influence on the evaluation of GEMSTRAC1. The flow field established during GEMSTRAC1 has been modeled assuming confined conditions, implying that flow to a well is derived entirely from the aquifer and resulting in a radial flow velocity that is inversely proportional to the distance from the well. However, leakage to the aquifer "dampens" the impact of a pumping well, leading to a radial flow velocity that decreases more rapidly with distance than that under confined conditions (Figure 3.15). As described in Chapter 3, the uncertainty in the magnitude of leakage leads to uncertainty concerning the influence on GEMSTRAC1 of pumping at two nearby high-capacity wells.

The water table at the site occurs in the silt and clay, typically at about 6 meters depth, subject to seasonal and annual fluctuations. Attempts to measure the ambient gradient in the aquifer were

unsuccessful because the measured lateral head differences at the site are not significantly larger than the combined errors in the measurements of depth to water and well casing elevation. The measurements indicate that the magnitude of the ambient gradient is probably no larger than 10^{-3}. Fader (1974) presents a water table map for the Kansas River valley from Topeka to Kansas City. This map indicates flow to the southeast, along the axis of the river valley, in the vicinity of the site, with a magnitude of about $5X10^{-4}$. Possible local influences on flow at the site include the persistent pumping at the two high-capacity wells several hundred meters to the west, the proximity of the valley wall a few hundred meters to the north, and the proximity of Mud Creek, approximately 80 meters to the west. It is unlikely that there is any immediate interaction between Mud Creek and flow in the aquifer, because the creek bed is separated from the aquifer by the overlying silt and clay.

Chemical characteristics

The groundwater in the Kansas River valley alluvium is generally of a calcium bicarbonate type and is very hard, with most reported total hardnesses exceeding 300 mg/l (as $CaCO_3$) and some as high as 800 mg/l (Dufford, 1958; Fader, 1974). Another naturally occurring water quality problem in the alluvial aquifer is the presence of fairly high concentrations of iron, typically several milligrams per liter, but ranging up to around 20 mg/l (Dufford, 1958; Fader, 1974; Denne *et al.*, 1998). In addition, samples from a number of wells in the valley exhibit high concentrations of nitrate, some approaching or exceeding the federal primary drinking water standard of 44.3 mg/l (Denne *et al.*, 1998; Fader, 1974).

The groundwater chemistry at GEMS is described in Macpherson and Schulmeister (1994), McElwee and Butler (1995), Macpherson *et al.* (1996), and Hall (1998). Groundwater samples collected at GEMS are similar in chemistry to those described above, with the dominant

dissolved species being calcium and bicarbonate. Measurements in one multilevel sampler show total dissolved solids (TDS) ranging from around 320 to 400 mg/l, with the higher TDS values occurring lower in the aquifer. GEMSTRAC1 involved the injection of 596 mg/l of KBr salt, leading to a TDS approximately 2.5 times higher than normal values. Such an increase in TDS would almost certainly lead to density-driven flow in the aquifer if the tracer were not distributed uniformly in the vertical. As described in Chapter 4, the vertical tracer distribution was decidedly nonuniform. However, the majority of the tracer initially entered lower portions of the aquifer, limiting the potential for density-induced sinking. In fact, there appears to be some evidence that tracer entering the lowermost portion of the aquifer might have been channeled upward into a high-conductivity zone about 2 meters above the base of the aquifer (Figures 4.31 and following).

As described in McElwee and Butler (1995), the presence of significant quantities of chloride (up to about 7 mg/l) at GEMS ruled out the use of a chloride salt as a tracer. KBr was deemed preferable to $CaBr_2$ and NaBr, because introduction of calcium would probably have led to oversaturation with respect to calcite, causing precipitation either in the mixing tank or in the aquifer, and introduction of sodium could lead to swelling of smectitic clays in the aquifer sediments.

Bromide is present in low concentrations at the site, with measured values ranging up to about 0.7 mg/l (McElwee and Butler, 1995). However, the detectable concentrations of bromide tended to occur in the upper portions of the aquifer. As described in Chapter 4, GEMSTRAC1 was effectively only a test of the lower portion of the aquifer, with very little injected tracer entering the upper half of the aquifer. Thus, there may have been very little background bromide present at many of the ports where discernible breakthrough curves were obtained. Nevertheless, the possible presence of low and variable background bromide concentrations in both the samples and the

calibration standard solutions (prepared with GEMS water) leads to considerable uncertainty in measured bromide concentrations below about 1 mg/l, as described in McElwee and Butler (1995) and discussed further in Chapter 3.

The nitrogen chemistry at the site reveals the presence of an upper reducing zone, in which ammonium is present, and a lower oxidizing zone containing significant quantities of nitrate (Macpherson and Schulmeister, 1994; Hall, 1998). The boundary between the two zones appears to be about 16 meters below land surface, or about 6 meters above the base of the aquifer. According to Hall (1998), a persistent plume of nitrate exists in the lower portion of the aquifer. The location of the plume front appears to move seasonally (Hall, 1998) and may move radically in response to large recharge events (Macpherson, pers. comm., 1998). The source of this nitrate is unknown.

III. OVERVIEW OF WORK TO DATE AT GEMS

A number of well-testing methodologies have been employed at GEMS, including pumping tests (Voegeli, 1991), slug tests (McElwee and Butler, 1995; Butler and McElwee, 1996), and single-well electrical tracer tests (Huettl, 1994; McElwee and Butler, 1995). Recent and ongoing work includes investigation of multilevel slug tests (McElwee, 1999), dipole flow tests (Butler *et al.*, 1998) and pumping tests employing pressure measurements obtained from MLS sampling tubes, allowing much greater vertical resolution of the drawdown response than that obtained from conventional observation wells (Butler *et al.*, 1997). In addition, core samples have been obtained from a number of boreholes and subjected to permeameter and grain size analysis (McElwee and Butler, 1995). The overall goal has been to develop techniques that allow accurate assessment of hydraulic conductivity variations while remaining practical for use in routine site characterization efforts. To remain practical, these techniques must

employ commonly available equipment and must not require inordinate amounts of time in the field.

Initially it was assumed that multilevel slug tests, in which short intervals of a fully-screened well are successively isolated with packers and tested, would prove to be a method of great utility for site characterization. However, the performance and analysis of slug tests at the site has been greatly complicated by nonlinear effects associated with the high aquifer permeability, requiring modifications of the testing procedures and development of a new model for analysis of these tests (McElwee and Zenner, 1998). McElwee (1998) employed this model to analyze a suite of multilevel slug tests recently performed in the injection well and obtained very promising results. Analysis of the single-well electrical tracer tests was also complicated, leading to somewhat ambiguous results (McElwee and Butler, 1995). However, recent work with the dipole flow test, in which circulating flow is established between two isolated chambers in a single well (Butler *et al.*, 1998; Zlotnik and Zurbuchen, 1998; Zlotnik and Ledder, 1996), has shown considerable promise. The performance of pumping tests with highly detailed drawdown observations obtained in MLS tubes, one implementation of a method we have termed "hydraulic tomography", has also shown some promise (Butler *et al.*, 1997). However, progress in this area has been hampered by complications in the development of the fiber optic pressure sensors we had originally intended to use to obtain drawdown measurements. Subsequent work with simpler and cheaper air pressure sensors has produced more promising results, but the use of these sensors is hampered by the design of the sampling ports used at GEMS.

Chapter 7 presents a comparative assessment of the results of GEMSTRAC1 and the various well-testing methodologies employed at the site.

CHAPTER 3: TRACER TEST DESIGN AND IMPLEMENTATION

I. INTRODUCTION

This chapter presents both the design modeling employed in planning the October 1994 tracer test (GEMSTRAC1) at GEMS and the details of the final test design and implementation. The design modeling involved development of code to compute tracer plume trajectories by numerically integrating analytical expressions for groundwater flow velocities due to pumping and injection at multiple wells. In addition, the radially convergent transport model described in Chapter 5 was used to simulate breakthrough curves at selected samplers in order to determine the expected duration of the test and required frequency of sampling. This chapter also presents an assessment of site characterization efforts that preceded GEMSTRAC1, including an analysis of the potential impact of leakage on the tracer test results.

Figure 2.3 shows the location of all the wells at the site, including the network of multilevel samplers used for the tracer test. An expanded view of the sampler network, using the injection well (IW) as the coordinate system origin, is shown in Figure 3.1. Appendix A contains the location survey data for the sampler network. The discharge well (DW) is 14.17 meters south 23° east from the injection well. Both IW and DW are essentially fully screened. The observation well TMO-1 has two screens, one extending from about 0.05 to .60 meters above the bottom of the aquifer, and the other extending from about 2.60 to 3.17 meters above the bottom of the aquifer.

All the multilevel samplers east (TME, TMEE) and west (TMW, TMWW) of the centerline are 'regular' samplers, with a 0.61-meter interval between each pair of ports. Thus the 17 ports extend throughout the 11-meter thickness of the aquifer. The odd-numbered samplers along the centerline (TMC) are also regular samplers.

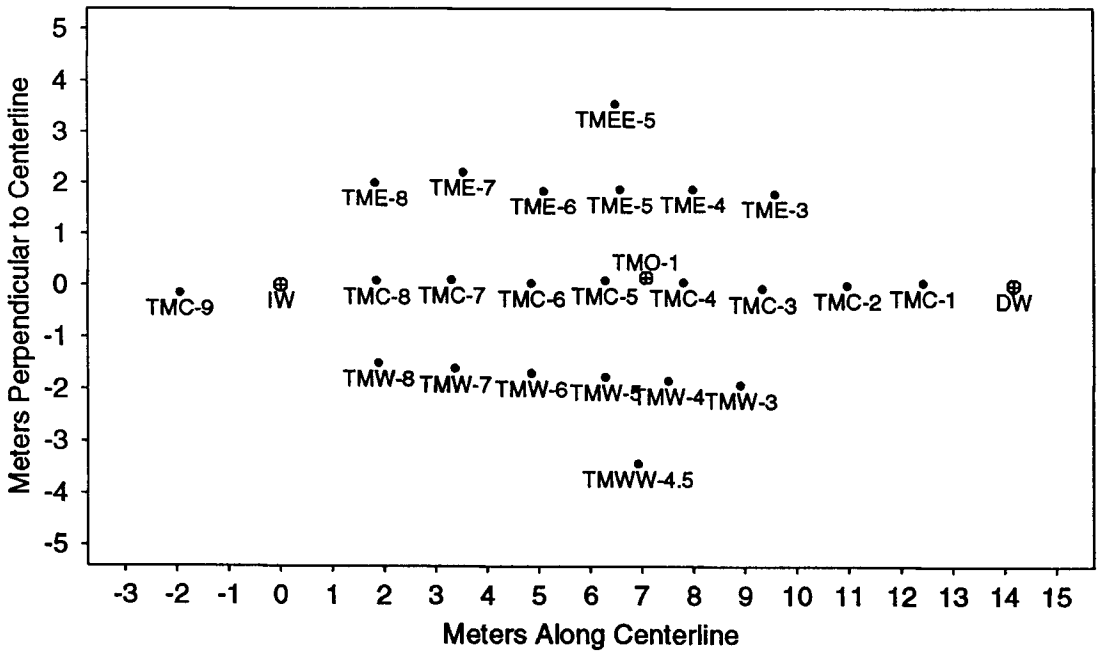

Figure 3.1. Areal view of sampling network.

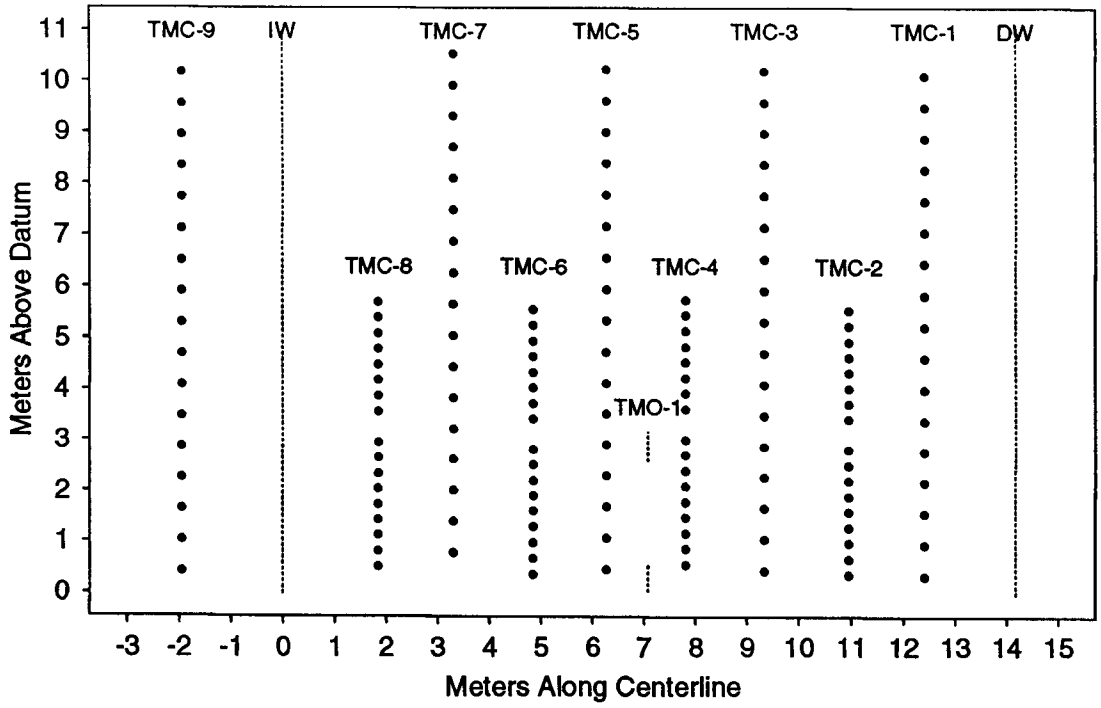

Figure 3.2. Locations of centerline sampling ports.

However, the even-numbered centerline samplers are 'detailed' samplers, with ports at 0.30-meter intervals, except for a 0.61-meter interval, between ports 9 and 10, to accommodate a coupler between sections of PVC. The ports for the detailed samplers extend only through the bottom half of the aquifer, approximately. Figure 3.2 displays the locations of sample ports along the centerline, along with the locations of well screens for IW, DW, and TMO-1. The elevations are in terms of meters above datum, which is 21.33 meters (70 feet) below the top of the Corps Stake, the elevation reference point for the site survey. Appendix A contains the survey data and the port elevations for all the samplers in the network.

II. DESIGN MODELING

The design modeling presented here helped to determine the hydraulic format of the tracer test (radially convergent versus dipole), the method of tracer introduction (instantaneous versus continuous), and the amount of tracer mass to introduce. In addition, these results yielded an estimate of the amount of time required to conduct the test and of the necessary sampling frequency.

Pre-test site characterization

In August and September of 1994, several pumping tests and slug tests were performed using wells in the tracer test network (IW, DW, and TMO-1, along with two observation wells located near TMWW-5). The purpose of these tests was to determine aquifer parameters to use in modeling expected tracer travel times and concentrations for a given pumping rate and injection scheme. However, the results of these tests raised more questions than they answered. In addition, while the vertical distribution of relative horizontal hydraulic conductivity has a profound influence on tracer test results, conservative transport in a stratified, steady state flow field is unaffected by the absolute value of hydraulic conductivity. In a

confined, homogeneous aquifer, the total volumetric flux across any cylindrical surface centered on a pumping well will be equal to the pumping rate, with the flux per unit cross-sectional area of aquifer decreasing in proportion to the surface area of the cylinder ($2\pi rb$, where r is the radius of the cylinder and b is the aquifer thickness). Thus the flow velocity at any point is determined solely by the pumping rate and the radial distance from the pumping well. In a confined aquifer with a layered conductivity distribution, the flux towards the well will be distributed in the vertical according to the relative distribution of horizontal hydraulic conductivity, but the absolute conductivity values will have no influence on the flow velocities. Therefore the bulk conductivity estimate yielded by a pumping test is in some respects irrelevant to tracer test design decisions. Slug tests can potentially yield useful information on the vertical variation of hydraulic conductivity (Butler *et al.*, 1994). However, the results of GEMSTRAC1 were influenced by a very fine scale of conductivity variation. It is unclear whether slug tests at the site can be configured to resolve such a fine scale. A further analysis of these issues can be found in Chapter 7.

The most important result of the pumping tests performed in August and September of 1994 was that the measured heads were clearly affected by the pumping of nearby rural water district (RWD) wells. This led us to perform some longer-term continuous monitoring of the head variation at the site, using pressure transducers in several wells. Figure 3.3 shows the head variation observed in well 0-1 over a two-day period from the afternoon of September 28, 1994, until the afternoon of September 30, 1994. These results clearly show the influence of the two rural water district wells, which are pumped alternately. It was estimated that each well was pumping approximately 30% of the time, with the nearer well (designated RWD1 in this report) pumping at approximately 69.3 m^3/hr and the farther well (RWD2) pumping at approximately 71.5 m^3/hr. RWD1 and RWD2 are approximately 366 meters and 533 meters, respectively, to the west of the network centerline. The locations of the RWD wells

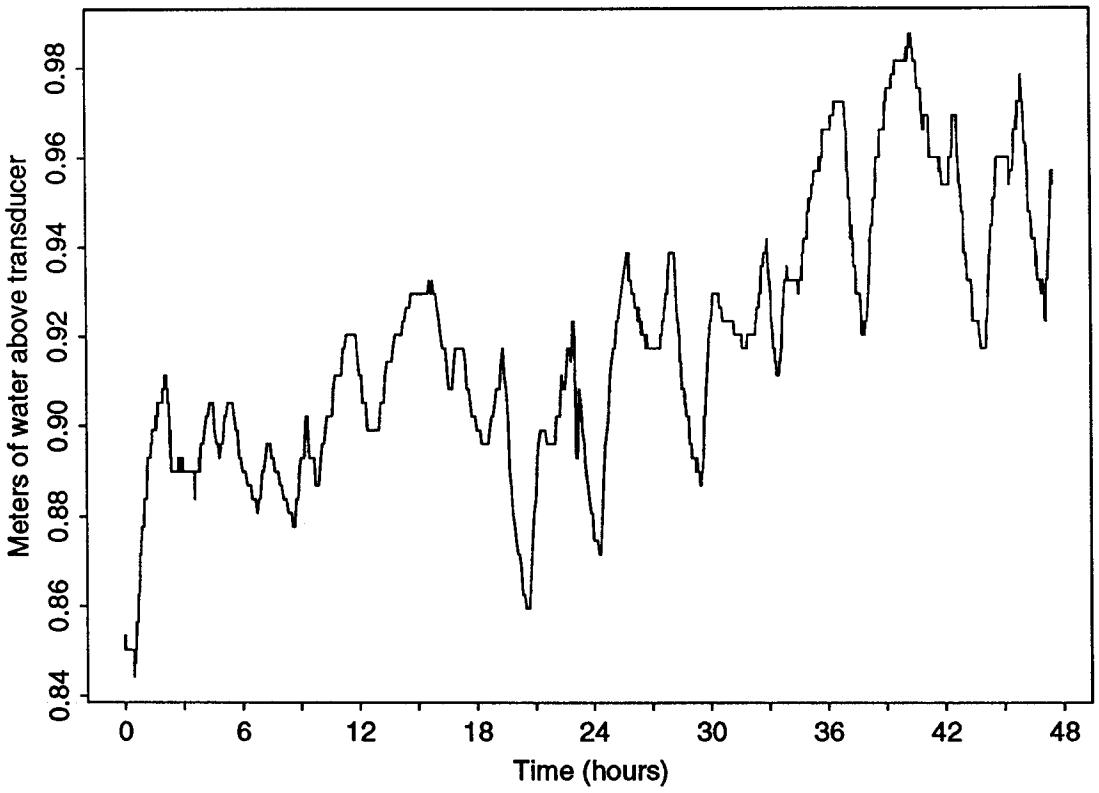

Figure 3.3. Head variation at well 0-1, 9/28/94-9/30/94

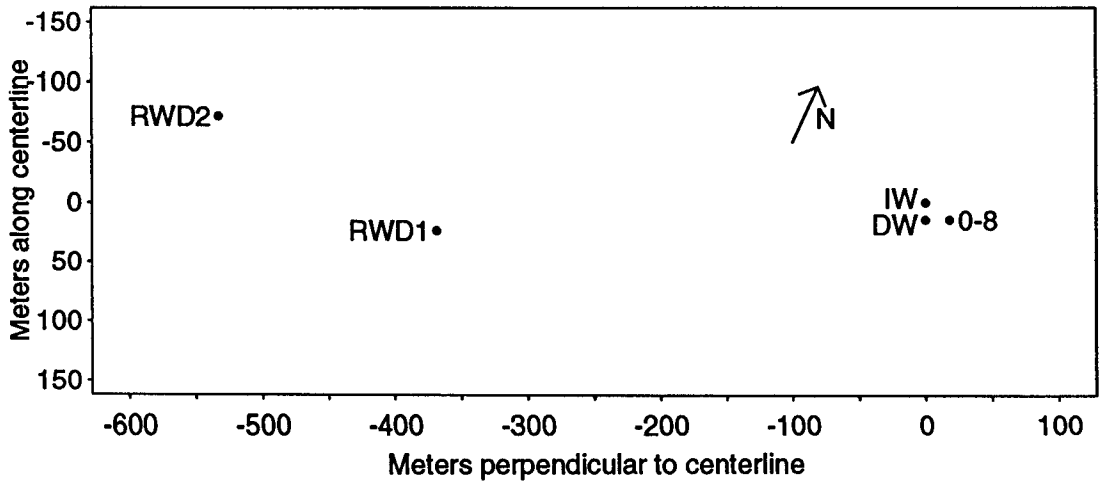

Figure 3.4. Locations of Rural Water District Wells

were estimated using an aerial photograph and a pace estimate of the distance between RWD1 and RWD2. The locations of these wells relative to the network centerline are shown in Figure 3.4. The location of GEMS well 0-8 is also included in this plot, since this well was ultimately used as a 'hydraulic compensator', to attempt to correct for the expected influence of the RWD wells, as discussed below.

Modeling of the Influence of Rural Water District Wells

Theoretical modeling was used to help identify an appropriate test format. Based on some initial design modeling and consideration of field logistics, we had originally decided to perform a radially convergent tracer test, with a zero fluid injection rate at the tracer injection well. That is, no water would be introduced at the injection well other than that which was necessary to introduce the tracer. The results would then be analyzed under the assumption that the tracer was transported in a radial flow field, considering the hydraulic effects of the injection process to be negligible. The alternative format would have been to inject water continuously at the injection well, setting up a dipole flow field between the two wells. The tracer mass would then be introduced over a much longer period, with the injected fluid. This results in the tracer being spread out over a much larger area, compared to the radially convergent test. Due to the spreading of tracer mass over both time and space, the dipole test with continuous tracer injection will have much lower concentrations for a given mass of tracer than the radially convergent test with pulse injection. In the latter test most of the tracer mass will remain near the line between the injection and discharge wells and should be contained in packets of relatively limited longitudinal extent, due to the pulse nature of the input. We had hoped that by performing a pulse-injection radially convergent test we would be able to focus our sampling efforts on the samplers along the network centerline and would also increase our chances of obtaining measurable concentrations at most ports sampled. In addition, results of a radially convergent tracer test could be analyzed

with an existing solution for transport in a radially convergent flow field (Moench, 1989, 1991).

The discovery of the potential influence of the RWD wells led us to reconsider a dipole format test, in hopes that a nonzero (fluid) injection rate would help to compensate for the tendency of the RWD wells to draw the tracer away from the centerline towards the west. The design modeling presented here demonstrates that a dipole format does little to reduce the deflection of flowlines caused by the RWD wells. Instead, an alternative scheme, involving pumping at a low rate at a GEMS well to the east of the network centerline (well 0-8) seems to compensate for the deflection caused by the RWD wells while still allowing us to perform a radially convergent test.

The computation of flow lines for different pumping scenarios is accomplished by numerically integrating analytical expressions for the x- and y-components of pore fluid velocity due to a number of point sources and sinks superimposed on a uniform regional flow field. These expressions can be found in Javandel *et al.* (1984). If u_x and u_y are the x- and y-components of the regional pore fluid velocity, and Q_i is the pumping rate (positive for extraction, negative for injection) at well i, located at (x_i,y_i), then the x- and y-components of the pore fluid velocity are given by

$$\begin{aligned}\frac{dx}{dt} &= v_x(x,y) = u_x - \sum_{i=1}^{N} \frac{Q_i}{2\pi bn} \frac{(x-x_i)}{(x-x_i)^2+(y-y_i)^2} \\ \frac{dy}{dt} &= v_y(x,y) = u_y - \sum_{i=1}^{N} \frac{Q_i}{2\pi bn} \frac{(y-y_i)}{(x-x_i)^2+(y-y_i)^2}\end{aligned} \tag{3.1}$$

where b is the aquifer thickness and n is the porosity. Flowlines for a given scenario are computed using a fourth-order adaptive stepsize Runge-Kutta algorithm (Press *et al.*, 1992) to integrate the above expressions from time zero at a specified starting point (x_s,y_s).

The following computations assume that the influence of the RWD wells can be represented using their overall average pumping rates. That is, since each well is on about 30% of the time, the overall average pumping rate at RWD1 is 0.3*(69.3 m^3/hr) = 20.8 m^3/hr and the pumping at RWD2 is 0.3*(71.5 m^3/hr) = 21.5 m^3/hr. The temporal variations in the actual pumping rates should not significantly influence the overall trajectory of the tracer cloud, but will instead produce somewhat greater apparent transverse dispersion than might occur otherwise due to the shifting of the hydraulic gradient as the RWD wells turn on and off.

Unfortunately, we are unable to obtain a useful measurement of the regional hydraulic gradient at the site; the differences in hydraulic head across the site due to the regional gradient are probably of the same magnitude as the errors in our measurements of the relative elevations of the tops of the well casings. Therefore the following computations will be based on the assumption that u_x and u_y are negligible in comparison to the pore-fluid velocities induced by pumping. At this point we have no way of confirming the validity of this assumption.

The pumping rate at the discharge well will be fixed at 15.9 m^3/hr, about the maximum rate obtainable with our equipment, for all simulations. Figures 3.5 and 3.6 show the computed flowlines for an injected pulse of two different widths, 2 meters and 3 meters, respectively, with a zero fluid injection rate at IW and no pumping at well 0-8, that is, with no attempts to compensate for the influence of the RWD wells. The middle line represents the trajectory of the center of the plume from the injection well at (0,0) to the discharge well at (14.17 m, 0). The two outer lines are the trajectories of the outer edges of the plume assuming negligible transverse dispersion. The design modeling presented here also assumed that the injected tracer solution would be distributed uniformly in a cylinder surrounding the injection

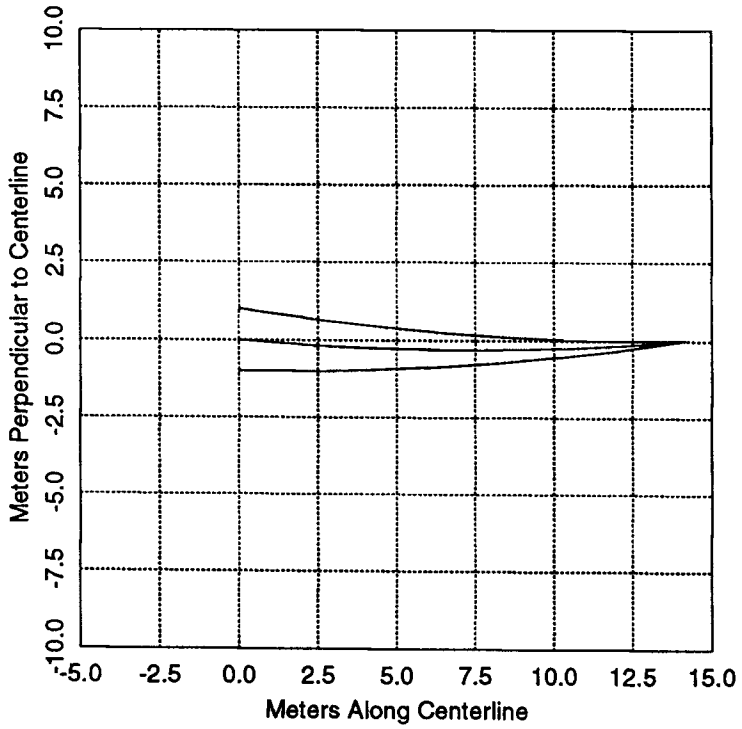

Figure 3.5. Flowlines for zero injection rate, 2-meter initial width.

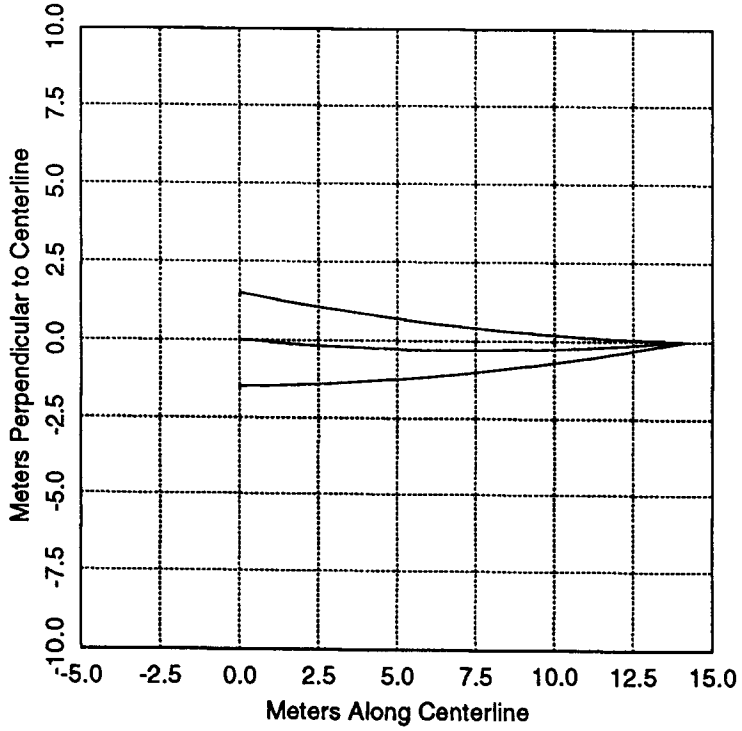

Figure 3.6. Flowlines for zero injection rate, 3-meter initial width.

well throughout the 11-meter aquifer thickness. This turned out to be a very poor assumption, but the extent to which it would be violated was not anticipated in advance. Using this simple model and employing a porosity of 0.28, the 2-meter and 3-meter injection widths (cylinder diameters) correspond to injected volumes of 9.65 m^3 (2550 gallons) and 21.7 m^3 (5733 gallons), respectively. The latter volume is considerably greater than we intended to inject.

In the simulations presented in Figures 3.5 and 3.6, the plume is deflected significantly from the network centerline. With a two-meter injected width, the simulated plume is just grazing the network centerline for approximately the final four meters of travel to the discharge well. This would potentially lead to low concentrations along the network centerline and also to substantial systematic deviations from the behavior predicted by a radially convergent transport model. With a three-meter injected width, the potential for 'missing' the injected plume is reduced but not entirely alleviated and the problem of a systematic deviation from a radially convergent transport model is unchanged.

Figures 3.7, 3.8, and 3.9 show the computed flowlines for dipole tests with three different fluid injection rates, 0.23 m^3/hr (1 gpm), 1.13 m^3/hr (5 gpm), and 2.27 m^3/hr (10 gpm), at well IW. It is clear that a non-zero injection rate at IW does little to reduce the deflection caused by pumping at the RWD wells. This would result in a systematic deviation from behavior predicted by a dipole transport model. In addition, the dipole format would require a much higher injected mass relative to the radially convergent format due to the spreading of tracer over a larger area and the longer time period of injection.

Since fluid injection at IW does little to compensate for the deflection of flowlines caused by the RWD wells, an alternative compensation scheme was proposed: pumping at a low rate in a well in the 0 nest, approximately east of the discharge well. Well 0-8, shown

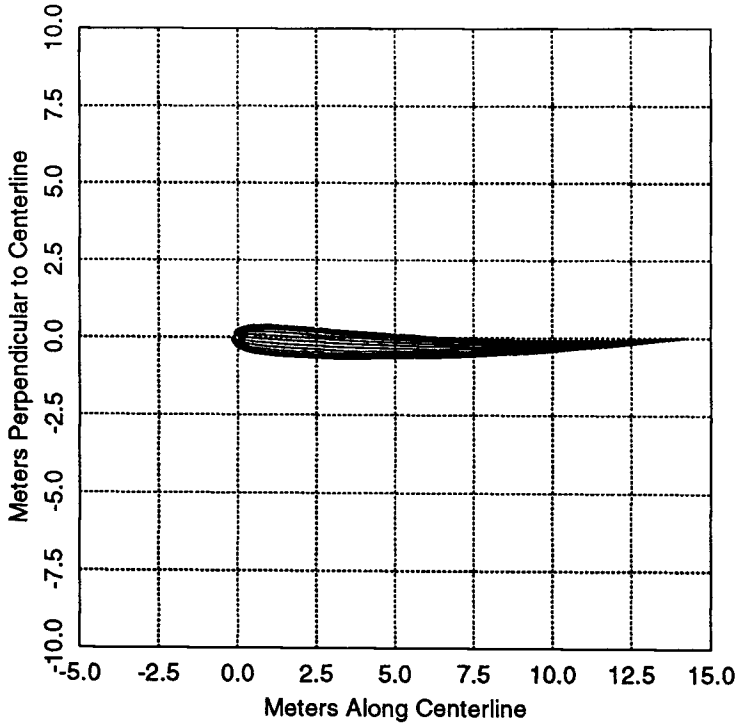

Figure 3.7. Flowlines with 0.23 m^3/hr (1 gpm) injection.

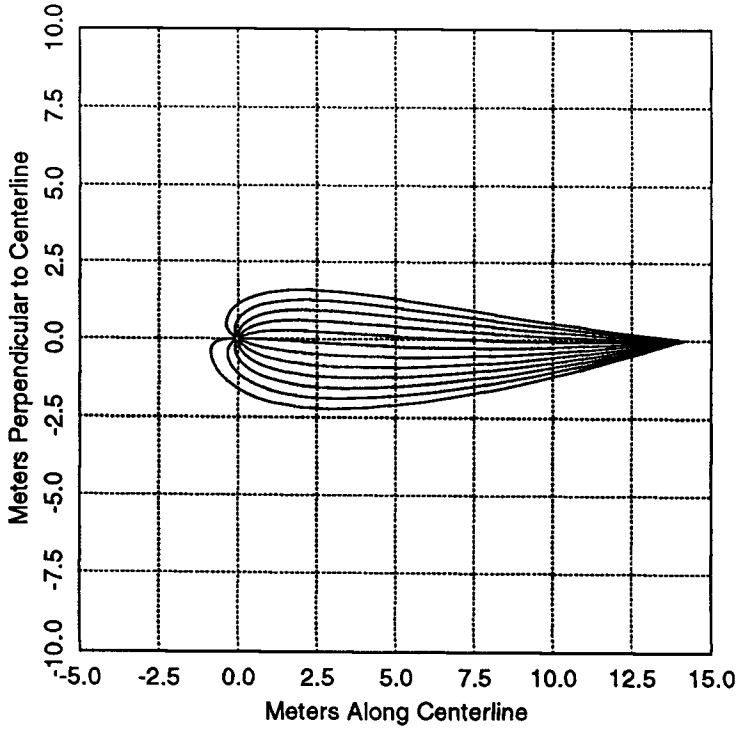

Figure 3.8. Flowlines with 1.13 m^3/hr (5 gpm) injection.

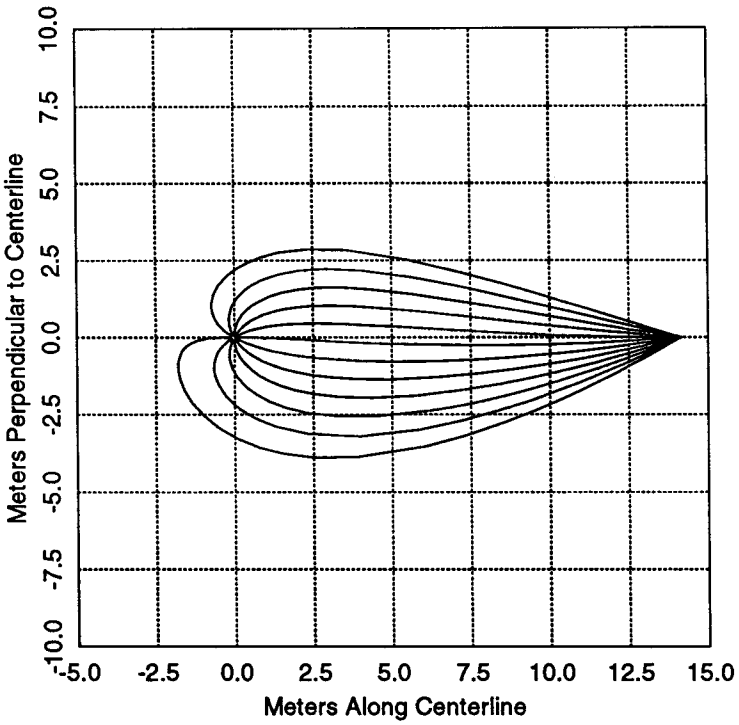

Figure 3.9. Flowlines with 2.27 m^3/hr (10 gpm) injection.

in Figure 3.4, was selected as the potential 'compensator' well. Figure 3.10 shows the flowlines computed using a 2.27 m^3/hr (10 gpm) flow rate at well 0-8 with a zero fluid injection rate at IW and assuming a two-meter injection width. The computed flowlines are nearly identical to those computed for a purely radial flow field. The eastward velocity components due to pumping at well 0-8 nearly cancel the westward components due to pumping at the RWD wells. Thus, the transport problem could reasonably be represented as radially convergent. Figures 3.11 and 3.12 show the sensitivity of the computed flowlines to our estimates of the average pumping rates at the RWD wells. Figure 3.11 shows the flowlines computed assuming 20% higher pumping rates at the two RWD wells, with the same pumping rate (2.27 m^3/hr) at well 0-8. The effects of a 20% lower pumping rate at the RWD wells are demonstrated in Figure 3.12. In both cases the center of the plume still remains reasonably close to the network centerline and

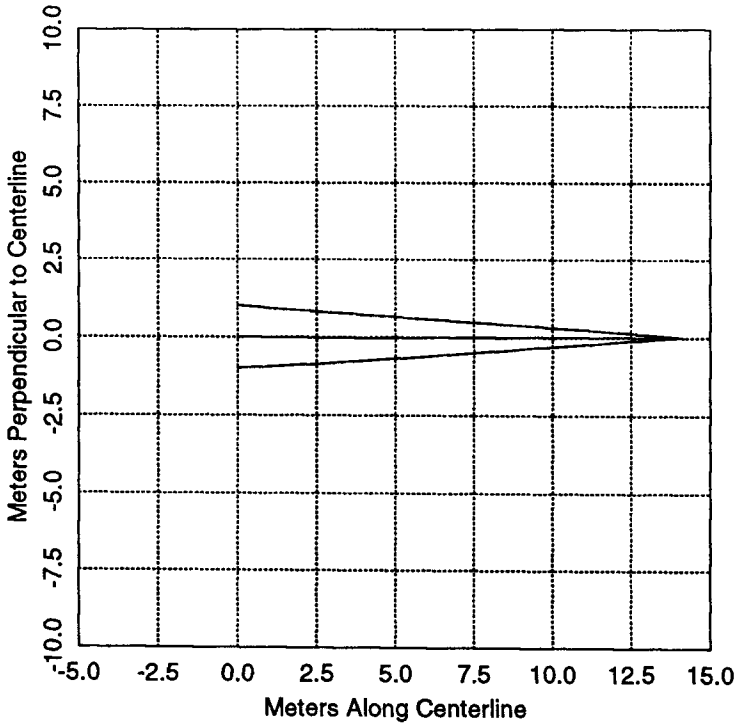

Figure 3.10. Flowlines with 2.27 m^3/hr pumping at well 0-8.

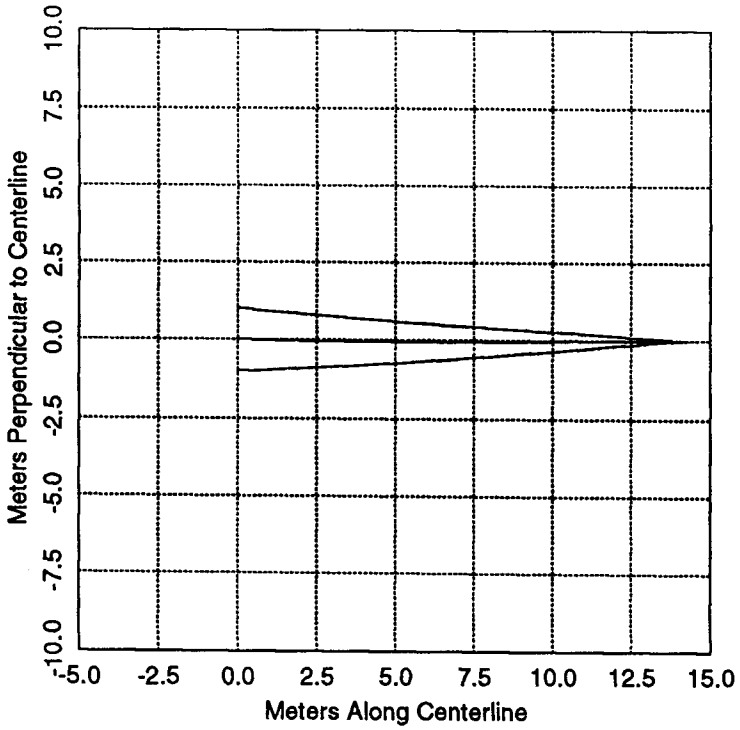

Figure 3.11. Flowlines with 20% higher pumping at RWD wells.

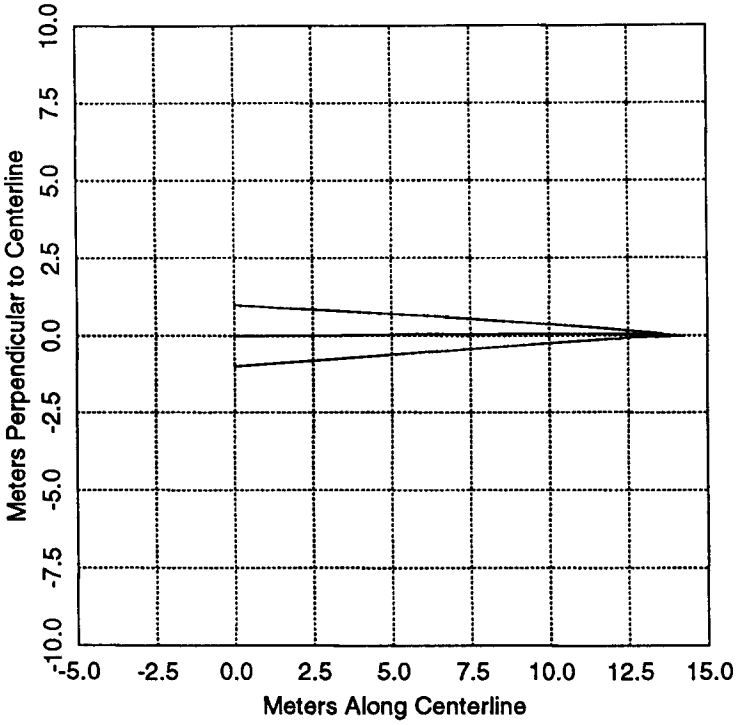

Figure 3.12. Flowlines with 20% lower pumping at RWD wells.

the flow is nearly radially convergent. Based on these simulations, we decided to pump well 0-8 at about 2.27 m^3/hr during the tracer test.

We failed to consider the possibility that the RWD wells might have negligible influence on the flow velocity at the site, despite their obvious influence on the time variation of the potentiometric surface. It is possible that the RWD pumping leads to an essentially uniform increase and decrease in heads across the site, with only an insignificant influence on the head gradient. This could be the case, for example, if a significant portion of the pumpage at the RWD wells was supplied by leakage from the overlying silts and clays. The effects of leakage are not accounted for in the modeling presented above, which assumes perfectly confined conditions. It may be reasonable to neglect leakage when computing the velocity components due to nearby wells, but the velocities due to pumping at distant wells will be significantly reduced by the leakage over the intervening aquifer volume. In

addition, the pseudo-steady state assumption employed above may contribute to an overprediction of the velocity components at the site due to pumping at the RWD wells. These factors are examined in detail in the next subsection. Figure 3.13 shows the flowlines computed when the RWD wells are assumed to have negligible influence on the flow velocities, but with the compensator well, 0-8, pumping at 2.27 m^3/hr. Not surprisingly, Figure 3.13 looks a great deal like Figure 3.5, with the plume now being deflected to the east (towards the compensation well) rather than to the west (towards the RWD wells). There is evidence that this eastward deflection may in fact have happened during the test.

Influence of leakage and storage on flow velocities

The flowline calculations presented above are based on flow velocities computed under the assumption of confined, steady state conditions. This subsection attempts to provide an estimate of the possible errors in the calculated velocities due to the influence of leakage from above or below the aquifer and transient effects due to release of water from storage.

Under purely confined conditions the steady state flow velocity in response to constant pumping at a single well can be computed on the basis of volumetrics. At a radial distance, r, from the pumping well, the pumping rate, Q, is distributed around a cylinder of radius $2\pi r$ and with a height, b, equal to the aquifer thickness. Assuming a constant porosity, n, the flow velocity at radius r under confined conditions is given by

$$v_c(r) = \frac{Q}{2\pi bn}\frac{1}{r} \qquad (3.2)$$

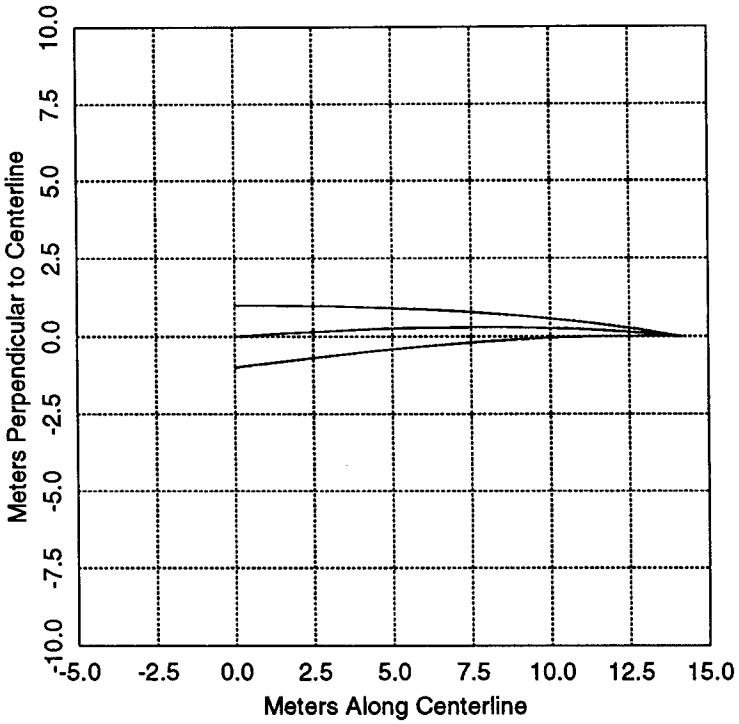

Figure 3.13. Flowlines with no pumping at RWD wells.

This velocity is directed towards a pumping well or away from an injection well. Equation 3.1 results from summing the x and y components of velocities due to a number of wells.

When water is also supplied by leakage into the aquifer from above or below, then the volumetric flux crossing the cylindrical surface of radius r decreases with increasing radius, since increasing proportions of the pumping rate are supplied by leakage over the intervening area. The simplest analytical models for pumping under leaky conditions consider two kinds of mechanisms for leakage, release of water from storage in an adjacent aquitard or leakage of water across an aquitard from an overlying or underlying formation, treated as a constant head reservoir. In practice it is difficult to distinguish these different leakage mechanisms, or to distinguish between leakage from above and leakage from below. However, storage effects contribute only transient components to the aquifer response; a constant head

reservoir must be present in order to obtain a steady state leaky solution that is distinct from the steady state solution under purely confined conditions.

Figure 3.14 shows the data from a 1988 pumping test at GEMS, along with the best-fit curves for three different pumping test models incorporating leakage (Reed, 1980). In this test, the Permanent Well (see Figure 2.3) was pumped at 38.6 m^3/hr (170 gpm) and drawdown was measured at well 0-1 over a three-day period. Well 0-1 is 21.3 meters from the Permanent Well and is screened throughout the aquifer thickness. The model in which leakage is derived solely from a constant head reservoir (i.e., there is no release of water from storage in the aquitard) is described by three parameters, the aquifer transmissivity, T, the aquifer storage coefficient, S, and the leakage coefficient, $L = \sqrt{K'/Tb'}$, where K' and b' are the vertical hydraulic conductivity and thickness of the aquitard. L has units of inverse length and increases with increasing leakage. For the two models including the effects of aquitard storage, the aquitard parameters K', b', and specific storage, S_s', must be specified or fit independently.

Table 3.1 shows the fitted parameter values and root mean squared residual (rmsr) for each of the three model fits. Clearly, all three models provide reasonable fits to the data, with the model incorporating both leakage mechanisms providing a marginally superior fit. Figure 3.14 shows that the third model, with no constant head reservoir, does not reproduce the apparent flattening of the drawdown response at late times.

Assuming that the leakage is supplied by a single constant head reservoir separated from the aquifer by an aquitard of thickness b' and hydraulic conductivity K', the steady state drawdown is given by

$$s(r) = \frac{Q}{2\pi T} K_0(rL) \qquad (3.3)$$

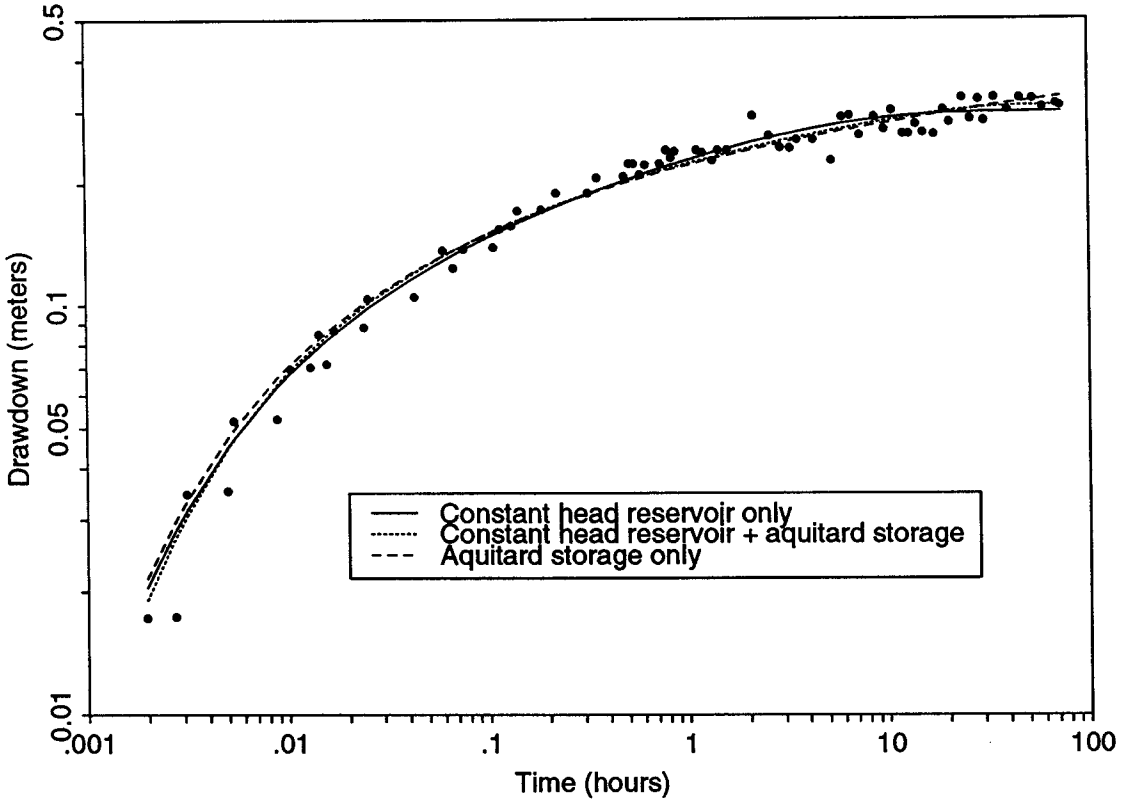

Figure 3.14. Model fits to 1988 pumping test.

Table 3.1. Parameter estimates for three different models based on analysis of the October, 1988, pumping test at GEMS. Model 1 includes leakage from a constant head reservoir only, Model 2 includes leakage from a constant head reservoir and release of storage from the aquitard, and Model 3 includes aquitard storage only.

	Model 1	Model 2	Model 3
T [m^2/hr]	84.2	71.4	74.9
S [-]	7.3×10^{-4}	7.3×10^{-4}	6.6×10-4
L [m^{-1}]	9.0×10^{-4}	NA	NA
K' [m/hr]	NA	6.9×10^{-4}	2.7×10^{-4}
S_s' [m^{-1}]	NA	1.5×10^{-3}	2.5×10^{-3}
b' [m]	NA	4.57	7.62
rmsr [m]	0.0158	0.0153	0.0156

where $K_0(x)$ is the modified Bessel function of the second kind and zero order. Since the derivative of $K_0(x)$ is the negative of $K_1(x)$, the first-order modified Bessel function of the second kind, the steady state radial velocity under leaky conditions is (Reed, 1980; Jacob, 1946)

$$v_\ell(r) = -\frac{K}{n}\frac{\partial s}{\partial r} = -\frac{T}{bn}\frac{\partial s}{\partial r} = \frac{Q}{2\pi bn} LK_1(rL). \qquad (3.4)$$

Thus the ratio of velocities under leaky and purely confined conditions at a radius r is given by

$$\frac{v_\ell}{v_c}(r) = \frac{LK_1(rL)}{1/r} = \left[xK_1(x)\right]_{x=rL}. \qquad (3.5)$$

This function is plotted in Figure 3.15, for dimensionless radii, r_L, ranging from 0.01 to 10. As either leakage coefficient or radius decreases, the steady state velocity under leaky conditions approaches that under purely confined conditions, implying that flow velocity computations assuming confined conditions may be sufficiently accurate within a certain radius of a pumping well, even when leakage is present. However, velocities for more distant points will be overestimated if leakage is neglected.

Using the leakage coefficient estimate of 9×10^{-4} m^{-1} derived from the analysis of the 1988 pumping test, the 14.17-meter distance from the tracer test discharge well, DW, to the injection well, IW, corresponds to a dimensionless radius of 0.013. The corresponding velocity ratio (Equation 3.5) is 0.9996, implying that the assumption of confined conditions would introduce negligible error in the computation of velocity components in the vicinity of the tracer network due to pumping at well DW in this case. The same is also true for the components due to pumping at the compensator well, 0-8. The distances from the center of the tracer network to wells RWD1 and RWD2 are around 370 and 540 meters, respectively. The velocity ratios

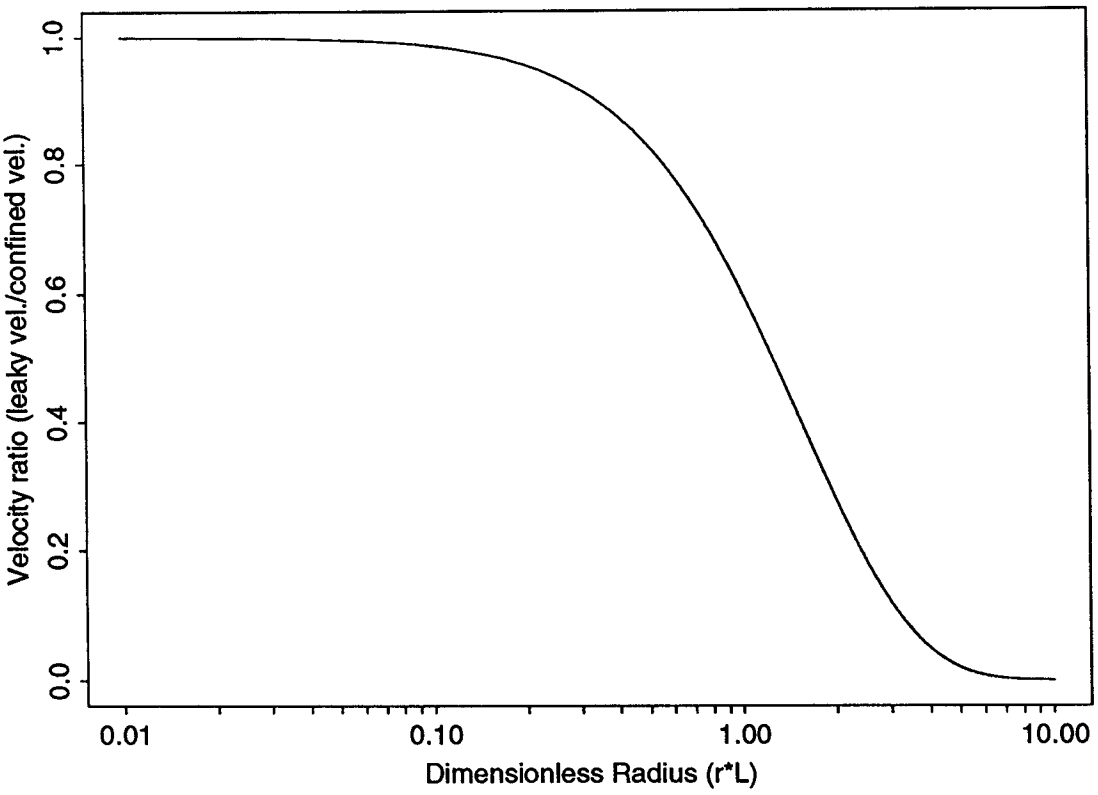

Figure 3.15. Velocity ratio for leaky versus confined conditions.

for these radii are .90 and .83, implying that the neglect of leakage would not appear to introduce more than a 20% error in the velocity components computed for these wells in the vicinity of the tracer network. As illustrated in Figure 3.12, an error of this magnitude does not significantly alter the plume trajectory. However, a somewhat larger leakage coefficient could lead to substantially lower velocity ratios. With a leakage coefficient of 1.8×10^{-3} m^{-1}, which also yields a plausible fit to the pumping test data, the velocity ratios are 0.75 and 0.61 for RWD1 and RWD2. With a leakage coefficient of 4.5×10^{-3} m^{-1}, five times the fitted value, the ratios are 0.37 and 0.20, indicating that the neglect of leakage would lead to a substantial overestimation of the flow velocities in this case. Although the larger leakage coefficient results in a fairly poor fit to the pumping test data, it is certainly possible that the pumping test analysis could underestimate the leakage coefficient by a factor of five or more, especially given the

limited radial distance between the pumping well and the observation well in this test. Thus it is conceivable that neglect of steady state leakage effects could have resulted in an overestimate of the influence of the RWD wells in the flowline calculations. However, even using a leakage coefficient ten times larger than the fitted value, the velocity ratio for distances on the order of the tracer test network length is 0.98, implying that steady state leakage has little affect on the flow velocities due to pumping at DW and well 0-8.

The neglect of transient effects due to storage in the aquifer and aquitard could also lead to overestimation of the computed flow velocities. Figure 3.16 shows the time variation of velocities at the center of the tracer test network due to a synthetic pumping record at RWD1, calculated using the three different leakage models with the parameters shown in Table 3.1. The synthetic pumping record has five pumping cycles per day, with two 2-hour pumping periods, one 1.2-hour pumping period, and two 1-hour pumping periods, for a total 7.2 hours of pumping per day. The two-day period shown in Figure 3.16 follows three days of pumping in the same pattern, allowing time to achieve a "steady state" cyclic drawdown response to the cyclic pumping. RWD1 is assumed to pump at 69.27 m^3/hr when it is on, resulting in an overall average pumping rate of 20.78 m^3/hr, the figure used in the velocity calculations in the previous section. The horizontal dashed line in Figure 3.16 corresponds to the velocity computed using the average pumping rate and assuming confined, steady state conditions. This velocity is 0.0030 m/hr. The time-varying velocities computed using the leaky models vary roughly about this constant value. The time-averaged velocities are 0.0027 m/hr, 0.0024 m/hr, and 0.0027 m/hr for the constant-head only, constant-head plus aquitard storage, and aquitard storage only models, respectively. That is, the velocity corresponding to confined, steady-state conditions does seem to provide a reasonable estimate of the overall average velocity

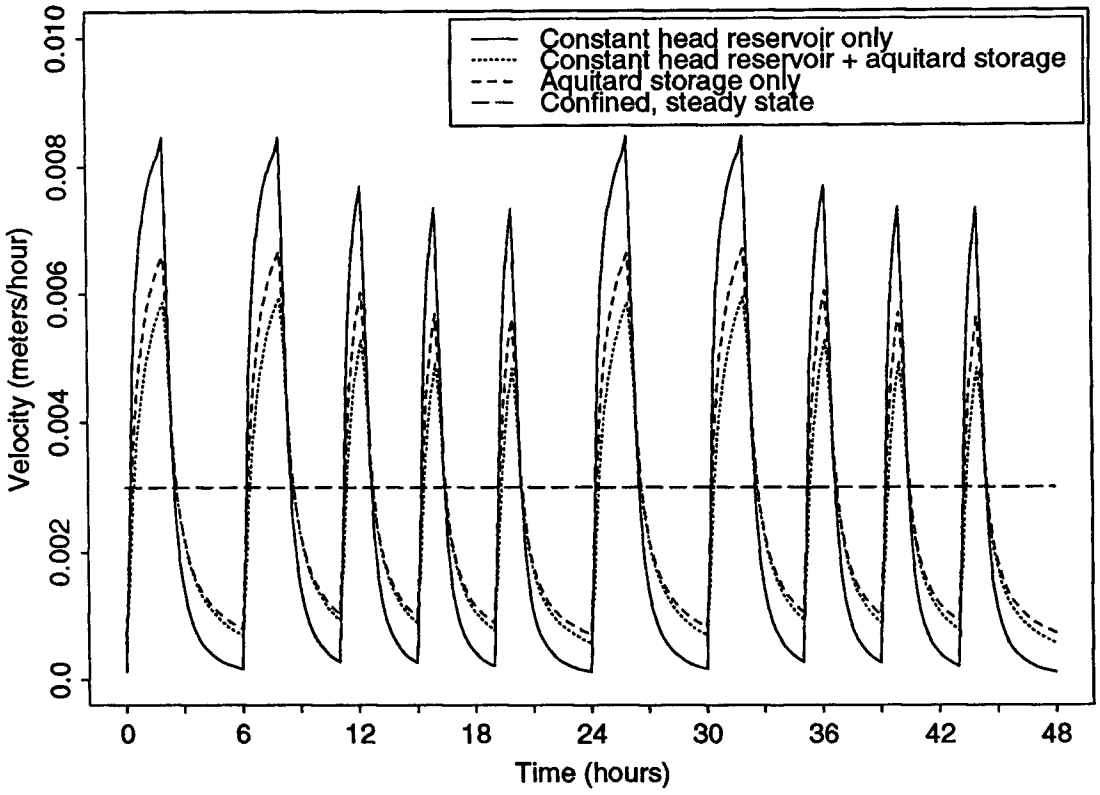

Figure 3.16. Velocities due to synthetic pumping at RWD1.

due to pumping at RWD1, even accounting for the delayed response due to leakage and storage.

Figure 3.17 shows the time-varying velocities at the center of the network due to a synthetic pumping record at RWD2, along with the constant velocity assuming confined, steady state conditions and using the assumed overall average pumping rate, 21.46 m^3/hr. The constant velocity is 0.021 m/hr, while the time-averaged velocities for the three different models are 0.0018 m/hr, 0.0015 m/hr, and 0.0018 m/hr. The constant velocity overestimates the overall average velocity somewhat in this case, but still would not introduce major errors in the flowline computations.

It is important to point out that the synthetic pumping records are only intended to emulate the approximate pumping rates,

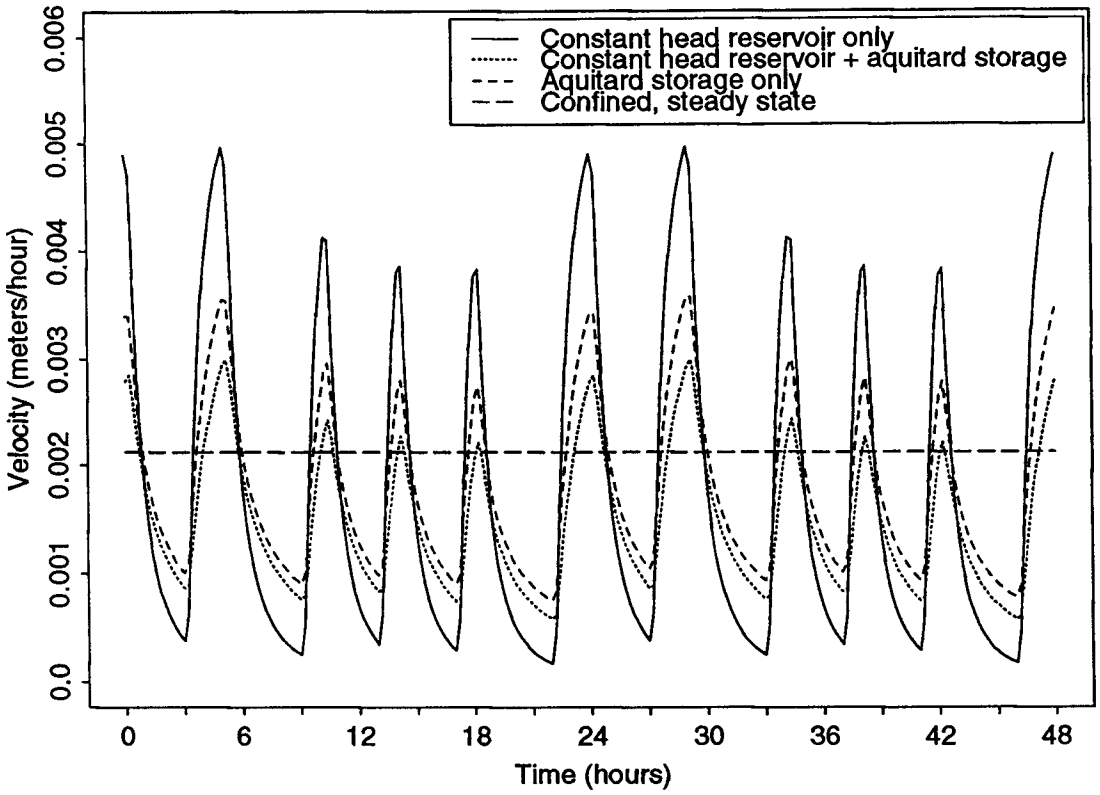

Figure 3.17. Velocities due to synthetic pumping at RWD2.

durations, and frequencies for the actual pumping records at the RWD wells, as we understand them. No attempt was made to match the drawdown history shown in Figure 3.3, the major features of which we attribute to RWD pumping. In fact, we have only very sketchy information about the actual pumping at the RWD wells. Nevertheless, the results shown in Figures 3.16 and 3.17 seem to indicate that the overall average velocities due to pumping at these wells can be reasonably approximated using the average pumping rates and assuming confined, steady-state conditions.

One might also wonder about the influence of transient effects on the velocities due to pumping at DW and well 0-8. Computations based on the three best-fit leakage models show that velocities at well IW due to constant-rate pumping at well DW essentially reach steady state values within a few hours of the beginning of pumping, with the

steady state velocity given by the steady state velocity for confined conditions multiplied by the velocity ratio given in Equation 3.5, which is essentially 1 in this case.

The basic conclusions of this analysis are that steady state leakage effects and transient storage effects introduce little error in the computed velocities due to pumping at DW and well 0-8. The overall average velocities due to pumping at the RWD wells can also be reasonably approximated using the average pumping rates at these wells and assuming confined, steady state conditions as long as the "true" leakage coefficient is no more than a factor of two or so larger than the estimate obtained from the analysis of the 1988 pumping test. Another factor that could contribute to overestimating the influence of the RWD wells is the use of incorrect information concerning the pumping rates or typical duration and frequency of pumping at these wells. The values used were based on a conversation with the manager of the rural water district operating the wells and were quite approximate. In addition, the above analysis has assumed that Mud Creek exerts no influence on the flow system, although it lies between the RWD wells and GEMS. It is assumed that a substantial thickness of silt and clay separates the bottom of the creek bed from the top of the sand and gravel, resulting in negligible interaction between Mud Creek and the aquifer. However, this assumption has never been tested.

Simulated Breakthrough Curves

The Moench (1989, 1991) solution for radially convergent, conservative transport, discussed in Chapter 5, was used to simulate breakthrough curves at the pumping well and at three multilevel samplers along the network centerline to help determine the expected duration of the test, the necessary sampling frequency, and the amount of injected mass required to obtain reasonable concentrations at most ports. The computed concentrations are in terms of mg/l per kg of injected bromide. Breakthrough curves for a range of dispersivity

values, from 0.1 meter to 2.5 meters, were computed. This range of values was selected based on dispersivities reported for tracer experiments in sand and gravel aquifers (see Gelhar *et al.*, 1992, for a review of such experiments). It was anticipated that smaller dispersivity values would represent 'local' dispersivities and thus more accurately predict breakthrough curves at individual ports whereas larger dispersivity values would represent 'whole-aquifer' dispersivities appropriate for modeling vertically averaged concentrations. Thus the breakthrough curves for smaller dispersivities are appropriate for estimating the sampling frequency necessary to define breakthrough curves at individual ports while the breakthrough curves for larger dispersivities are appropriate for determining the expected duration of the test.

These simulated breakthrough curves were computed using a Dirac delta function to represent the injection (that is, assuming negligible injection duration) and also assuming that the mixing volume associated with the initial injection was the volume of the injection well itself. The first assumption produces results that are almost indistinguishable from those computed using the actual injection duration of two hours. However, as discussed in Chapter 5, the assumption that the mixing volume is equivalent to the injection well volume is probably not appropriate for GEMSTRAC1. It would be more appropriate to assume a much larger mixing volume representing a cylinder of aquifer surrounding the injection well. However, the design modeling presented here was done prior to the realization of the potential importance of the mixing volume estimate.

Breakthrough curves computed at the discharge well are shown in Figure 3.18. These results are computed using a pumping rate of 15.9 m^3/hr (70 gpm) and assuming a porosity of 0.28. Because the pumping well concentration represents a vertically mixed sample, the breakthrough curves for larger dispersivities are probably more appropriate in this case. These curves give some indication of the

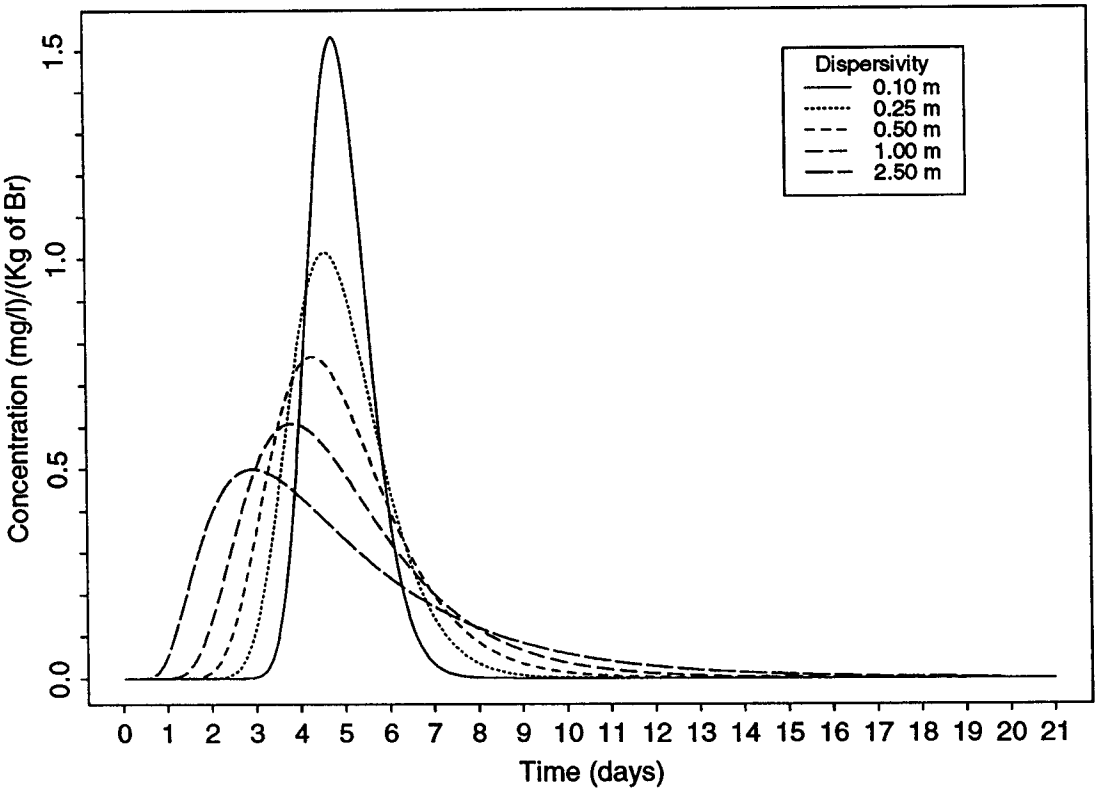

Figure 3.18. Computed breakthrough curves at discharge well (DW).

expected duration of the test. The curve for the largest dispersivity, 2.5 meters, indicates that negligible tracer mass would remain in the aquifer after about three weeks of pumping.

Figures 3.19 through 3.21 show the breakthrough curves computed for TMC-7, TMC-4, and TMC-1. In order to be appropriate for concentrations at locations other than the pumping well, Moench's solution must be multiplied by the factor $2\pi r_L/\Delta y$, where r_L is the distance from the injection well to the pumping well and Δy is the transverse width of the initial injected pulse. As discussed in Chapter 5, this factor accounts for the fact that Moench's solution treats the injected mass as if it were distributed uniformly around the pumping well, although it is in fact contained within a narrow wedge encompassing an angle determined by the initial width of injection. The breakthrough curves shown here have been computed assuming

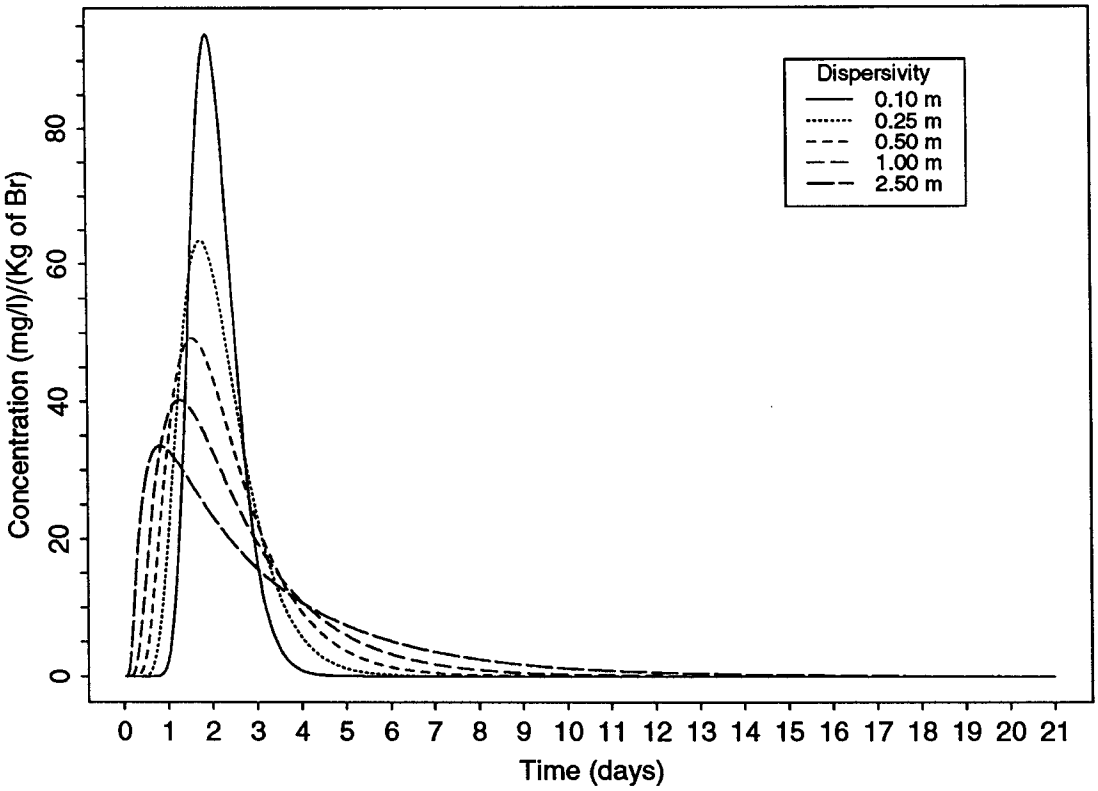

Figure 3.19. Computed breakthrough curves at TMC-7.

Δy = 2 meters, implying that $2\pi r_L/\Delta y$ = 44.5. This is the primary reason for the large difference in concentration scales between Figure 3.18 (for the pumping well) and for Figures 3.19 through 3.21 (for the three multilevel samplers).

The breakthrough curves for TMC-7 (Figure 3.19) are fairly sharp for all dispersivity values, due to the limited travel distance (3.3 m) from the injection well to TMC-7. For the smallest dispersivity, 0.1 meter, the breakthrough occurs over a period of about three days. A good data density will be somewhat arbitrarily defined here as meaning at least 15 samples within the non-negligible portion of the breakthrough curve. Thus, about five sample rounds per day would be required to clearly define this peak. The breakthrough curve for a dispersivity of 2.5 meters, more indicative of the 'whole-aquifer'

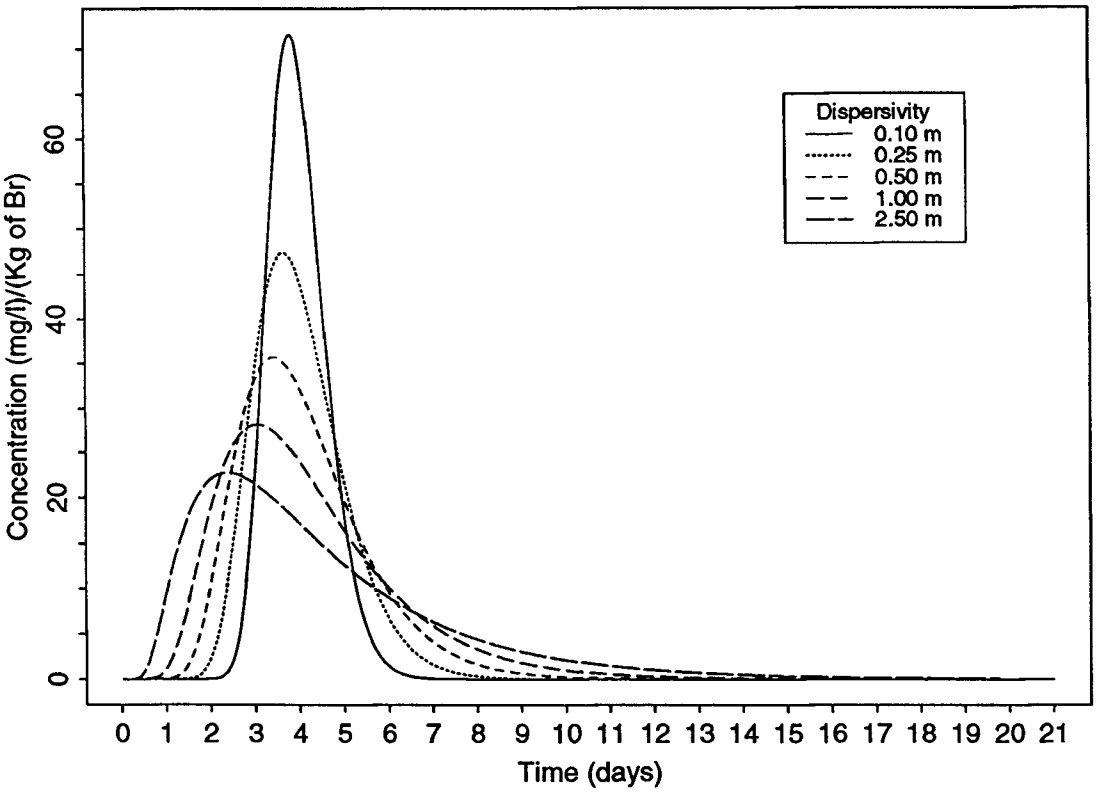

Figure 3.20. Computed breakthrough curves at TMC-4.

behavior, indicates that non-negligible concentrations would be expected to occur in some ports of TMC-7 over a period of 10 to 12 days.

Figure 3.20 contains the breakthrough curves computed for TMC-4, approximately in the middle of the network (7.8 meters from the injection well, 6.4 meters from the discharge well). Here the sharpest peak occurs

over a period of about four to five days, requiring a sampling frequency of three or four times per day for good definition. The breakthrough curve for the largest dispersivity indicates that non-negligible concentrations would be expected to occur in some ports over a period of about two weeks. The breakthrough curves computed for TMC-1 (Figure 3.21), 1.8 meters from the discharge well, are of a similar

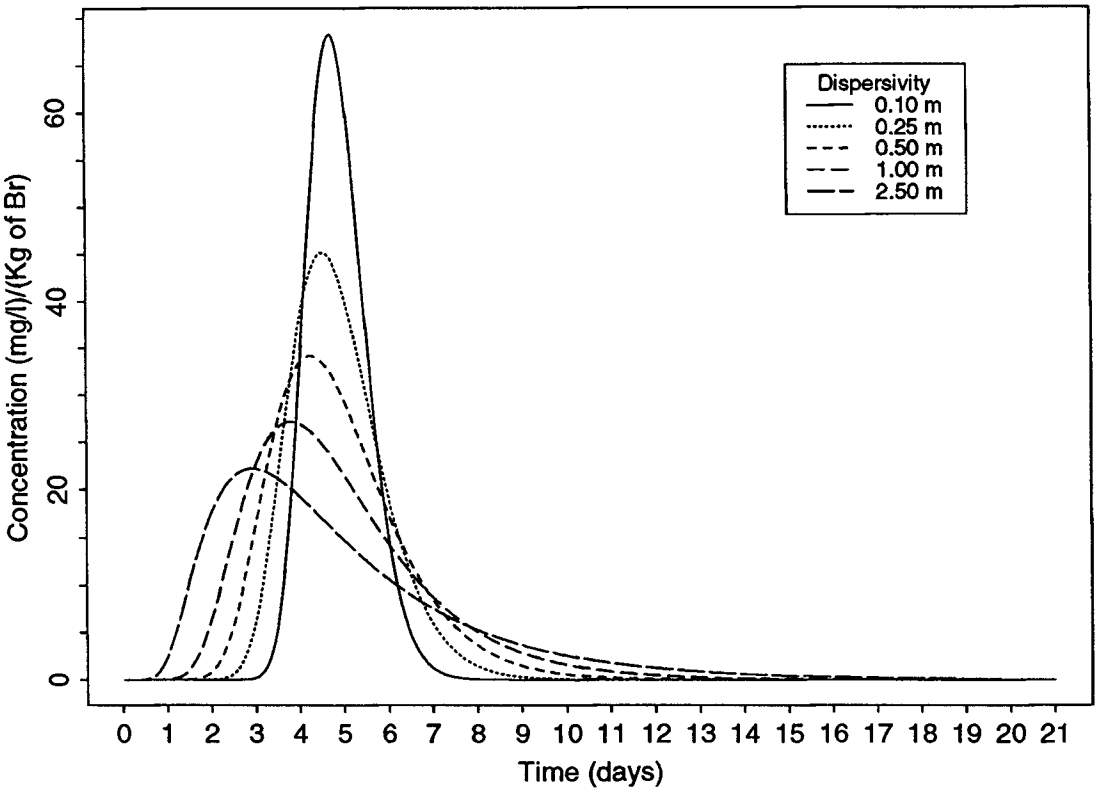

Figure 3.21. Computed breakthrough curves at TMC-1.

duration as those computed for TMC-4, requiring approximately the same sampling frequency and duration.

In all cases, measurable concentrations are computed at all sampler locations given one kilogram of injected bromide. Due to the possibility that a large portion of the mass could enter a few zones, an injected mass of a few kilograms of bromide would probably be appropriate, in order to increase the chances of obtaining measurable concentrations at most ports.

Concluding remarks on design modeling

The validity of the above design modeling can now be discussed in retrospect by comparing the predictions to the actual tracer test results, described in Chapter 4. In some respects the design modeling

was quite successful. A number of the breakthroughs at individual ports did indeed occur over a period of several days and, in general, vertically averaged breakthroughs at most samplers were approximately complete after a period of about two weeks. However, we failed to take into account the full ramifications of the stratified flow model implicit in our analyses. The 'whole-aquifer' dispersion is created primarily by differential advection between different vertical zones of the aquifer, with faster flow occurring at some levels and slower flow at others. If the breakthrough curves computed for larger dispersivities represent concentrations averaged across these different flow zones, then the steep early rise in these curves represents contributions from very rapidly moving, sharp fronts at certain levels in the aquifer. For example, the breakthrough curve for a dispersivity of 2.5 meters at TMC-1 (Figure 3.21) indicates that substantial amounts of mass could have moved all the way along the centerline by just two days into the test. In fact, this is exactly what occurred in the actual tracer test: large quantities of tracer mass entered narrow, highly permeable zones and moved rapidly toward the discharge well. We did not anticipate such rapid movement downgradient and focused our sampling efforts on those samplers near the injection well during the first couple days of the test. Thus, peak concentrations had already passed some ports in samplers further downgradient by the time we sampled them. In retrospect, it is clear that we should have incorporated some design modeling runs using a range of flow rates and small dispersivities, appropriate for modeling the transport in individual zones, in order to anticipate the effects of the vertical variation in flow velocity. However, the tracer test results revealed that the magnitude of this variation was much greater than we would have anticipated based on prior work at the site.

III. FINAL DESIGN FOR GEMSTRAC1

For reasons described above, we chose to run GEMSTRAC1 as a radially convergent tracer test, with the discharge well, DW, pumping

at a steady rate of about 15.7 m^3/hr (69 gpm) throughout the test and with injection at well IW limited to that required to introduce the tracer. The injection process is described in more detail below. In addition, well 0-8 was pumped at a rate of about 2.3 m^3/hr (10 gpm) throughout the test in an attempt to compensate for the expected influence of pumping at the Rural Water District wells to the west. We focused our sampling efforts on the centerline of the sampler network, with spot checks of samplers to the east and west of the centerline to determine the extent of lateral spreading or lateral deviation of the tracer plume. Early in the test we sampled every four to five hours during the day, with sampling frequency dropping off as the test continued. Throughout most of the test, at least one complete sampling of the centerline samplers was performed every day. The test lasted for 32 days, with a total of almost 6000 samples being collected and analyzed during that time.

IV. SAMPLER DESIGN AND INSTALLATION

A total of 24 multilevel samplers (MLS) were constructed for use at GEMS, 23 of which were used in the sampling network employed during GEMSTRAC1. The first sampler constructed was installed in the southeast corner of the site and employed during a set of single-well injection-withdrawal tests at that location (Huettl, 1994). Each sampler consists of 17 0.64-cm (1/4-inch) polyethylene tubes threaded through 3.2-cm (1 1/4-inch) PVC casing. The PVC casing consists of 3.05-meter (10-foot) sections. Most samplers have ports at 0.61-meter (2-foot) intervals, with the first port located 0.30 meter (1 foot) above the bottom end of the lowermost section. These are termed "regular" samplers. Regular samplers have 5 ports in each of the first (lowermost) three sections of PVC and 2 ports in the fourth section. The uppermost port (port 17) is 9.8 meters (32 feet) above the lowermost port (port 1) and 10.1 meters (33 feet) above the bottom end of the sampler. We attempted to install the samplers so that the bottom end was located approximately at the boundary between the

sand and gravel aquifer and the underlying sandstone bedrock. Thus, the 17 ports of a regular sampler extend approximately throughout the full thickness of the aquifer.

The even-numbered samplers on the network centerline (TMC-8, TMC-6, TMC-4, and TMC-2) are "detailed" samplers, with ports located at 0.30-meter (1-foot) intervals, except for a 0.61-meter (2-foot) gap to accommodate the coupling between the two sections of PVC. Detailed samplers have 9 ports in the lowermost section and 8 ports in the next section up. Port 1 is located 0.30 meter (1 foot) above the lower end of the sampler and port 17 is located 5.5 meters (18 feet) above the lower end. Thus the ports of the detailed samplers extend only through the lower half of the aquifer, approximately. The detailed samplers were installed because we felt that there could be significant variability in the tracer concentration at a vertical scale smaller than the 0.62-meter port spacing of the regular samplers. In fact, the detailed samplers did capture detail that we would have missed with the regular samplers alone.

Table 3.2 shows the depth of each port below the top of the PVC casing after installation. A sequence of different colors of tubing was used to help in the rapid identification of ports during the sampling process, as shown in Table 3.2. In addition, each tube was labeled with the port number and depth below top of casing. The labels were covered with clear heat shrink tubing for protection. The port elevation data in Table A.3 (Appendix A) were computed from the survey data in Table A.1 and the depth data shown in Table 3.2. The elevations of the centerline sample ports relative to datum are shown in Figure 3.2. Datum corresponds roughly with the top of the bedrock underlying the aquifer.

The ports were constructed by first marking the intended port locations on each section of PVC and then drilling an angled hole through the PVC about three inches above each port location. A piece

Table 3.2. Port locations for regular and detailed multilevel samplers.

Regular MLS Depth Below TOC, meters (feet)	Regular MLS PVC Section Number	Port Number and Color	Detailed MLS PVC Section Number	Detailed MLS Depth Below TOC, meters (feet)
11.6 (38)	4	17. Natural	2	16.2 (53)
12.2 (40)	4	16. Natural	2	16.5 (54)
12.8 (42)	3	15. Natural	2	16.8 (55)
13.4 (44)	3	14. Black	2	17.1 (56)
14.0 (46)	3	13. Blue	2	17.4 (57)
14.6 (48)	3	12. Green	2	17.7 (58)
15.2 (50)	3	11. Orange	2	18.0 (59)
15.8 (52)	2	10. Red	2	18.3 (60)
16.5 (54)	2	9. Yellow	1	18.9 (62)
17.1 (56)	2	8. Natural	1	19.2 (63)
17.7 (58)	2	7. Yellow	1	19.5 (64)
18.3 (60)	2	6. Red	1	19.8 (65)
18.9 (62)	1	5. Orange	1	20.1 (66)
19.5 (64)	1	4. Green	1	20.4 (67)
20.1 (66)	1	3. Blue	1	20.7 (68)
20.7 (68)	1	2. Black	1	21.0 (69)
21.3 (70)	1	1. Natural	1	21.3 (70)

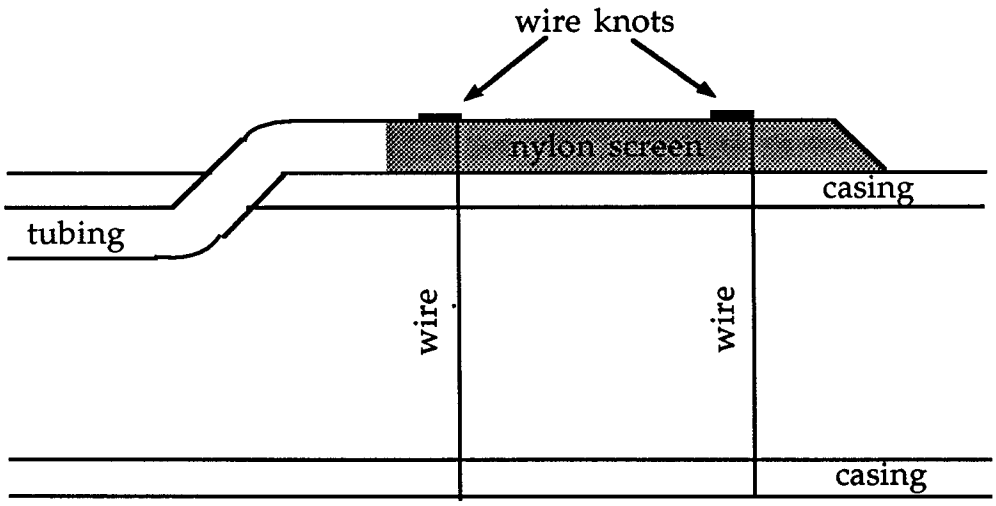

Figure 3.22. Sample port construction (after McElwee and Butler, 1995, Figure 2, Section V).

of the polyethylene tubing was threaded through each hole so that about three inches protruded from the PVC. The end of the tubing was cut at a 45° angle and then covered with a piece of nylon hose, serving as a screen. The hose was secured to the tubing and both the hose and tubing were secured to the PVC, with the end of the tubing placed at the marked port location, using two pieces of stainless steel wire, as shown in Figure 3.22 (McElwee and Butler, 1995).

We installed the samplers by first augering a hole through the overlying 11 meters of silt and clay, then lowering steel drive casing (6-cm inner diameter, 6.9-cm outer diameter) through the augers to the top of the aquifer and driving it through the aquifer using a jackhammer. A cap at the lower end of the steel casing kept the saturated sand from flowing into the casing during driving. After the lower end of the steel casing had been driven to the top of the bedrock, we lowered drill rod through the drive casing and used it to push off the end cap. We then lowered the MLS into place inside the casing. The 3-meter sections of PVC were put together using collars and stainless steel screws as the MLS was lowered. After the MLS was in

place, the drive casing was then withdrawn using the drill rig's hydraulics. The aquifer material collapsed back against the MLS as the casing was withdrawn. The auger flights were then withdrawn.

In order to keep the saturated sand from flowing into the drive casing, we had to keep the drive casing filled with water (thus maintaining a higher head in the casing than in the aquifer) from the time the end cap was pushed off until withdrawal of the casing was complete. The water was supplied by pumping from another well at the site. During installation of one sampler (TMC-7), some sand did in fact flow into the drive casing, locking the MLS inside the casing. We were able to wash the sand out and free the MLS, but only after the MLS had been pulled up about 0.3 meters. Thus the ports for TMC-7 are approximately 0.3 meters higher than the corresponding ports in other regular samplers.

By installing the samplers inside driven casing of the smallest possible diameter, we hoped to minimize aquifer disturbance. Nevertheless, there is clearly some disturbance induced by the compression of the aquifer materials by the driven casing and the subsequent collapse during the withdrawal of the casing. Nevertheless, this disturbance is considerably less than that associated with augering, which causes considerable vertical movement and mixing of the aquifer sediments.

Of the 408 total ports in the MLS network, only five failed to yield samples. Furthermore, although we have not performed direct evaluations of the amount of interference or mixing between ports, the results of the tracer test seem to indicate that these factors are negligible. Very sharp concentration contrasts occur between vertically adjacent ports, even in the detailed samplers. Thus, overall, the sampler design and installation process appear to have been quite successful.

V. INJECTION PROCEDURES

The GEMSTRAC1 tracer test began on the morning of Friday, October 7, 1994, with the introduction of approximately 4.5 kg of KBr (3.02 kg of Br^-) over a two-hour period into the injection well, IW. Pumping at the discharge well, DW, started at 7:32 that morning and was maintained at approximately 15.7 m^3/hr (69 gpm) throughout the test. It is likely that an approximately steady state response to this pumping had been established before the start of injection several hours later. The injected KBr was mixed with 7.57 cubic meters (2000 gallons) of water pumped from DW, leading to a concentration of 399 mg/l Br^- in the injected solution. The discharge from DW was used to fill a 1.89 cubic meter (500-gallon) tank four times, with portions of the KBr added at regular intervals during each filling. Filling the tank took about 7.5 minutes each time. A jet pump was used to increase circulation in the tank, providing for more uniform mixing of the injectate. The jet pump was started about one minute after the beginning of filling the tank. The jet pump continued to operate in recirculating mode for about 10 minutes after the tank was filled. The outflow from the jet pump was then diverted to a hose leading to the injection well, beginning the injection process. The time required to drain the tank into IW was a little over 16 minutes, implying an injection rate of about 7.1 m^3/hr (31 gpm). Injection from the first tank began at 10:13:00 and was completed by 10:29:12. Injection from the second tank began at 10:49:00 and ended at 11:05:05. Tank 3 injection lasted from 11:24:00 to 11:40:06 and injection from the fourth tank lasted from 11:59:00 until 12:15:24.

Prior to the tracer test, extensive head surveys had been conducted in both the discharge and injection wells, in order to ensure that constant head conditions existed throughout the screened intervals for conditions similar to those that would exist during the tracer test. In addition, a velocity diffuser, consisting of 1.4 meters of 10-cm PVC casing filled with coarse gravel, was placed in the injection

well in order to minimize head losses due to the inertial energy of the falling water. Measurements in IW during injection indicated that the velocity diffuser was successful in providing constant head conditions along the well screen.

Unfortunately, a constant head along the well screen did not ensure a constant rate of flux of the injected solution out of the well. It is quite apparent from the tracer test data (Chapter 4) that most of the tracer mass entered high permeability zones in the lower half of the aquifer, with very little mass entering the upper half of the aquifer. To a large extent, this nonuniform vertical mass distribution reflects the vertical distribution of the pumping flux across the aquifer thickness, which in turn reflects the vertical distribution of horizontal hydraulic conductivity. However, other factors may also have influenced the vertical mass distribution. It is possible that the injected solution may have tended to concentrate near the bottom of the well due to a density contrast with the native aquifer water or simply due to downward momentum remaining after its passage through the velocity diffuser. Any tendency for the tracer to concentrate lower in the well would compound the influence of the higher permeability zones lower in the aquifer.

The final injection ceased at 12:15 p.m. Soon after that, at 12:19, a pump in well 0-8 was started, with an initial pumping rate of about 2.7 m^3/hr (12 gpm). At 12:58, the pumping rate was adjusted to 2.3 m^3/hr (10 gpm), the pumping rate estimated to be appropriate to compensate for the influence of the rural water district wells to the west of the site. The pumping from well 0-8 was maintained at approximately 10 gpm throughout the test.

VI. SAMPLING PROCEDURES

Samples were collected using two 10-channel peristaltic pumps, allowing simultaneous pumping of all 17 ports of a single MLS. A

sampling cart was constructed to hold the peristaltic pumps and associated tubing. The cart also had a shelf for a tray holding the 50-ml sample vials. The outlet ends of the tubes running from the pumps passed through holes in a template above the shelf. The pattern of the template matched the pattern of the vial tray, which contained a hole for each sample vial, marked with the port number. In addition, a round template was constructed for each MLS, with 17 numbered holes near the outer perimeter. This template held the tubes apart and allowed for rapid identification of each MLS sample tube, each of which had to be attached to the inlet tube running to the appropriate peristaltic pump.

Most sample tubes could be pumped at 150 ml/min or more using the peristaltic pumps. Although sampling procedure varied somewhat earlier in the test, the protocol used throughout most of the test was to pump the sample tubes for at least four minutes prior to collecting the sample, in order to flush stagnant water from the tubes. After the four minutes of pumping, the pumps were turned off, the tray of sample vials was inserted, and the pumps were turned on again and run until most sample vials were nearly full. The sample vials, labeled with date, sample time, sampler identification, and port number, were then packed in boxes, using specially designed trays, for transport to the lab. The time of sampling was taken to be the time at which the flushing of tubes ceased, since the samples consisted of the water residing in the tubes at that time. Once the routine was established, a single MLS could be sampled in about 10 minutes, including the time required for hooking up the tubes, flushing the tubes, preparing the vials, collecting the sample, labeling and storing the vials, and unhooking the tubes. Two people were required for this operation, one handling the sampling cart setup and sampling and the other handling vial preparation, labeling, and storage.

The initial intention was to concentrate sampling near the injection well and to move sampling downgradient as the tracer

moved. However, at some levels in the aquifer the tracer moved much more rapidly than anticipated, so that by the fourth day of the test (Monday, October 10) we had decided to shift the focus of our efforts to sampling the network centerline along its entire length, with only spot checking of off-center samplers. A routine developed involving four sample rounds a day, generally with four MLSs sampled at 6:00 a.m., eight at 11:00 am, eight at 4:00 p.m., and four again at 11:00 p.m., providing a total of 408 samples per day, most of which were analyzed in the lab the following day. The frequency of sampling was reduced as the test progressed, so that by the week of October 24 we were performing only one sample round per day. Sampling essentially ended on Monday, October 31, although a final sample round was performed on Tuesday, November 8, in order to ensure that no significant tracer mass remained in the system. The discharge well pump and the pump in well 0-8 were both turned off on Thursday, November 11.

VII. SAMPLE ANALYSIS

The samples from GEMSTRAC1 were analyzed in the lab using Orion bromide-selective electrodes paired with Orion single-junction reference electrodes (Orion Research, 1991). When the electrode pair is immersed in a sample solution, the potential developed between the electrodes is approximately proportional to the log of the bromide concentration in the solution, at least over a certain range of concentration values. This potential can be converted to a concentration value by comparing it to the electrode response to calibration solutions of known concentration. The calibration solutions and sample solutions must be about the same temperature, since the electrical potential is also temperature-dependent. In addition, because the electrode response tends to vary over time, the calibration step must be repeated at regular intervals during analysis. For GEMSTRAC1, calibration solutions were prepared using site water so that the samples and standards would have a similar ionic

composition and hopefully a similar ionic strength. The electrodes actually respond to ion activity, rather than ion concentration. However, calibrations against standards of known concentration can be used directly as long as the standard solution and sample solution have approximately the same ionic strength.

To keep from running out of sample vials, samples from the field had to be analyzed rapidly and discarded so the vials could be washed and reused. Typically, the samples analyzed on a given day were those collected the day before. At the peak of sampling activity, early in the test, this amounted to analyzing at least 408 samples per day. In order to expedite the analysis, we developed a system that allowed us to analyze five samples simultaneously, with the data being recorded electronically for later processing. A device was developed which held five pairs of electrodes in a sliding rack. A tray containing five sample vials was inserted under the sliding rack and then the electrodes were lowered into the vials. After the electrodes had equilibrated with the solutions (a process taking one to three minutes), the electrode pair potentials were recorded using a Campbell Scientific CR10 data logger attached to a PC. In addition, the readings were recorded by hand on data sheets, as a backup.

Each pair of electrodes remained in the same location on the rack and remained connected to the same channel of the data logger throughout the analysis period. As a shorthand, we began referring to the electrode pairs themselves as 'channels', with channel 1 referring to the leftmost electrode pair on the rack and 'channel 5' referring to the rightmost pair. The samples from the seventeen ports of each sampler were always analyzed in the same order, with ports 1-5 analyzed in the first 'bank' of samples, 6-10 in the second bank, 11-15 in the third bank, and finally ports 16 and 17 in the fourth bank (with channels 3 through 5 empty). This created four records on the data file, one for each bank, with a given port always being recorded in the same channel. Two people were required in the lab, one operating the PC

controlling the data logger and washing the electrodes between analyses and the other dealing with the logistics of loading and unloading the sample vials from the tray. Once we became proficient at these tasks, the seventeen samples from one sampler could be analyzed in eight to ten minutes, with the main bottleneck being the time required for the electrodes to equilibrate with the solution.

We calibrated every 1.5 to 2 hours, by recording the electrode responses to our standard solutions. Three standard solutions were used, covering the expected range of concentrations: a low standard of 1 mg/l, a medium standard of 50 mg/l, and a high standard of 300 mg/l. The calibration responses for a given channel were then used to convert the electrode responses for the sample solutions measured in that channel to concentrations. The calibration responses varied over time, most notably for the low concentration standard, sometimes changing quite significantly between successive calibrations. Figures 3.23 through 3.25 show the low, medium, and high calibration responses over time for channel five (the rightmost electrode pair). The calibration responses over a given day could be quite erratic, although the long-term trend over the entire month of analysis is fairly clear. Therefore it was decided to use the median calibration responses for a given day as the 'standards' for that day; that is, all the samples analyzed in channel five on the first day were converted to concentrations using a calibration equation developed from the median low standard response, median medium standard response, and median high standard response for channel five for that day. This particular calibration curve is shown in Figure 3.26. A similar calibration equation was computed for each of the five channels for each day of analysis.

Measured concentrations below about 1 mg/l are subject to a great deal of uncertainty due to several factors: 1) the nonlinearity of the electrode responses for concentrations below 1 mg/l has not been taken into account in the calibration, 2) the precision of the electrode

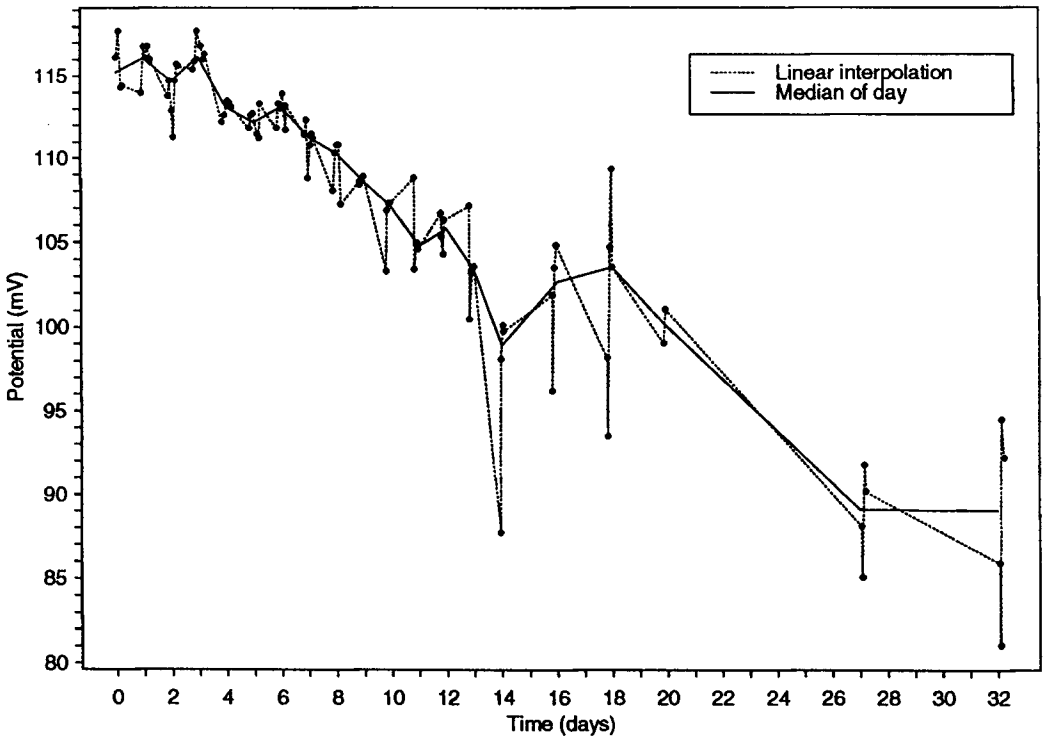

Figure 3.23. 1 mg/l calibration response over time for channel 5.

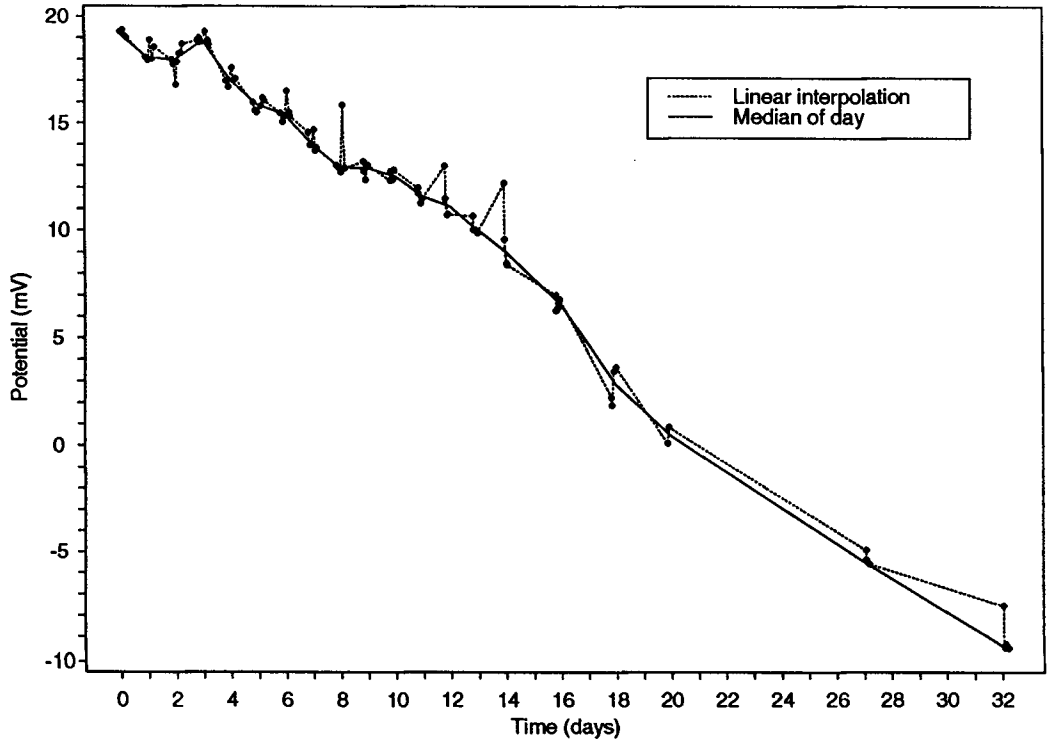

Figure 3.24. 50 mg/l calibration response over time for channel 5.

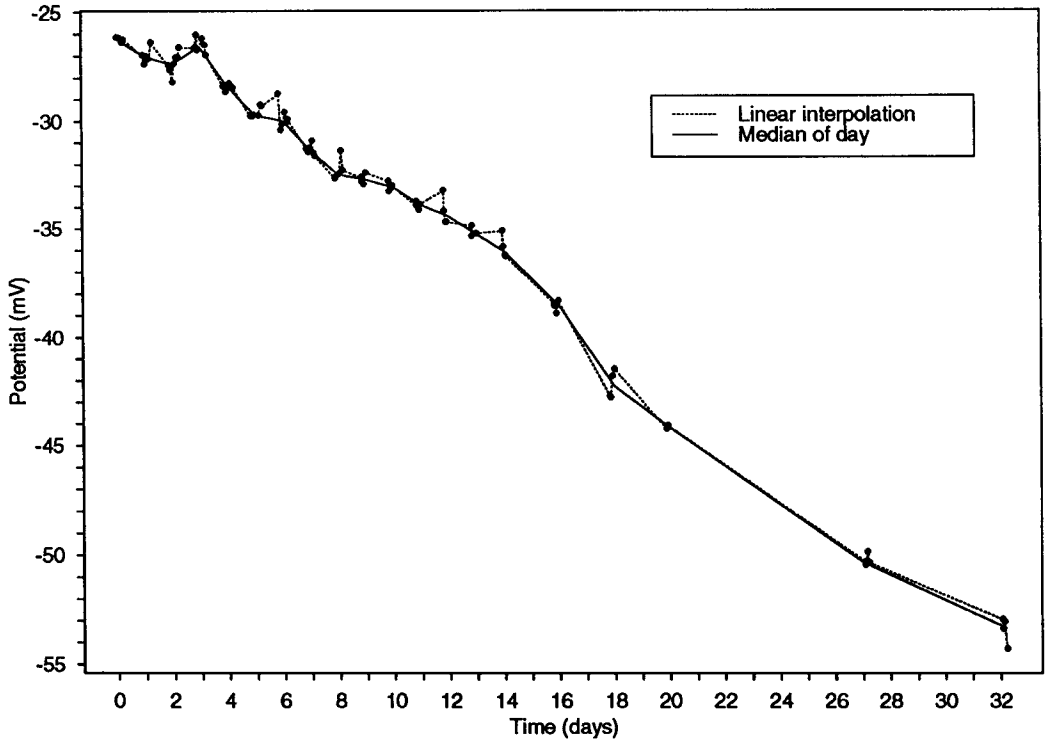

Figure 3.25. 300 mg/l calibration response over time for channel 5.

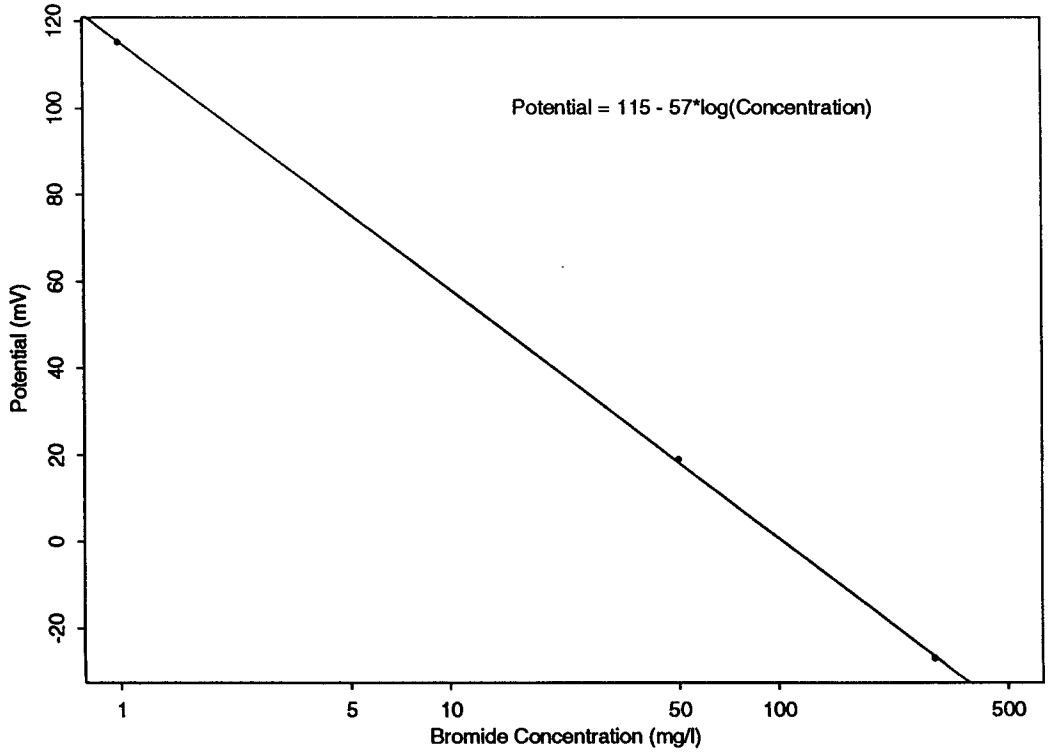

Figure 3.26. Calibration curve for channel 5, 10/8/94.

measurements decreases as the concentration decreases, ranging from about 3% at 0.8 mg/l to about 20% at .4 mg/l, and 3) the low and variable background concentration of Br^- in water from the site implies that unknown background concentrations of Br^- were present both in the samples themselves and in the water used to prepare the calibration solutions. One motivation for preparing the calibration solutions in site water was the hope that both the samples and the standards would be approximately equally affected by the background Br^- concentration, thus canceling out its effect on the computed concentrations. However, such a result would only occur if the background concentration were constant in space and time, and thus the same in all samples and calibration solutions. As described in McElwee and Butler (1995), the site water obtained for one set of calibration solutions was analyzed for background Br^- concentration using the method of standard additions. This analysis gave an estimated background concentration of about 0.11 mg/l. Earlier assessment of Br^- concentrations at GEMS showed a concentrations ranging from below detection limit to about 0.7 mg/l. The effects of this variability on measured concentrations is confounded by the nonlinearity of the electrode responses at low concentrations. However, analyses of very low concentration calibration solutions, prepared both in site water and distilled water, seemed to indicate that estimated concentrations above 1 mg/l were reasonably accurate. Above this limit, the electrode response is reasonably linear. In addition, for any concentration above about 10 mg/l, the contribution of background Br^- is almost certainly negligible. Further details regarding the estimation of background concentrations and analysis of low concentration samples can be found in McElwee and Butler (1995).

Most ports showing discernible breakthrough curves during GEMSTRAC1 had peak concentrations ranging from tens to hundreds of milligrams per liter. These breakthrough curves were analyzed assuming a background concentration of zero since the background concentration is in fact quite small relative to concentrations of this

magnitude. However, some clear breakthrough curves were seen in ports whose peak concentrations were only a few milligrams per liter, and the presence of a non-zero background concentration is apparent in these data. Several breakthrough curves were analyzed after subtracting out a background concentration estimated from visual inspection of the data. However, the low concentration values from which this estimate was made were subject to the complications described above, calling the background concentration estimate itself into question.

CHAPTER 4: EXPLORATORY ANALYSIS OF TRACER DATA

I. INTRODUCTION

Earth science data often contain features that cannot be explained by any model of reasonable complexity. In fact, it is the deviations from expected behavior that most often lead to development of new scientific insight. Therefore it is important to examine data carefully prior to fitting models to them. This chapter presents the results of the GEMSTRAC1 tracer test in graphical form, both as sets of breakthrough curves at individual samplers and as profiles of tracer concentration along the network centerline at specific times. In addition, this chapter discusses an animation of the centerline concentrations over time. These graphical presentations of the data reveal a considerable amount of information about the distribution of hydraulic conductivity at the site. However, they also reveal some flaws in the execution of GEMSTRAC1, the most important of which was our failure to sample the entire network centerline early in the test.

II. BREAKTHROUGH CURVES AT SELECTED SAMPLERS

Figures 4.1 through 4.12 show tracer breakthrough curves for those samplers where we obtained an adequate number of samples, specifically, all the centerline samplers except TMC-9 (upgradient from the injection well) and four "eastern" samplers, TME-6, TME-5, TME-4, and TME-3. The concentration scales vary from one figure to the next, with the scale for each figure determined by the maximum concentration observed over all ports at the particular sampler. Chapter 6 contains figures in which the concentration data at each port are scaled relative to the maximum at that particular port, revealing more detail in the low-concentration curves. While comparing the data from different samplers, one should keep in mind that TMC-8, TMC-6, TMC-4, and TMC-2 have ports at 0.30-meter intervals

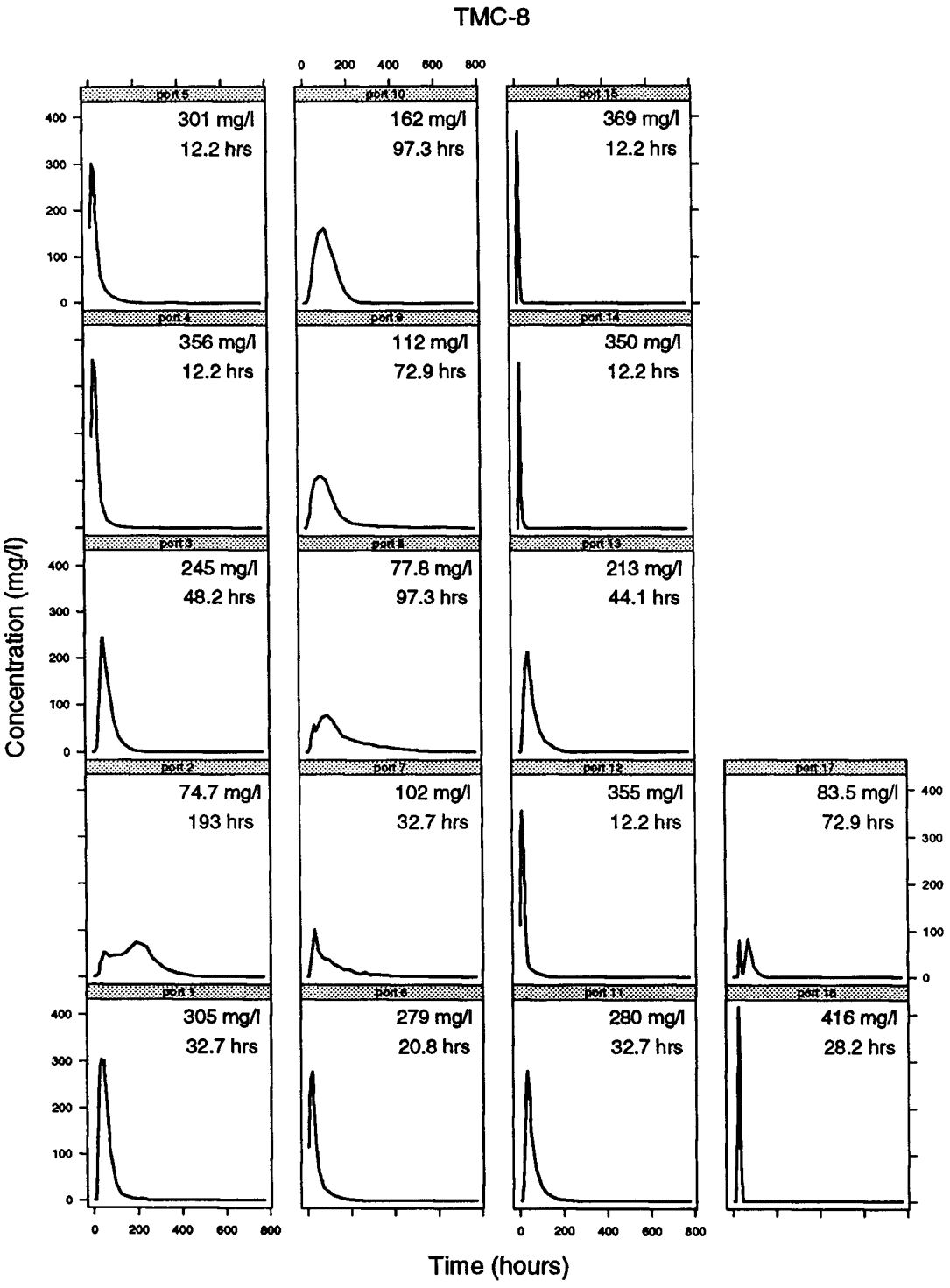

Figure 4.1. Breakthrough curves at TMC-8, with peak concentration and time of peak concentration at each port.

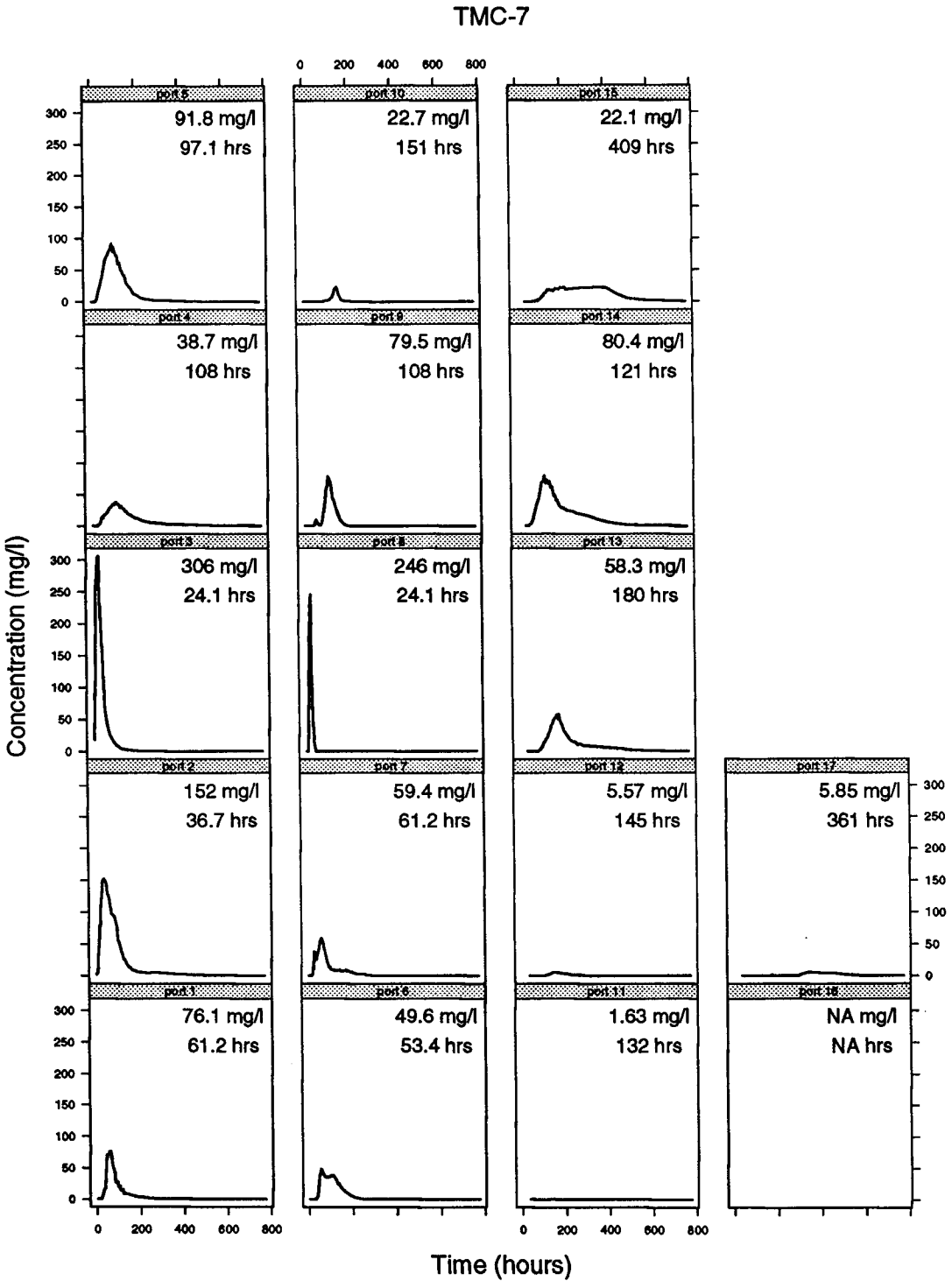

Figure 4.2. Breakthrough curves at TMC-7.

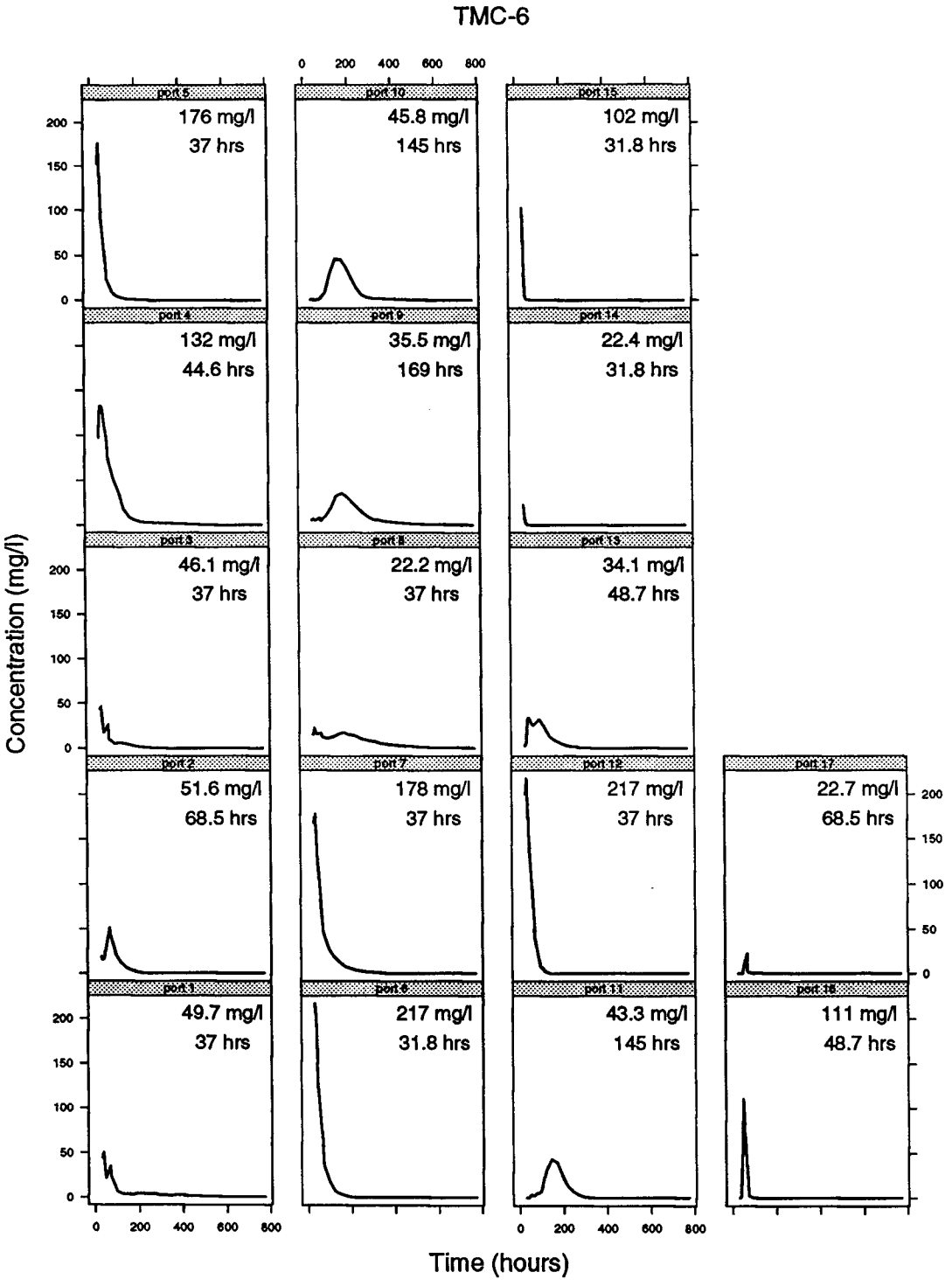

Figure 4.3. Breakthrough curves at TMC-6.

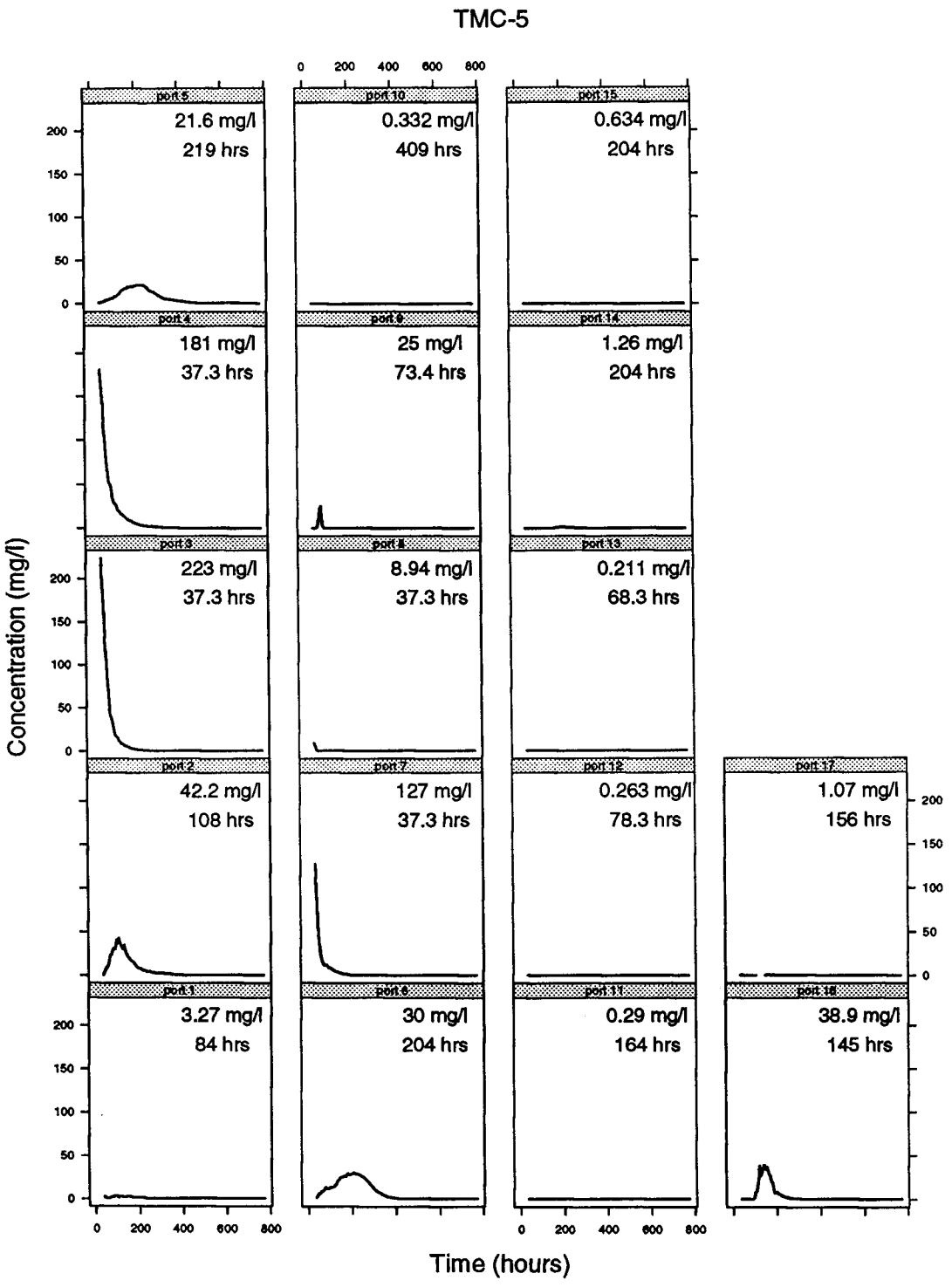

Figure 4.4. Breakthrough curves at TMC-5.

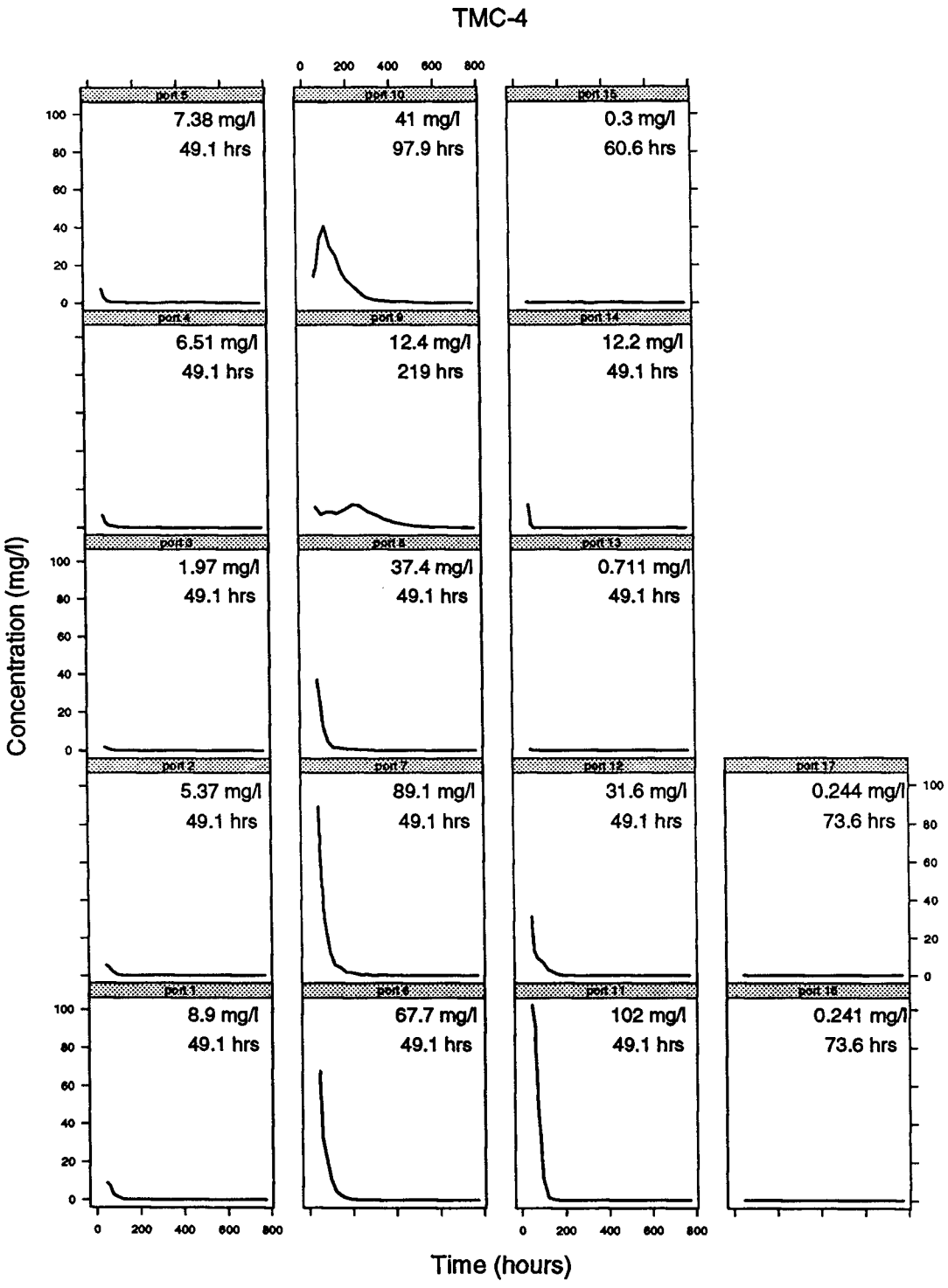

Figure 4.5. Breakthrough curves at TMC-4.

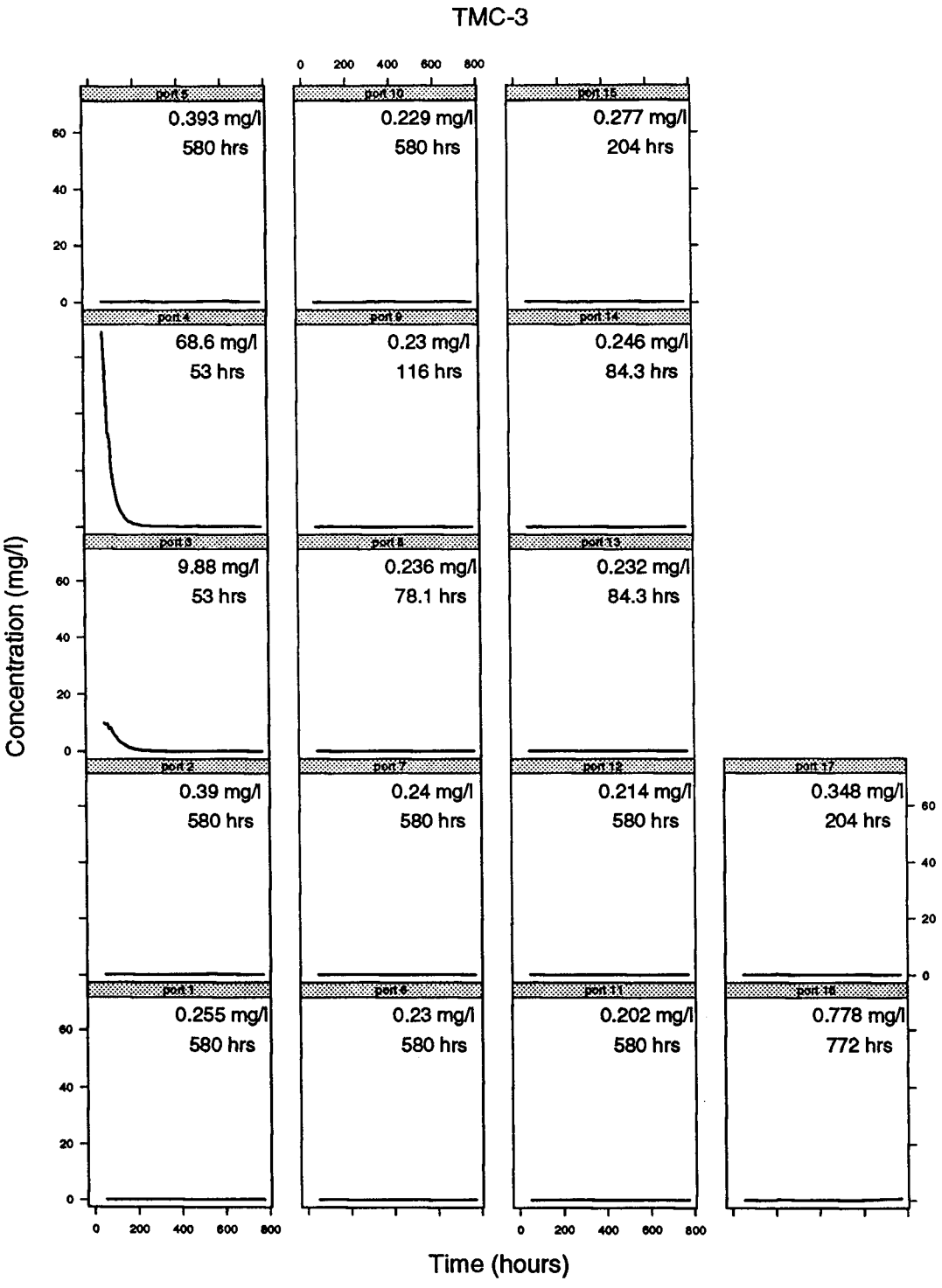

Figure 4.6. Breakthrough curves at TMC-3.

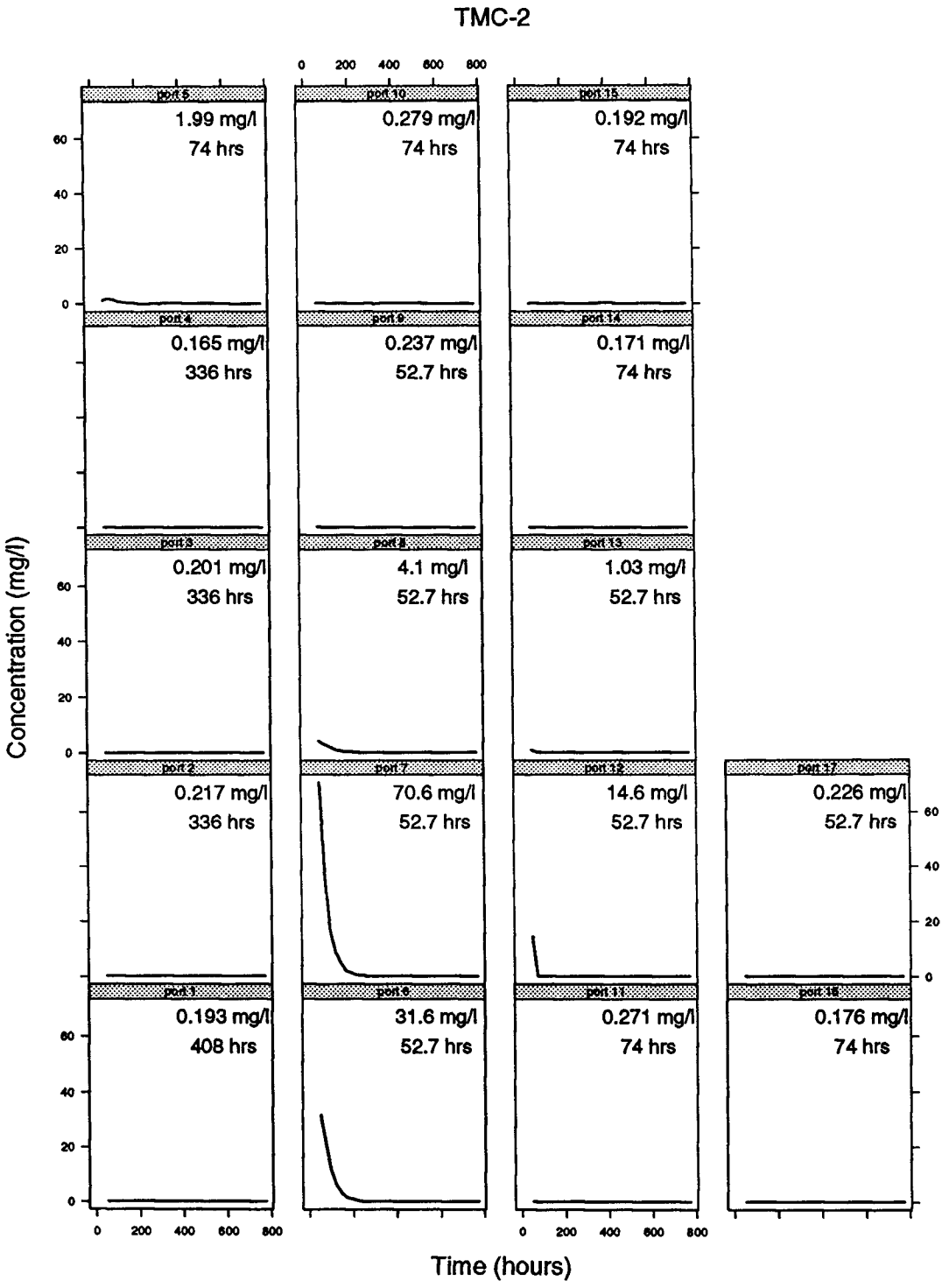

Figure 4.7. Breakthrough curves at TMC-2.

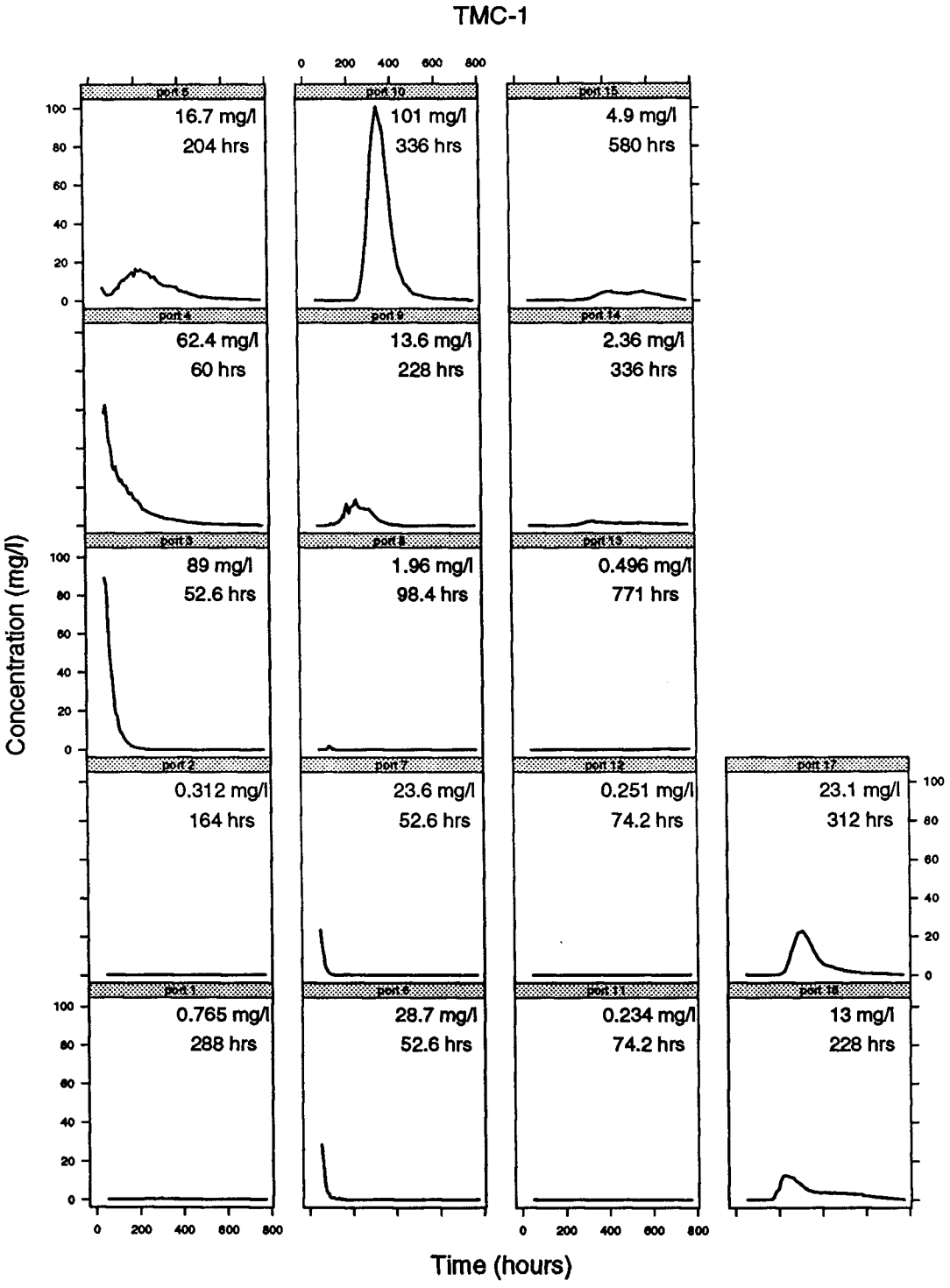

Figure 4.8. Breakthrough curves at TMC-1.

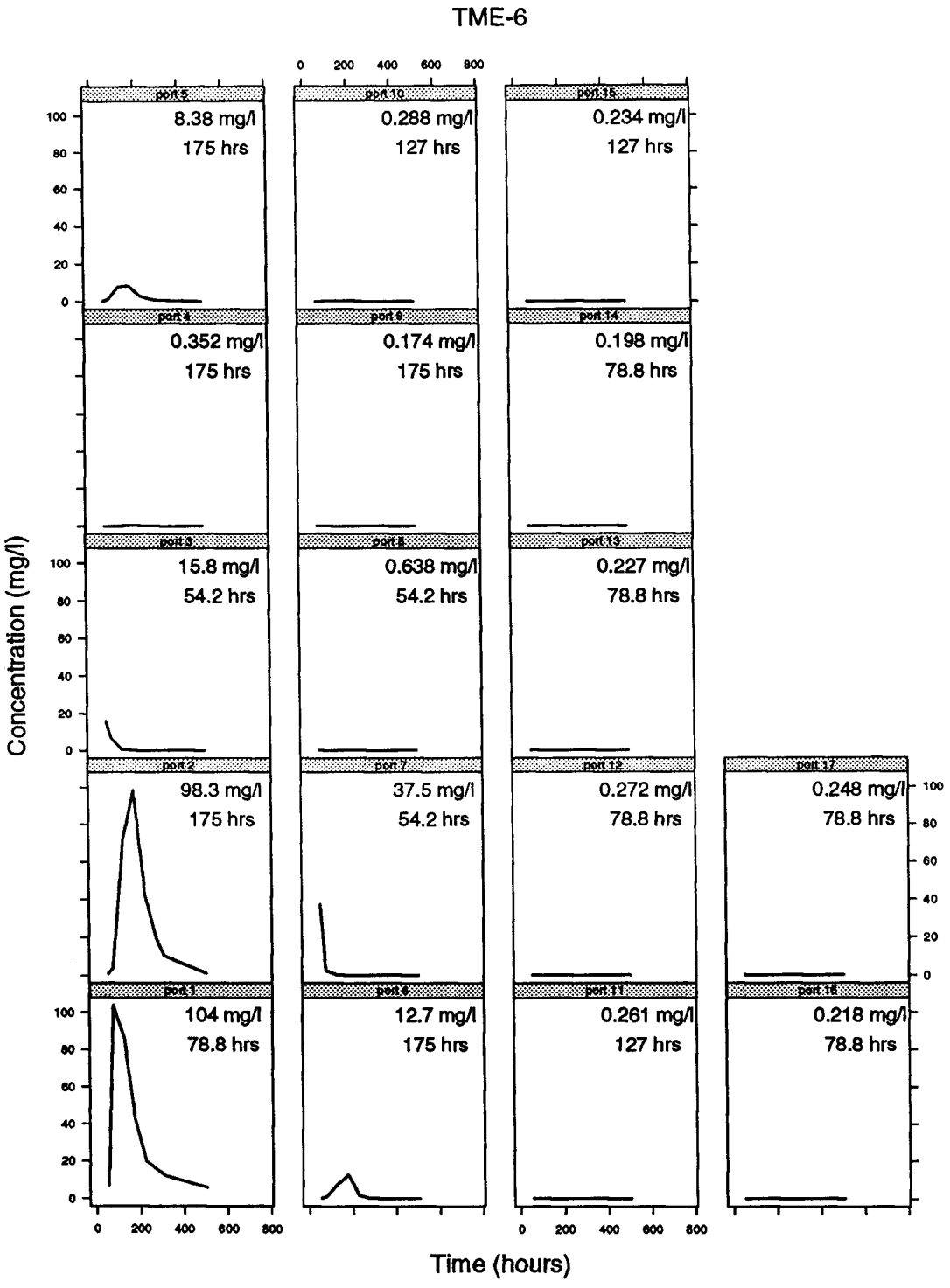

Figure 4.9. Breakthrough curves at TME-6.

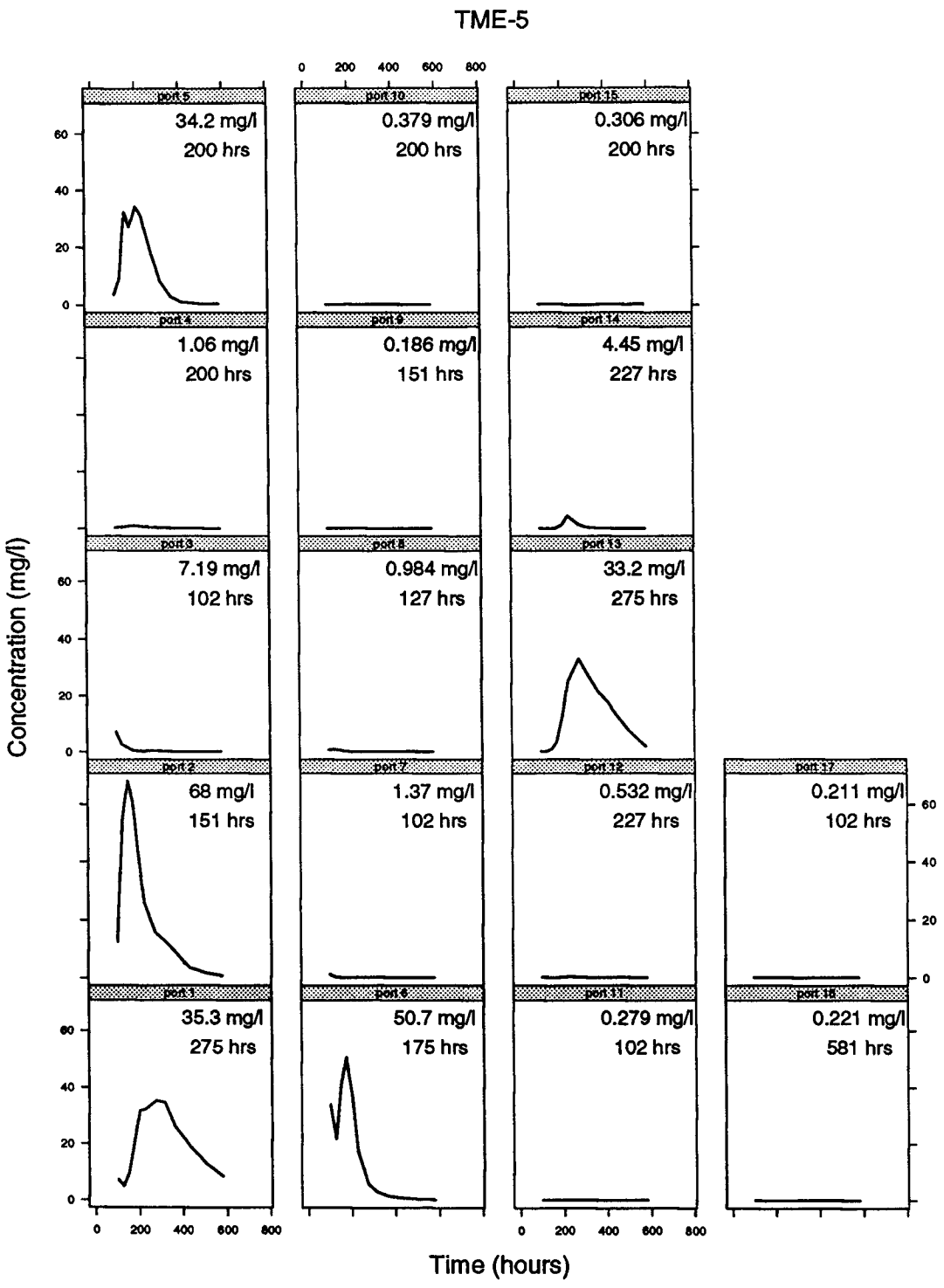

Figure 4.10. Breakthrough curves at TME-5.

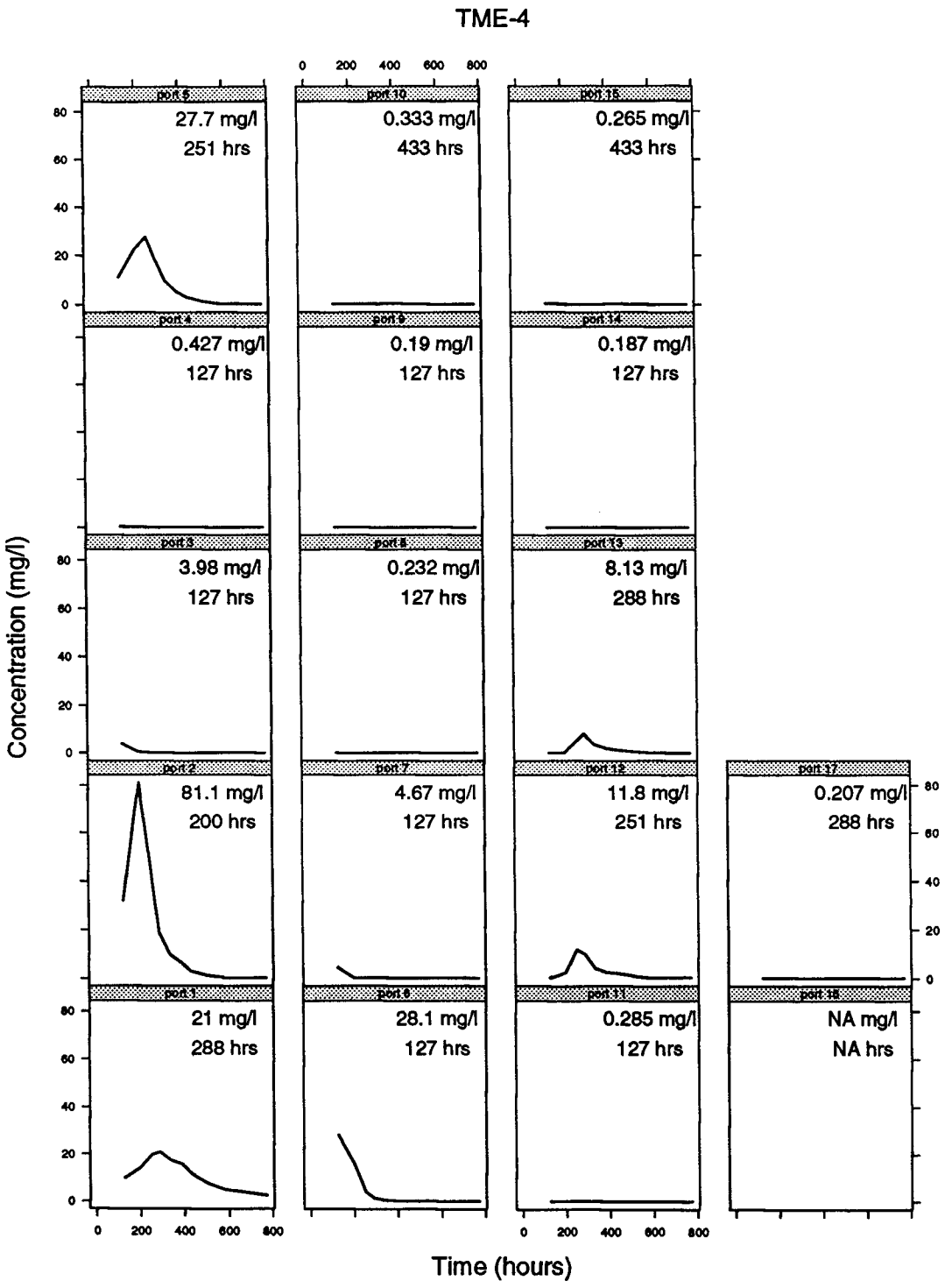

Figure 4.11. Breakthrough curves at TME-4.

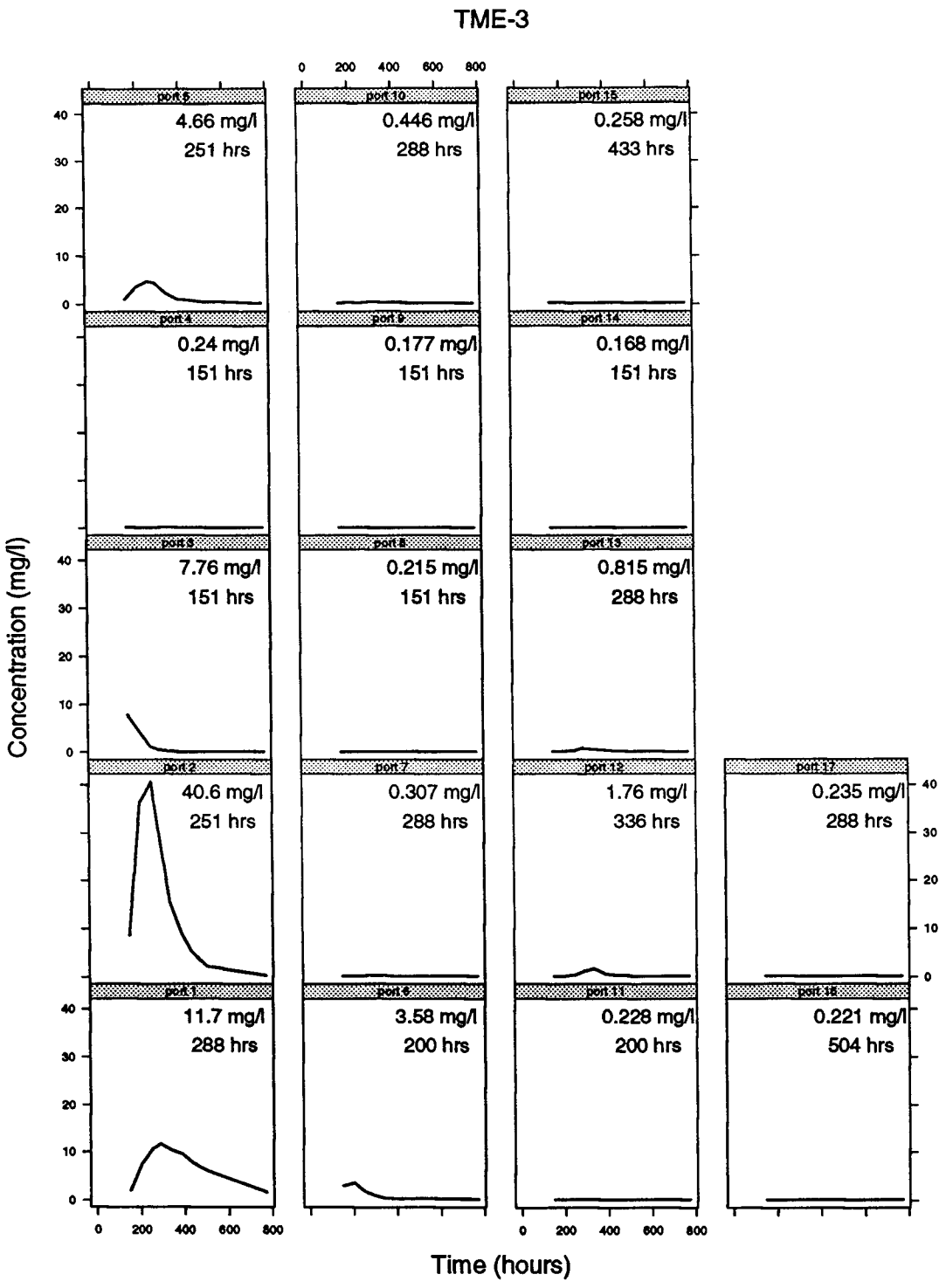

Figure 4.12. Breakthrough curves at TME-3.

throughout the bottom half of the aquifer, and the remaining samplers have ports at 0.61-meter intervals throughout the entire aquifer thickness. Furthermore, it is quite possible that there might be significant differences in results observed at corresponding ports of different samplers, due to the slight differences in vertical locations of the ports and due to deviations of the flow and transport processes from perfectly stratified, horizontal behavior. Most notably, the ports in TMC-7 are approximately 0.30 meter higher than those of the other regular samplers, due to the sandlocking of this sampler inside the drive casing during installation.

III. CENTERLINE CONCENTRATION PROFILES AT SELECTED TIMES

Figures 4.13 through 4.30 show profiles of the tracer concentration along the network centerline for selected times. The sample time shown is the average of the sample times for all the samplers included in the figure. In some cases sample rounds lasted up to two hours, a time which is not insignificant compared to the time between sample rounds, especially early in the test. The vertical scale is in terms of meters above datum. Datum is 21.33 meters (70 feet) below the top of the Corps Stake (the reference point employed in the site survey) and corresponds roughly with the bottom of the aquifer. (See Table A.3, Appendix A, for the actual port elevation values.) The concentration scale in each figure is determined according to the maximum concentration observed in that sample round, so care must be taken in comparing the different figures. The panel for a particular MLS is empty if the MLS was not sampled during the sample round depicted. The concentration values are connected by straight lines in order to clarify the vertical order. There is no reason to believe that such a smooth variation in concentration actually exists between ports. Given some of the sharp contrasts in concentration between ports even in the detailed samplers, it is quite possible that significant vertical

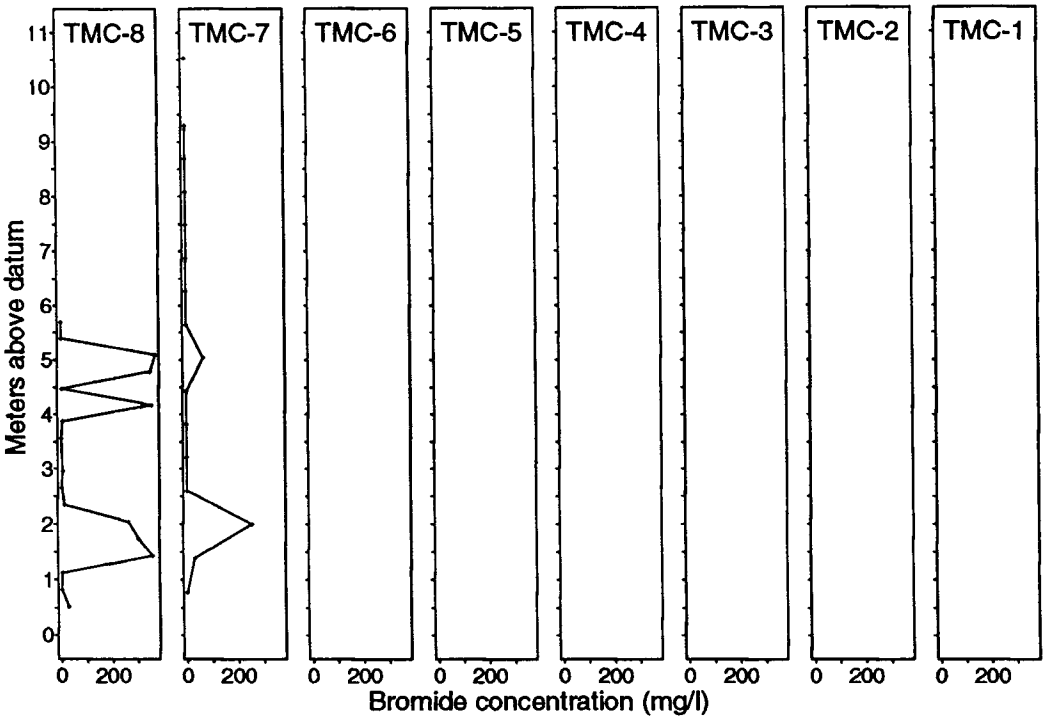

Figure 4.13. Profile at 12.5 hours (0.52 days, sample round 3)

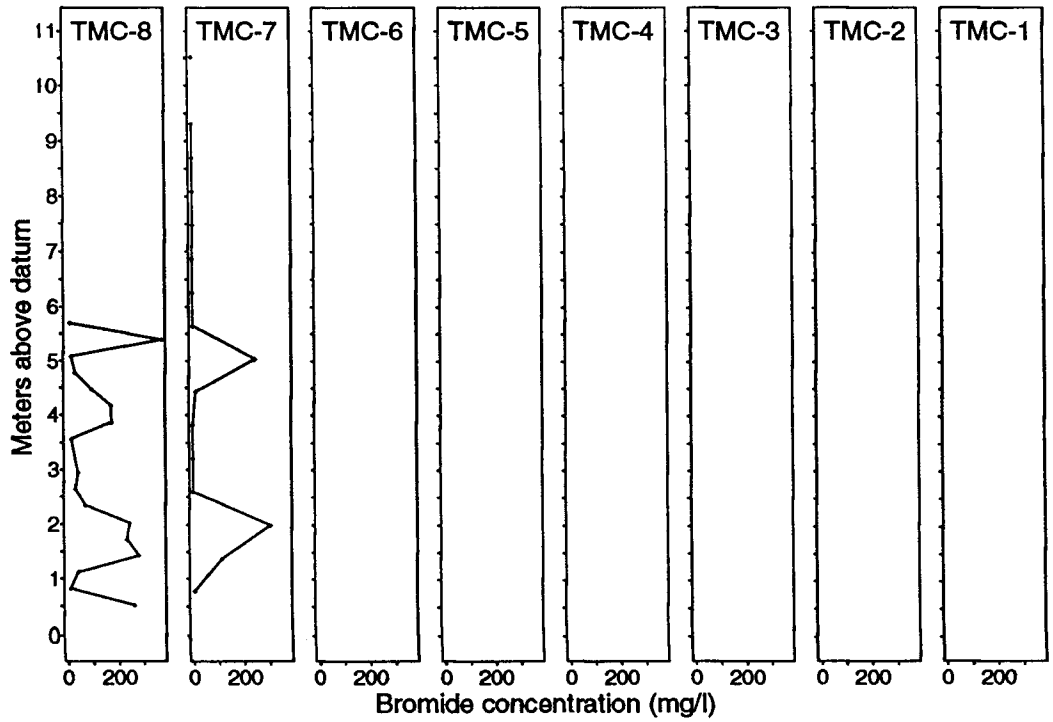

Figure 4.14. Profile at 24.5 hours (1.02 days, sample round 5)

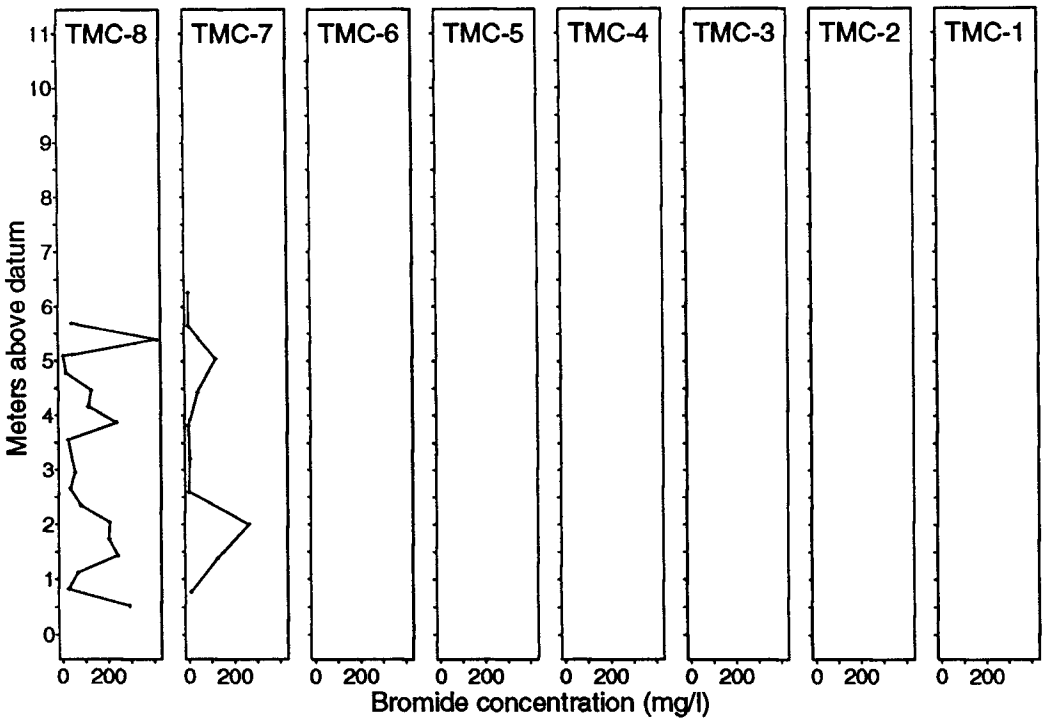

Figure 4.15. Profile at 28.3 hours (1.18 days, sample round 6).

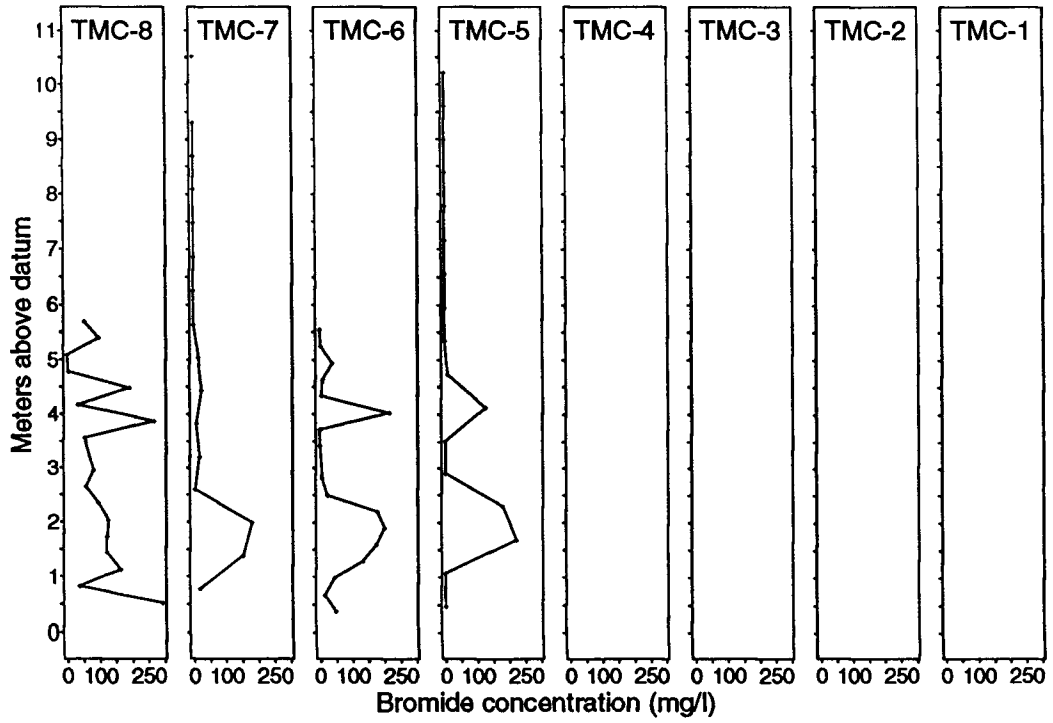

Figure 4.16. Profile at 36.7 hours (1.53 days, sample round 8).

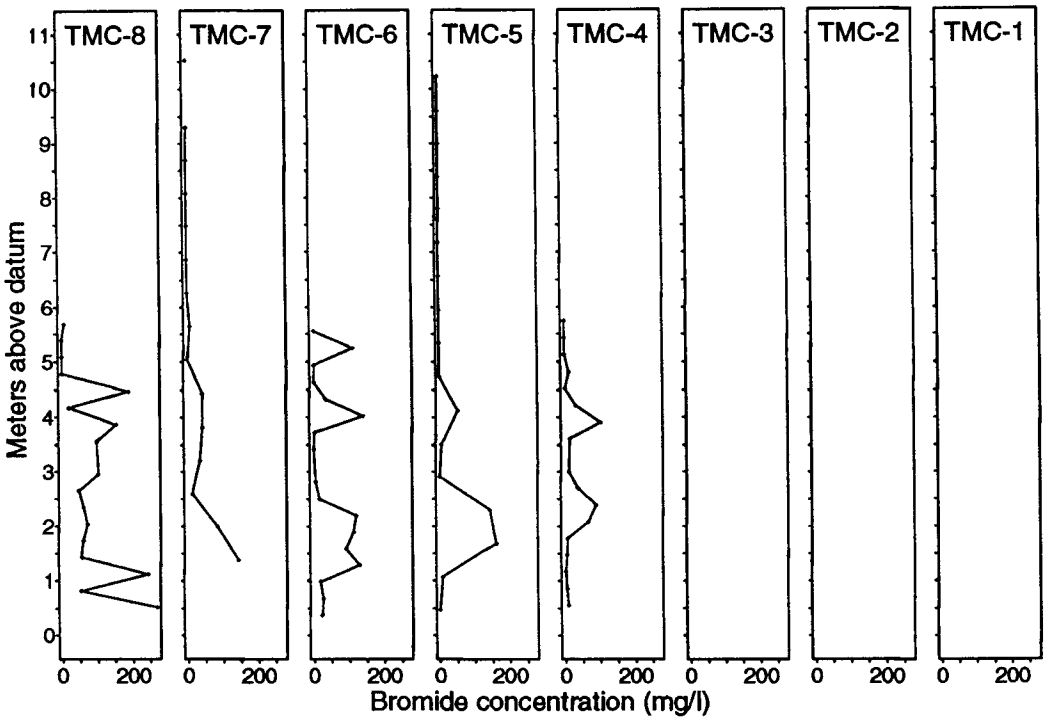

Figure 4.17. Profile at 48.5 hours (2.02 days, sample round 10).

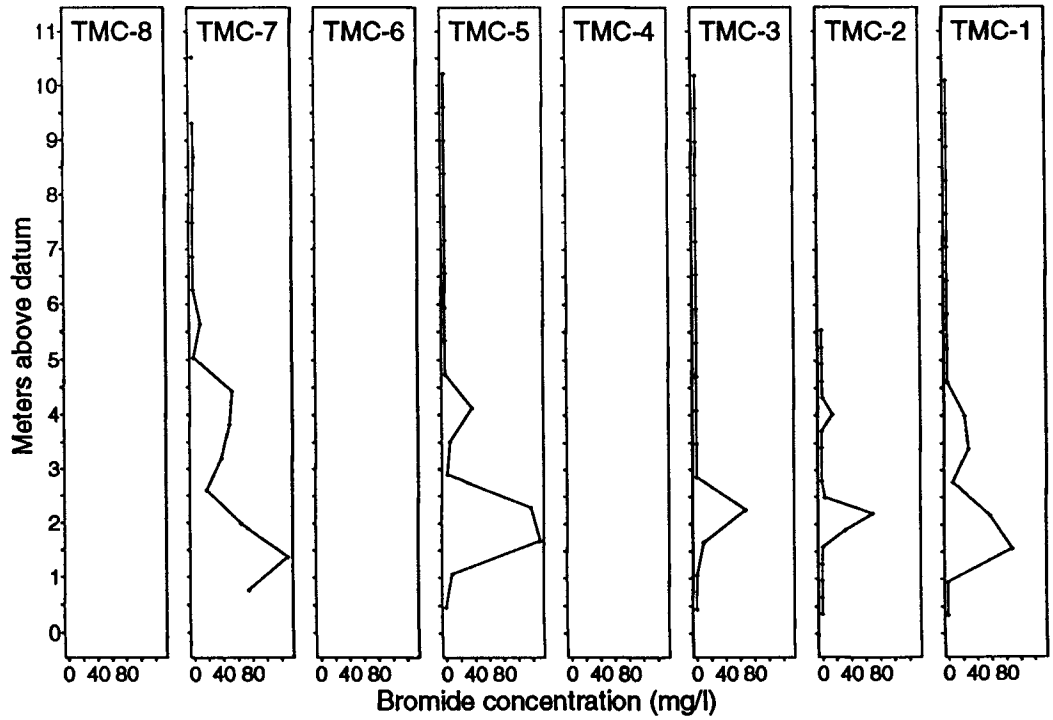

Figure 4.18. Profile at 53.3 hours (2.22 days, sample round 11).

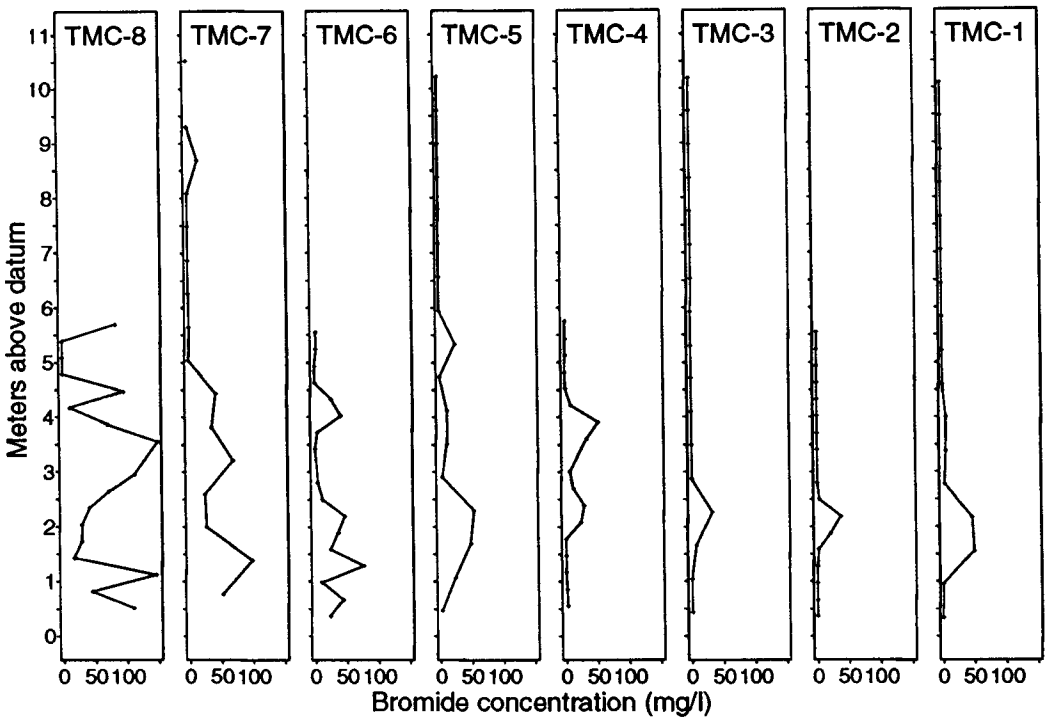

Figure 4.19. Profile at 73.4 hours (3.06 days, sample round 14).

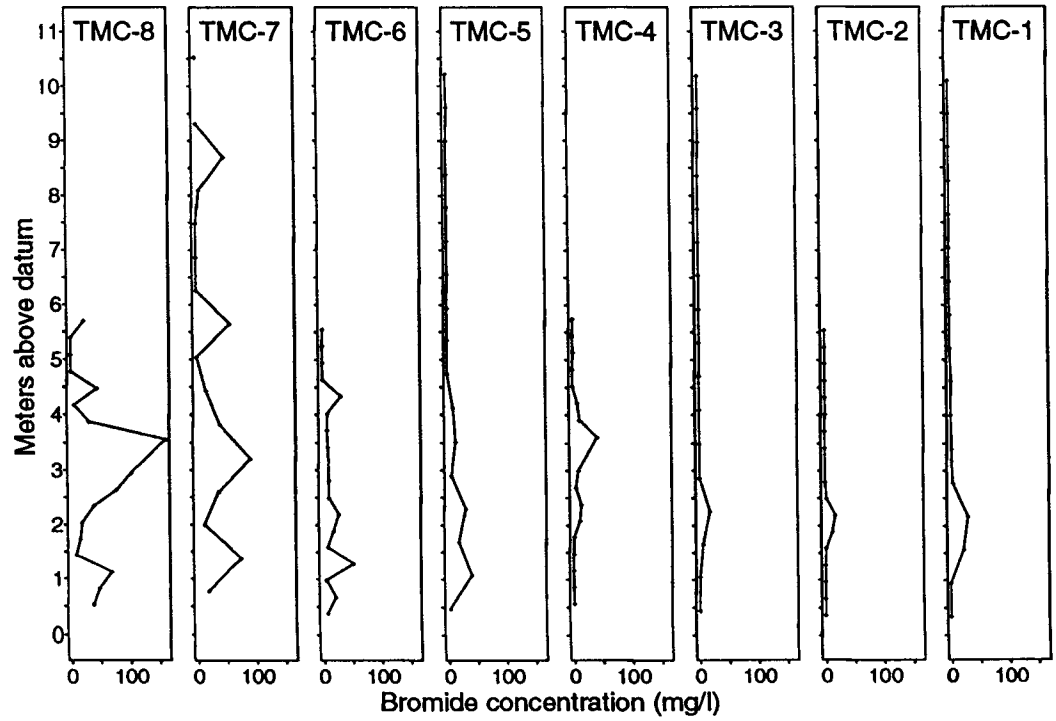

Figure 4.20. Profile at 97.7 hours (4.07 days, sample round 18).

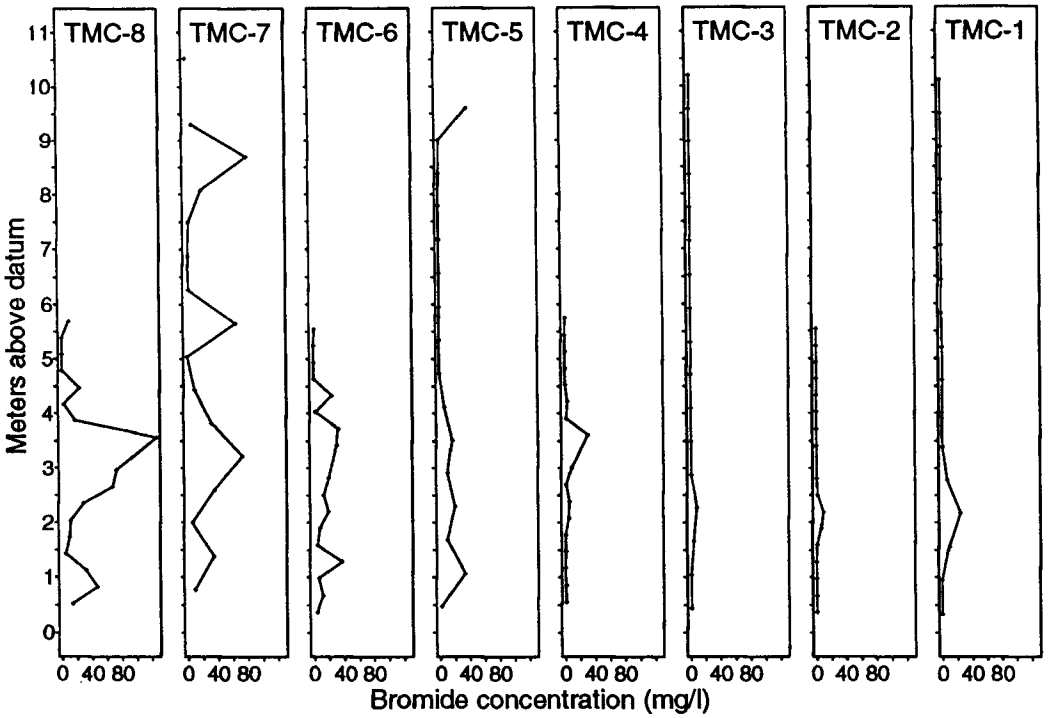

Figure 4.21. Profile at 121.4 hours (5.06 days, sample round 22).

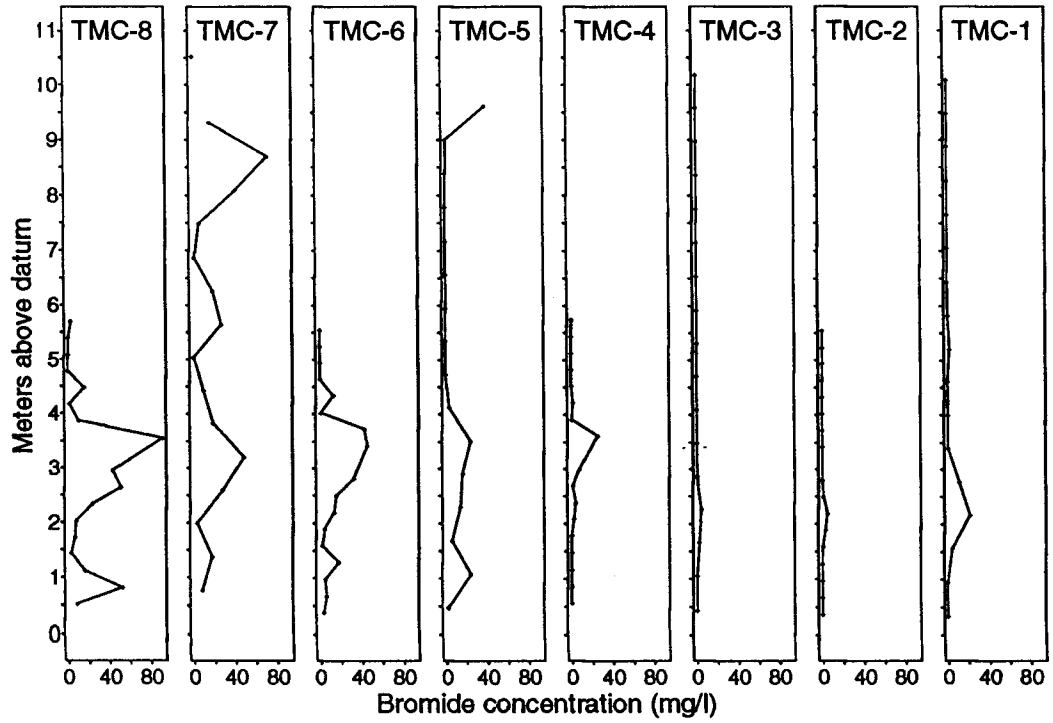

Figure 4.22. Profile at 145.4 hours (6.06 days, sample round 26).

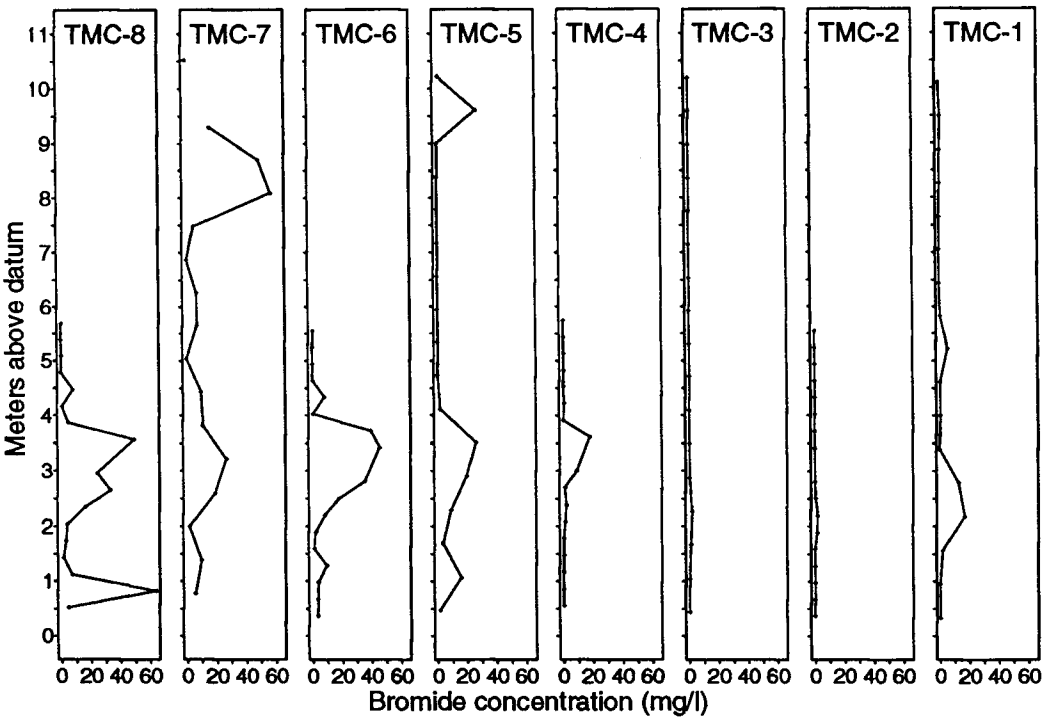

Figure 4.23. Profile at 169.4 hours (7.06 days, sample round 30).

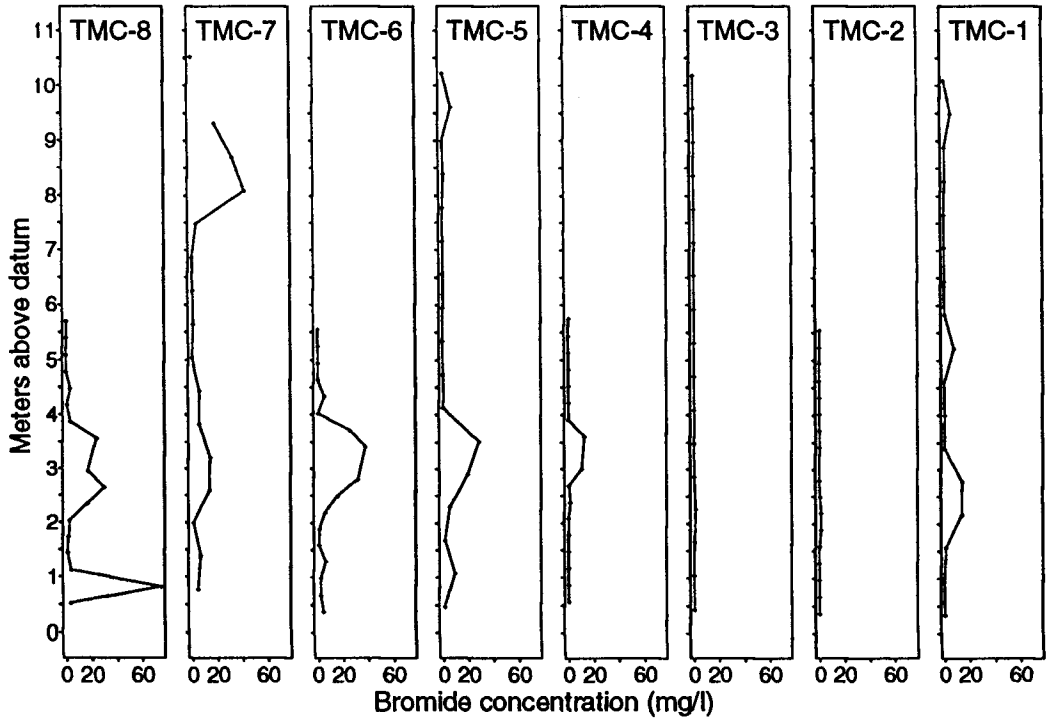

Figure 4.24. Profile at 193.7 hours (8.07 days, sample round 34).

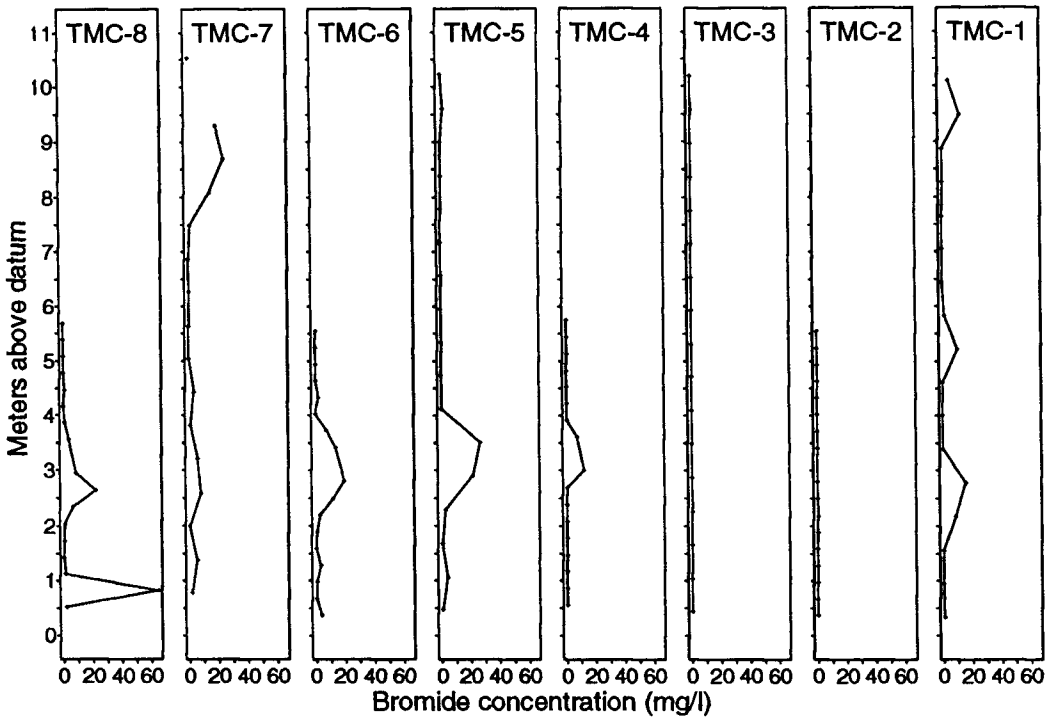

Figure 4.25. Profile at 241.0 hours (10.04 days, sample round 39).

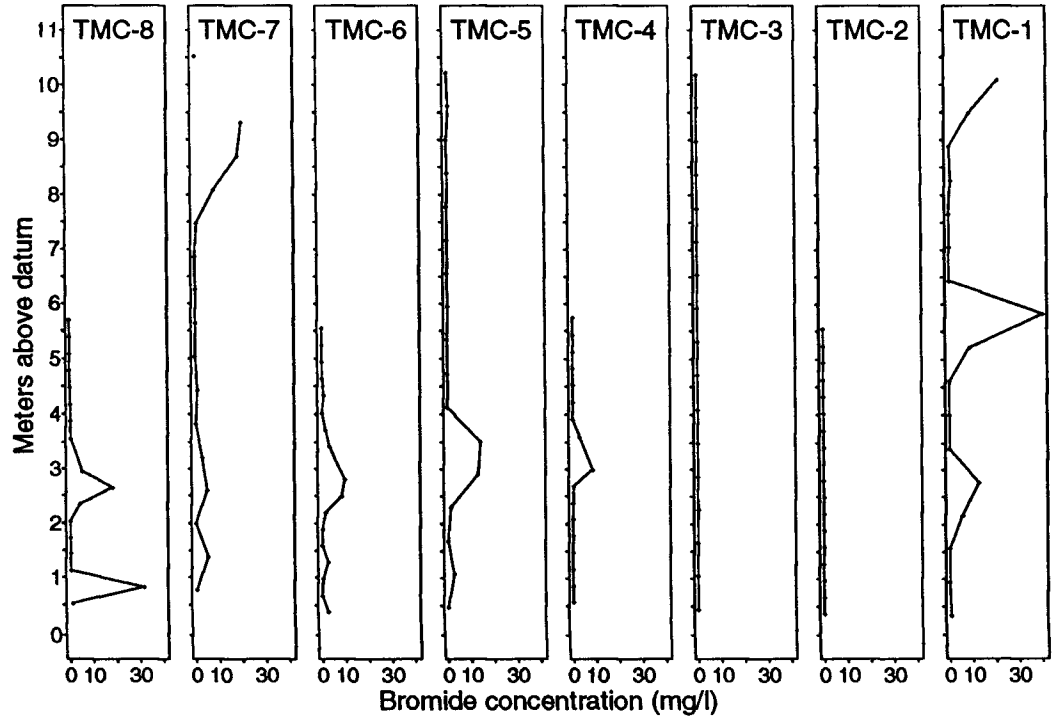

Figure 4.26. Profile at 288.5 hours (12.02 days, sample round 43).

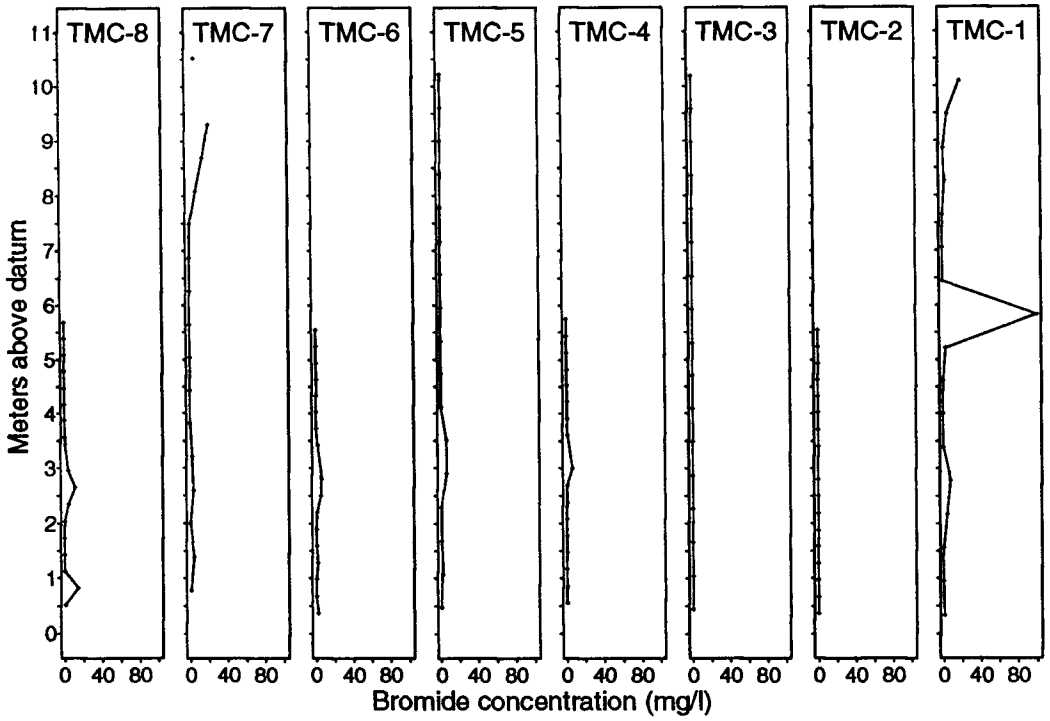

Figure 4.27. Profile at 336.2 hours (14.01 days, sample round 45).

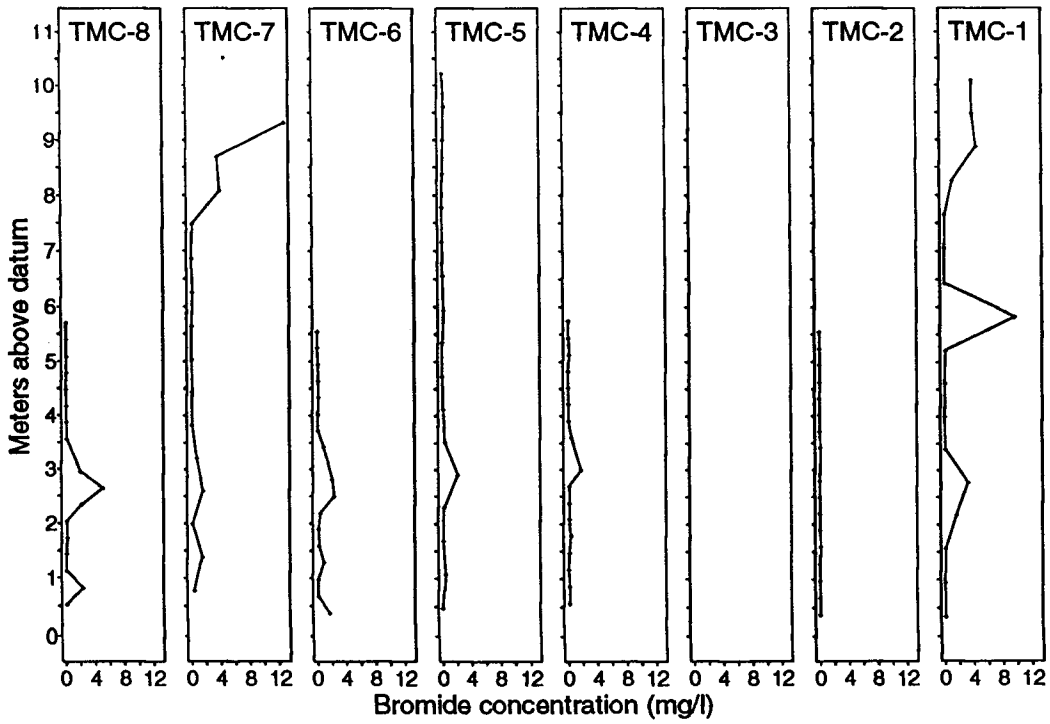

Figure 4.28. Profile at 456.2 hours (19.01 days, sample round 50).

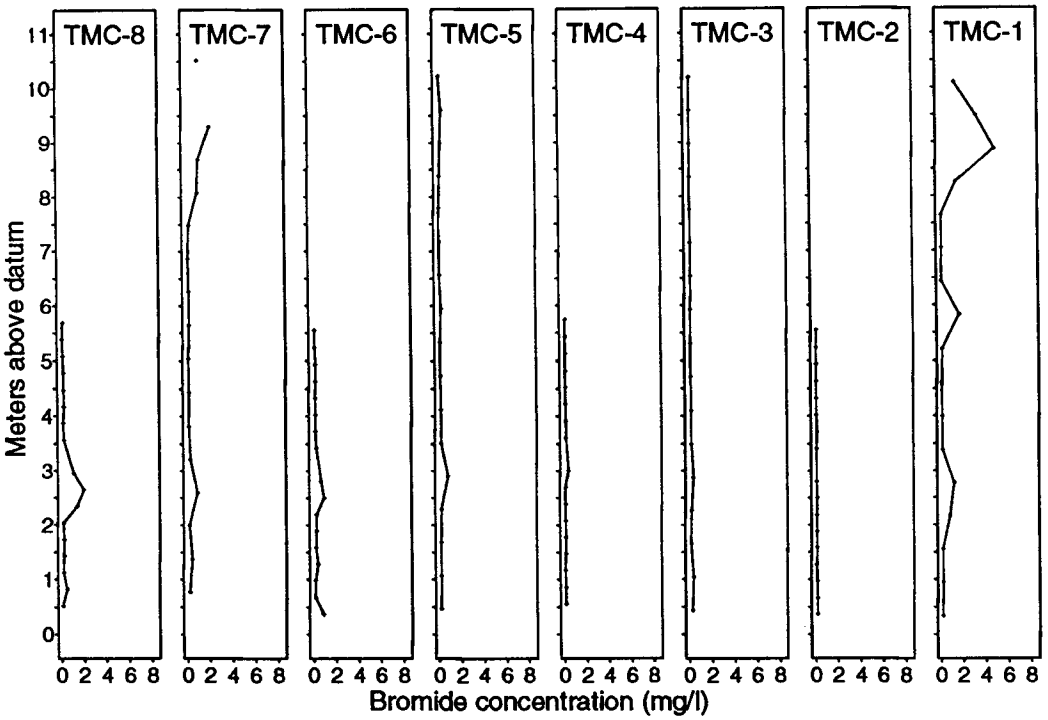

Figure 4.29. Profile at 580.8 hours (24.20 days, sample round 52).

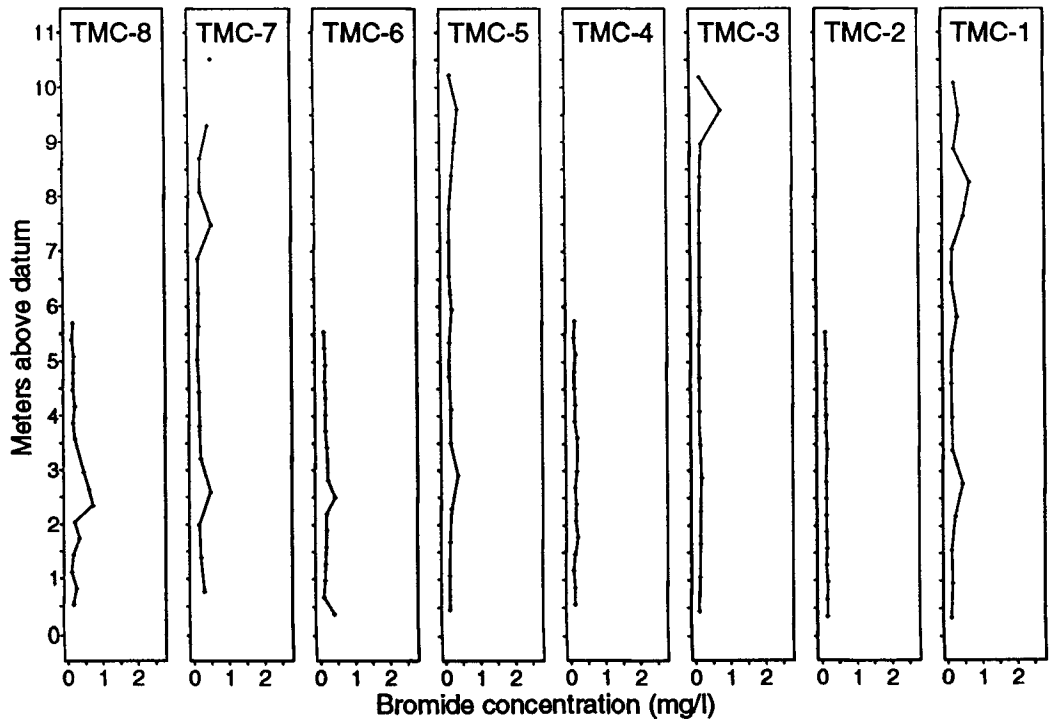

Figure 4.30. Profile at 772.3 hours (32.18 days, sample round 53).

variation in the concentration occurs at scales smaller than the port spacing.

Figures 4.13 through 4.18 show the gradual movement of our sampling efforts downgradient, with sample round 11 at 53.3 hours (Figure 4.18) being the first sample round reaching all the way to TMC-1. Unfortunately, significant amounts of mass had already moved through the entire system by this point, as evidenced by the relatively large concentrations in TMC-1 and TMC-2. In fact, we had missed the peak concentrations in many of the ports in these samplers. After this point in the test we started collecting at least one full-centerline sample round every day until 19 days into the test, when we ceased collecting samples on a daily basis. Figures 4.19 through 4.28 show a number of these "daily snapshots", with Figures 4.29 and 4.30 showing profiles from the last two sample rounds. The final sample round at 32 days (Figure 4.30) confirmed that concentrations had decreased to near-background levels along the network centerline.

IV. ANIMATION OF CENTERLINE CONCENTRATIONS WITH TIME

In order to convey a sense of the overall movement of the tracer along the centerline, an animation was prepared consisting of a large number of "frames" at six-hour intervals, with each frame displaying interpolated concentration using a color scale that was held constant over time. Figures 4.31 through 4.44 show gray-scale versions of selected frames of this animation. In a sense, these figures represent an interpretation of the centerline profiles presented in Figures 4.13 through 4.30, with the "correlations" of similar concentration values between samplers being drawn according to the spatial correlation model employed in the interpolation algorithm. While this augmentation of the raw data helps to convey a better sense of the tracer movement, these figures represent only one of many possible interpretations of the data. A different interpolation scheme would

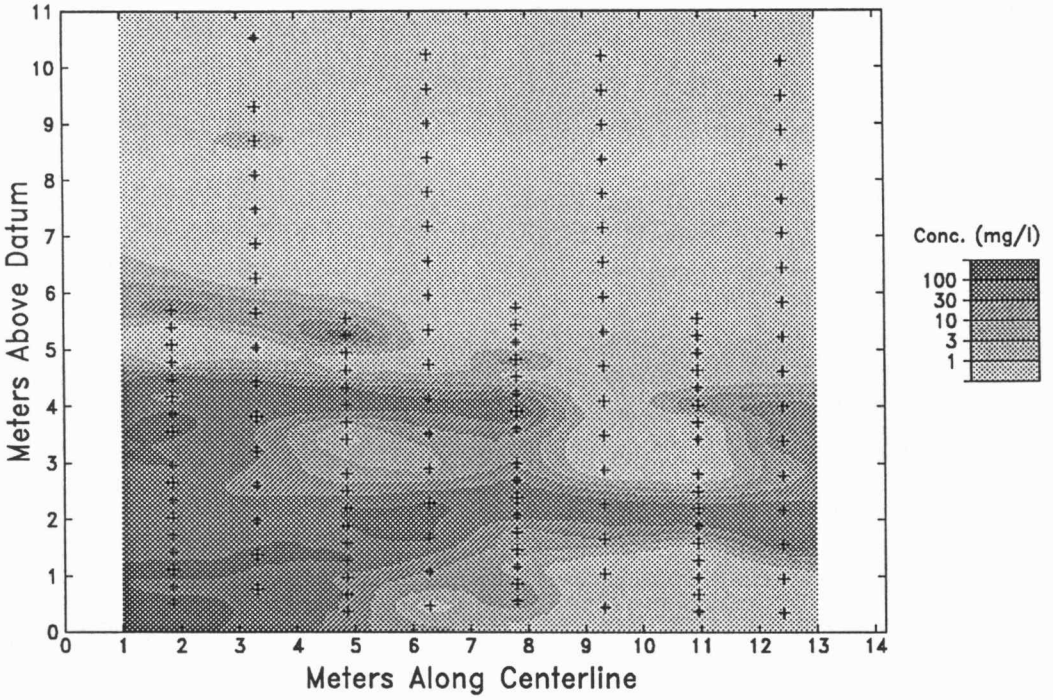

Figure 4.31. Interpolated centerline concentrations at 54 hours (2.25 days)

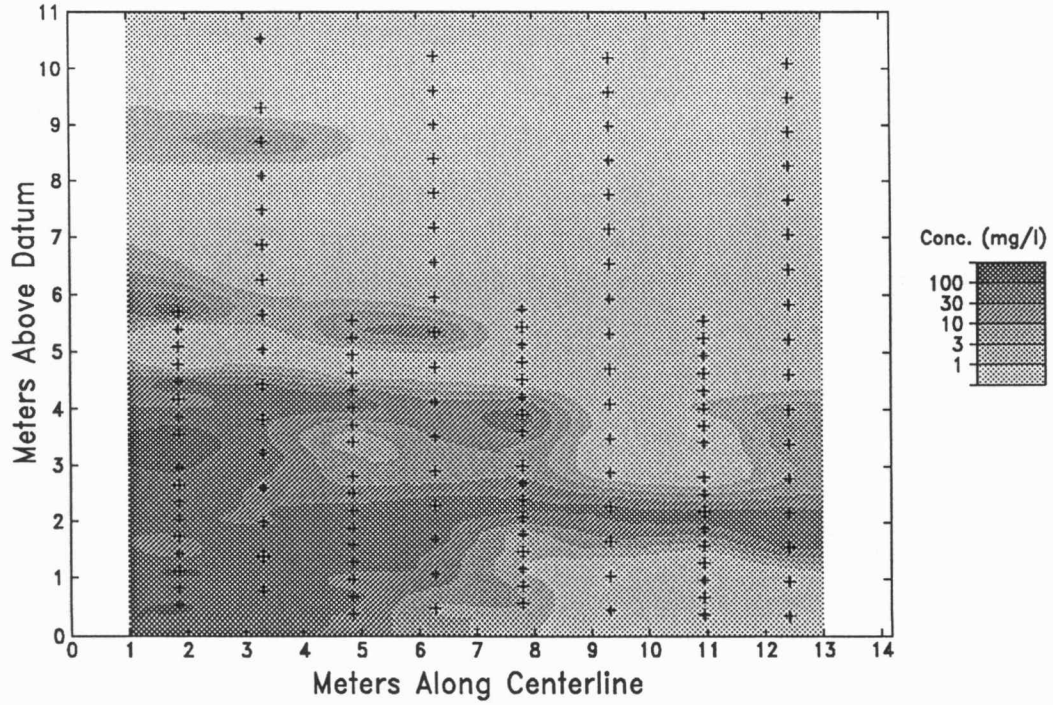

Figure 4.32. Interpolated centerline concentrations at 72 hours (3 days)

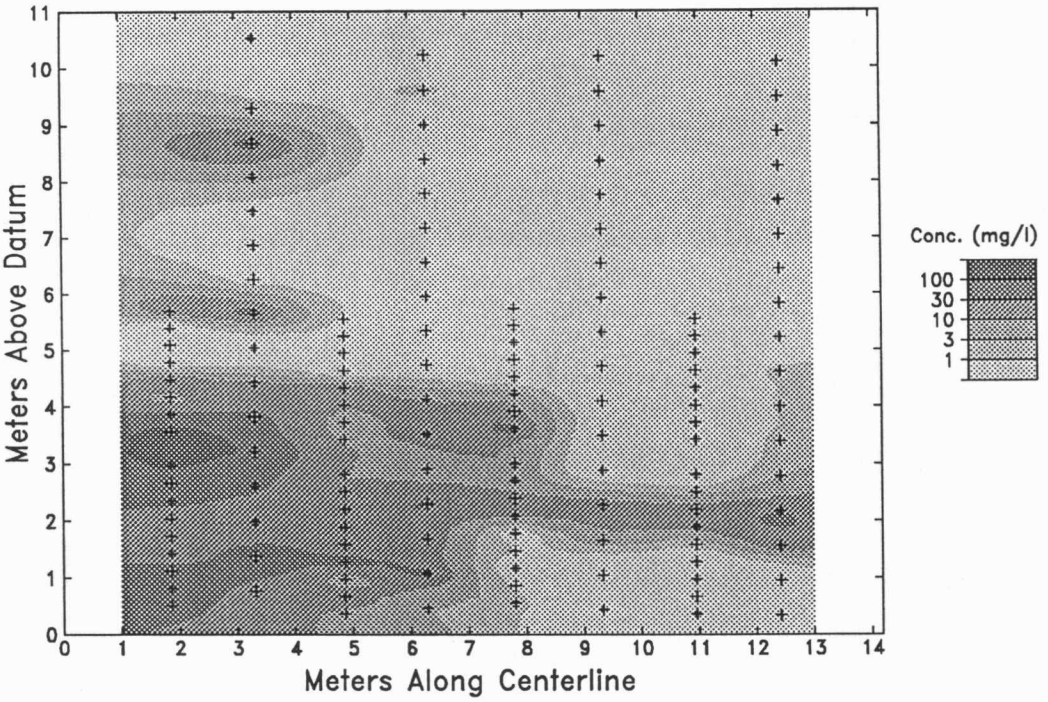

Figure 4.33. Interpolated centerline concentrations at 96 hours (4 days)

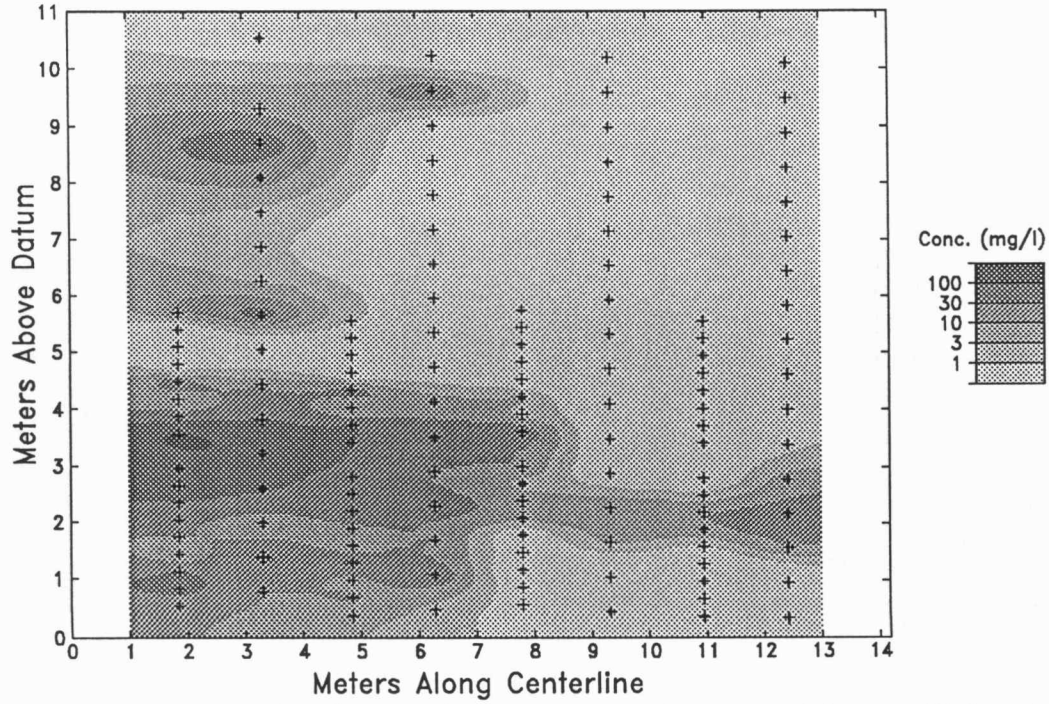

Figure 4.34. Interpolated centerline concentrations at 120 hours (5 days)

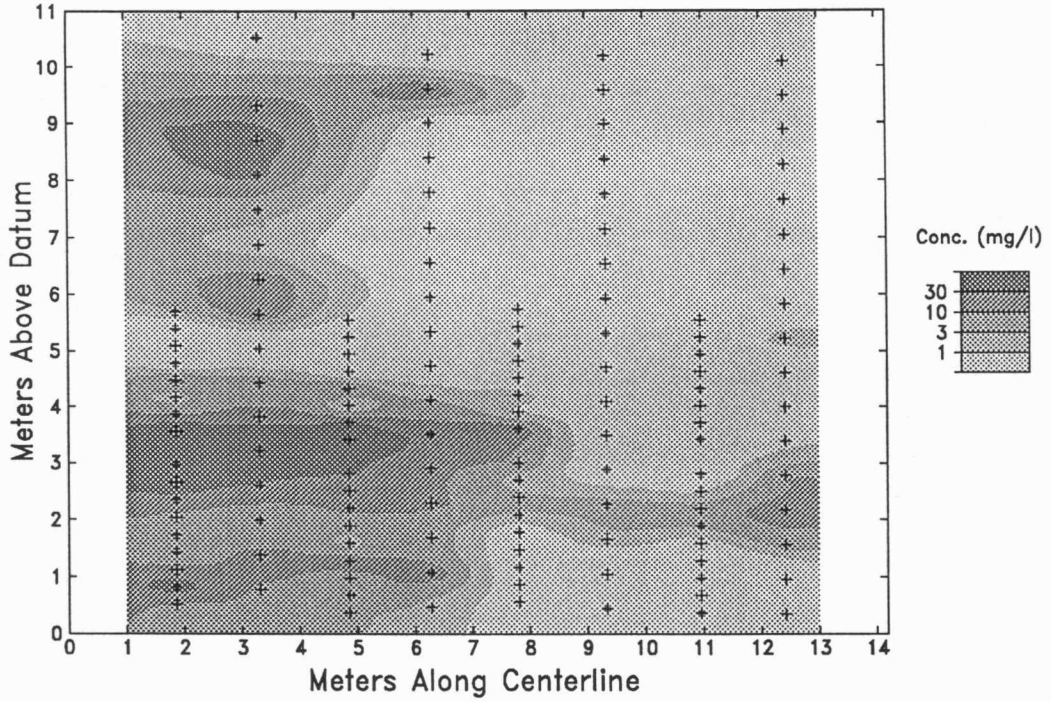

Figure 4.35. Interpolated centerline concentrations at 144 hours (6 days)

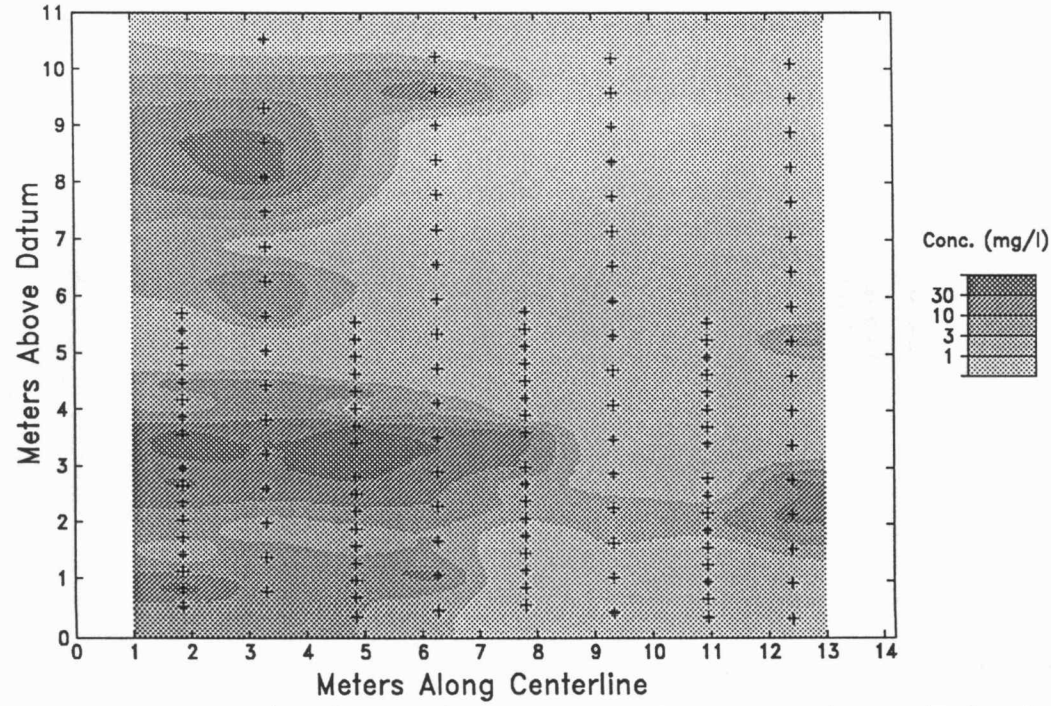

Figure 4.36. Interpolated centerline concentrations at 168 hours (7 days)

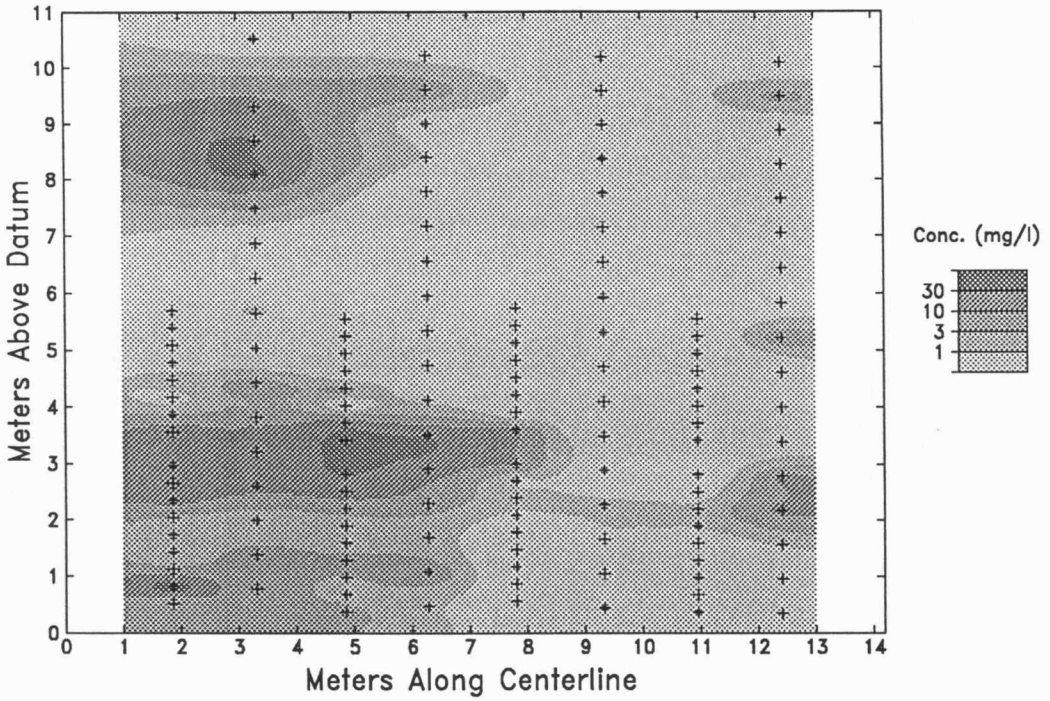

Figure 4.37. Interpolated centerline concentrations at 192 hours (8 days)

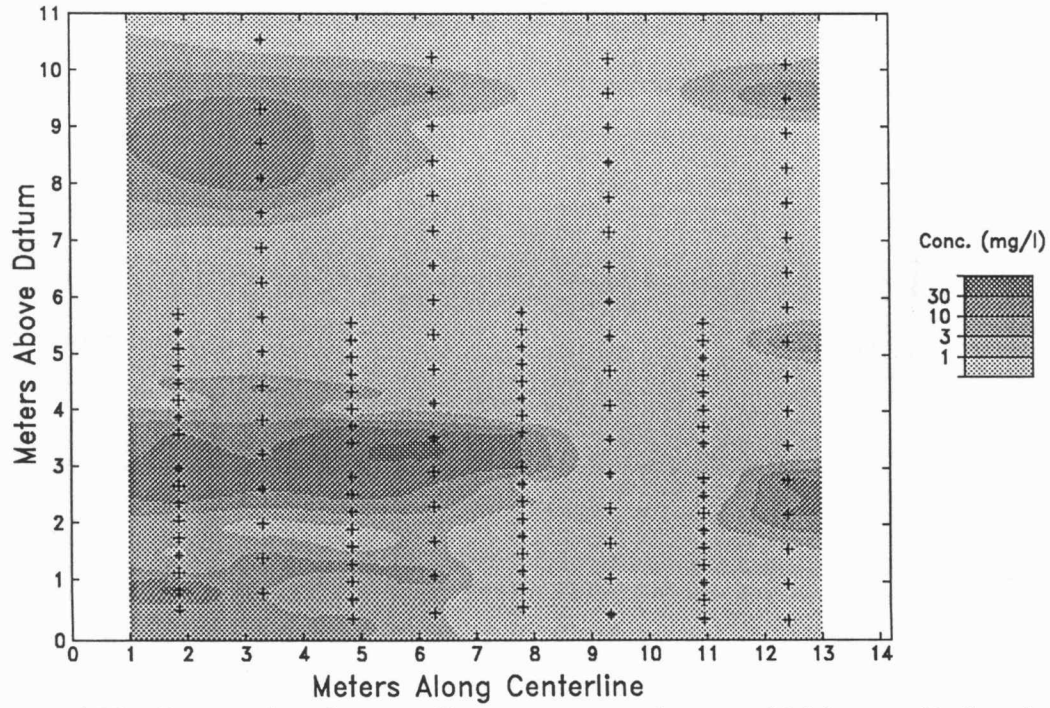

Figure 4.38. Interpolated centerline concentrations at 216 hours (9 days)

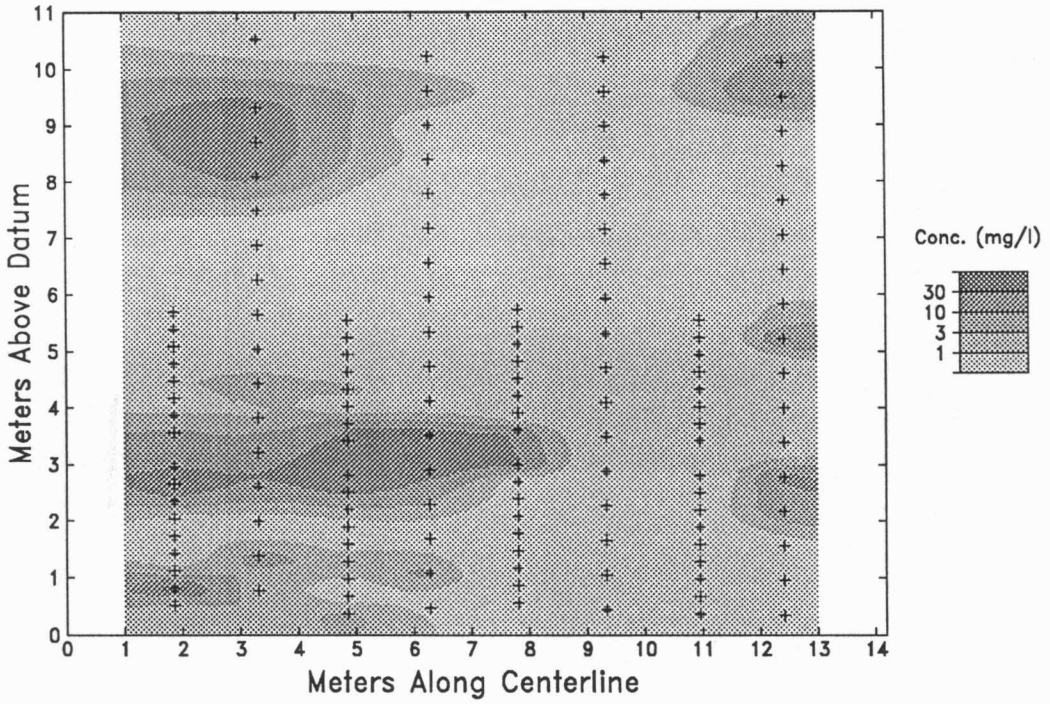

Figure 4.39. Interpolated centerline concentrations at 240 hours (10 days)

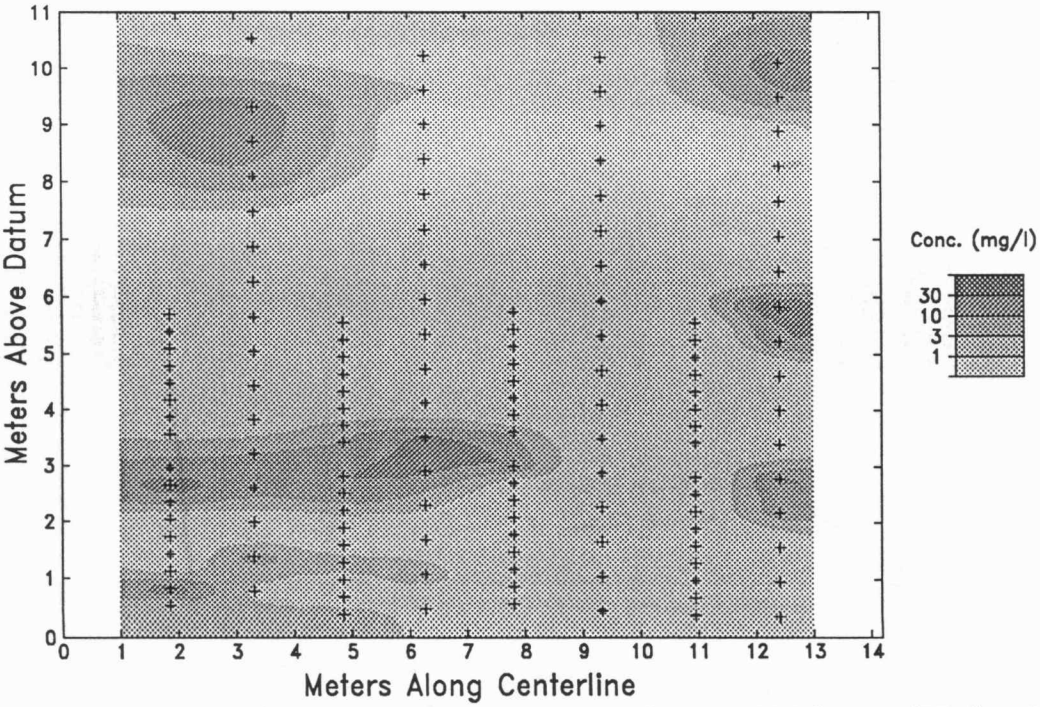

Figure 4.40. Interpolated centerline concentrations at 288 hours (12 days)

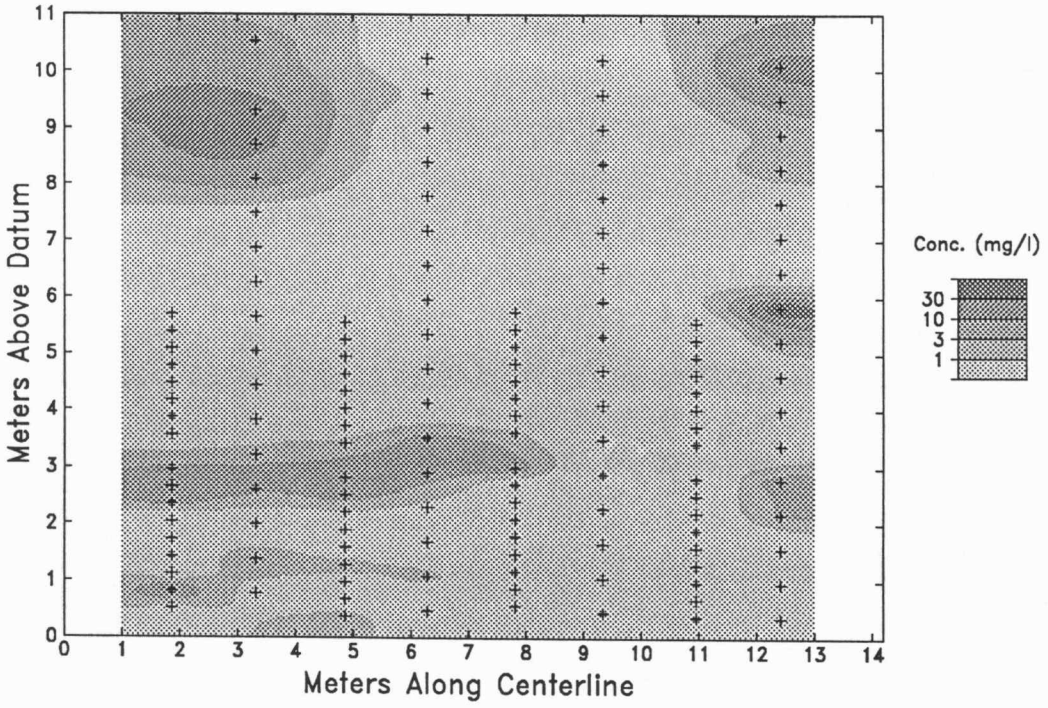

Figure 4.41. Interpolated centerline concentrations at 336 hours (14 days)

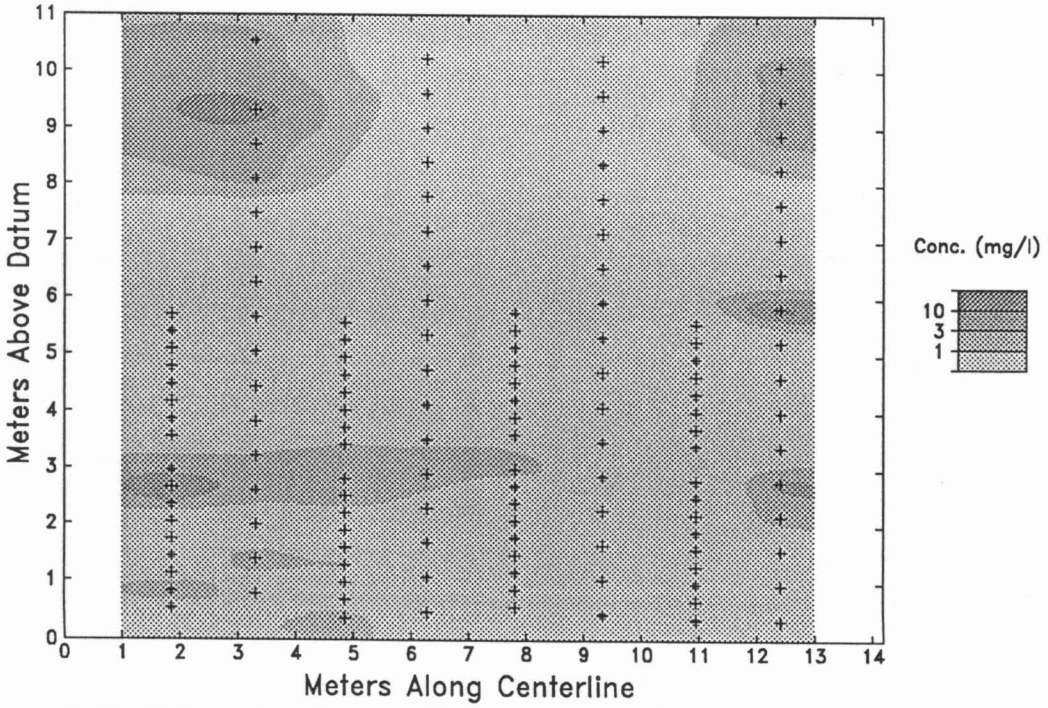

Figure 4.42. Interpolated centerline concentrations at 432 hours (18 days)

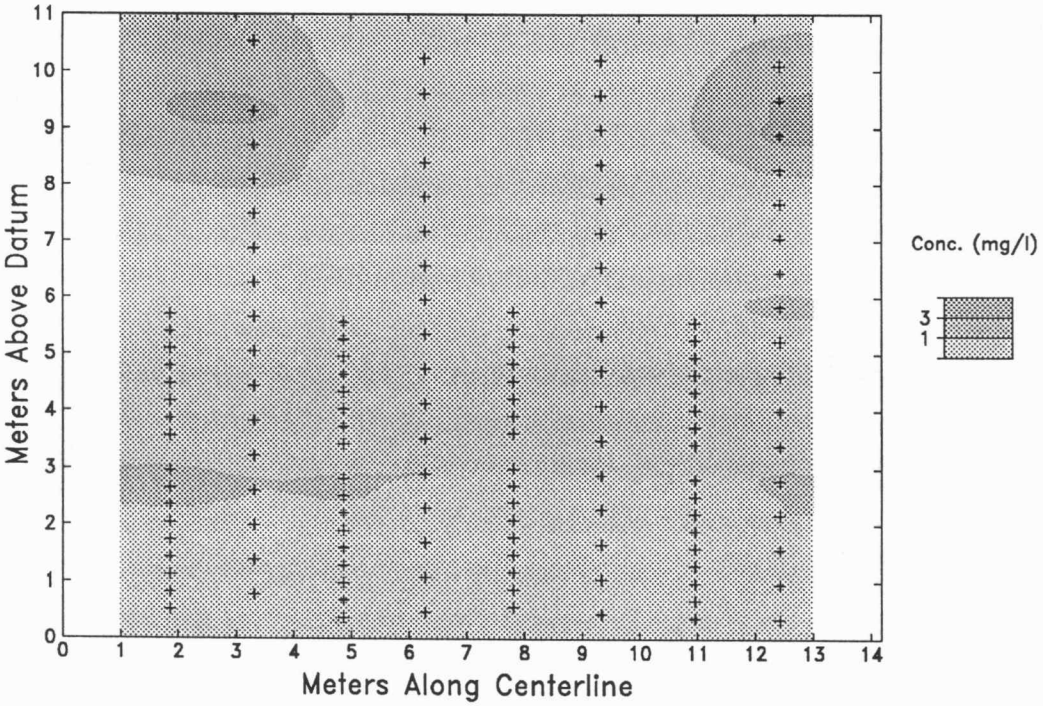

Figure 4.43. Interpolated centerline concentrations at 528 hours (22 days)

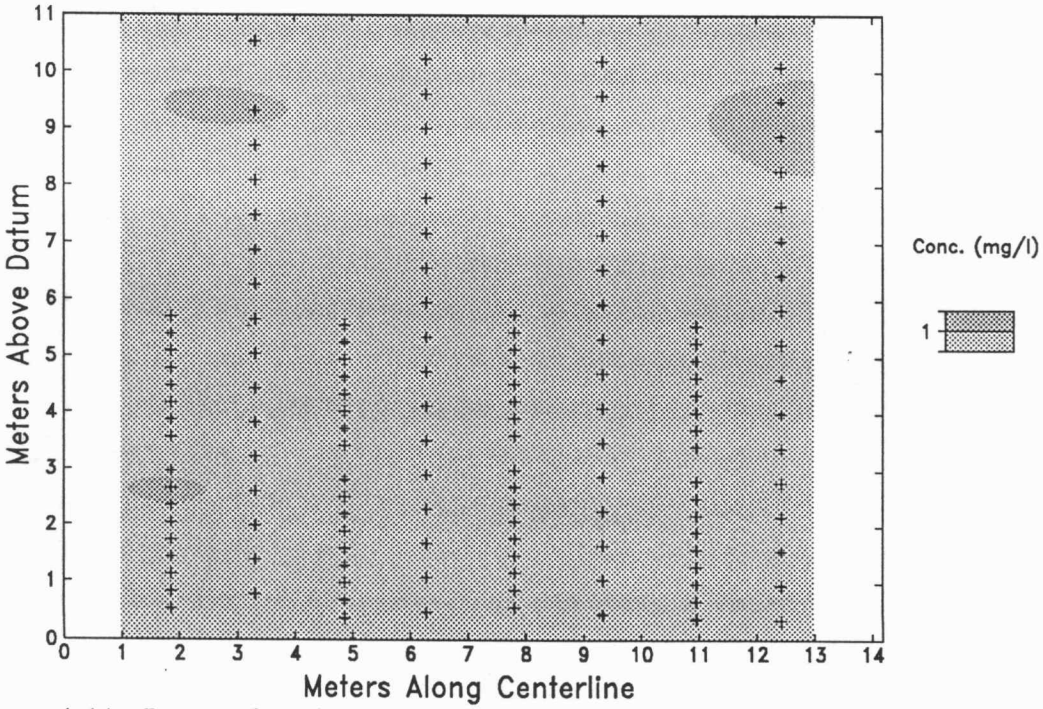

Figure 4.44. Interpolated centerline concentrations at 672 hours (28 days)

convey a different overall sense of the data, possibly quite different if it employed a drastically different model of spatial correlation than that employed here.

The first step in creating the animation was to interpolate the concentration data at each port to regular six-hour intervals using simple linear interpolation between observation times. The first frame is at six hours into the test and the last is at 768 hours (32 days). However, concentrations were not interpolated outside the limits of actual observation times at any sampler. Due to our delay in obtaining samples all the way along the centerline, the first complete frame (showing concentrations along the entire centerline) is at 54 hours (Figure 4.31).

The temporally-interpolated concentration values at each six-hour interval were then interpolated from the port locations, represented in meters from the injection well and meters above datum, to the nodes of a regular grid. In fact, the concentration values were not interpolated directly. Instead, logarithms of the concentration values were interpolated and the gridded log values were then backtransformed to concentration values. The smoothing effect of the logarithmic transformation made the log concentration values somewhat more amenable to interpolation than the original concentration values. The grids contained 121 nodes in the horizontal, ranging from 1 meter to 13 meters along the centerline at a 0.1-meter spacing, and 111 nodes in the vertical, ranging from 0 to 11 meters above datum, also at a 0.1-meter spacing.

The interpolation was performed using a GSLIB program for ordinary kriging, okb2dm (Deutsch and Journel, 1992). The ordinary kriging estimate of a spatially varying property at an unsampled location is given by a linear combination of measured values of that property at n surrounding data locations. Using z_0 to represent the

value being estimated and z_i to represent the property value at each of the n data points, the ordinary kriging estimator is given by

$$z_0 = \sum_{i=1}^{n} \lambda_i z_i \tag{4.1}$$

where the n kriging weights, λ_i, are chosen to minimize the expected estimation error variance subject to the constraint $\sum \lambda_i = 1$, which guarantees unbiasedness. Minimizing the error variance involves solving a set of linear equations (the normal equations) for the kriging weights. The coefficients in these equations consist of the correlations between pairs of data points, derived from a model for the spatial autocorrelation of the property being estimated. Further details regarding ordinary kriging can be found in Deutsch and Journel (1992) and Isaaks and Srivastava (1989).

The interpolation of the log concentration values employed an anisotropic exponential autocorrelation model, in which the correlation between log concentration values separated by a lag vector **h** is given by

$$\rho(\mathbf{h}) = \exp\left(-\sqrt{\left(\frac{h_1}{\ell_1}\right)^2 + \left(\frac{h_2}{\ell_2}\right)^2} \right) \tag{4.2}$$

where h_1 is the component of **h** in the direction of maximum correlation and h_2 is the component of **h** in the direction of minimum correlation, perpendicular to the direction of maximum correlation. The three parameters in this model are the maximum and minimum correlation lengths, ℓ_1 and ℓ_2, and the orientation angle of the direction of maximum correlation. For the results presented here, the parameters of the correlation model were determined through cross-validation using the log concentration values at the port locations for every six-hour increment from 54 hours (the first "full-centerline"

frame) to 240 hours (at which point the amount of mass in the system was becoming quite small). The selected direction of maximum correlation was 2° down from horizontal, implying that ℓ_1 and ℓ_2 essentially represent the horizontal and vertical correlation lengths. The selected correlation lengths were ℓ_1 = 5 meters and ℓ_2 = 1.5 meters.

The port locations are posted as crosses in Figures 4.31 through 4.44. The left edge of each figure represents the location of the injection well and the right edge represents the location of the discharge well (14.2 meters from the injection well). Note that port 16 of TMC-7 (second sampler from the left) is not posted, because this port never yielded any samples. The strong horizontal to vertical anisotropy specified in the correlation model is readily apparent in the figures, which contain many thin, horizontally persistent features. Again, the interpolated results represent an interpretation of the raw data, with the assumptions of the interpretation represented primarily in the imposed model of spatial correlation. Use of a different correlation model could significantly alter the overall appearance of these figures. However, the results shown here generally match our expectations regarding the nature of the tracer distribution and there do not appear to be too many features in the interpolated results that are not warranted by the data at the port locations.

VI. PRELIMINARY ASSESSMENT OF TEST RESULTS

A number of conclusions can be drawn directly from the experimental breakthrough curves and profiles. First of all, it is clear that sharp contrasts in concentration between vertically adjacent ports were maintained throughout the test. These contrasts seem to indicate that minimal mixing occurred between ports. Possibly the simultaneous pumping of all 17 ports created flow divides between vertically adjacent ports, minimizing the mixing between zones. Regardless of the exact mechanics, the procedure seems to be quite successful in sampling from isolated zones around each port.

However, breakthrough curves at some ports show a double-peaked behavior that indicates sampling from two different transport zones, as evidenced by the correspondence of one peak with that in an adjacent port. Perhaps the clearest example of this is the breakthrough curve for port 17 of TMC-8 (Figure 4.1), which has two distinct peaks. The first peak, at 32.7 hours, lags just slightly behind the single peak in port 16, at 28.2 hours (the previous sample time at TMC-8). The breakthrough curve for port 8 exhibits an early peak lagging only four hours behind the peak at port 7, although it is somewhat obscured by the broader main peak at port 8. Similar behavior can be seen between other pairs of ports. This does not necessarily indicate a problem with the sampling strategy. It could simply indicate that the vertical thicknesses of certain packets of tracer are comparable to the port spacing. A smaller peak at a port may represent sampling from the upper or lower edge of such a packet.

The analysis of breakthrough curves presented in Chapter 6 assumes that the tracer movement can be conceptualized as vertically stratified, horizontal transport. The presence of double peaks in certain breakthrough curves complicates the analysis, but does not necessarily undermine the utility of this conceptual model. In fact, the distinctness of separate peaks and the correspondence of secondary peaks with peaks at adjacent ports would tend to argue for the validity of conceptualizing the tracer as moving in separate packets with different velocities in different vertical zones, although possibly with some overlap in sampling at certain ports due to the lack of perfect stratification or separation between these transport zones.

It is clear that we missed the peak concentrations at a number of ports in samplers TMC-5 through TMC-1 (Figures 4.4 through 4.8), and possibly even in TMC-6 (Figure 4.3). Based on our design modeling we decided to concentrate our sampling efforts on samplers close to the injection well during the first few days of the test. We intended to use

results obtained from these early sample rounds to guide further sampling efforts. However, in some zones the tracer moved out much faster than anticipated and peaks had already passed some ports before we extended our sampling down the centerline. By the time we finally sampled all the way along the centerline, about two days into the test, a significant amount of tracer had already moved all the way through the system (Figures 4.8 4.18, and 4.31).

The hydraulic compensation pump in well 0-8 proved to be unnecessary if not detrimental. Large concentrations were observed in some ports in samplers on the east side of the network, the side toward the compensation well, as shown in Figures 4.9 through 4.13. Only small concentrations were observed in samplers on the west side, the side toward the rural water district wells, except at TMW-8, where concentrations in a few ports rapidly rose and fell in the first few days of the test. Thus it is likely that the pumping at the RWD wells had little effect on the test while the pumping at the compensation well might even have drawn the plume to the east of the centerline. As discussed in Chapter 3, our initial assessment of the potential influence of the RWD wells failed to account for the impact of leakage on flow velocities, possibly leading to an overestimate of the influence of pumping at the RWD wells. The samplers on the west side were sampled fairly infrequently, based on their apparent lack of activity.

Taken together, the centerline samplers TMC-3, TMC-2 and TMC-1 (Figures 4.6 through 4.8) exhibit rather mysterious behavior. All but two ports at TMC-3 and most ports at TMC-2 exhibited negligible concentrations throughout the tracer test. However, non-negligible concentrations occurred in most ports at TMC-1, closer to the injection well. The tracer seems to have missed samplers TMC-3 and TMC-2 at most vertical levels in the aquifer. This behavior is quite apparent in the interpolated concentrations shown in Figures 4.31 through 4.44. Two possible explanations for this are that a vertically extensive region of low permeability material exists in the vicinity of

TMC-2 and TMC-3 or that the hydraulic compensator well actually caused the tracer to follow a curved path in the horizontal, bypassing TMC-3 and TMC-2, but returning to the centerline before reaching TMC-1. The latter explanation is possibly supported by the anomalous appearance of a very large spike at port 10 in TMC-1 relatively late in the test (peaking at 14 days). No hint of this spike occurs anywhere upgradient along the centerline, or in the samplers in the east line, for that matter. Either this particular packet of tracer is of extremely limited vertical extent and passed between ports in the upgradient centerline samplers TMC-3, TMC-5 and TMC-7 or it is of limited horizontal extent and missed or skirted the centerline until it reached TMC-1.

The breakthrough curves for TMC-8 (Figure 4.1) and the first centerline profile (Figure 4.13) show that a great deal of the tracer mass moved rapidly into three distinct zones, one between about 1.5 and 2 meters above datum (ports 4 through 6 of TMC-8), another at around 4 meters above datum (port 12), and another from about 4.8 to 5.4 meters above datum (ports 14 through 16). Presumably these are zones of higher hydraulic conductivity, into which the tracer-laden water flowed most readily. It is also possible that some of the non-uniformity of tracer distribution was caused by vertical variability in the extent of development of the well screen, although both the injection and discharge wells were both extensively developed prior to the tracer test. Any variability in well development would probably also reflect vertical variability in the aquifer conductivity, with portions of the well screen adjacent to higher conductivity zones tending to be better developed (Butler and Healey, 1998).

The high conductivity zone centered at about two meters above datum appears to be the most persistent in the horizontal, as evidenced by early breakthroughs in ports at a similar level in all the centerline samplers. It is almost certain that a large fraction of the tracer mass was transported rapidly through this narrow zone to the discharge well,

with much of the rest of the mass being transported through the zone at about four meters above datum, which also appears to be fairly persistent. It is apparent from Figures 4.31 through 4.44 that very little mass entered the upper half of the aquifer. What little mass did enter the upper half of the aquifer tended to show up as isolated blobs at particular ports, rather than as horizontally persistent stringers of tracer. Thus the test revealed very little about the transport properties of the upper portion of the aquifer, due to undersampling of this region. The injection process for any future tracer tests should be modified to attempt to create a more uniform vertical distribution of tracer mass, perhaps by successively isolating different vertical intervals with packers and injecting equal amounts of tracer into each of these intervals.

CHAPTER 5: DEVELOPMENT OF THE TRANSPORT MODEL

I. INTRODUCTION

This chapter describes the radially convergent transport model used to analyze the breakthrough curves at the centerline sampling ports during GEMSTRAC1. Moench (1989, 1991) presents a model describing the vertically and azimuthally averaged concentration resulting from transport in a radially convergent flow field in a confined aquifer. To be used in the analysis of the GEMSTRAC1 data, this model has to be modified to account for both vertical and azimuthal concentration variations. In addition, the boundary condition associated with the injection well needs to be considered with some care, since the injection process employed in GEMSTRAC1 almost certainly violated assumptions employed by Moench (1989, 1991). Furthermore, our inability to completely characterize the initial injection geometry leads to the addition of two unknown parameters to the model-fitting process, contributing to a high degree of parameter nonuniqueness in some cases.

II. THE MOENCH RADIALLY CONVERGENT TRANSPORT MODEL

Moench (1989) presents the equation governing advective-dispersive transport in a radially convergent flow field in a confined aquifer:

$$\frac{1}{r}\frac{\partial}{\partial r}\left(rD_L\frac{\partial C}{\partial r}\right)-v\frac{\partial C}{\partial r}=R\frac{\partial C}{\partial t} \qquad (5.1)$$

where r is the radial distance from the center of the pumping well, C is the vertically averaged tracer concentration, D_L is the dispersion coefficient, v is the vertically averaged advective velocity, and R is the retardation coefficient. Figure 5.1 illustrates the configuration of a

radially convergent tracer test. Under confined flow conditions, the advective velocity v is given by

$$v(r) = -\frac{Q}{2\pi bnr} \tag{5.2}$$

where Q is the pumping rate, and b and n are the aquifer thickness and porosity. Moench assumes that the dispersion coefficient is given by $D_L = \alpha_L|v|$, where α_L is the aquifer dispersivity (with units of length).

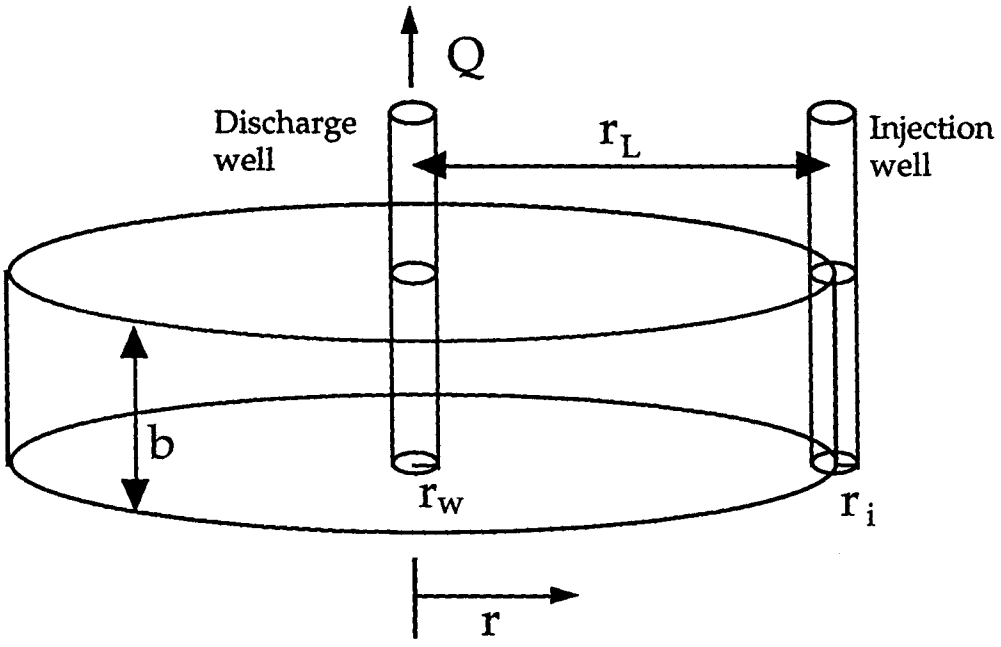

Figure 5.1. Geometry of radially convergent tracer test (after Moench, 1989, Figure 1).

Moench (1989) presents a solution describing concentration in the pumping well, which represents both a vertical and azimuthal average. Because the concentration in the pumping well is insensitive to the vertical and azimuthal distribution of tracer, the injected mass can be treated as if it were distributed uniformly around the pumping

well. This leads to simplification of the boundary conditions. The boundary condition at the pumping well is

$$2\pi r_w bn\left[D_L \frac{\partial C}{\partial r} - vC\right]_{r=r_w} = QC_w + \pi r_w^2 b_w \frac{\partial C_w}{\partial t} \qquad (5.3)$$

where r_w and b_w are the pumping well radius and mixing length and C_w is the concentration in the pumping well. Under the assumption of instantaneous mixing, $C_w = C(r=r_w)$, this boundary condition reduces to

$$2\pi r_w bn\left[D_L \frac{\partial C}{\partial r}\right] = \pi r_w^2 b_w \frac{\partial C}{\partial t}, \quad r = r_w. \qquad (5.4)$$

The outer (injection well) boundary condition needs to be considered with some care, since it embodies a number of assumptions concerning the injection process and geometry. Moench (1989) presents outer boundary conditions describing both instantaneous and continuous mass injection, and Moench (1991) includes the additional option of using a tophat (boxcar) input function. Zlotnik and Logan (1996) suggest using a more generalized representation, in which the mass injection rate as a function of time is simply represented by $\dot{M}$. In this case, the outer boundary condition becomes

$$2\pi r_L bn\left[D_L \frac{\partial C}{\partial r} - vC\right]_{r=r_L} = \dot{M} - \pi r_i^2 b_i \frac{\partial C_b}{\partial t} \qquad (5.5)$$

where r_L is the radial distance from the pumping well to the injection well, r_i and b_i are the radius and mixing length of the injection well, and C_b is the concentration of the well-mixed fluid in the wellbore. The second term on the right-hand side of Equation 5.5 represents the release of solute from storage in the wellbore. Moench (1989) eliminates C_b from this boundary condition using the mistaken assumption that the azimuthally averaged concentration at r_L, $C(r=r_L)$, is equal to the wellbore concentration, C_b, yielding

$$2\pi r_L bn\left(D_L \frac{\partial C}{\partial r} - vC\right) = \dot{M} - \pi r_i^2 b_i \frac{\partial C}{\partial t}, \quad r = r_L. \tag{5.6}$$

The next section discusses modifications to this boundary condition required for the analysis of GEMSTRAC1.

For the analysis of GEMSTRAC1 we will use the tophat (finite duration) mass input function suggested by Moench (1991). In this case the mass injection is represented as $\dot{M}(t) = M\Pi_{t_p}$, where M is the total injected mass, t_p is the duration of injection, and

$$\Pi_{t_p} = \begin{cases} 1/t_p, & 0 \le t \le t_p \\ 0, & \text{otherwise} \end{cases}. \tag{5.7}$$

The advective travel time from the injection well to the pumping well is given by

$$t_a = \pi bn\left(r_L^2 - r_w^2\right)/Q. \tag{5.8}$$

The numerator in Equation 5.8 is the pore volume contained between the radii r_w and r_L, so that t_a represents the time required to remove one pore volume at rate Q. A convenient reference concentration is given by dividing the total injected mass by the same pore volume, or

$$C_i = M/\left[\pi bn\left(r_L^2 - r_w^2\right)\right] \tag{5.9}$$

Using these definitions for advective travel time and reference concentration, a set of dimensionless transport equations can be defined as (Moench, 1989):

$$\text{PDE:} \quad \frac{1}{Pe}\frac{\partial^2 C_D}{\partial r_D^2}+\frac{\partial C_D}{\partial r_D}=\frac{2r_D R}{\left(1-r_{wD}^2\right)}\frac{\partial C_D}{\partial t_D}, \quad r_{wD}<r_D<1 \qquad (5.10a)$$

$$\text{Inner BC:} \quad \frac{1}{Pe}\frac{\partial C_D}{\partial r_D}=\mu_w\frac{\partial C_D}{\partial t_D}, \quad r_D=r_{wD} \qquad (5.10b)$$

$$\text{Outer BC:} \quad \frac{1}{Pe}\frac{\partial C_D}{\partial r_D}+C_D=\Pi_{t_{pD}}-\mu_i\frac{\partial C_D}{\partial t_D} \qquad (5.10c)$$

$$\text{IC:} \quad C_D(r_D,0)=0, \quad r_{wD}<r_D<1 \qquad (5.10d)$$

where the dimensionless quantities are

$$\text{time:} \quad t_D=t/t_a \qquad (5.11a)$$

$$\text{injection duration:} \quad t_{pD}=t_p/t_a \qquad (5.11b)$$

$$\text{radius:} \quad r_D=r/r_L \qquad (5.11c)$$

$$\text{pumping well radius:} \quad r_{wD}=r_w/r_L \qquad (5.11d)$$

$$\text{Peclet number:} \quad Pe=r_L/\alpha_L \qquad (5.11e)$$

$$\text{concentration:} \quad C_D=C/C_i \qquad (5.11f)$$

$$\text{pumping well mixing factor:} \quad \mu_w=\frac{r_w^2 b_w}{nb\left(r_L^2-r_w^2\right)} \qquad (5.11g)$$

$$\text{injection well mixing factor:} \quad \mu_i=\frac{r_i^2 b_i}{nb\left(r_L^2-r_w^2\right)} \qquad (5.11h)$$

The injection well and pumping well mixing factors represent the ratio of the mixing volume of each well to the pore volume between r_w and r_L. As described below, the application of this model to analysis of GEMSTRAC1 requires modifications of the definitions of μ_i, C_i, and t_a. However, these modifications do not change the forms of the

dimensionless equations and the code described by Moench (1989, 1991) can still be used to analyze the GEMSTRAC1 breakthrough curves.

Moench (1989) uses a Laplace transform to remove the time derivatives in Equations 5.10 and then uses a sequence of variable substitutions to reduce the Laplace space differential equation to the Airy equation, which has a known solution. Backsubstitution of the variables and use of the transformed boundary conditions leads to a Laplace space solution of the form

$$\overline{C}_D(s) = \psi(s) \exp\left[\frac{Pe}{2}(1 - r_{wD})\right] \overline{G}(r_D, s) \qquad (5.12)$$

where s is the Laplace space variable. $\overline{G}(r_D, s)$ is an expression involving Airy functions whose arguments depend on the Peclet number (Pe), the retardation coefficient (R), the dimensionless discharge well radius (r_{wD}), and the dimensionless observation radius (r_D). $\overline{G}(r_D, s)$ also includes terms depending on the two mixing factors, μ_w and μ_i. $\psi(s)$ represents the Laplace transform of the dimensionless injection function. For the tophat injection function,

$$\psi(s) = \frac{1}{s t_{pD}}\left(1 - e^{-s t_{pD}}\right). \qquad (5.13)$$

The limit of the above expression as $t_{pD} \rightarrow 0$ is 1, the Laplace transform of the Dirac delta function, representing a pulse injection at time zero.

The computations presented herein employ the code described in Moench (1991), which uses the de Hoog *et al.* (1982) algorithm to numerically backtransform the Laplace space solution shown in Equation 5.12. The Airy functions employed in this code (Amos, 1986) allow evaluation for Peclet numbers up to 1350, or dispersivities down to 1 cm for GEMSTRAC1 (with r_L = 14.2 m).

III. QUESTIONS REGARDING THE MOENCH MODEL

Outer (injection well) boundary condition

A more generalized version of the outer boundary condition is given by

$$2\pi r_L bn\left[D_L\frac{\partial C}{\partial r}-vC\right]_{r=r_L}=\dot{M}-V_m\frac{\partial C_m}{\partial t} \qquad (5.14)$$

where $V_m\frac{\partial C_m}{\partial t}$ represents the rate of change of mass in a mixing volume, V_m, encompassing the injection well. This mixing volume is characterized by concentration C_m, which may differ from the concentration of the injected fluid. Different results are obtained depending on the assumptions made regarding V_m and the relationship between $C_m(t)$ and the azimuthally averaged concentration, $C(r_L,t)$. The following development employs the assumption that $C(r_L,t)=\gamma C_m(t)$, where γ is a proportionality constant determined by the flow geometry in the vicinity of the injection well, an approach suggested by Zlotnik and Logan (1996).

The outer boundary condition presented by Moench (1989) is based on the assumption that the tracer is swept passively out of the injection well by the water flowing past due to pumping at the discharge well, i.e., that the injection itself has negligible influence on the flow system. In this case the mixing volume is that of the injection well, $V_m=\pi r_i^2 b_i$, and $C_m(t)$ is the same as $C_b(t)$, which Moench describes as "the concentration of well-mixed fluid in the well bore." Moench (1989) further assumes that the azimuthally averaged concentration at $r = r_L$ is equal to $C_b(t)$, i.e., that $\gamma = 1$, an error pointed out by Zlotnik and Logan (1996) and acknowledged by Moench (1996). Under these assumptions, the outer boundary condition is that shown in Equation

5.6 and the injection well mixing factor is that shown in Equation 5.11h.

Zlotnik and Logan (1996) point out that $C(r=r_L)$ must be much smaller than C_b, since the tracer is contained within a narrow wedge, of aperture angle θ, emanating from the pumping well, whereas the definition of $C(r=r_L)$ involves averaging around the entire circle surrounding the pumping well. Like Moench (1989), Zlotnik and Logan (1996) assume that the tracer is swept passively out of the injection well. If the injection well is far enough from the pumping well, the flow in the immediate vicinity of the injection well can be modeled using the results

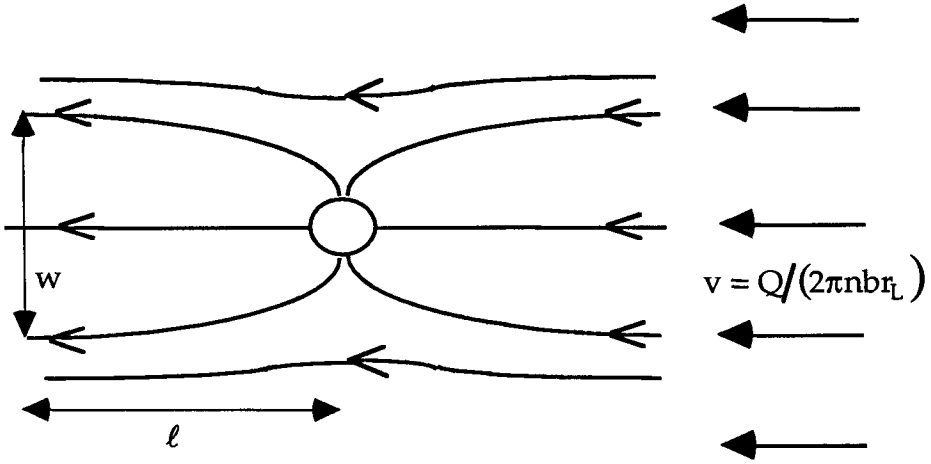

Figure 5.2. Flow configuration in the vicinity of the injection well assuming negligible injection rate (after Zlotnik and Logan, 1996, Figure 4).

for a highly conductive cylinder in an approximately uniform ambient flow field, characterized by the velocity $v = Q/(2\pi nbr_L)$ (Bidaux and Tsang, 1991; Wheatcraft and Winterberg, 1985). In this case the tracer-laden water from the injection well is swept out to a certain maximal width, w, within a certain distance, ℓ, downstream of the well, as

illustrated in Figure 5.2. This width determines the azimuth angle of the tracer-laden wedge, that is

$$\theta \cong \frac{w}{r_L}. \tag{5.15}$$

Zlotnik and Logan (1996) assume that ℓ is negligible in comparison to r_L and that the concentration in the wedge at $r_L - \ell \cong r_L$ is the same as that in the wellbore, C_b. In this case

$$C(r_L,t) \cong C(r_L - \ell,t) = \frac{\theta}{2\pi} C_b(t) \cong \frac{w}{2\pi r_L} C_b(t) \tag{5.16}$$

so that the outer boundary condition becomes

$$2\pi r_L bn\left(D_L \frac{\partial C}{\partial r} - vC\right) = \dot{M} - \frac{\pi r_i^2 b_i}{\gamma} \frac{\partial C}{\partial t}, \quad r = r_L \tag{5.17}$$

and the revised mixing factor becomes

$$\mu_i = \frac{1}{\gamma} \frac{r_i^2 b_i}{nb\left(r_L^2 - r_w^2\right)} \tag{5.18}$$

with $\gamma = \theta/2\pi \cong w/2\pi r_L$.

Since the width of the tracer wedge, w, will generally be quite small in comparison to the circumference $2\pi r_L$, the mixing factor proposed by Zlotnik and Logan (1996) will generally be quite a bit larger than the original mixing factor proposed by Moench (1989). In the absence of a well skin, $w = 4r_i$ (Wheatcraft and Winterberg, 1985), so that $\gamma \cong 2r_i/\pi r_L$. For GEMSTRAC1, $r_L = 14.2$ m and $r_i = 0.07$ m, so that $\gamma \cong 0.003$ and $\mu_i \cong 0.03$ (assuming $b_i = b$ and using n = 0.28). Without Zlotnik and Logan's correction, the mixing factor would be $\mu_i \cong 8.9 \times 10^{-5}$. Figure 5.3 illustrates the effect of mixing factor on

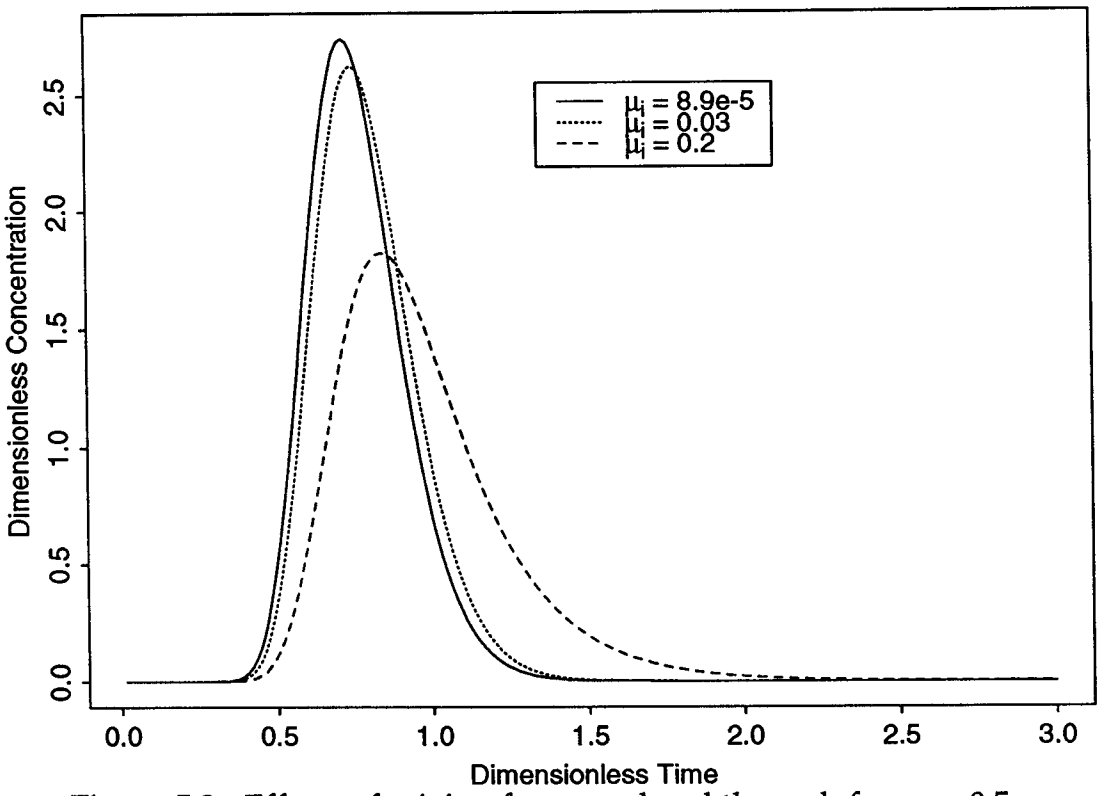

Figure 5.3. Effects of mixing factor on breakthrough for $r_D = 0.5$.

dimensionless breakthrough curves calculated at a dimensionless observation radius of 0.5 for a Peclet number of 100 and using a dimensionless injection duration, t_{pD}, of 0.01 (both numbers approximately representative of conditions during GEMSTRAC1). Breakthrough curves are shown for the two injection well mixing factors mentioned above, along with a larger mixing factor of 0.2, deemed to be more representative of the actual GEMSTRAC1 injection process, as discussed below. Variation with mixing factor is more pronounced for higher Peclet numbers (less dispersive transport). Clearly, use of an inappropriate mixing factor could lead to bias in estimates of both the advective travel time and the dispersivity. In particular, use of too small a mixing factor would lead to an overestimation of the dispersivity.

The outer boundary conditions proposed by Moench (1989) and Zlotnik and Logan (1996) both employ the assumption that the injection rate, q, is negligible in comparison to the rate of flow through the injection well due to pumping at the discharge well, γQ. However, quite the opposite was true during GEMSTRAC1. As described in Chapter 3, GEMSTRAC1 began with the injection of 7.57 cubic meters of tracer-laden solution over a period of about two hours, introduced in four separate injections of 1.89 cubic meters (500 gallons), each lasting about 16 minutes. This implies an overall average injection rate of about 3.8 m^3/hr over the two hours or 7.1 m^3/hr during each of the actual injection periods. Using the estimate $\gamma \cong 0.003$, as above, and the discharge rate of 15.7 m^3/hr leads to $\gamma Q = 0.047\ m^3/hr$, a value much smaller than the overall average or actual instantaneous injection rate. That is, for GEMSTRAC1, $\gamma Q << q$ rather than $q << \gamma Q$, as assumed by Moench (1989) and Zlotnik and Logan (1996). Therefore, the tracer was almost certainly driven out of the injection well by the injection process itself, rather than being swept out passively. The following presents the development of a revised outer boundary condition based on the assumption that $\gamma Q << q$, in which case a concentric cylinder of tracer-laden water forms around the injection well (Guvanasen and Guvanasen, 1987).

Figure 5.4 is an idealized representation of the geometry of the injected plume immediately following the end of injection. In this case the volume occupied by the tracer is

$$V_m = \pi\left(r_m^2 - r_i^2\right)nb + \pi r_i^2 b_i = \pi\left[r_m^2 + \left(\frac{b_i}{nb} - 1\right)r_i^2\right]nb \cong \pi r_m^2 nb \quad (5.19)$$

where r_m is the radius of the injection zone. The approximation $V_m \cong \pi r_m^2 nb$ results from the assumption that $\left(\frac{b_i}{nb} - 1\right)r_i^2 << r_m^2$, i.e., that the small correction for the inclusion of the wellbore volume can be ignored. This is almost certainly true for GEMSTRAC1, because the

injection well has a radius of 0.07 m and the injection radii were probably on the order of 1 meter.

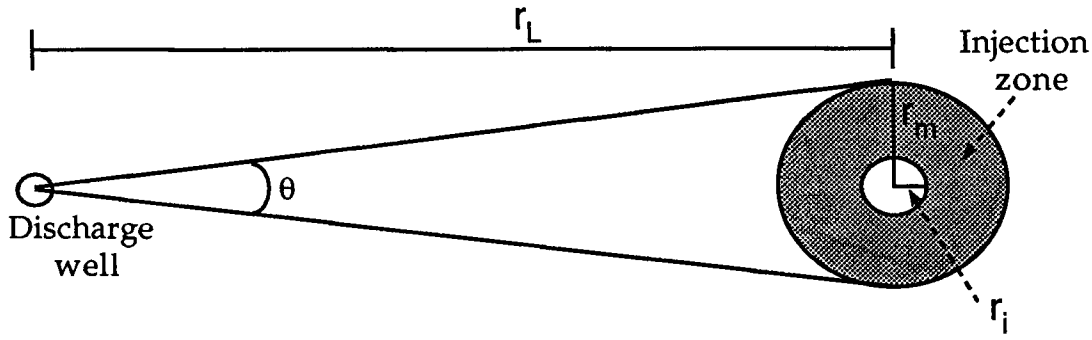

Figure 5.4. Idealized plume geometry immediately after injection.

In addition, the angle of the wedge encompassing the tracer, shown in Figure 5.4, can be approximated as

$$\theta = 2\tan^{-1}(r_m/r_L) \cong 2r_m/r_L \tag{5.20}$$

because θ is small. This implies that the proportionality constant relating $C(r=r_L)$ to C_m, the concentration in the injection zone, can be approximated as

$$\gamma = \theta/2\pi \cong r_m/\pi r_L . \tag{5.21}$$

In this case the mixing term in Equation 5.12 can be written as

$$V_m \frac{\partial C_m}{\partial t} = \frac{V_m}{\gamma}\frac{\partial C}{\partial t} \cong \pi^2 r_m r_L nb \frac{\partial C}{\partial t} \tag{5.22}$$

and the corresponding injection zone mixing factor is

$$\mu_i = \frac{1}{\gamma}\frac{V_m}{\pi nb\left(r_L^2 - r_w^2\right)} \cong \frac{\pi r_L}{r_m}\frac{\pi r_m^2 nb}{\pi nb\left(r_L^2 - r_w^2\right)} \cong \frac{\pi r_m}{r_L} \tag{5.23}$$

where the final approximation employs the fact that $r_w^2 << r_L^2$. A mixing radius of 1 meter would imply an injection zone mixing factor equal to 0.22 for GEMSTRAC1, since r_L = 14.2 m. A dimensionless breakthrough curve for $\mu_i = 0.2$ is included in Figure 5.3. Clearly, this curve differs considerably from that for the much smaller mixing factors derived from the "passive injection" assumption employed by Moench (1989) and Zlotnik and Logan (1996).

The injection process for GEMSTRAC1 was very poorly characterized, so that we do not know either r_m or C_m directly. In fact, both of these quantities almost certainly varied with depth, so that both the injection zone mixing factor and the reference concentration must be treated as unknown parameters, potentially different for each port elevation.

The two most questionable simplifications built into this treatment of the injection well boundary condition are that the longitudinal dimension of the injected pulse is treated as negligible and that the relationship between $C_m(t)$ and $C(r_L,t)$ is characterized by a simple proportionality constant. Although the injection zone mixing factor attempts to account for the time variation in $C(r_L,t)$ due to storage of tracer mass in the injection volume, it does not truly account for the finite spatial dimensions of the initially injected plume. All the mass is still treated as if it were introduced at the radius $r = r_L$. Furthermore, one could easily imagine the injection process coupled with the movement of tracer due to pumping at the discharge well creating a more complicated injection zone geometry and a more complicated relationship between $C_m(t)$ and $C(r_L,t)$. Guvanasen and Guvanasen (1987) present a thorough analysis of the influence of injection rate and discharge rate on the geometry of the injected plume, along with a method for computing breakthrough curves at any location for fairly arbitrary injection geometries.

Pointwise versus azimuthally averaged concentrations

Although Moench (1989) developed a solution describing tracer breakthroughs for any arbitrary observation radius, his solution is not applicable to the description of breakthrough curves obtained from a particular sampler or observation well, because it describes azimuthally averaged, rather than pointwise concentrations. Instead, Moench focuses on analysis of concentrations in the discharge well, which do in fact represent azimuthal averages. Because the discharge well draws in and mixes water from the full 360° surrounding it, the concentrations in the discharge well are totally insensitive to the azimuthal distribution of tracer mass in the surrounding aquifer. This allows the outer boundary condition to be stated in terms of an azimuthal average, as described above.

In GEMSTRAC1 we sampled concentrations from within the actual tracer wedge. These concentrations are much higher than the azimuthally averaged concentrations at the same radii. Assuming that the tracer is distributed uniformly across the wedge, the azimuthally averaged concentration given by Moench's solution and the concentration in the wedge, C*(r,t), are related by

$$C^*(r,t) = \frac{2\pi}{\theta} C(r,t) = \frac{1}{\gamma} C(r,t) \tag{5.24}$$

where θ is the angle encompassed by the wedge, as shown in Figure 5.4, and γ is the same scaling factor introduced in the modification of the injection zone mixing factor. The necessary scaling of the concentration in this case can be accomplished by redefining the reference concentration (Equation 5.9) as

$$C_i = \frac{1}{\gamma} \frac{M}{\pi bn\left(r_L^2 - r_w^2\right)} \cong \frac{2\pi r_L}{2r_m} \frac{M}{\pi bn\left(r_L^2 - r_w^2\right)} \tag{5.25}$$

yielding a solution that is applicable for describing breakthroughs in the tracer wedge. The second form of the equation shows that the scaling factor is simply the ratio of the circumference of the circle passing through the injection well to the initial width of the injected plume. It is important to note that although this modification of the reference concentration involves the same geometric factor as the modification of the injection zone mixing factor, it arises from fundamentally different considerations and produces substantially different results. The modification of the injection zone mixing factor is the more fundamental deviation from Moench's original formulation, because it amounts to an alteration of a boundary condition parameter and influences the fundamental form of the solution, as shown in Figure 5.3. The modification of the reference concentration is simply a scaling to account for a difference in sampling procedures. It does not change the form of the dimensionless breakthrough curve.

In the analysis of GEMSTRAC1, the reference concentration shown in Equation 5.25 will be treated as an unknown parameter, due to our inability to characterize the vertical variation in injected mass and injection radius. We have no way to independently determine how the factor $M/(2\pi r_m bn)$, representing the injected mass per unit pore area transverse to flow, varied with depth.

Resident versus flux-averaged concentrations

The tracer transport solution described above yields results for the resident or volume-averaged concentration, defined as the mass of solute per unit volume of water in the pore space at a given time. The resident concentration must be distinguished from the flux-averaged concentration, defined as the ratio of the solute flux density to the specific discharge (Parker and van Genuchten, 1984). In other words, the flux-averaged concentration, C_f, is defined so that the solute flux density for radial transport is given by

$$J = n\left[vC - D_L \frac{\partial C}{\partial r}\right] = nvC_f. \qquad (5.26)$$

This implies that the flux-averaged and resident concentrations are related by

$$C_f = C - \frac{D_L}{v}\frac{\partial C}{\partial r} = C - \frac{\alpha_L |v|}{v}\frac{\partial C}{\partial r} = C + \alpha_L \frac{\partial C}{\partial r}. \qquad (5.27)$$

The change of sign occurs because v is a negative quantity for radially convergent flow. Expressed in terms of dimensionless quantities, Equation 5.27 becomes (Moench, 1989)

$$C_{fD} = C_D + \frac{1}{Pe}\frac{\partial C_D}{\partial r_D}. \qquad (5.28)$$

Parker and van Genuchten (1984) point out that C and C_f obey the same partial differential equation but different boundary conditions for the same transport problem. They discuss the relationship between C and C_f for linear flow problems and Chen (1987) investigates that relationship for radially divergent flow and transport. The critical issue in all cases is to properly identify sampled concentrations as either resident or flux-averaged and analyze them appropriately. Sampled concentrations are clearly flux-averaged when the sampling process consists of capturing the flow that is driving the transport, as when samples consist of fluid that has flowed out the end of a laboratory column (Parker and van Genuchten, 1984) or of fluid from the discharge well in a radially convergent tracer test (Moench, 1989). In fact, the discharge well boundary condition resulting from the assumption of instantaneous mixing (Equation 5.10b) essentially enforces an equality of resident and flux-averaged concentrations at the discharge well in most situations, since μ_w is usually very small and

thus $\partial C_D/\partial r_D \cong 0$ at $r_D = r_{wD}$. However, resident and flux-averaged concentrations clearly differ away from the discharge well.

When the sampling process involves the imposition of an "artificial" flow field, as when sampling ports are pumped to draw in water, it is not clear how the sampled concentrations relate to the resident concentrations in the aquifer; the samples in fact represent flux averages determined by the sampling flow field. The only unambiguous way to measure a resident concentration would be to instantaneously extract a portion of aquifer and measure the overall concentration in the contained pore fluid. The data from GEMSTRAC1 have been analyzed based on the assumption that they represent resident concentrations, that is, that the sampling process closely approximates instantaneous extraction of all the pore fluid in a small volume surrounding each port. We have no way of verifying this assumption, but it seems at least plausible. The samples clearly cannot be regarded as the flux-averaged concentrations described by Equation 5.26, as the sampling flow field is completely different from that driving tracer transport.

IV. FACTORS COMPLICATING THE ANALYSIS OF GEMSTRAC1

Vertical stratification of flow and transport

The breakthrough curves and concentration profiles shown in Chapter 4 clearly demonstrate that the tracer moved at dramatically different rates and with varying rates of spreading at different elevations in the aquifer. They also show that there appears to be at least some horizontal continuity in the flow and transport parameters. In order to apply the Moench model to GEMSTRAC1, we must assume that the flow and transport are horizontally stratified, so that each elevation in the aquifer can be treated as if it were a very thin confined aquifer. In this case we assume that the total discharge rate is distributed in the vertical in accordance with the vertical distribution

of horizontal hydraulic conductivity, so that each elevation, z, is characterized by a particular flow rate per unit pore-thickness

$$q_0(z) = \frac{Q}{nb}(z) \tag{5.29}$$

and by a particular dispersivity, $\alpha_L(z)$. The entire ratio on the right-hand side of Equation 5.29 is written as a function of z to indicate that not only flux rate but also porosity may vary with depth. As described further below, the format of GEMSTRAC1 has not allowed us to obtain an independent estimate of porosity. Instead, the porosity must be incorporated into the unknown parameters q_0, C_i, and μ_i.

In the initial round of analysis the breakthrough curve from each port is fitted with a different set of parameters. These can be regarded as apparent parameters applying to the flow path from the injection well to the particular port. Consistency among fitted parameters for ports at similar elevations would indicate that the stratified flow and transport assumption is at least plausible and the fitted q_0 values could be taken as a reflection of the vertical distribution of hydraulic conductivity. This approach is very similar to that taken by Thorbjarnarson and Mackay (1994) in their analysis of the induced gradient tracer test at the Borden site. A second round of fitting will involve attempts to simultaneously fit breakthrough curves from similar depths with a single set of parameters.

Nonuniform vertical distribution of mass

It is clear from the results presented in Chapter 4 that the injection process did not create a uniform distribution of mass in the vertical. Instead, most of the mass entered the lower half of the aquifer, particularly the high conductivity zones centered around 2 and 4 meters above datum, with very little mass entering the upper portion of the aquifer. Furthermore, it seems reasonable to expect that the

injection radius also varied with depth. This implies that both the reference concentration (Equation 5.25) and the injection zone mixing factor (Equation 5.23) must also vary with depth. Ideally these factors would be known, so that breakthrough curves could be analyzed in terms of a two-parameter model involving only q_0 and α_L. The inclusion of C_i and μ_i as unknown parameters leads to a four-parameter model with high parameter correlations in many cases.

Inadequate sampling during early stages of the test

As described in Chapter 4, portions of the tracer plume moved much more rapidly than we had anticipated. As a result, we missed the peak concentration at a number of ports in samplers TMC-1 through TMC-3, catching only the falling limb of the breakthrough curve. The lack of information concerning the timing and magnitude of the peak concentration, along with the parameter correlations inherent in the four-parameter transport model, leads to highly nonunique fits for these particular ports.

V. SENSITIVITY ANALYSIS OF REVISED TRANSPORT MODEL

This section explores the sensitivity of modeled concentrations to the four model parameters, C_i, q_0, α_L, and μ_i. For the sake of generality, we will examine dimensionless normalized sensitivities, describing the change in dimensionless concentration induced by a ratio change in a parameter value. A raw sensitivity coefficient (McElwee, 1982; Knopman and Voss, 1987) is given by the first derivative of the response with respect to a parameter. For example, the sensitivity of concentration to q_0 is given by $\partial C(r,t)/\partial q_0$. As described in McElwee *et al.* (1995), normalization is performed by multiplying the sensitivity coefficient by the parameter value itself, so that the normalized sensitivity to q_0 is given by

$$q_0 \frac{\partial C(r,t)}{\partial q_0} = \frac{\partial C(r,t)}{\partial q_0 / q_0} \tag{5.30}$$

The second form shows that the normalized sensitivity describes the response to a small ratio change in a parameter. A normalized sensitivity coefficient has the same dimensions as the response variable, allowing normalized sensitivities to different parameters to be compared on the same scale.

In this study we will look at dimensionless sensitivity coefficients, produced by dividing normalized sensitivities by the reference concentration, C_i. The dimensionless normalized sensitivities can be expressed entirely in terms of the dimensionless parameters appearing in Equation 5.10, revealing the fundamental sensitivity behavior of the model (McElwee *et al.*, 1995). For example, the dimensionless normalized sensitivity to q_0 is given by

$$\left(q_0 \frac{\partial C}{\partial q_0} \right) \Big/ C_i = q_0 \frac{\partial (C/C_i)}{\partial q_0} = q_0 \frac{\partial C_D}{\partial q_0} = q_0 \frac{\partial C_D}{\partial t_D} \frac{\partial t_D}{\partial q_0} \tag{5.31}$$

The chain rule has been used for the right-most equality, in order to isolate the dimensionless derivative $\partial C_D / \partial t_D$. Combining Equations 5.8 and 5.29 yields the relationship between advective travel time and q_0 for a given layer:

$$t_a = \pi \left(r_L^2 - r_w^2 \right) / q_0 \tag{5.32}$$

so that the factor multiplying $\partial C_D / \partial t_D$ in Equation 5.31 reduces to t_D:

$$q_0 \frac{\partial t_D}{\partial q_0} = q_0 \frac{\partial}{\partial q_0} \left(\frac{t}{t_a} \right) = q_0 \frac{\partial}{\partial q_0} \left(\frac{q_0 t}{\pi \left(r_L^2 - r_w^2 \right)} \right) = \frac{q_0 t}{\pi \left(r_L^2 - r_w^2 \right)} = \frac{t}{t_a} = t_D \tag{5.33}$$

Thus, the dimensionless normalized sensitivity to q_0 is given by

$$q_0 \frac{\partial C_D}{\partial q_0} = t_D \frac{\partial C_D}{\partial t_D} . \tag{5.34}$$

The dimensionless normalized sensitivity to the reference concentration is simply the dimensionless concentration itself, as shown by

$$\left(C_i \frac{\partial C}{\partial C_i} \right) \Big/ C_i = \frac{\partial C}{\partial C_i} = C_D . \tag{5.35}$$

The dimensionless normalized sensitivity to dispersivity is the negative of the normalized sensitivity of C_D to Pe, since

$$\begin{aligned} \left(\alpha_L \frac{\partial C}{\partial \alpha_L} \right) \Big/ C_i &= \alpha_L \frac{\partial C_D}{\partial \alpha_L} = \alpha_L \frac{\partial C_D}{\partial Pe} \frac{\partial Pe}{\partial \alpha_L} \\ &= \alpha_L \frac{\partial C_D}{\partial Pe} \left(-\frac{r_L}{\alpha_L^2} \right) = -\frac{r_L}{\alpha_L} \frac{\partial C_D}{\partial Pe} = -Pe \frac{\partial C_D}{\partial Pe} \end{aligned} . \tag{5.36}$$

Finally, the dimensionless normalized sensitivity to μ_i is given simply by

$$\left(\mu_i \frac{\partial C}{\partial \mu_i} \right) \Big/ C_i = \mu_i \frac{\partial C_D}{\partial \mu_i} \tag{5.37}$$

because μ_i is already a dimensionless parameter.

Like the concentration, each sensitivity is a function of radius and time. The set of sensitivities computed at the discrete observation times and locations can be collected into a matrix, termed the Jacobian matrix, in which each column represents the sensitivity to a particular parameter and each row represents a particular observation. That is,

the i,jth element of the Jacobian, $[J]_{i,j}$, represents the sensitivity of observation i to parameter j. The Jacobian contains the first-order information on the variation of the response variable with each parameter and is employed in the iterative solution of the nonlinear parameter estimation problem, as described in the next chapter.

Figure 5.5 shows the temporal behavior of the sensitivities to the four unknown parameters for a dimensionless observation radius r_D = 0.5 and a dimensionless injection duration t_{pD} = 0.01. Sensitivity curves are shown for the six different combinations of $1/Pe = \alpha_L/r_L$ = .001, .01, and .1 (from bottom to top) and μ_i = .02 (on the left) and .2 (on the right). Clearly the sensitivities vary considerably with varying parameter values, leading to changes in correlation among the four sensitivities. The magnitudes of and correlations among the sensitivities influence the variances of and correlations between the parameter estimates, because the covariance matrix for the parameters can be estimated as (McElwee et al, 1995; Beck and Arnold, 1977)

$$V \cong \sigma^2 (J'J)^{-1} \tag{5.38}$$

where J' is the transpose of the Jacobian and σ^2 represents the error variance of the measurements. That is, apart from the constant σ^2, the parameter covariance matrix is approximated by the inverse of the inner product of the Jacobian matrix with its transpose. Using a matrix of dimensionless normalized sensitivities in 5.38 yields a matrix, V, containing normalized variances and covariances, such as $Var[C_i]/C_i^2$ and $Cov[C_i, q_0]/C_i q_0$. The square root of each diagonal element of V is the coefficient of variation (the standard deviation of the estimate divided by the estimate itself) for the corresponding parameter.

In general, low overall sensitivities to a given parameter lead to a high estimation variance in that parameter and high correlations among the sensitivities lead to high correlations among the

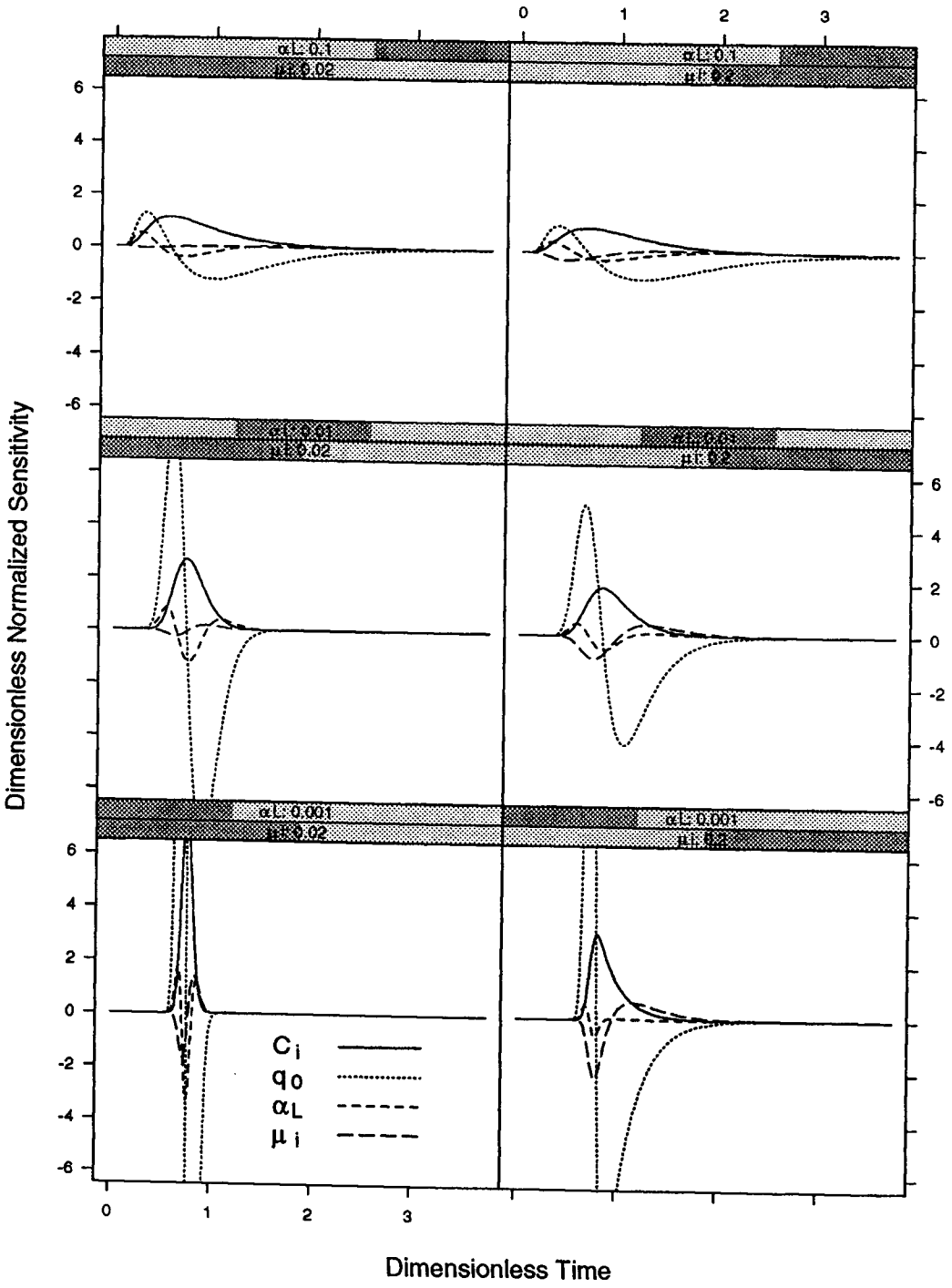

Figure 5.5. Sensitivities to four unknown parameters at $r_D = 0.5$.

parameters. A high correlation between two parameters implies that the parameters have a similar influence on the measured responses, reducing the investigator's ability to obtain independent estimates of these parameters. Sensitivity magnitudes and correlations among sensitivities interact. For example, a parameter associated with a low overall sensitivity which is strongly correlated with the sensitivity to another parameter will have a higher estimation variance than a parameter associated with a comparably low but relatively independent sensitivity.

Tables 5.1 through 5.7 show the coefficients of variation (main diagonal) for the parameter estimates and the parameter correlations (upper triangle) computed under a number of different scenarios. The coefficients of variation have all been computed using a data standard deviation of $\sigma = 0.1$ (a data variance of $\sigma^2 = 0.01$). The value of σ is somewhat immaterial to a comparative analysis as presented here, because the parameter correlations are unaffected by σ and the coefficients of variation all scale uniformly with σ. In addition, all the results have been computed using a dimensionless injection duration of $t_{pD} = 0.01$. This corresponds to the actual injection time of two hours divided by an advective travel time of 200 hours (8.3 days), which is approximately representative of average conditions for GEMSTRAC1. Analyses were also carried out using $t_{pD} = .07$, which corresponds roughly with the largest values of q_0 estimated from the actual test. The latter results did not differ significantly from those for $t_{pD} = .01$, shown here.

Table 5.1 shows the coefficients of variation and parameter correlations corresponding to the sensitivity curves shown in Figure 5.5, which represent a dimensionless observation radius of 0.5. These results have been computed using a dense and extensive temporal sampling scheme, with 250 samples ranging in dimensionless time from 0.015 to 3.75 in increments of 0.015. This will be referred to as "full temporal sampling", since it represents almost continuous

Table 5.1. Coefficients of variation (main diagonal) and parameter correlations (upper triangle) for $r_D = 0.5$ with full temporal sampling.

A. μ_i=.02, α_L/r_L=.001	C_i	q_0	α_L	μ_i
C_i	0.009	0.705	-0.527	0.709
q_0		0.005	-0.937	0.994
α_L			0.049	-0.939
μ_i				0.215
B. μ_i = .02, α_L/r_L = .01	C_i	q_0	α_L	μ_i
C_i	0.708	1.000	-0.997	1.000
q_0		0.709	-0.998	1.000
α_L			0.409	-0.998
μ_i				27.7
C. μ_i = .02, α_L/r_L = .1	C_i	q_0	α_L	μ_i
C_i	0.520	0.999	0.988	1.000
q_0		0.522	0.985	1.000
α_L			0.311	0.987
μ_i				20.9
D. μ_i = .2, α_L/r_L =.001	C_i	q_0	α_L	μ_i
C_i	0.013	0.500	-0.090	0.669
q_0		0.002	-0.414	0.706
α_L			0.080	-0.529
μ_i				0.028
E. μ_i = .2, α_L/r_L = .01	C_i	q_0	α_L	μ_i
C_i	0.024	0.822	-0.574	0.848
q_0		0.015	-0.845	0.964
α_L			0.093	-0.843
μ_i				0.107
F. μ_i = .2, α_L/r_L = .1	C_i	q_0	α_L	μ_i
C_i	0.850	1.000	-0.993	1.000
q_0		0.853	-0.994	1.000
α_L			0.533	-0.993
μ_i				4.500

sampling over the range of significant sensitivities for all the cases shown in Tables 5.1 through 5.7.

Table 5.1 shows that the ability to obtain reliable and independent estimates of the four parameters depends strongly on the interaction between the injection zone mixing factor and the dispersivity. Not only is it difficult to distinguish between these two mixing processes, the inclusion of both factors as unknowns contributes to high correlations among the other parameters. In three of the six cases shown (cases B, C, and F in the table), it is clearly impossible to obtain independent estimates of all four parameters, because all the estimates are essentially perfectly correlated. Based on the arguments above, it is expected that the larger mixing factor value of $\mu_i = 0.2$ is more appropriate for GEMSTRAC1 than the lower value. In this case, the sensitivity analysis indicates that it may be possible to obtain reliable parameter estimates for low to moderate dispersivity values, but not for higher dispersivity values. This does not bode well for model fitting, because all four of these factors are truly unknown in GEMSTRAC1. Results are similar or slightly worse when observations are obtained at $r_D = 0.1$ (Table 5.2) and slightly better, although still not very promising, when observations are obtained at $r_D = 0.9$ (Table 5.3). Observations obtained at $r_D = 0.9$ are more likely to be influenced by deviations of the injection process from the ideal conditions specified in the model, somewhat reducing their utility.

The behavior of the inverse problem improves considerably if the mixing factor is removed from the analysis and is specified as known. Table 5.4 shows the coefficients of variation and parameter correlations for full temporal sampling at $r_D = 0.5$ with μ_i specified as known in each case. That is, the Jacobian matrix here has been reduced to a three-column matrix containing the sensitivities to C_i, q_0, and α_L. Comparing these results to those in Table 5.1 reveals the dramatic reduction in parameter variances and correlations gained by removal of μ_i from the analysis. Unfortunately, the appropriate μ_i to use for

Table 5.2. Coefficients of variation and parameter correlations for r_D = 0.1 with full temporal sampling.

A. μ_i =.02, α_L/r_L=.001	C_i	q_0	α_L	μ_i
C_i	0.009	0.662	-0.490	0.667
q_0		0.004	-0.943	0.995
α_L			0.052	-0.944
μ_i				0.247
B. μ_i = .02, α_L/r_L = .01	C_i	q_0	α_L	μ_i
C_i	8.14	1.000	-1.000	1.000
q_0		8.14	-1.000	1.000
α_L			7.86	-1.000
μ_i				412
C. μ_i = .02, α_L/r_L = .1	C_i	q_0	α_L	μ_i
C_i	0.680	1.000	0.962	1.000
q_0		0.683	0.957	1.000
α_L			0.179	0.961
μ_i				34.1
D. μ_i = .2, α_L/r_L =.001	C_i	q_0	α_L	μ_i
C_i	0.013	0.477	-0.082	0.653
q_0		0.002	-0.449	0.715
α_L			0.078	-0.540
μ_i				0.028
E. μ_i = .2, α_L/r_L = .01	C_i	q_0	α_L	μ_i
C_i	0.023	0.781	-0.543	0.817
q_0		0.013	-0.863	0.964
α_L			0.094	-0.849
μ_i				0.110
F. μ_i = .2, α_L/r_L = .1	C_i	q_0	α_L	μ_i
C_i	2.50	1.000	-1.000	1.000
q_0		2.50	-1.000	1.000
α_L			2.36	-1.000
μ_i				14.9

Table 5.3. Coefficients of variation and parameter correlations matrix for $r_D = 0.9$ with full temporal sampling.

A. μ_i =.02, α_L/r_L=.001	C_i	q_0	α_L	μ_i
C_i	0.009	0.798	-0.564	0.808
q_0		0.005	-0.877	0.982
α_L			0.033	-0.883
μ_i				0.071
B. μ_i = .02, α_L/r_L = .01	C_i	q_0	α_L	μ_i
C_i	.104	0.997	-0.688	0.997
q_0		0.106	-0.723	0.999
α_L			0.030	-0.714
μ_i				1.16
C. μ_i = .02, α_L/r_L = .1	C_i	q_0	α_L	μ_i
C_i	0.138	0.994	0.934	0.996
q_0		0.143	0.907	0.993
α_L			0.102	0.930
μ_i				1.54
D. μ_i = .2, α_L/r_L =.001	C_i	q_0	α_L	μ_i
C_i	0.143	0.628	-0.158	0.768
q_0		0.005	-0.342	0.696
α_L			0.097	-0.463
μ_i				0.025
E. μ_i = .2, α_L/r_L = .01	C_i	q_0	α_L	μ_i
C_i	0.039	0.948	-0.753	0.957
q_0		0.032	-0.848	0.972
α_L			0.108	-0.853
μ_i				0.098
F. μ_i = .2, α_L/r_L = .1	C_i	q_0	α_L	μ_i
C_i	0.140	0.992	-0.339	0.993
q_0		0.146	-0.403	0.992
α_L			0.062	-0.374
μ_i				0.348

Table 5.4. Coefficients of variation and parameter correlations for r_D = 0.5 with μ_i specified as known and full temporal sampling.

A. μ_i =.02, α_L/r_L=.001	C_i	q_0	α_L
C_i	0.006	-0.011	0.570
q_0		0.001	-0.088
α_L			0.017
B. μ_i = .02, α_L/r_L = .01	C_i	q_0	α_L
C_i	0.011	-0.026	0.535
q_0		0.003	-0.261
α_L			0.026
C. μ_i = .02, α_L/r_L = .1	C_i	q_0	α_L
C_i	0.016	0.170	0.265
q_0		0.013	-0.504
α_L			0.049
D. μ_i = .2, α_L/r_L =.001	C_i	q_0	α_L
C_i	0.010	0.053	0.419
q_0		0.002	-0.067
α_L			0.068
E. μ_i = .2, α_L/r_L = .01	C_i	q_0	α_L
C_i	0.013	0.035	0.496
q_0		0.004	-0.224
α_L			0.050
F. μ_i = .2, α_L/r_L = .1	C_i	q_0	α_L
C_i	0.017	0.176	0.262
q_0		0.014	-0.497
α_L			0.061

each breakthrough curve obtained in GEMSTRAC1 is truly unknown, so there is no way to remove this fundamental uncertainty. However, the results shown here indicate that it might be prudent to formally remove μ_i from the automated fitting process used to estimate the parameters and instead fit the three remaining parameters for several different fixed values of μ_i . Again, this will not reduce the fundamental nonuniqueness of the fits. However, it will increase the likelihood that the parameter estimation algorithm, described in Chapter 6, will produce physically reasonable results, assuming that the candidate μ_i values are reasonable. When all four parameters are analyzed simultaneously, it is quite possible for the fitting algorithm to find an "optimal" combination of parameters which is not physically plausible.

The above analyses have all employed the full temporal sampling scheme described above. The real sampling process employed in GEMSTRAC1 was far from such an ideal. The most extensive sampling was performed at TMC-7, for which there are 51 measurements beginning 5 hours after injection and ending 773 hours (32 days) after injection, with four samples per day being collected early in the test. An essentially complete breakthrough curve was obtained from every port of TMC-7 (except port 16, which never yielded a sample). Almost complete breakthroughs were also measured at TMC-8, although the rising limbs of a few of the curves were truncated. However, sampling is much less ideal in the remaining samplers, especially those downgradient, in which peak breakthroughs were missed in a number of ports. These factors greatly increase the estimation variances of the parameters and the nonuniqueness of the resulting fits. Table 5.5 contains the coefficients of variation and parameter correlations that result from using a limited temporal sampling scheme at $r_D = 0.5$, with μ_i specified as known, as in Table 5.4. This sampling scheme uses 30 measurements ranging from a dimensionless time of 0.8 to 3.7 in increments of 0.1. The very late starting time of 0.8 was chosen to reflect the worst problem in the

Table 5.5. Coefficients of variation and parameter correlations for r_D = 0.5 with μ_i specified as known and limited temporal sampling.

A. μ_i =.02, α_L/r_L=.001	C_i	q_0	α_L
C_i	11.0	1.000	1.000
q_0		0.881	1.000
α_L			11.1
B. μ_i = .02, α_L/r_L = .01	C_i	q_0	α_L
C_i	0.271	0.985	0.973
q_0		0.049	0.945
α_L			0.347
C. μ_i = .02, α_L/r_L = .1	C_i	q_0	α_L
C_i	0.787	0.993	0.977
q_0		0.297	0.957
α_L			1.03
D. μ_i = .2, α_L/r_L =.001	C_i	q_0	α_L
C_i	0.698	0.999	0.999
q_0		0.163	0.999
α_L			5.24
E. μ_i = .2, α_L/r_L = .01	C_i	q_0	α_L
C_i	0.119	0.896	0.946
q_0		0.028	0.838
α_L			0.401
F. μ_i = .2, α_L/r_L = .1	C_i	q_0	α_L
C_i	0.361	0.958	0.954
q_0		0.134	0.869
α_L			0.707

actual GEMSTRAC1 sampling process: In some zones the tracer moved much faster than expected so that we began sampling too late at many downgradient ports. Comparing Table 5.5 to Table 5.4 reveals the deleterious effects of this tardiness in sampling. The coarseness of sampling also has some influence on the results, but is not nearly as serious a deficiency as the late starting time.

The above analyses have assumed that the breakthrough curve from each port will be analyzed separately to determine an optimal set of parameters associated with the breakthrough at that port. This is not an unreasonable approach for GEMSTRAC1, because one cannot assume that a given "horizontal" row of ports actually sample a single transport zone. First of all, the sample installation process did not produce perfectly horizontal rows of ports, and secondly there is no guarantee that the transport zones (if they exist) are perfectly horizontal. However, if a certain set of ports could be assumed to fall in a single transport zone, then the breakthrough curves from these ports could be analyzed simultaneously to obtain a single set of parameters. The simultaneous analyses of observations from different radii greatly increase the accuracy and independence of the parameter estimates, as shown in Table 5.6, containing results associated with simultaneous analysis of breakthrough curves obtained at r_D = 0.1, 0.5, and 0.9 using the full temporal sampling scheme and including all four unknown parameters in the analysis. Comparing these results to those in Tables 5.1 through 5.3 reveals that the use of multiple observation radii vastly improves the independence and accuracy of the parameter estimates, allowing simultaneous estimation of all four parameters in all cases. In particular, inclusion of information on the radial variation of the breakthrough curves enables one to distinguish the influence of dispersion from that of injection zone mixing. Even using the limited temporal sampling, as shown in Table 5.7, fitting of the four-parameter model is still viable if multiple observation radii are employed (although the correlations between μ_i and q_0 are rather high in most cases).

Table 5.6. Coefficients of variation and parameter correlations for r_D = 0.1, 0.5, and 0.9 with full temporal sampling.

A. μ_i =.02, α_L/r_L=.001	C_i	q_0	α_L	μ_i
C_i	0.004	0.229	0.355	0.284
q_0		0.001	-0.412	0.822
α_L			0.011	-0.442
μ_i				0.018
B. μ_i = .02, α_L/r_L = .01	C_i	q_0	α_L	μ_i
C_i	0.006	0.360	0.477	0.480
q_0		0.002	-0.138	0.769
α_L			0.014	0.058
μ_i				0.061
C. μ_i = .02, α_L/r_L = .1	C_i	q_0	α_L	μ_i
C_i	0.012	0.566	0.343	0.714
q_0		0.010	-0.240	0.636
α_L			0.026	0.251
μ_i				0.192
D. μ_i = .2, α_L/r_L =.001	C_i	q_0	α_L	μ_i
C_i	0.007	0.460	-0.054	0.665
q_0		0.001	-0.358	0.644
α_L			0.047	-0.474
μ_i				0.014
E. μ_i = .2, α_L/r_L = .01	C_i	q_0	α_L	μ_i
C_i	0.010	0.648	-0.199	0.723
q_0		0.005	-0.641	0.876
α_L			0.038	-0.625
μ_i				0.031
F. μ_i = .2, α_L/r_L = .1	C_i	q_0	α_L	μ_i
C_i	0.019	0.815	-0.167	0.873
q_0		0.018	-0.513	0.875
α_L			0.036	-0.311
μ_i				0.071

Table 5.7. Coefficients of variation and parameter correlations for r_D = 0.1, 0.5, and 0.9 with limited temporal sampling.

A. μ_i =.02, α_L/r_L=.001	C_i	q_0	α_L	μ_i
C_i	0.019	0.356	0.094	0.273
q_0		0.007	-0.853	0.985
α_L			0.091	-0.898
μ_i				0.394
B. μ_i = .02, α_L/r_L = .01	C_i	q_0	α_L	μ_i
C_i	0.042	0.798	-0.316	0.786
q_0		0.050	-0.731	0.995
α_L			0.091	-0.729
μ_i				2.39
C. μ_i = .02, α_L/r_L = .1	C_i	q_0	α_L	μ_i
C_i	0.138	0.454	0.589	0.042
q_0		0.118	-0.371	0.889
α_L			0.276	-0.667
μ_i				6.35
D. μ_i = .2, α_L/r_L =.001	C_i	q_0	α_L	μ_i
C_i	0.025	0.521	0.300	0.452
q_0		0.004	0.090	0.507
α_L			0.207	-0.493
μ_i				0.048
E. μ_i = .2, α_L/r_L = .01	C_i	q_0	α_L	μ_i
C_i	0.034	0.579	-0.141	0.548
q_0		0.019	-0.756	0.927
α_L			0.181	-0.808
μ_i				0.150
F. μ_i = .2, α_L/r_L = .1	C_i	q_0	α_L	μ_i
C_i	0.116	0.776	-0.134	0.621
q_0		0.134	-0.691	0.957
α_L			0.346	-0.805
μ_i				0.762

In the next chapter, breakthrough curves from the centerline sampling ports will first be analyzed individually, using the optimization algorithm to produce estimates of C_i, q_0, and α_L for several different candidate values of μ_i, as described above. An attempt will then be made to identify a few transport zones based on examination of the individual fits. Breakthrough curves from ports in each transport zone will then be analyzed simultaneously in order to identify a single set of parameters characterizing that zone.

CHAPTER 6: FITTING OF TRANSPORT MODEL TO TRACER DATA

I. INTRODUCTION

This chapter presents the results of fitting the radially convergent transport model presented in Chapter 5 to the bromide breakthrough curves obtained during GEMSTRAC1. The initial analysis involves fitting breakthrough curves at individual ports, adjusting the parameters of the model to obtain a match between the observed and predicted bromide concentrations at each port. In addition, the breakthrough curves from certain groups of ports have been analyzed simultaneously, in an attempt to reduce parameter correlation and to test the assumption of stratified, horizontal transport implicit in the use of the transport model. The simultaneous analysis of multiple breakthrough curves has met with limited success: reasonably coherent results can be obtained for ports in the high-velocity zone between about 1.5 and 2 meters above datum if the injection zone mixing factor (μ_i) is allowed to take on values larger than those initially considered to be physically meaningful. Less coherent results are obtained for ports in the apparent high conductivity zones at 4 meters above datum and 4.75 to 5 meters above datum. Attempts at simultaneous analysis of breakthroughs at ports in lower conductivity zones merely serve to point out the lack of consistency in these data.

II. FITTING PROCEDURES

Nonlinear least-squares regression has been used to determine optimal parameters for producing a match between the transport model and observed breakthroughs. As described in Chapter 5, the unknown parameters in the radially convergent transport model are taken to be the reference concentration, C_i, the pumping rate per unit thickness, q_0, the longitudinal dispersivity, α_L, and the injection zone mixing factor, μ_i. Parameter correlations for this four-parameter model

are very high in many cases, causing difficulties for the parameter estimation process. In order to decrease the chances that the optimization algorithm would find physically unreasonable "optimal" values, the injection zone mixing factor was formally removed from the fitting process. Instead, the remaining three parameters were fit using three different candidate values of μ_i, 0.11, 0.22, and 0.44, and the best of these three results was retained as the optimal fit. These three μ_i values correspond to injection radii of 0.5 m, 1.0 m, and 2.0 m respectively (see Equation 5.23). For each μ_i value, the fitting algorithm was run four times using four different initial values for α_L (0.03 m, 0.15 m, 0.3 m, and 0.6 m) but with the same initial values for C_i and q_0 (70 mg/l and 5.6 m^2/hr, respectively). Multiple initial α_L values were used to help compensate for the relative insensitivity of model results to α_L (see Tables 5.4 and 5.5).

The parameters were estimated using the S-Plus function nlregb, which performs bounded nonlinear least-squares regression (Statistical Sciences, 1995). The nlregb function uses the "trust-region" algorithm described by Dennis *et al.* (1981) and Gay (1984) to minimize the least-squares objective function given by

$$f(\mathbf{p}) = \sum_{i=1}^{n} [y_i - g_i(\mathbf{p})]^2 \qquad (6.1)$$

where y_i represents one of the n observed data values and $g_i(\mathbf{p})$ represents the modeled response corresponding to observation *i* using the set of parameters represented by the vector **p**. In this application, y_i represents an observed concentration and $g_i(\mathbf{p})$ represents the modeled concentration at the corresponding port location and measurement time based on the current values of C_i, q_0, and α_L. The algorithm iteratively adjusts the parameter values, beginning from the user-specified initial values, in order to reduce $f(\mathbf{p})$. Like many other nonlinear regression algorithms, the nlregb algorithm employs the Jacobian matrix (described in Chapter 5) to compute the gradient and an

approximate Hessian (second derivative matrix) of f(**p**), using these values to determine the parameter update vector at each iteration. In this application, the Jacobian is computed using a finite-difference approximation, perturbing each parameter in turn and determining the resulting change in computed concentration.

Once the final parameter estimates are determined, the approximate covariance matrix of the parameters can be computed as

$$V \cong \sigma^2 (J'J)^{-1} \tag{6.2}$$

where J is the Jacobian matrix computed using the final parameter values and σ^2 is the estimated data variance. Equation 6.2 will yield a good approximation of the parameter covariance matrix if the residuals are small and the behavior of g(**p**) is nearly linear with respect to parameter variations in the vicinity of the optimal parameter values. The approximation will be worse for larger residuals and increasing nonlinearity in g(**p**). Hopefully the residuals will be fairly small in the vicinity of the optimal parameters. Large residuals are often indicative of systematic lack-of-fit, in which case the applicability of g(**p**) and thus of Equation 6.2 should be questioned anyway.

III. RESULTS FOR INDIVIDUAL PORT FITS

Figures 6.1 through 6.8 show the observed breakthrough curves for the ports along the network centerline, along with fitted breakthrough curves for most ports. Each plot is scaled relative to the maximum observed concentration at that port, which is noted on the plot. No fitting was done for ports showing a peak concentration less than 1 mg/l. It is interesting to note, however, that some evidence of tracer breakthrough is apparent even at some of these low-concentration ports, for example, port 16 of TMC-3 (Figure 6.6). At several ports with peak concentrations of 1 to 2 mg/l, such as port 17 of

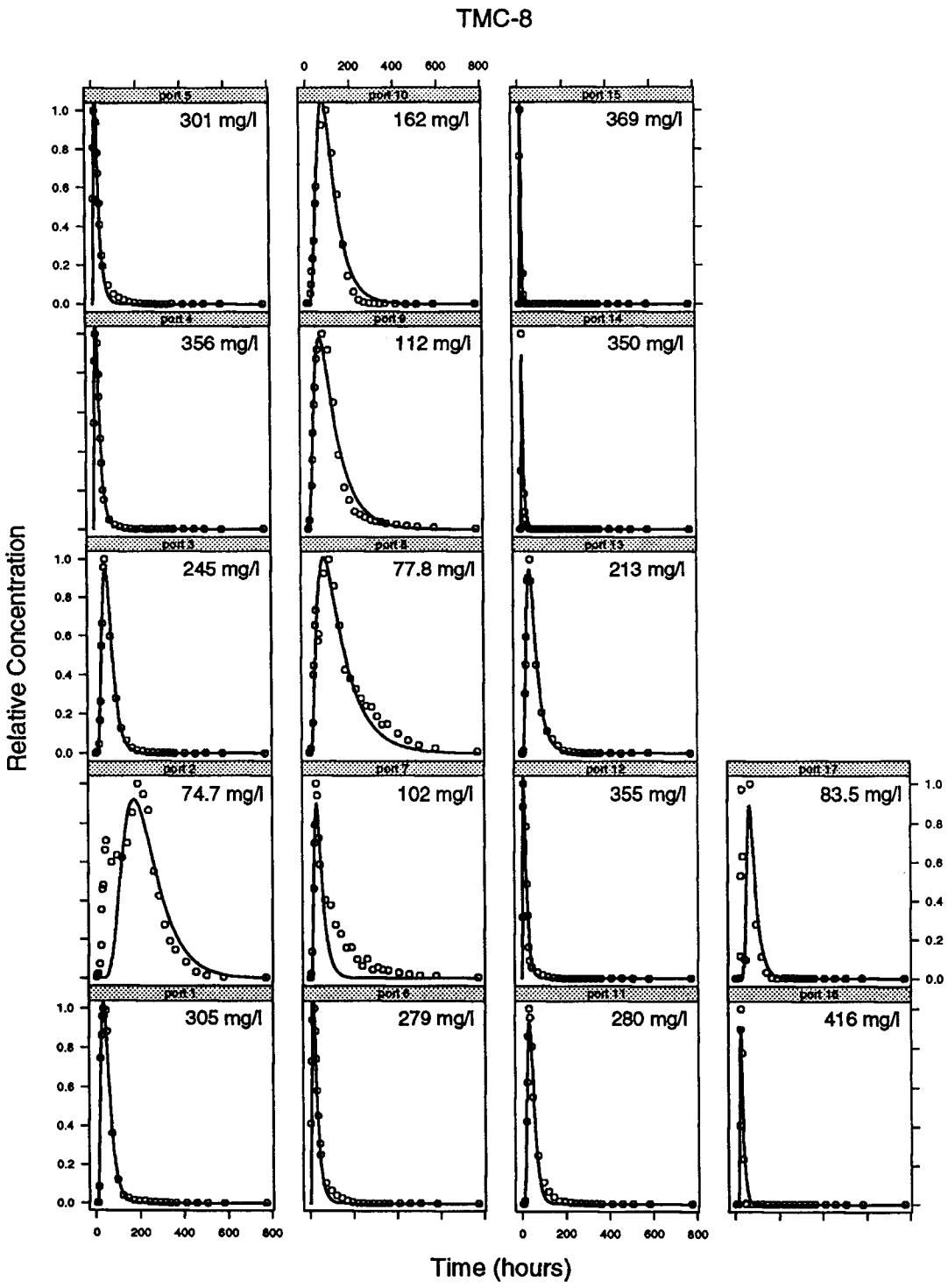

Figure 6.1. Fitted breakthrough curves at TMC-8. Scale is relative to maximum observed concentration, which is noted in each panel.

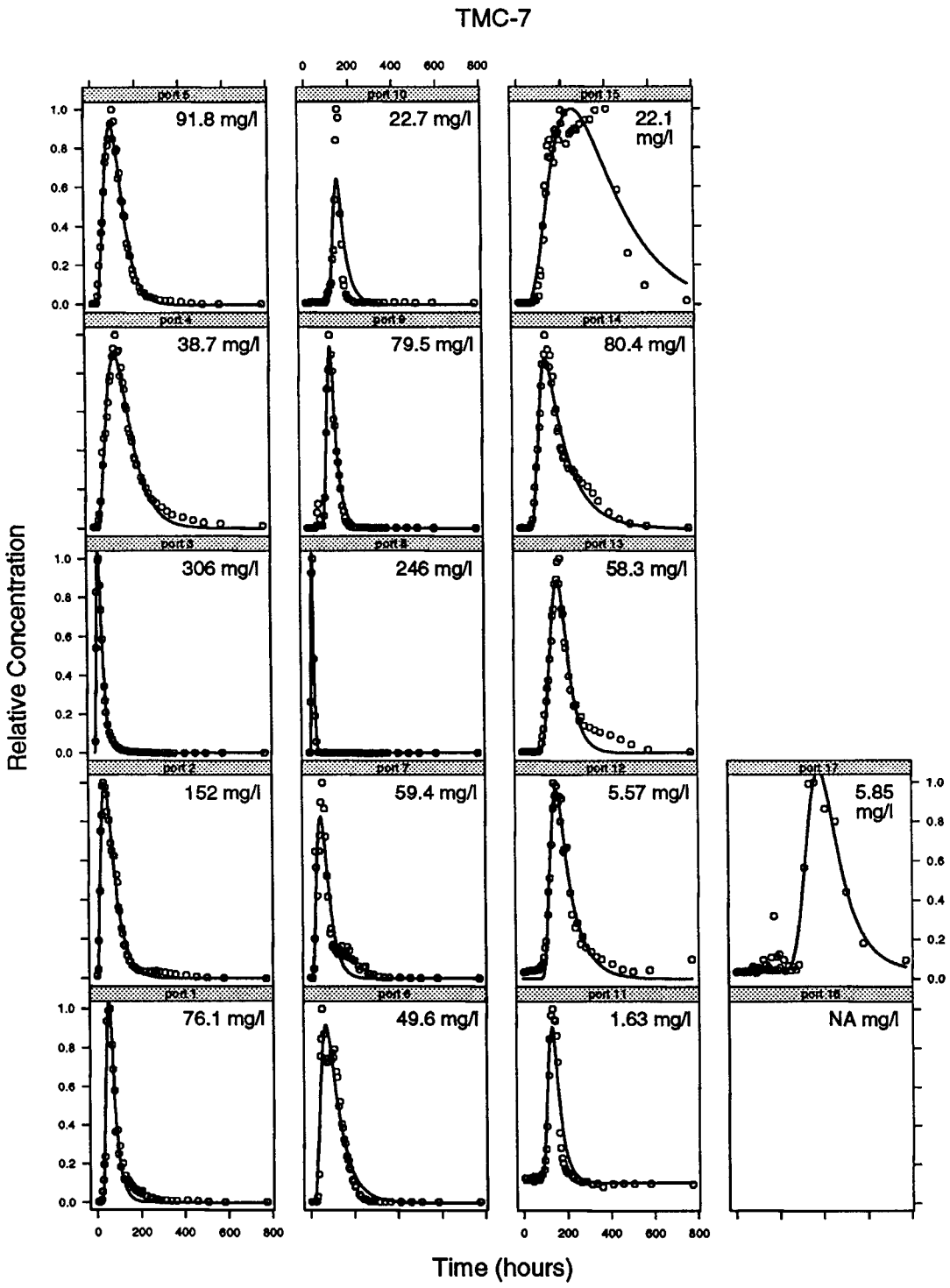

Figure 6.2. Fitted breakthrough curves at TMC-7.

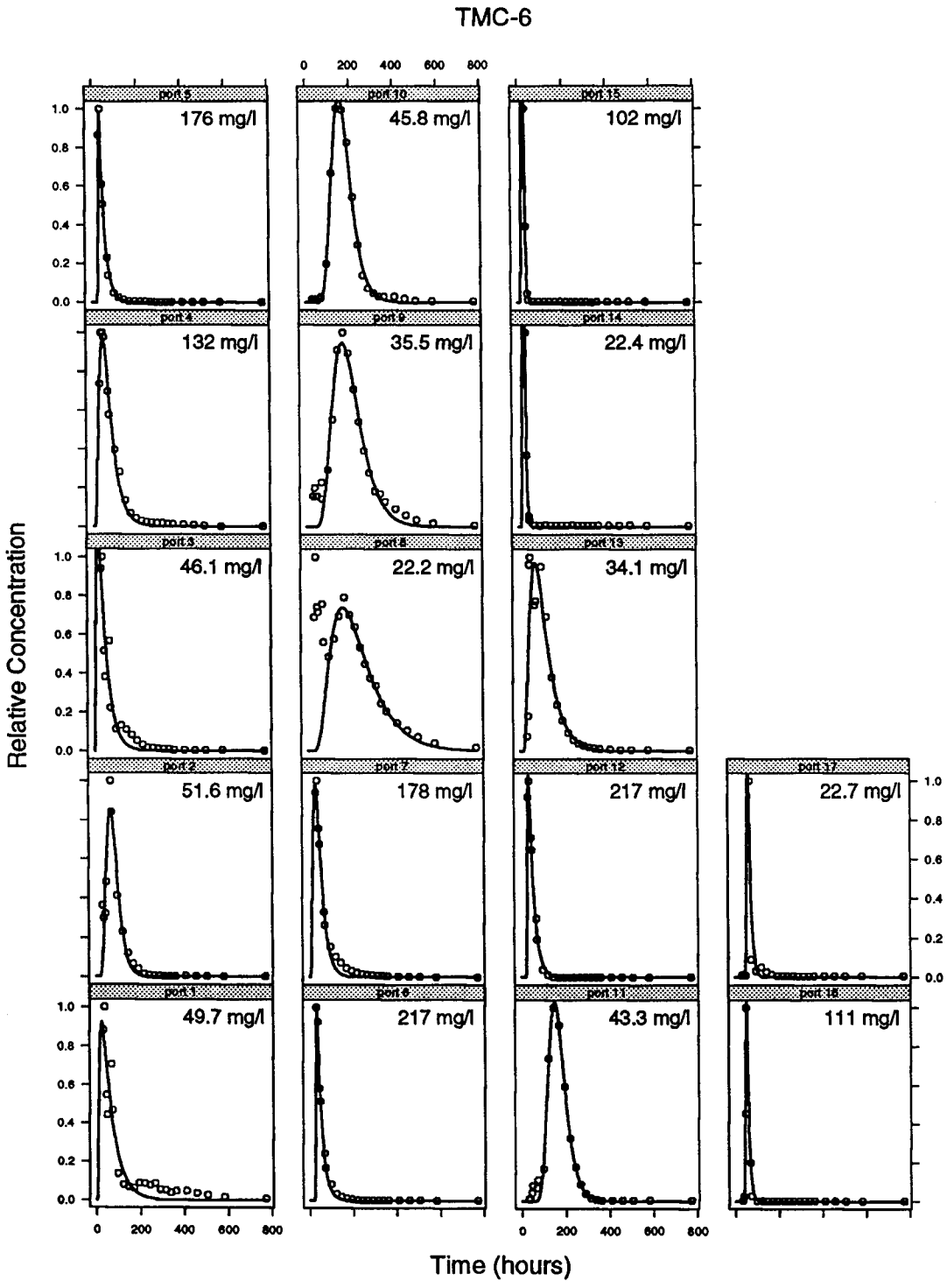

Figure 6.3. Fitted breakthrough curves at TMC-6.

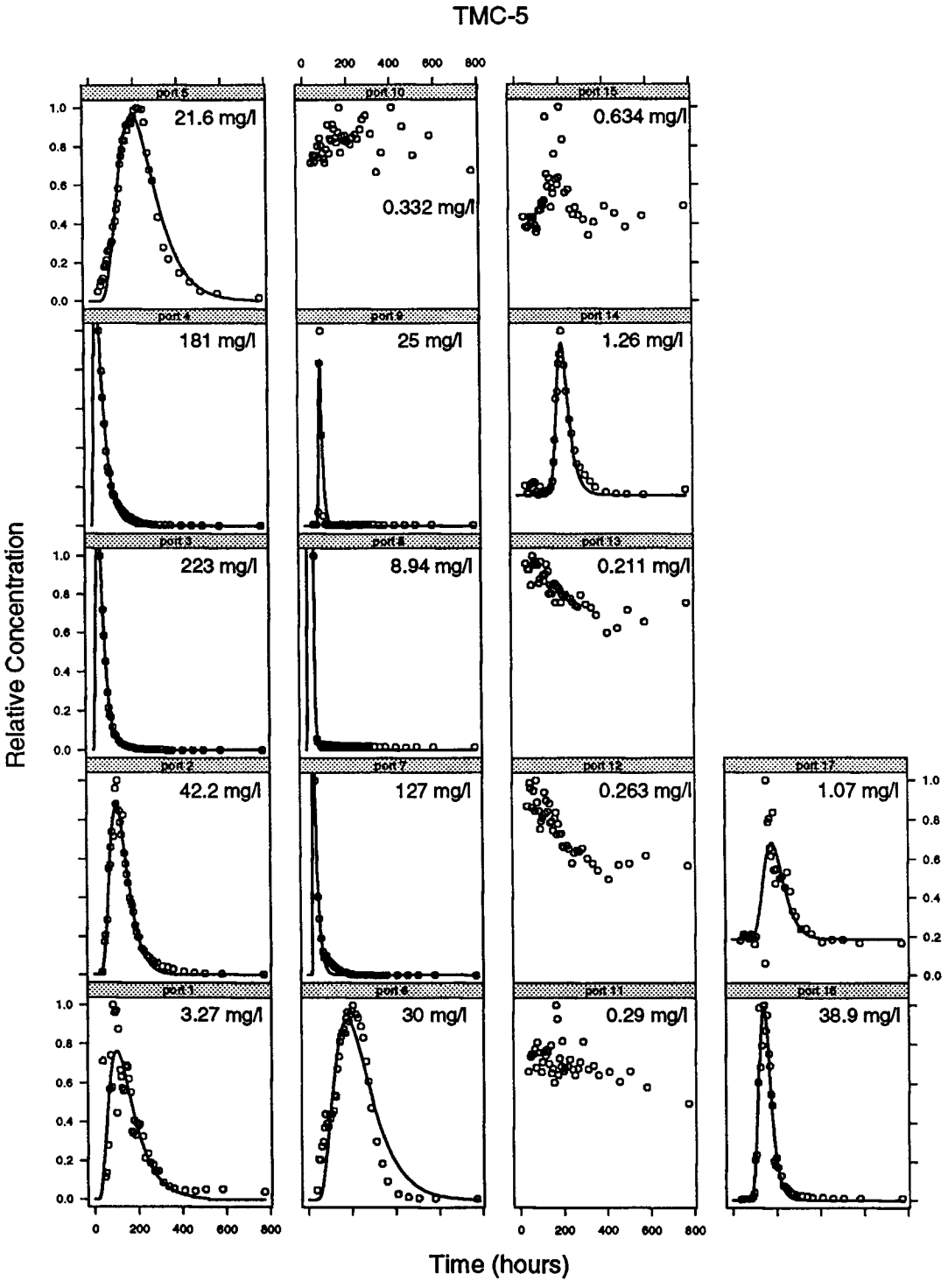

Figure 6.4. Fitted breakthrough curves at TMC-5.

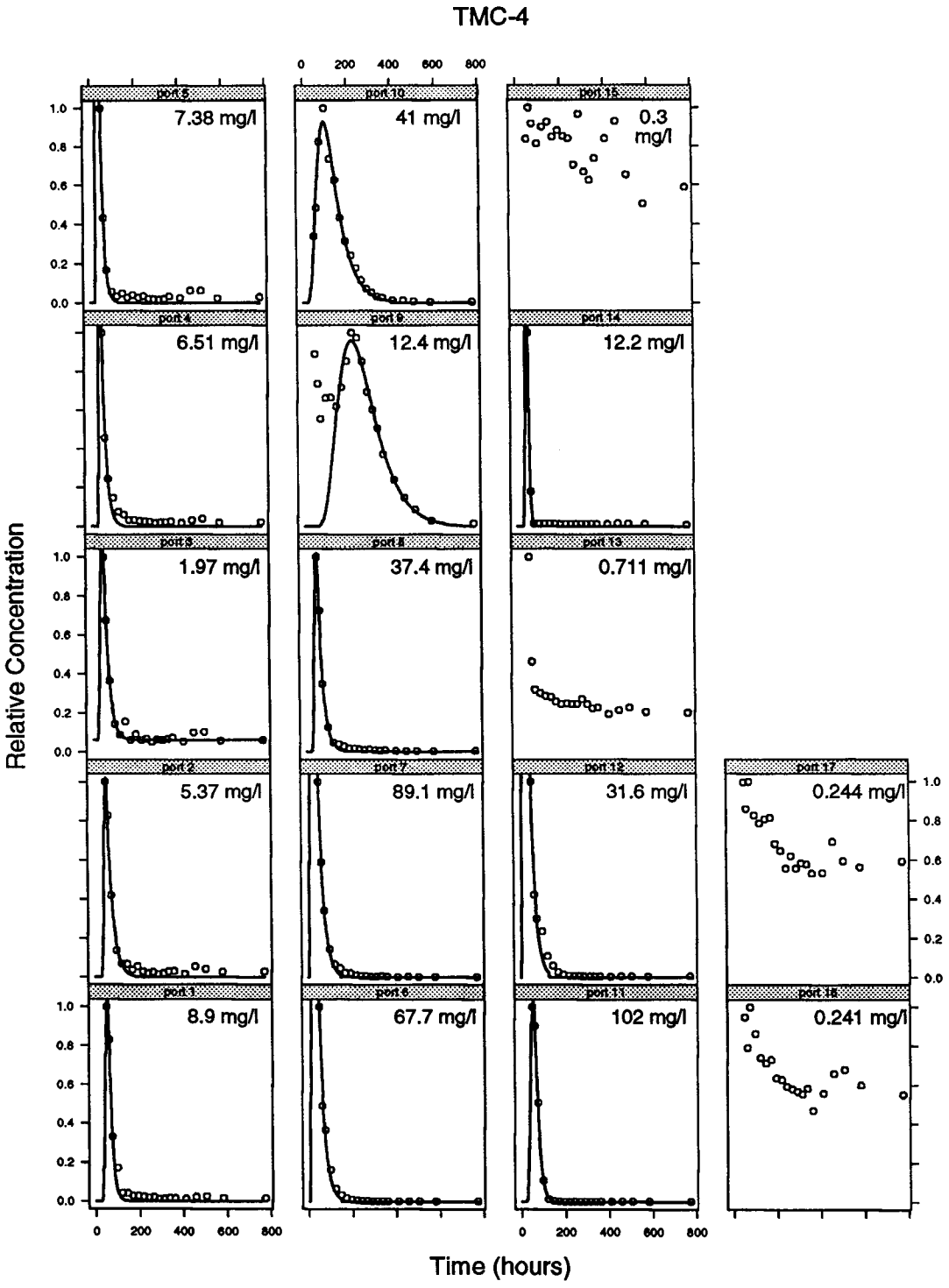

Figure 6.5. Fitted breakthrough curves at TMC-4.

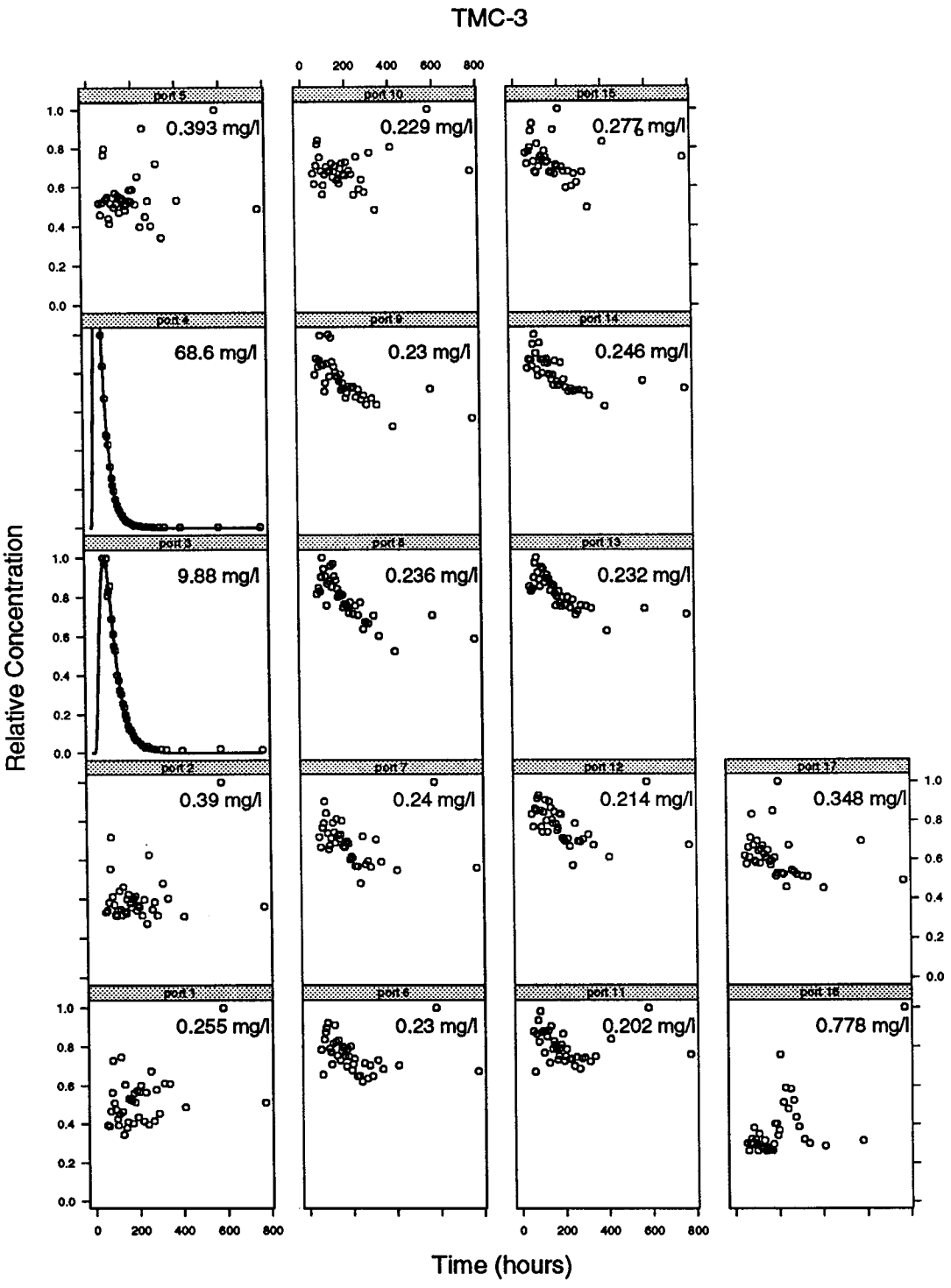

Figure 6.6. Fitted breakthrough curves at TMC-3.

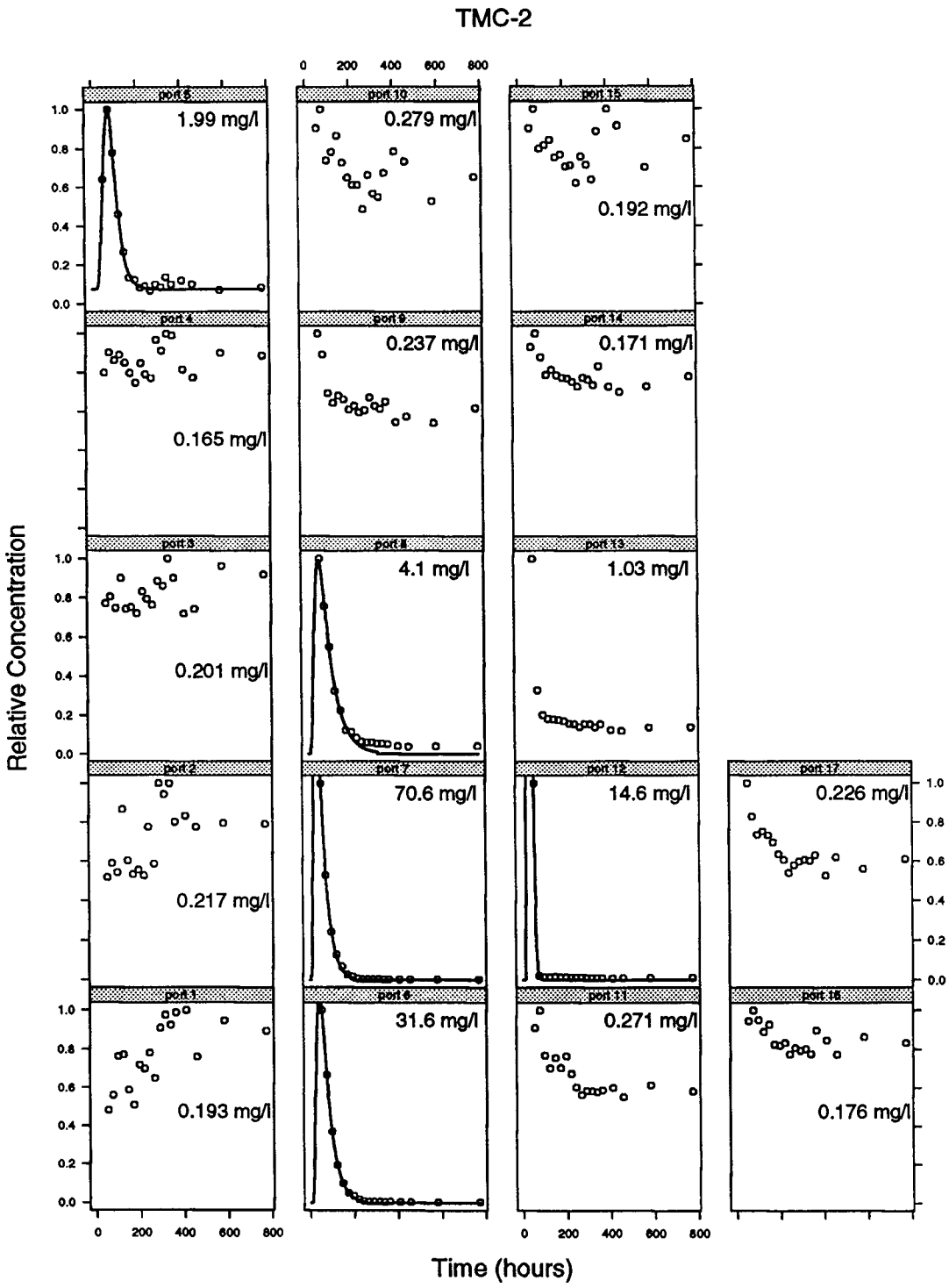

Figure 6.7. Fitted breakthrough curves at TMC-2.

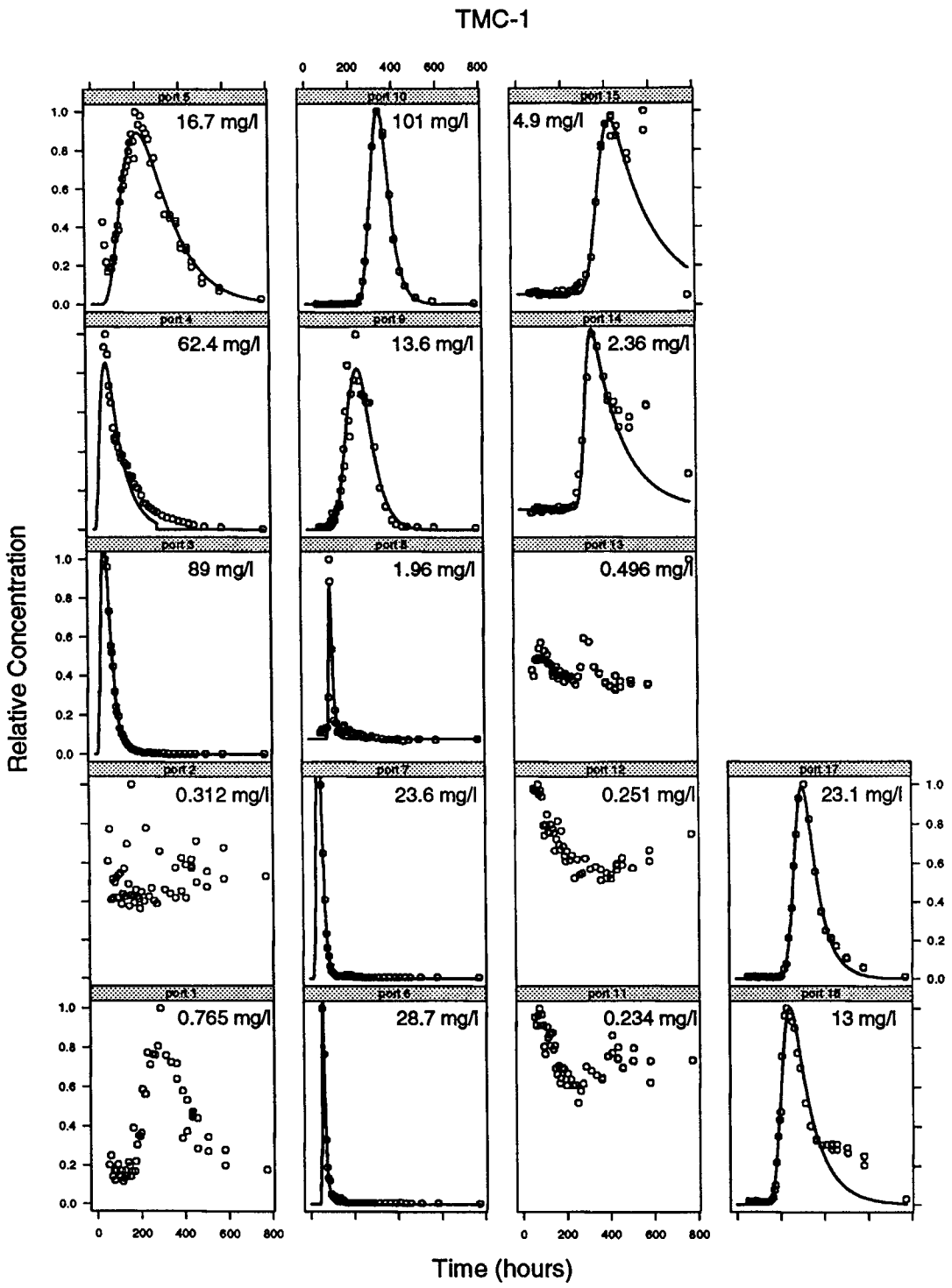

Figure 6.8. Fitted breakthrough curves at TMC-1.

TMC-5 (Figure 6.4), an estimated background concentration was subtracted from the observed concentration values prior to fitting. This background concentration was estimated by eye from the observed data. No attempt was made to estimate background concentration at ports with higher concentrations, because the correction would have little influence on the fits at these ports.

Figures 6.1 through 6.8 show that the fitted and observed breakthrough curves match quite well at many of the ports. However, there are two kinds of systematic lack-of-fit apparent at a number of ports: dual-peaked behavior and excessive tailing. One of the clearest examples of dual-peaked behavior is seen at port 2 of TMC-8 (Figure 6.1). As discussed in Chapter 4, this behavior could result from the sampling of two different velocity zones by a single port. When the breakthrough curve at a port revealed two distinct peaks, as at port 2 of TMC-8, variable weighting was used in the fitting process in order to emphasize the primary peak. Thus the fit for TMC-8, port 2, essentially ignores the earlier peak. It is possible that the excessive tailing seen at some ports, such as TMC-8, port 7, and TMC-7, port 13, is also indicative of overlapping sampling from different velocity zones. Li *et al.* (1994) describe numerical and laboratory experiments demonstrating that mixed sampling from a two-layer stratified transport system can produce behavior ranging from the presence of two distinct peaks to a single apparent peak. Between these two extremes is what Li *et al.* (1994) describe as "transitional transport", characterized by excess tailing much like that seen at TMC-7, port 13, with a distinct break in slope leading into the tail of the breakthrough curve. Variable weighting was also used to fit several of the breakthrough curves with excessive tails, in order to emphasize the peak and de-emphasize the tail.

Tables 6.1 through 6.8 show the fitted parameters for all the centerline ports where fitting was possible, along with the port elevation above datum, number of observations (n) at the port, and root-mean-squared error (rmse) for the fit. In cases where variable

Table 6.1. Fitted parameters for breakthrough curves at TMC-8, with port elevation (elev.), number of data (n) and root-mean-squared error (rmse).

port	elev. [m]	n	C_i [mg/l]	q_0 [m^2/hr]	α_L [m]	μ_i [-]	C_b [mg/l]	rmse [mg/l]
1	0.52	28	128.7	5.01	0.305	0.11	0	8.44
2	0.82	28	22.9	1.01	0.148	0.11	0	4.91
3	1.13	28	77.7	3.57	0.153	0.11	0	7.00
4	1.43	28	325.2	18.24	0.385	0.44	0	27.10
5	1.74	28	252.2	17.25	0.156	0.44	0	31.97
6	2.04	28	234.0	15.99	0.159	0.44	0	24.33
7	2.35	28	42.3	6.03	0.151	0.22	0	4.53
8	2.65	28	62.4	3.13	0.309	0.44	0	7.24
9	2.95	28	87.1	3.86	0.310	0.44	0	5.75
10	3.56	28	78.4	2.65	0.151	0.22	0	8.62
11	3.87	28	88.0	5.33	0.152	0.11	0	10.48
12	4.17	28	274.4	22.72	0.193	0.44	0	20.19
13	4.48	28	92.8	4.94	0.153	0.22	0	5.40
14	4.78	28	106.0	18.27	0.031	0.22	0	15.95
15	5.09	28	99.3	19.20	0.030	0.11	0	3.12
16	5.39	28	82.0	7.22	0.030	0.11	0	31.33
17	5.70	28	16.1	2.68	0.031	0.11	0	3.96

Table 6.2. Fitted parameters for breakthrough curves from TMC-7.

port	elev. [m]	n	C_i [mg/l]	q_0 [m^2/hr]	α_L [m]	μ_i [-]	C_b [mg/l]	rmse [mg/l]
1	0.77	50	36.4	5.85	0.093	0.22	0	3.71
2	1.38	51	154.1	8.05	0.656	0.44	0	5.04
3	1.99	51	250.1	14.86	0.764	0.22	0	4.85
4	2.60	51	23.3	2.96	0.413	0.22	0	1.80
5	3.21	51	42.6	3.01	0.327	0.11	0	3.48
6	3.82	51	37.9	5.04	0.249	0.44	0	4.30
7	4.43	51	32.1	5.93	0.375	0.22	0	5.51
8	5.04	51	88.9	15.22	0.107	0.11	0	7.99
9	5.65	51	16.4	2.70	0.021	0.11	0	2.63
10	6.26	51	3.0	1.98	0.015	0.11	0	2.56
11	6.87	47	0.3	2.25	0.031	0.11	0.17	0.13
12	7.48	47	2.0	2.00	0.033	0.22	0	0.30
13	8.09	47	15.1	1.78	0.060	0.11	0	3.12
14	8.70	47	46.6	2.81	0.070	0.44	0	4.20
15	9.31	47	13.5	0.98	0.600	0.11	0	2.39
16	9.92							
17	10.53	47	1.4	0.77	0.030	0.11	0.22	0.29

Table 6.3. Fitted parameters for breakthrough curves at TMC-6.

port	elev. [m]	n	Ci [mg/l]	q_0 [m^2/hr]	α_L [m]	μ_i [-]	C_b [mg/l]	rmse [mg/l]
1	0.37	23	46.7	9.19	3.048	0.11	0	4.99
2	0.68	23	25.4	5.54	0.345	0.11	0	4.02
3	0.98	23	54.8	12.58	3.048	0.11	0	4.08
4	1.29	23	143.6	9.70	0.721	0.44	0	4.89
5	1.59	23	97.7	12.37	0.015	0.44	0	4.36
6	1.90	23	129.5	13.11	0.023	0.44	0	3.59
7	2.20	23	196.6	14.37	0.736	0.44	0	5.56
8	2.51	23	13.9	2.30	0.686	0.22	0	0.49
9	2.81	23	19.1	2.22	0.331	0.11	0	3.13
10	3.42	23	21.1	2.47	0.157	0.11	0	0.92
11	3.72	23	17.9	2.63	0.124	0.11	0	1.45
12	4.03	23	138.8	12.55	0.036	0.44	0	3.24
13	4.33	23	35.2	6.18	0.573	0.44	0	4.36
14	4.64	23	22.1	17.71	0.106	0.11	0	0.20
15	4.94	23	93.2	17.44	0.105	0.11	0	0.91
16	5.25	23	25.0	7.85	0.015	0.11	0	2.17
17	5.55	23	5.5	6.52	0.015	0.11	0	2.29

Table 6.4. Fitted parameters for breakthrough curves from TMC-5.

port	elev. [m]	n	C_i [mg/l]	q_0 [m^2/hr]	α_L [m]	μ_i [-]	C_b [mg/l]	rmse [mg/l]
1	0.47	43	3.0	4.90	0.873	0.44	0	0.47
2	1.08	43	29.2	4.62	0.428	0.22	0	1.79
3	1.69	43	261.0	13.66	1.535	0.11	0	2.84
4	2.30	43	243.8	12.69	3.048	0.11	0	4.46
5	2.91	43	15.7	2.14	0.627	0.11	0	1.57
6	3.52	43	22.4	2.25	0.785	0.11	0	3.64
7	4.13	43	132.8	18.85	0.015	0.44	0	3.42
8	4.73	43	215.2	30.84	0.415	0.11	0	0.20
9	5.34	43	4.7	6.74	0.015	0.11	0	1.61
10	5.95							
11	6.56							
12	7.17							
13	7.78							
14	8.39	43	0.3	2.30	0.027	0.11	0.20	0.05
15	9.00							
16	9.61	43	14.2	3.37	0.083	0.11	0	2.60
17	10.22	37	0.3	2.57	0.171	0.11	0.20	0.13

Table 6.5. Fitted parameters for breakthrough curves at TMC-4.

port	elev. [m]	n	C_i [mg/l]	q_0 [m^2/hr]	α_L [m]	μ_i [-]	C_b [mg/l]	rmse [mg/l]
1	0.56	20	5.0	11.04	0.109	0.22	0	0.29
2	0.87	20	3.8	11.76	0.059	0.44	0	0.18
3	1.17	20	1.8	14.30	0.176	0.44	0.12	0.05
4	1.48	20	6.7	15.57	0.015	0.44	0	0.25
5	1.78	20	16.6	19.97	0.016	0.44	0	0.24
6	2.09	20	171.7	17.36	2.621	0.11	0.	1.94
7	2.39	20	235.2	17.36	2.792	0.11	0	1.26
8	2.69	20	29.3	12.90	0.108	0.44	0	0.64
9	3.00	20	9.3	2.22	0.621	0.11	0	0.38
10	3.61	20	45.7	6.00	0.742	0.44	0	1.40
11	3.91	20	69.5	10.84	0.217	0.22	0	0.26
12	4.22	20	106.3	19.81	3.048	0.11	0	1.58
13	4.52							
14	4.83	20	6.2	12.92	0.062	0.11	0	0.16
15	5.13							
16	5.44							
17	5.74							

Table 6.6. Fitted parameters for breakthrough curves at TMC-3.

port	elev. [m]	n	C_i [mg/l]	q_0 [m^2/hr]	α_L [m]	μ_i [-]	C_b [mg/l]	rmse [mg/l]
1	0.44							
2	1.05							
3	1.66	38	10.6	7.63	1.826	0.11	0	0.24
4	2.27	38	123.2	13.03	2.978	0.11	0	0.99
5	2.88							
6	3.49							
7	4.10							
8	4.71							
9	5.32							
10	5.93							
11	6.54							
12	7.15							
13	7.76							
14	8.36							
15	8.97							
16	9.58							
17	10.19							

Table 6.7. Fitted parameters for breakthrough curves at TMC-2.

port	elev. [m]	n	C_i [mg/l]	q_0 [m^2/hr]	α_L [m]	μ_i [-]	C_b [mg/l]	rmse [mg/l]
1	0.37							
2	0.67							
3	0.98							
4	1.28							
5	1.58	18	1.6	7.45	0.754	0.11	0.15	0.04
6	1.89	18	38.8	10.18	2.425	0.11	0	0.16
7	2.19	18	116.9	13.01	2.771	0.11	0	0.42
8	2.50	18	4.7	8.05	3.048	0.11	0	0.14
9	2.80							
10	3.41							
11	3.72							
12	4.02	18	157.3	21.95	0.332	0.11	0	0.16
13	4.33							
14	4.63							
15	4.94							
16	5.24							
17	5.55							

Table 6.8. Fitted parameters for breakthrough curves at TMC-1.

port	elev. [m]	n	C_i [mg/l]	q_0 [m^2/hr]	α_L [m]	μ_i [-]	C_b [mg/l]	rmse [mg/l]
1	0.34							
2	0.95							
3	1.56	51	100.7	11.45	1.432	0.11	0	1.31
4	2.17	51	82.6	8.68	3.048	0.44	0	3.94
5	2.78	51	17.0	2.60	1.373	0.22	0	1.56
6	3.39	51	10.8	12.52	0.015	0.22	0	0.43
7	4.00	51	28.8	16.27	0.495	0.22	0	0.26
8	4.61	51	0.4	6.60	0.015	0.11	0.15	0.09
9	5.22	51	7.0	2.75	0.302	0.11	0	0.92
10	5.83	51	34.6	1.96	0.054	0.11	0	0.96
11	6.44							
12	7.05							
13	7.66							
14	8.27	51	1.3	2.06	0.019	0.44	0.25	0.07
15	8.88	51	3.1	1.66	0.059	0.44	0.25	0.09
16	9.49	51	9.9	2.96	0.094	0.44	0	1.05
17	10.10	51	10.6	2.26	0.059	0.22	0	0.49

weighting was used during the fitting process, the rmse was recomputed without the variable weighting after the final parameters were obtained. That is, the rmse values reported in the tables reflect the actual discrepancies between the observed and modeled concentration values. Any non-zero background concentration (C_b) values shown were estimated from visual inspection of the breakthrough curve, as mentioned above. This value was subtracted from the observed concentrations prior to fitting. The "fitted" μ_i value shown for each port is whichever of the three candidate values produced the minimum fit.

Figures 6.9 through 6.12 show profiles of the estimated values of C_i, q_0, α_L, and μ_i. The profiles of C_i (Figure 6.9) and q_0 (Figure 6.10) reveal some tantalizing consistency, although it is impossible to trace zones of similar values all the way along the centerline, due primarily to the "missing" breakthroughs in the downgradient half of the centerline, especially at TMC-3 and TMC-2. These plots also reveal that GEMSTRAC1 was essentially a tracer test in the lower half of the aquifer, with almost no mass entering the upper half. If the stratified transport assumption employed in the analysis is considered valid, then the estimated q_0 values should reflect the vertical distribution of relative horizontal hydraulic conductivity. That is, the total flux to the pumping well should be distributed in the vertical in proportion to the horizontal hydraulic conductivity at each depth. The fitted q_0 values shown in Figure 6.10 do show considerable horizontal consistency, implying the presence of horizontally persistent zones of similar conductivity. The correlation of q_0 values between the first two detailed samplers, TMC-8 and TMC-6, is particularly striking. If one assumes that the narrow high-velocity zone at approximately four meters elevation (port 12 of TMC-8 and TMC-6) was simply not sampled by any port in TMC-7, then the results for TMC-7 are also quite consistent with those for TMC-8 and TMC-6.

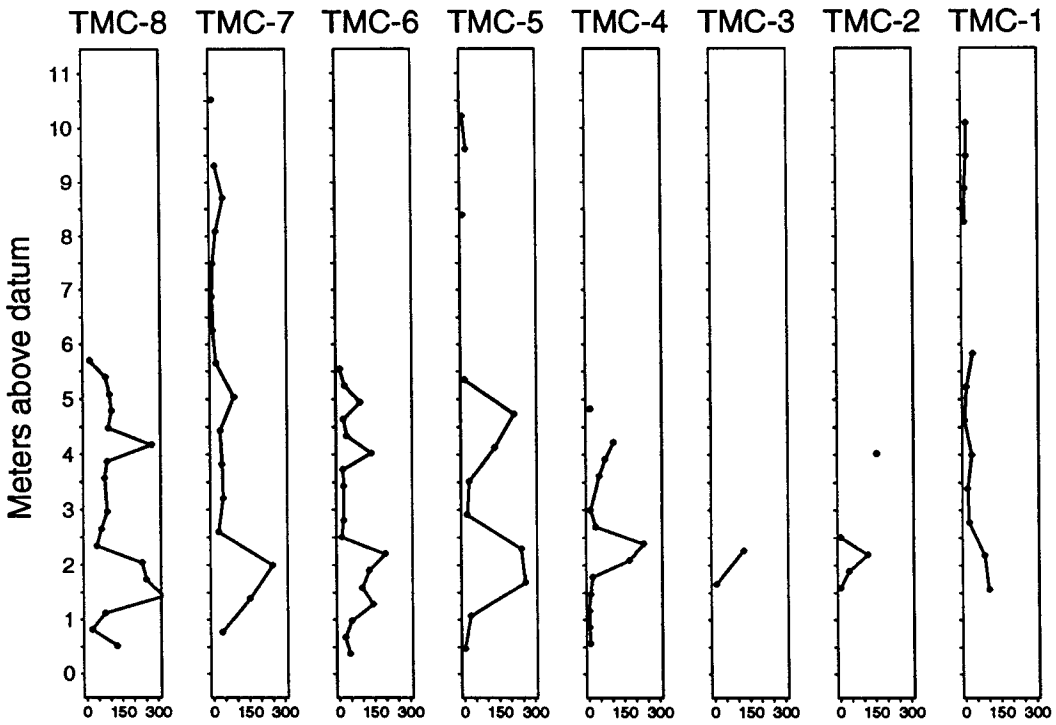

Figure 6.9. Estimated C_i values [mg/l] at centerline ports.

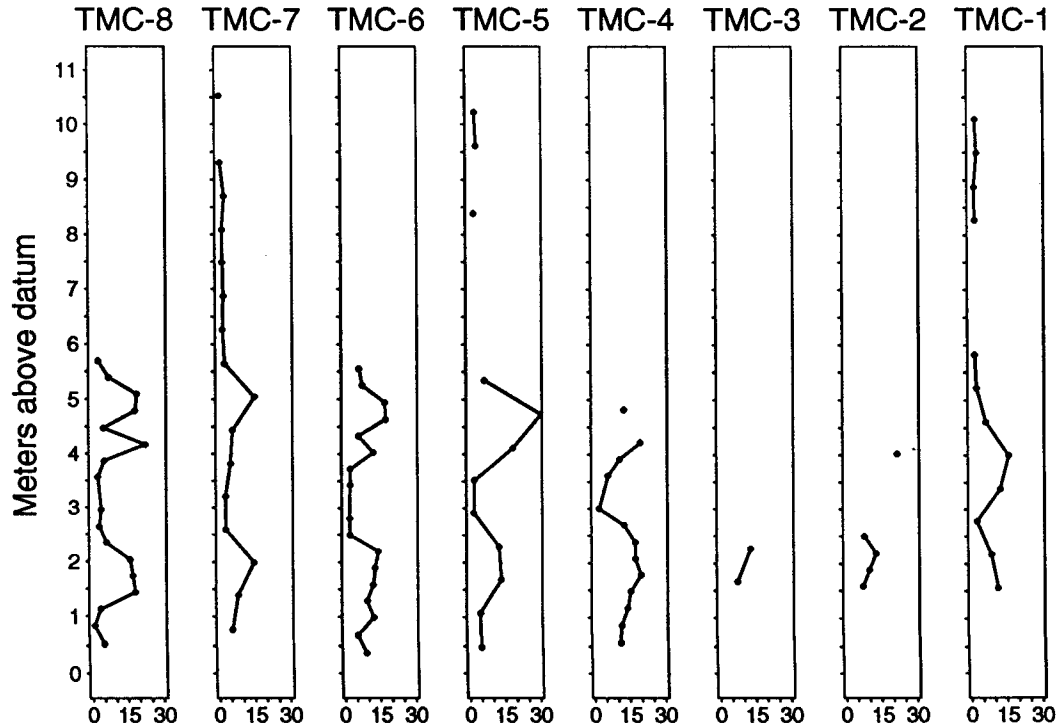

Figure 6.10. Estimated q_0 values [m^2/hr] at centerline ports.

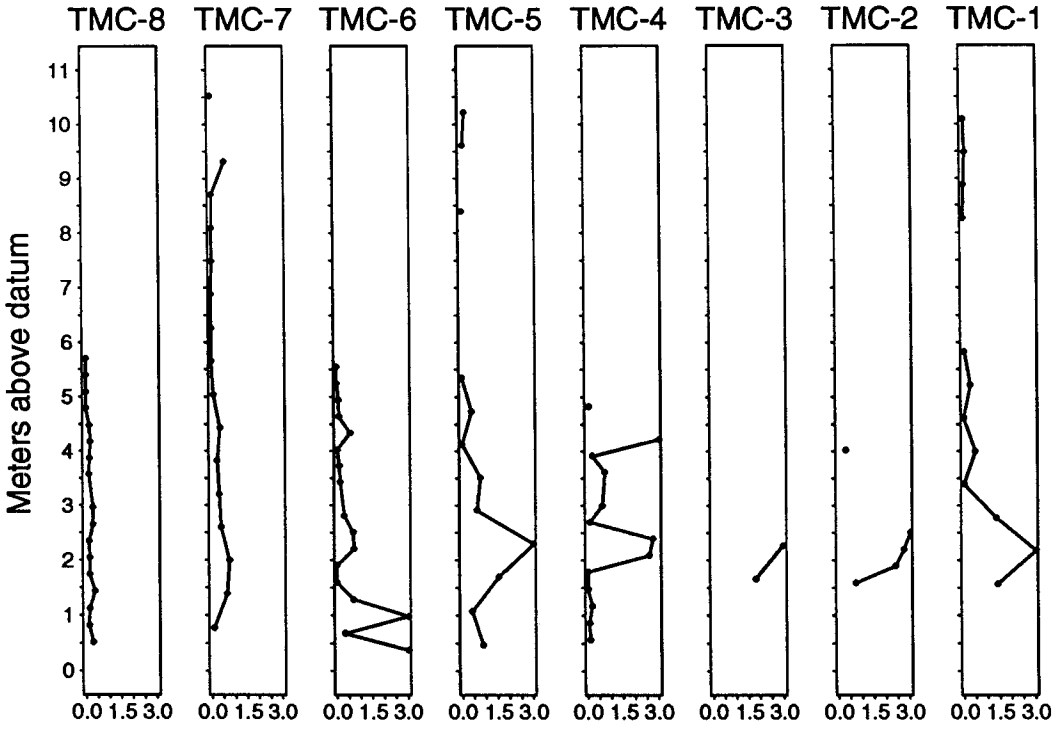

Figure 6.11. Estimated α_L values [m] at centerline ports.

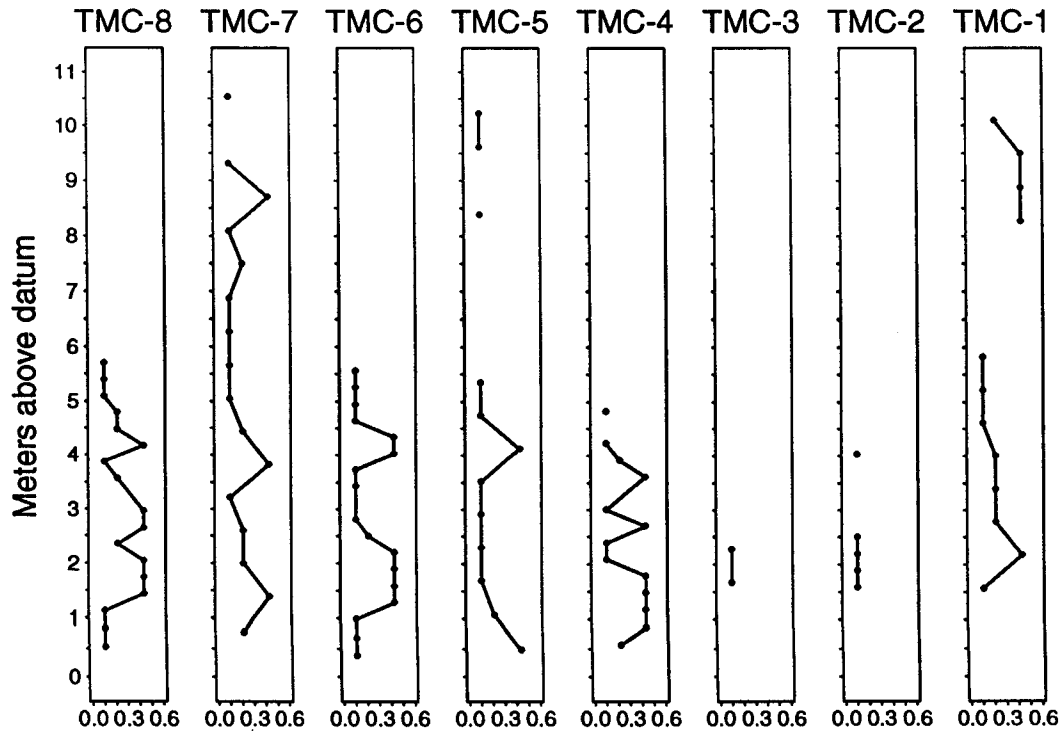

Figure 6.12. Estimated μ_i values [-] at centerline ports.

The spatial distribution of fitted C_i values (Figure 6.9) is strongly correlated with that of the fitted q_0 values, implying that most of the injected tracer entered high conductivity zones. As discussed in Chapter 4, this was a shortcoming of the test, as it resulted in undersampling of low-conductivity zones, and particularly of the upper half of the aquifer. Figures 6.9 and 6.10 seem to reveal a gradual rising of the lower high-velocity zone, represented by ports 4, 5, and 6 (from 1.4 to 2.0 meters elevation) at TMC-8. In fact, the fitted C_i values seem to indicate channeling of tracer in this zone into a narrower vertical zone, represented by ports 6 and 7 (2.1 and 2.4 meters elevation) at TMC-4. This effect also appears in the animation described in Chapter 4. Due to the coarseness of sampling at TMC-7 and TMC-5 and missing results for TMC-4 through TMC-2, it is difficult to assess the behavior of the upper two high-velocity zones, represented at TMC-8 by port 12, at 4.2 meters elevation, and ports 14 and 15, at 4.8 and 5.8 meters elevation. Nevertheless, the zone at 4 meters elevation appears to persist across the centerline, appearing as one of the few significant breakthroughs at TMC-2 (port 12, at 4.0 meters elevation) and also at port 7 (4.0 meters elevation) of TMC-1.

It may seem inconsistent to interpret the fitted parameters in terms of inclined zones of transport or channeling of tracer, as presented above, since these mechanisms clearly violate the assumption of vertically stratified horizontal transport inherent in the model used to obtain the parameters. Nevertheless, it is clear that the fitted flux rate will reflect the speed of transport from the injection well to a port and the fitted reference concentration will reflect the amount of mass reaching that port, despite deviations of the transport process from the assumed form. Deviations from purely horizontal transport, caused either by lack of perfect stratification in the conductivity distribution or by vertical diffusion of the tracer, almost certainly have influenced the parameter estimates to some extent, but the large-scale distribution of q_0 and C_i can probably still be taken as reasonable representations of the spatial distribution of flux and tracer mass.

Tables 6.9 through 6.12 present the coefficients of variation and correlations for the fitted parameters obtained at several ports. The ports have been chosen to reflect the range of variation of results. The parameter covariance matrix in each case is determined from Equation 6.2, using the mean squared error for each fit as an estimate for the data variance, σ^2. The mean squared error (mse) is the sum squared error (sse) divided by the degrees of freedom (df), given by the number of data (n), minus the number of estimated parameters. The rmse values shown in Tables 6.1 through 6.8 were computed on the basis of n, rather than df, so that the mse values employed here are related to the displayed rmse values by $mse = sse/df = (n/df)*rmse^2$.

In fact, the mean squared error almost certainly overestimates σ^2 in those cases showing significant lack-of-fit. However, we have no means of obtaining an independent estimate of σ^2, which should represent "random" (non-systematic) variation in the concentration values. An attempt was made to estimate the concentration measurement error from repeat samples at TMC-1. Unfortunately, these repeat measurements were not made until later in the test, when concentrations were low, diffuse, and slowly changing. An estimate of σ^2 based on these repeat runs would be unrealistically low. Even if these results could be taken as representative of sample repeatability for the entire test, it is likely that they would still provide underestimates of σ^2, since variability induced by the sampling process and laboratory analysis procedures represent only two contributions to the possible "random" variation in the data. That is, "sub-systematic" (effectively stochastic) aspects of the transport process itself will also contribute to σ^2.

In Tables 6.9 through 6.12, the parameter covariance values are presented in terms of correlation coefficients for easier interpretation. The parameter variances (on the main diagonal) are presented in terms of coefficients of variation, representing the standard deviation of the

Table 6.9. Correlations (upper triangle) and coefficients of variation (diagonal) for estimated parameters at TMC-7, port 5.

A. μ_i known, σ^2 = sse/df = 616.7/48 = 12.8				
	C_i	q_0	α_L	
C_i	0.014	0.075	0.460	
q_0		0.008	-0.362	
α_L			0.046	
B. μ_i unknown, σ^2 = sse/df = 616.7/47 = 13.1				
	C_i	q_0	α_L	μ_i
C_i	0.394	0.999	-0.992	0.999
q_0		0.384	-0.995	1.000
α_L			0.461	-0.995
μ_i				2.170

Table 6.10. Correlations (upper triangle) and coefficients of variation (diagonal) for estimated parameters at TMC-8, port 12.

A. μ_i known, σ^2 = sse/df = 11419/25 = 457				
	C_i	q_0	α_L	
C_i	0.044	0.332	0.513	
q_0		0.033	0.111	
α_L			0.269	
B. μ_i unknown, σ^2 = sse/df = 11419/24 = 476				
	C_i	q_0	α_L	μ_i
C_i	0.142	0.939	-0.616	0.948
q_0		0.118	-0.709	0.958
α_L			0.423	-0.761
μ_i				0.295

estimate over the estimated value itself. The coefficients of variation are proportional to σ, the estimated error standard deviation, and thus are questionable in those cases in which the mean squared error provides a poor estimate for σ^2. However, the parameter correlation values are independent of the estimate of σ.

Table 6.9 demonstrates that the identifiability of the parameters depends critically on whether the injection zone mixing factor is considered known or unknown. This table presents parameter

Table 6.11. Correlations (upper triangle) and coefficients of variation (diagonal) for estimated parameters at TMC-6, port 15.

A. μ_i known, σ^2 = sse/df = 19.0/20 = 0.95				
	C_i	q_0	α_L	
C_i	12.737	1.000	1.000	
q_0		2.692	1.000	
α_L			13.451	
B. μ_i unknown, σ^2 = sse/df = 19.0/19 = 1.00				
	C_i	q_0	α_L	μ_i
C_i	13.275	1.000	1.000	0.176
q_0		2.808	1.000	0.181
α_L			13.960	0.151
μ_i				0.226

Table 6.12. Correlations (upper triangle) and coefficients of variation (diagonal) for estimated parameters at TMC-1, port 10.

A. μ_i known, σ^2 = sse/df = 46.8/48 = 0.97				
	C_i	q_0	α_L	
C_i	0.005	0.221	0.368	
q_0		0.001	-0.154	
α_L			0.017	
B. μ_i unknown, σ^2 = sse/df = 46.8/47 = 1.00				
	C_i	q_0	α_L	μ_i
C_i	0.008	0.729	-0.471	0.714
q_0		0.003	-0.837	0.958
α_L			0.033	-0.849
μ_i				0.040

correlations and coefficients of variation for the fit to the breakthrough curve at TMC-7, port 5, where a good match to a complete breakthrough was obtained. Table 6.9A shows the parameter correlations and coefficients of variation for the case in which μ_i is considered known, i.e., when the fit is regarded as a three-parameter fit. Table 6.9B shows the corresponding values when the fit is regarded as a four-parameter fit, with μ_i considered unknown. As mentioned above, μ_i was not formally included as an unknown parameter in the optimization algorithm. Instead, the optimization algorithm was run

using three different candidate values of μ_i and the value corresponding to the best fit was retained as the estimate of μ_i. Thus, table 6.9A represents characteristics of the problem as the optimization algorithm saw it (in the neighborhood of the final parameter estimates). These three-parameter results appear to be quite good, with low parameter correlations and coefficients of variation. The maximum coefficient of variation of 4.6% (for α_L) is quite acceptable.

Unfortunately, μ_i is truly an unknown quantity and Table 6.9B is probably a more realistic representation of the reliability of the parameter estimates. The inclusion of μ_i as a fitting parameter induces strong correlation among all the parameters, implying that it is essentially impossible to obtain an independent estimate of any parameter. The high correlations contribute to the exceedingly large error bounds on the individual parameters, with coefficients of variation of 39%, 38% and 46% for C_i, q_0, and α_L, respectively, and 217% for μ_i, implying that the estimated value of μ_i (0.11 in this case) is essentially meaningless.

When looking at Tables 6.9 through 6.12, it is important to keep in mind that each table shows results for only one fit, with the corresponding parameters for each fit shown in the appropriate row in Tables 6.1 through 6.8. However, the fit is interpreted as a three-parameter fit in part A of the table and as a four-parameter fit in part B of the table.

The results shown in Table 6.9 are typical of the fits at a number of ports from TMC-8 and TMC-7, although somewhat extreme in the contrast between the three-parameter results and the four-parameter results. In fact, some of the four-parameter results, such as those for TMC-8, port 12 (Table 6.10), are much less objectionable. For the three-parameter results, the dispersivity is invariably the most poorly estimated parameter, with coefficients of variation as high as 50%. For

the four-parameter results, either α_L or μ_i exhibits the highest coefficient of variation.

High parameter correlations for the fits at TMC-8 and TMC-7 are largely a result of the inadequate characterization of the injection process, requiring the inclusion of C_i and μ_i as unknown parameters. Results at TMC-6 and TMC-5 begin to show the additional influence of the failure to sample the entire centerline early in the test. At several of the ports in TMC-6 and TMC-5 we sampled only the descending tail of the breakthrough curve, which leads to highly nonunique fits even when μ_i is considered as a known quantity, as shown by the results for TMC-6, port 15 (Table 6.11). The perfect correlations shown in Table 6.11A indicate that various combinations of C_i, q_0, and α_L could match the tail of the breakthrough curve equally well. Considering μ_i as an additional unknown does not significantly change the results for the other three parameters in this case. Results for TMC-6 and TMC-5 ports with more complete breakthrough curves are similar to those for TMC-8 and TMC-7.

Because most of the breakthrough curves obtained at TMC-4, TMC-3, and TMC-2 are incomplete, most of the corresponding fits also display very high or perfect correlations among the fitted parameters. As might be expected, the situation is worse for the earlier, sharper peaks than for the later, broader peaks. The extreme case is represented by the breakthrough at TMC-2, port 12, where only one observation has a significant concentration, 14 mg/l. Whether regarded as a three-parameter fit or a four-parameter fit, the results for this port exhibit perfect correlation among all the parameters and absurdly large coefficients of variation.

The results for TMC-1 cover the entire range of possibilities seen above, from perfect parameter correlations at port 6, where only the descending tail of the breakthrough was sampled, to the alarmingly good fits at port 10 and port 17. The correlations and coefficients of

variation for the port 10 fit are shown in Table 6.12 and those for the port 17 fit are similar. Looking at these results alone, one might conclude that the radially convergent transport model has done an excellent job of explaining the data. However, these breakthroughs seem to have appeared out of nowhere; no precursors for either of them are apparent in any of the upgradient centerline samplers. As discussed in Chapter 4, there is some evidence that significant quantities of mass might have traveled in a path that bypassed or skirted the centerline for most of the network length, possibly converging to the centerline in the vicinity of TMC-1. However, there is no evidence of significant breakthroughs at these levels in the TME samplers either (Figures 4.9 through 4.12), although our sampling of the non-centerline MLSs was too sparse to be conclusive.

IV. RESULTS FOR MULTIPLE PORT FITS

As discussed in Chapter 5, the simultaneous analysis of breakthrough curves at different radii can greatly improve the identifiability of the estimated parameters, potentially resulting in acceptable results even for the four-parameter model with limited temporal sampling (Table 5.7). Furthermore, simultaneous analysis of breakthroughs at multiple ports provides a check on the assumption of stratified horizontal transport. If this assumption were strictly valid, then it would be possible to use a single set of parameters to match breakthroughs at different ports within the same "layer" or transport zone. However, as described in Chapter 4, any attempts to match up results from different ports are complicated by the lack of horizontal alignment of ports from different samplers and, of course, by lack of perfect horizontal stratification of the actual aquifer properties, particularly the hydraulic conductivity.

This section presents the results of simultaneous analyses of breakthroughs from various groups of ports. Groups of ports that appeared to represent distinct and consistent transport zones were

initially determined from the results of the single-port fits, primarily on the basis of the estimated q_0 values and secondarily on the basis of the C_i values. Simultaneous fits were then attempted and groupings modified until a set of ports was determined that could be matched with reasonable accuracy by a single set of parameters. This exercise was only marginally successful. Reasonably consistent results could be obtained for ports in samplers closer to the injection well that were in high-velocity, high-concentration transport zones. However, the results from samplers further downgradient are inconsistent with those nearer the injection well. It was not possible to determine satisfactorily consistent results for breakthroughs at ports in lower-concentration, slower transport zones.

The fits presented here were obtained in much the same fashion as the single-port fits, except that the injection zone mixing factor was formally included as a fitting parameter in the calls to the minimization algorithm. The improved conditioning of the problem resulting from the inclusion of multiple observation radii allowed μ_i to be included as a fitting parameter. However, sixteen initial parameter vectors were employed, resulting from the combination of four initial values of α_L (0.03 m, 0.15 m, 0.3 m, and 0.6 m) and four initial values of μ_i (0.11, 0.22, 0.44, and 1.0). The same initial C_i and q_0 values as before, 70 mg/l and 5.6 m^2/hr, were employed for each fit. The initial μ_i value of 1.0 was included because preliminary analyses indicated that μ_i values of this magnitude were required to obtain consistency among the breakthroughs for ports in the high-velocity zone at about 1.5 to 2 meters above datum. However, if μ_i is interpreted according to Equation 5.23, then a value of $\mu_i = 1.0$ implies an injection radius of 4.5 meters, meaning the initial ring of injected tracer would reach almost to TMC-6 (4.8 meters from IW). Such an interpretation would clearly invalidate the transport model, which treats the mass as if it all originates at the radius $r = r_L$. Thus, an estimated μ_i of this magnitude would require that we either reject the radially convergent transport

model employed here or that we at least reinterpret the meanings of the fitting parameters.

Figure 6.13 shows the simultaneous fit to breakthroughs at 15 ports falling within the apparent high-velocity zone about 1.5 to 2 meters above datum. Table 6.13 shows the estimated parameters for this fit, along with the parameter correlations and coefficients of variation. Overall, the consistency of results from samplers TMC-8 through TMC-5 is quite good, although port 7 of TMC-6 and port 4 of TMC-5 both exhibit somewhat longer tails than predicted by the model. Since we missed the peak breakthroughs for the ports in TMC-4, TMC-3, and TMC-2, it is impossible to determine whether the discrepancies between the data and fitted model at these ports are due primarily to timing of the peak, the magnitude of the peak, the shape of the peak, or some combination of those three factors.

There is some hint that we just barely caught the peak concentrations in ports 3 and 4 of TMC-1. If so, then the predicted peak is too high and too early relative to the observed breakthroughs at these ports. Based on the estimated parameters, the predicted peak concentration at TMC-1 is 268 mg/l at 30 hours. The observed peak for port 3 is 89 mg/l at 52.6 hours (the first measurement) and that for port 4 is 62.4 mg/l at 60.1 hours (the second measurement). These results seem to indicate a substantial loss of mass with increased travel distance, as well as a lower acceleration than that predicted by the radially convergent transport model. Of course, vertical and transverse dispersion, which have been neglected in this analysis, would contribute to an apparent loss of mass. In addition, a circuitous transport path could contribute to the apparent late arrival of the tracer at TMC-1.

Although there are some high parameter correlations for this fit (Table 6.13B), particularly between μ_i and both C_i and q_0, the parameters are not completely unidentifiable, as with many of the single-port fits.

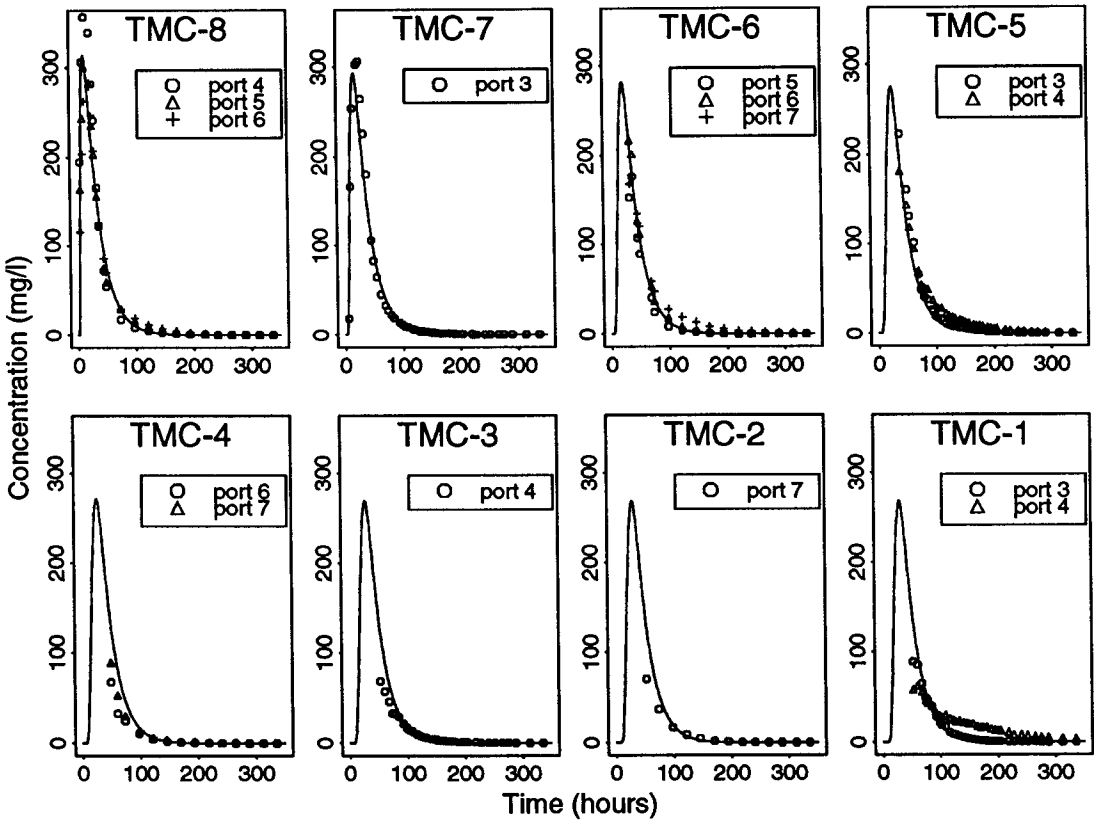

Figure 6.13. Simultaneous fit for ports in high velocity zone between about 1.5 and 2 meters above datum; individual port identified in each panel.

Table 6.13. Results of simultaneous fit to 15 ports in high-velocity zone between about 1.5 and 2 meters above datum.

A. Mean squared error (σ^2) and parameter estimates				
σ^2	C_i	q_0	α_L	μ_i
255 [mg/l]^2	446 mg/l	26.2 m^2/hr	0.54 m	0.92
B. Correlations (upper triangle) and coefficients of variation (diagonal)				
	C_i	q_0	α_L	μ_i
C_i	0.099	0.897	-0.661	0.962
q_0		0.072	-0.817	0.930
α_L			0.263	-0.737
μ_i				0.192

In particular, the values for C_i and q_0 appear to be reasonably accurately estimated, with coefficients of variation of 9.9% and 7.2% respectively. However, the values for α_L and μ_i are much more poorly estimated, with coefficients of variation of 26.3% and 19.2%. Based on these results, an approximate 95% confidence interval for μ_i would range from 0.57 to 1.27, notably larger than that expected from the development presented in Chapter 5.

Figure 6.14 shows the results of attempting a simultaneous fit to six ports whose individual fits seem to indicate a high-velocity zone at about four meters above datum. Unfortunately, no port in TMC-7 appeared to sample this zone, which would apparently fall between ports 6 and 7 of TMC-7. However, the zone is well defined at TMC-8 and TMC-6 and possibly extends to the samplers further downgradient. Figure 6.14 shows that there is in fact some discrepancy between the timing of the peaks at port 12 of TMC-8 and port 12 of TMC-6. The fitted model, which matches both the timing and magnitude of the observed peak at TMC-8, predicts a peak concentration of 317 mg/l at 19 hours at TMC-6. In fact, the observed peak concentration for TMC-6, port 12, was 217 mg/l at 37 hours (the second measurement). The fitted model appears to match the observed breakthrough at TMC-5, port 7, reasonably well, although the observed concentrations show excessive tailing relative to the model. The results for TMC-4, TMC-2, and TMC-1 are similar to those shown for the high-velocity zone at 1.5 to 2 meters above datum: Because we missed the peak breakthroughs at these ports, it is impossible to determine whether the discrepancies between observed and predicted concentrations are due to a significant loss of mass or a discrepancy in timing or shape of the peak.

This fit has somewhat higher parameter correlations and coefficients of variation (Table 6.14B) than that for the high velocity zone at 1.5 to 2 meters above datum (Table 6.13B). The 25.2% coefficient of variation for the injection zone mixing factor implies an approximate 95% confidence interval of 0.26 to 0.76 for μ_i in this case.

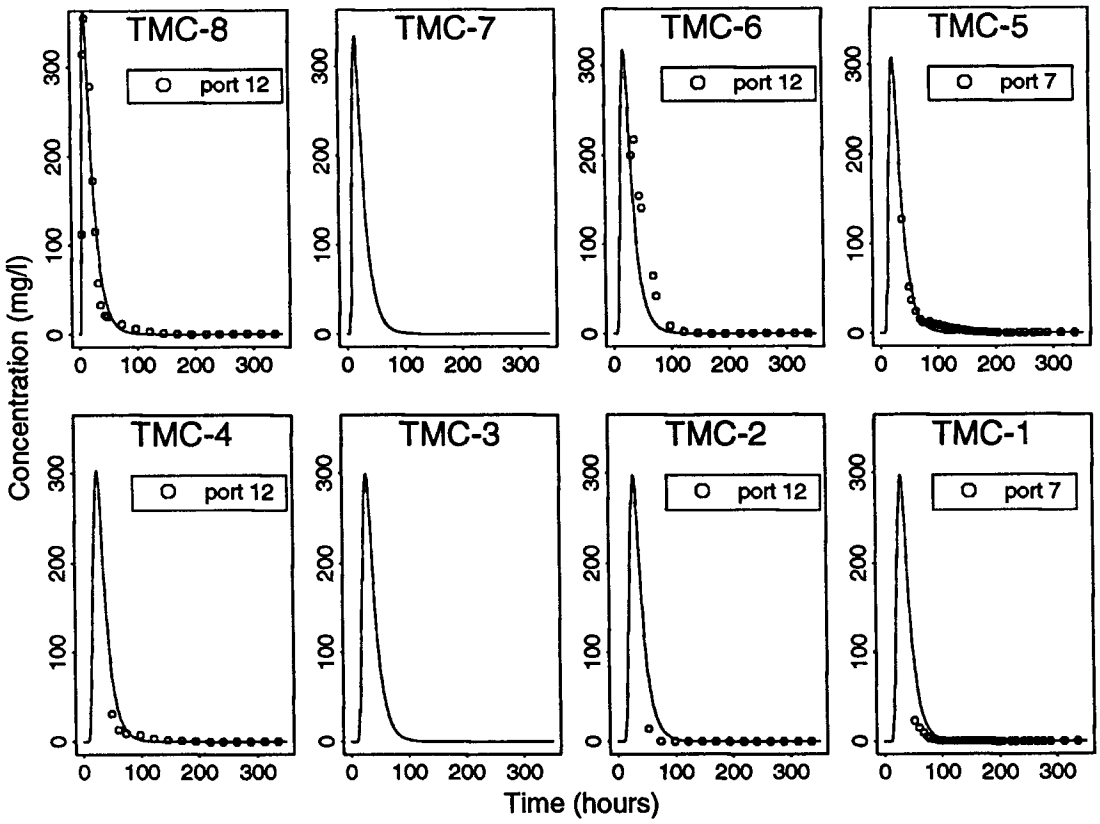

Figure 6.14. Simultaneous fit for ports in high velocity zone at about 4 meters above datum. No ports at TMC-7 or TMC-3 were included in this analysis.

Table 6.14. Results of simultaneous fit to six ports in high-velocity zone at about 4 meters above datum.

A. Mean squared error (σ^2) and parameter estimates				
σ^2	C_i	q_0	α_L	μ_i
280 [mg/l]^2	320 mg/l	25.2 m^2/hr	0.32 m	0.51
B. Correlations (upper triangle) and coefficients of variation (diagonal)				
	C_i	q_0	α_L	μ_i
C_i	0.124	0.978	-0.629	0.968
q_0		0.094	-0.678	0.982
α_L			0.173	-0.697
μ_i				0.252

That is, the mixing factor could fall within the range expected from the development in Chapter 5.

Figure 6.15 shows the results of an attempted fit to ports in the apparent high-velocity zone at about 4.75 to 5 meters above datum. (Perhaps it would be more appropriate to call it a medium-velocity zone, since the estimated q_0 value is 18.5 m^2/hr, notably lower than that for the previous two fits.) Table 6.15 shows that the parameters are in fact very poorly determined in this case. Although the parameter correlations are not as high as that for the previous fit, the mean squared error (166 $[mg/l]^2$) is fairly high relative to the overall magnitudes of the observed breakthroughs. It is apparent from Figure 6.15 that the breakthroughs at TMC-5, TMC-4, and TMC-1 contribute almost no information to the fit and that there is some inconsistency among the breakthroughs at TMC-8, TMC-7, and TMC-6.

Finally, Figure 6.16 and Table 6.16 show the results of a simultaneous analysis of ports in the apparent low-velocity zone from about 2.5 to 3.5 meters above datum. In this case the fitted model really only serves to highlight the differences among the results at the different ports, although the fitted q_0 value (2.3 m^2/hr) does seem to yield a reasonable compromise estimate of the timing of the various peaks. Attempts to find a more consistent fit to subsets of these ports showed little more success. Similarly, attempts to find consistent fits to ports in the lower velocity region near the bottom of the aquifer were also unsuccessful.

V. ASSESSMENT OF RESULTS

Overall, the attempts at simultaneous analysis of breakthrough curves from different ports have cast some doubt on the applicability of the radially convergent transport model to GEMSTRAC1. Nevertheless, it is clear that high velocity zones with some lateral persistence are present at least in the vicinity of the upgradient end of

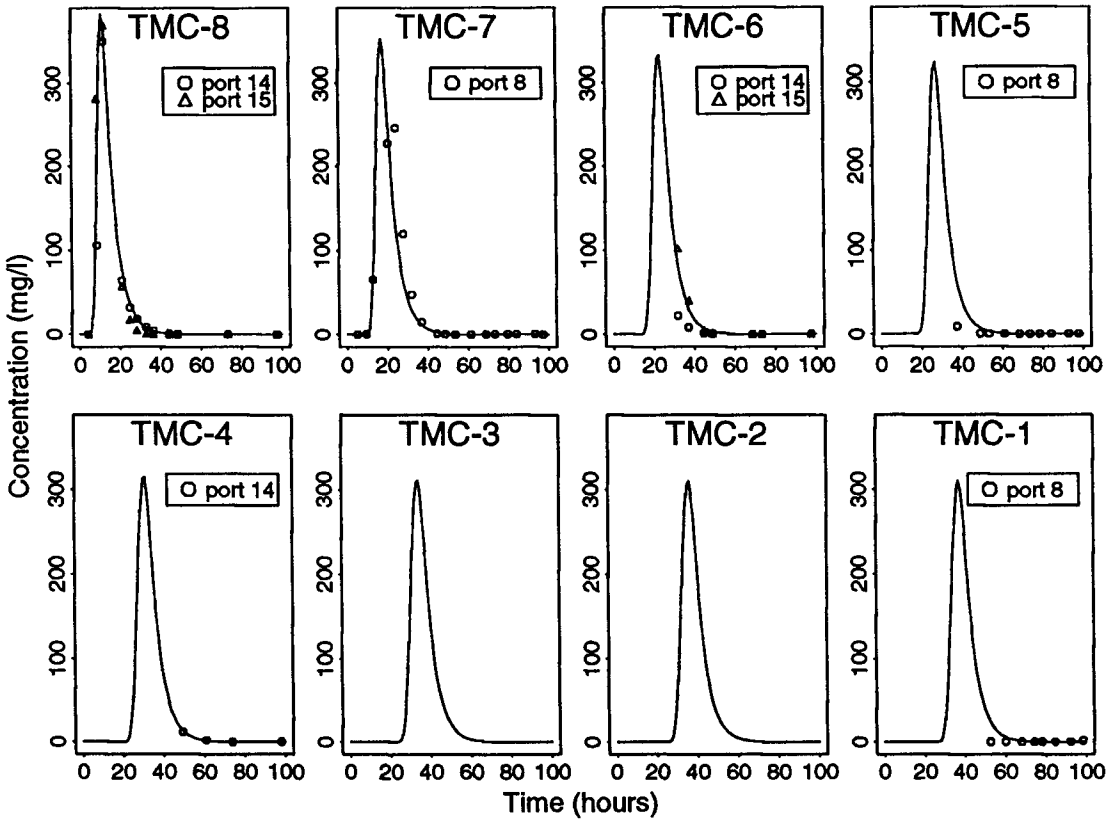

Figure 6.15. Simultaneous fit for ports in high velocity zone at about 4.75 to 5 meters above datum. No ports at TMC-4, TMC-3, or TMC-2 were included in this analysis.

Table 6.15. Results of simultaneous fit to eight ports in high-velocity zone at about 4.75 to 5 meters above datum.

A. Mean squared error (σ^2) and parameter estimates				
σ^2	C_i	q_0	α_L	μ_i
166 [mg/l]^2	102 mg/l	18.5 m^2/hr	0.03 m	0.15
B. Correlations (upper triangle) and coefficients of variation (diagonal)				
	C_i	q_0	α_L	μ_i
C_i	0.655	0.908	-0.678	0.967
q_0		0.486	-0.812	0.931
α_L			1.769	-0.740
μ_i				1.179

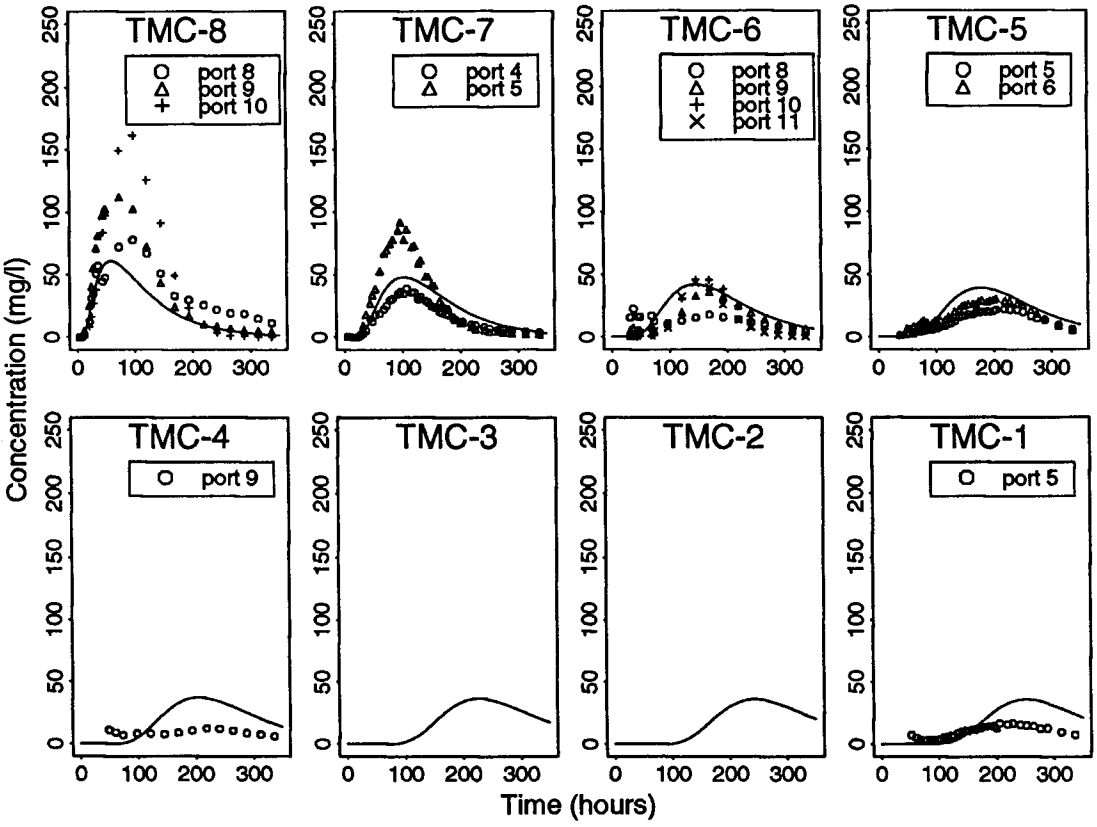

Figure 6.16. Simultaneous fit for ports in low velocity zone at about 2.5 to 3.5 meters above datum. No ports at TMC-3, or TMC-2 were included in this analysis.

Table 6.16. Results of simultaneous fit to thirteen ports in high-velocity zone at about 2.5 to 3.5 meters above datum.

A. Mean squared error (σ^2) and parameter estimates				
σ^2	C_i	q_0	α_L	μ_i
231 [mg/l]^2	28 mg/l	2.3 m^2/hr	0.60 m	0.09
B. Correlations (upper triangle) and coefficients of variation (diagonal)				
	C_i	q_0	α_L	μ_i
C_i	0.097	0.867	-0.467	0.941
q_0		0.078	-0.715	0.931
α_L			0.176	-0.587
μ_i				0.273

the tracer network and that these features played a dominant role in the transport of the tracer. The fact that less coherent results were found in the lower velocity zones could indicate that a significant component of the flow and transport in these zones is in fact directed upward or downward toward nearby high-velocity zones, where the bulk of the transport occurs. Flow and transport in the high-velocity zones is almost certainly predominantly horizontal, allowing for a reasonably consistent fit to different breakthrough curves observed in these zones.

As described in Chapter 7, an August 1997 pumping test revealed some evidence that well DW appears to be effectively partially penetrating, despite the fact that the screen extends across the entire aquifer. In this case, there would be significant vertical flow in the vicinity of well DW, with the flow becoming indistinguishable from that due to a fully penetrating well with increasing distance from DW. Such a phenomenon would contribute to the deterioration of the quality of fit between the transport model (which assumes horizontal flow) and the observed breakthroughs with increasing travel distance (decreasing distance from DW). The comparison of C_i and q_0 values fitted to individual-port breakthroughs (Figures 6.9 and 6.10), along with the simultaneous analysis of breakthroughs at multiple ports (Figures 6.13 through 6.16) show that it is possible to obtain reasonably coherent results at samplers TMC-8, TMC-7, and TMC-6. The consistency of C_i and q_0 profiles among these three samplers appears to validate the assumption of horizontally stratified flow in this region. The inconsistency of results with the horizontally stratified transport model for those samplers further downgradient could be caused in part by increasing importance of vertical flow with decreasing distance from well DW.

CHAPTER 7: COMPARATIVE ASSESSMENT OF CHARACTERIZATION EFFORTS AT GEMS

I. INTRODUCTION

The primary purpose for performing GEMSTRAC1 was to provide a point of reference for assessing the effectiveness of different well testing methodologies in delineating heterogeneities controlling contaminant transport in groundwater. Unfortunately, various complications have slowed progress in implementing these methods at the site. Nevertheless, this chapter presents an assessment of the results obtained so far, comparing hydraulic conductivity estimates provided by each technique to a composite relative conductivity distribution developed from the results of GEMSTRAC1. The characterization methodologies employed so far include pumping tests, slug tests, and permeameter analysis of core samples, along with preliminary work on hydraulic tomography (pumping tests employing high-resolution drawdown data) and single-well dipole flow tests. Numerical simulations have been used to supplement the limited field results obtained so far for hydraulic tomography. This modeling has been done using a two-dimensional finite-difference radial flow model developed specifically for this work.

II. COMPOSITE RELATIVE CONDUCTIVITY DISTRIBUTION

Figure 7.1 shows the fitted flux per unit thickness (q_0) values derived from the individual-port fits for GEMSTRAC1 (Tables 6.1 through 6.8), along with a composite flux distribution based on the fitted q_0 values for TMC-8, TMC-7, TMC-6, and TMC-5. The composite flux profile was created by combining the q_0 versus elevation profiles from these four samplers and then smoothing the resulting combined profile. The estimated q_0 values from TMC-4 through TMC-1 were not included in the development of the composite flux profile due to the preponderance of nonunique fits for these ports, along with the loss of

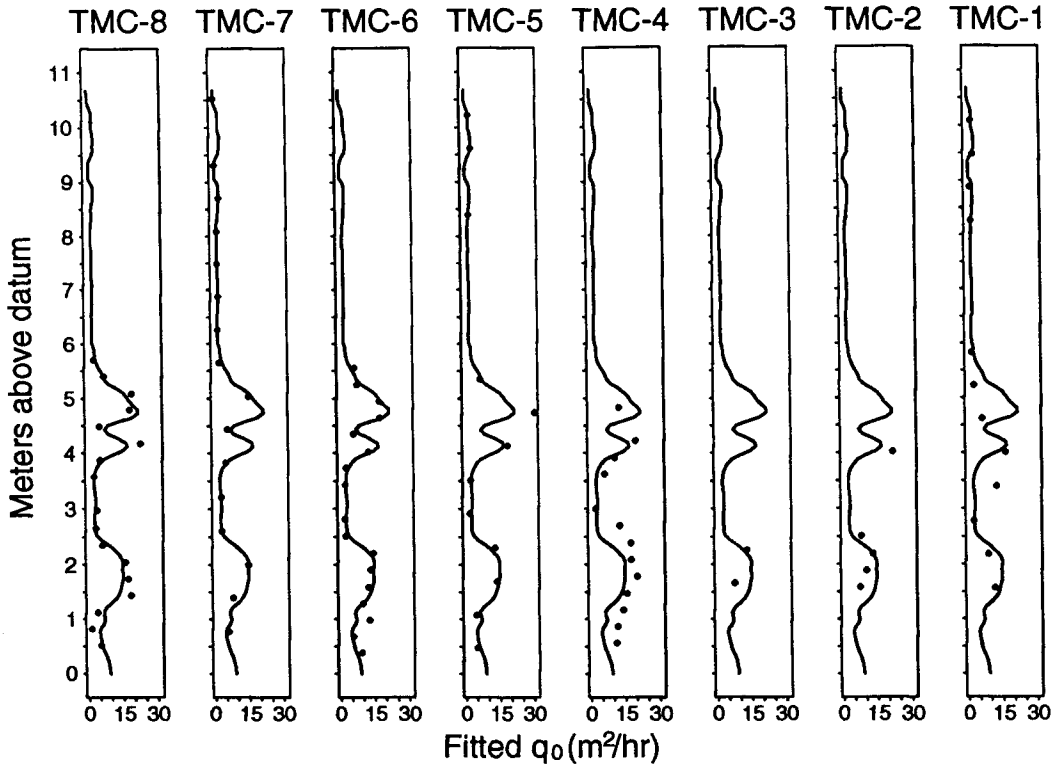

Figure 7.1. Fitted q_0 values from centerline ports (points) with composite profile (line, same for all plots).

coherence and definition of the high- and low-conductivity zones further downgradient from the injection well. It is clear that the composite profile does indeed represent a reasonable compromise among the results obtained at samplers TMC-8 through TMC-5. The composite flux profile also matches the fitted q_0 values at TMC-4 reasonably well, apart from the apparent broadening of the high-flux zone centered at around two meters above datum observed in the fitted values for this sampler. The results from TMC-3 and TMC-2 are too sparse to allow for reasonable comparison. The results from TMC-1 contradict the generalized profile most strongly, possibly indicating a lowering and merging of the two high-flux zones centered at about 4.3 and 4.9 meters above datum in the composite profile.

The mean value of the composite flux distribution is 5.77 m^2/hr. This mean value should be related to the pumping rate at the discharge well according to the vertically integrated version of equation 5.29:

$$\overline{q}_0 = \frac{Q}{nb} \tag{7.1}$$

Using the overall pumping rate (Q) of 15.7 m^3/hr and aquifer thickness (b) of 10.67 m, an average flux rate of 5.77 m^2/hr would correspond to a porosity (n) of 25.5%. This is somewhat lower than the overall average porosity of about 28% computed from the core samples obtained at the site, but nevertheless indicates that the computed average flux value is certainly not unreasonable, especially considering that the effective porosity could be somewhat lower than the total porosity. The flux rate values in the composite profile range from 0.77 to 21.74 m^2/hr. As described in Chapter 5, for horizontal, stratified flow, the flux should be distributed in the vertical according to the relative vertical distribution of horizontal conductivity. Thus the flux profile has been converted to a relative conductivity profile simply by dividing the flux value at each elevation by the overall average flux rate (5.77 m^2/hr), creating relative conductivity values ranging from 0.13 to 3.77. The pumping tests described below indicate that the aquifer has an average horizontal conductivity of about 1.5×10^{-3} m/s. This average value has been used to convert the relative conductivity profile into an absolute conductivity profile, with conductivities ranging from about 0.20×10^{-3} to 5.7×10^{-3} m/s.

III. PUMPING TESTS

Pumping tests at GEMS have revealed the overall high conductivity of the sand and gravel aquifer, along with the impact of leakage from the overlying silt and clay. Analysis of a 1988 pumping test is presented in Chapter 3, with the fits of three different analytical models presented in Figure 3.14 and corresponding parameter

estimates in Table 3.1. The first model, in which the leakage properties of the overlying silt and clay are summarized in the lumped leakage parameter, L, provides an estimate of 84.2 m^2/hr for the aquifer transmissivity, corresponding to a conductivity estimate of about 2.2×10^{-3} m/s. This is a very high conductivity, typical of conductivity values for clean sand or gravel (Freeze and Cherry, 1979). The pumping tests conducted in August and September of 1994 yielded conductivity estimates of 1.3×10^{-3} m/s and 1.6×10^{-3} m/s when analyzed with the same model, also in the range of values expected for clean sand or gravel. Two more recent pumping tests, performed in May and August of 1997 using wells within the tracer network, both yielded conductivity estimates of 1.5×10^{-3} m/s. As discussed in Butler (1990), pumping tests yield parameter estimates averaged over a volume that is generally much too large to be of use in predicting the detailed pathways that a contaminant will follow. However, the averaged conductivity value obtained from a pumping test can be used to complement the information obtained from tests which are sensitive to the vertical distribution of relative conductivity but insensitive to absolute conductivity, such as induced gradient tracer tests (Molz *et al.*, 1988).

IV. SLUG TESTS

As discussed in Chapter 2, it was hoped that an extensive program of multilevel slug tests at GEMS would yield a detailed picture of the hydraulic conductivity distribution at the site. However, unanticipated complications in the performance and analysis of slug tests at the site have kept us from achieving this goal. Because of the high permeability of the sediments, slug tests performed at GEMS last only a few seconds and involve very high water velocities, both in the well and in the portion of the aquifer adjacent to the screen. These high velocities lead to a number of effects not predicted by traditional linear slug test models (Hvorslev, 1951; Cooper *et al.*, 1967), invalidating any parameter estimates obtained from analysis of the

tests based on these models. Work in recent years has led to development of a more sophisticated model for slug test analysis, incorporating the nonlinear and inertial effects that influence slug tests in high permeability media (McElwee and Zenner, 1998). Application of this model to slug tests performed in twelve piezometers at GEMS produced the hydraulic conductivity estimates shown in Table 7.1. The locations of the wells are shown in Figure 2.3.

Table 7.1. Hydraulic conductivity estimates from slug tests at GEMS (from McElwee and Butler, 1995, and McElwee and Butler, 1996).

Well #	Height of bottom of screen above datum (m)	Length of screen (m)	K (10^{-3} m/s)
00-1	4.74	0.76	3.05
0-1	0.16	9.14	0.893
0-2	7.77	0.70	0.671
0-5	2.05	0.70	0.518
0-7	5.32	0.70	1.71
0-9	4.91	0.76	1.65
1-1	7.63	0.76	0.735
1-5	1.56	9.14	1.69
1-7	0.39	9.14	1.84
2-2	7.17	0.56	0.506
2-5	0.48	9.14	0.537
2-6	1.61	9.14	0.730

The results shown in Table 7.1 are in reasonable agreement with the results of the pumping tests described above, in that the conductivity estimates derived from wells screened throughout most of the aquifer (0-1, 1-5, 1-7, 2-5, 2-6) are comparable to those obtained from the pumping tests. The overall average conductivity value estimated from the slug tests (with each estimate weighted according to screen length) is 1.1×10^{-3} m/s.

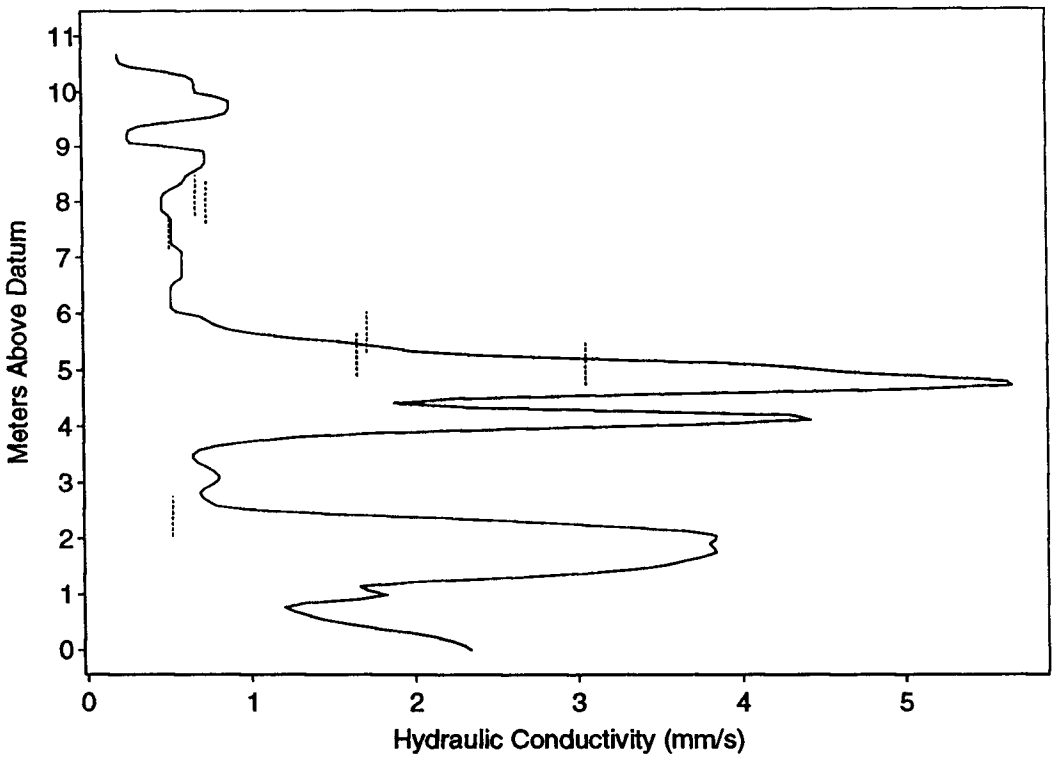

Figure 7.2. Hydraulic conductivity estimates from slug tests in short-screened wells (dashed lines at screen locations) with composite conductivity distribution determined from GEMSTRAC1.

Figure 7.2 compares the conductivity estimates obtained from the slug tests in short-screened wells (00-1, 0-2, 0-5, 0-7, 0-9, 1-1, and 2-2) to the conductivity distribution determined from GEMSTRAC1. The few slug test results that are available show some tantalizing similarities with the tracer test results, especially if one allows for the possibility of lateral changes of elevation of given zones. Unfortunately, the data are too sparse to allow for a thorough evaluation of the potential of multilevel slug tests for site characterization.

McElwee (1998) recently performed a suite of multilevel slug tests in well IW, using packers to isolate and test 17 successive two-foot intervals throughout the aquifer. He analyzed the results of these tests

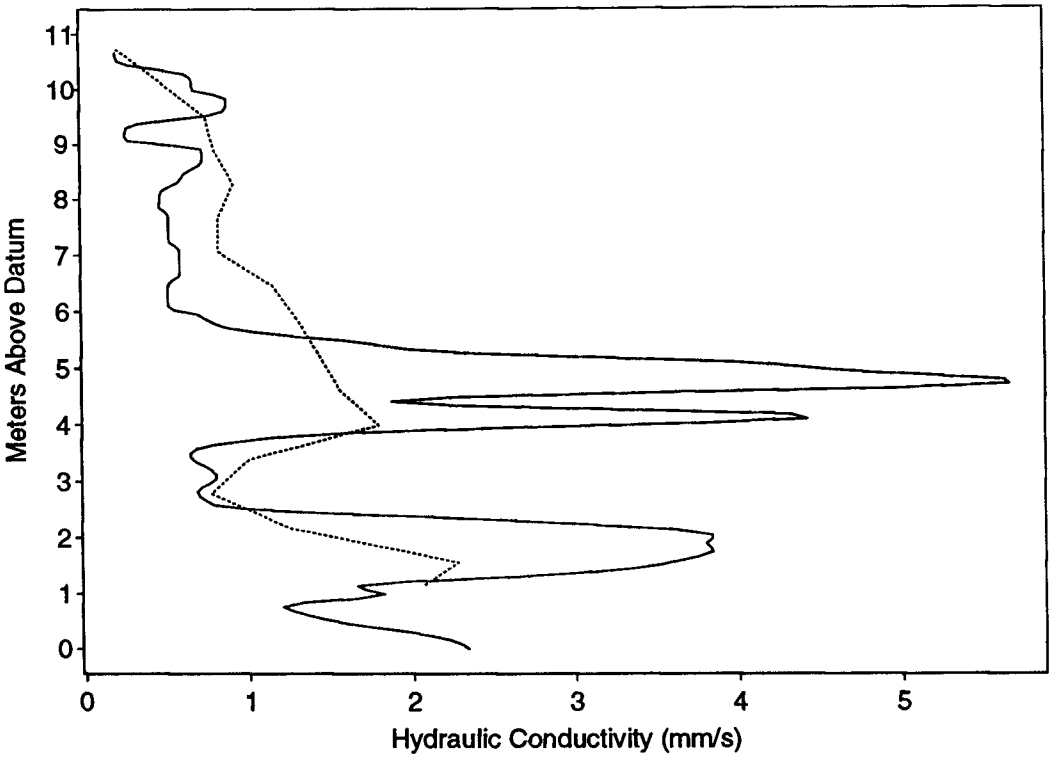

Figure 7.3. Hydraulic conductivity estimates from multilevel slug tests in well IW (dashed line) with composite conductivity distribution from GEMSTRAC1 (solid line).

using the model developed by McElwee and Zenner (1998) and obtained an estimated conductivity profile that agrees quite well with that derived from GEMSTRAC1, as shown in Figure 7.3. Results such as these are extremely encouraging , considering that multilevel slug tests represent an economical and efficient characterization technique, well within the reach of most practitioners.

V. CORE SAMPLING AND ANALYSIS

Relatively undisturbed core samples were obtained at GEMS utilizing a sampler designed for use in saturated, unconsolidated sand and gravel deposits (McElwee *et al.*, 1991). To date, 16 wells at the site have been cored through the sand and gravel, with an overall

sediment recovery rate of 75.3%. The cores were cut into segments ranging from 10 to 20 centimeters in length and the hydraulic conductivity, grain size distribution, and porosity of each segment were measured in the lab. Details of the coring and core sample analysis procedures can be found in McElwee and Butler (1995).

Figure 7.4 shows the mean grain size, in ϕ units, of core samples from three boreholes within and near the tracer test network, arranged from north to south. Unfortunately, the "Depth Below Reference" shown on the vertical axis is relative to a reference marker at each borehole, so that the results cannot be referenced to a common datum. Although the sediments are quite coarse overall, primarily consisting of coarse to very coarse sand, the results show a fairly clear fining upward sequence, as expected from the sedimentological history of the site. Not shown in Figure 7.4 are results for 18 clay-rich segments from TME-8 and four from TMO-1 whose conductivities were too low to be measured in the conventional permeameter and for which grain size data are not available. Although these clay-rich segments were primarily in the upper portions of each borehole, some were present in TME-8 at depths as great as 21 meters. Thus it is clear that lenses or layers of clay occur within the sand and gravel, even at greater depths in the aquifer.

The hydraulic conductivity of each core segment was measured twice, first in its original, relatively undisturbed state and then after disaggregation and repacking. The original and repacked hydraulic conductivities versus depth for TME-8, TMO-1, and well 00-1 are shown in Figure 7.5. Because water flows vertically through each core segment in the permeameter, the permeameter results reflect the vertical conductivity of each segment. Vertical conductivities are usually lower than horizontal conductivities, due to the presence of small-scale horizontal laminae in the sediments which impede flow in the vertical direction. We therefore expect the original conductivities

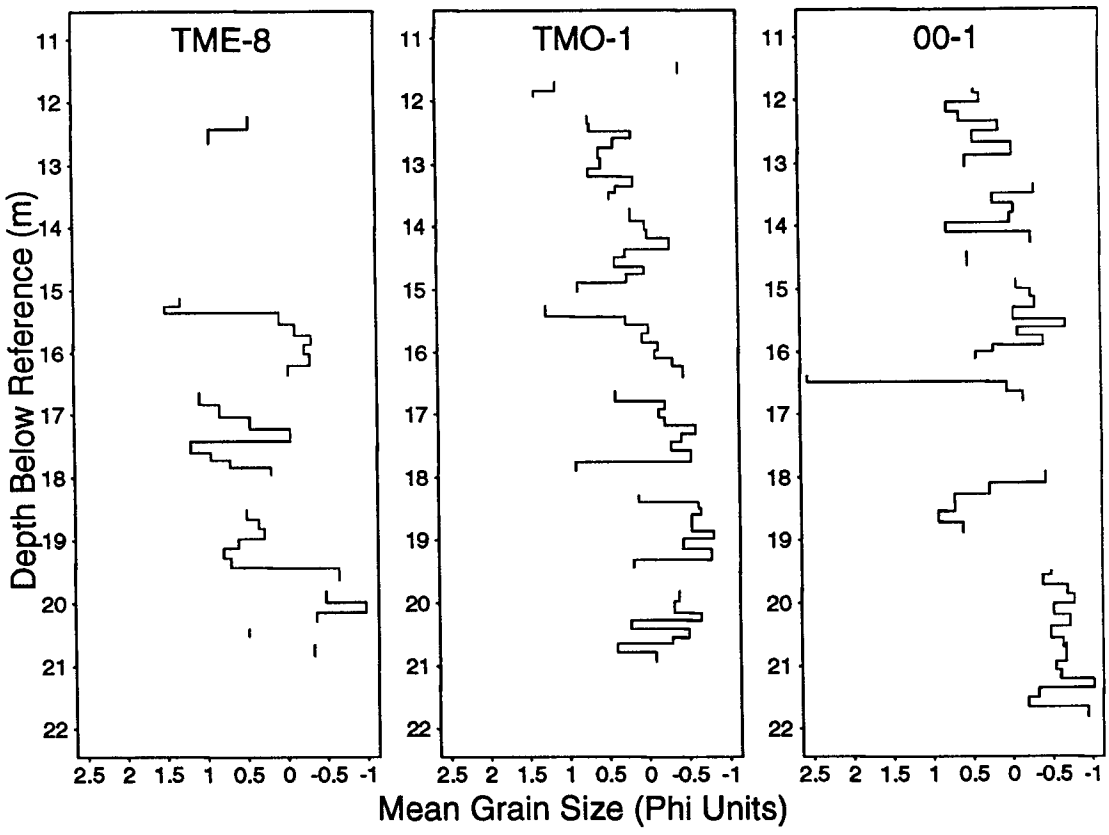

Figure 7.4. Mean grain size in ϕ units ($-\log_2$(mm)) versus depth for three GEMS wells.

measured in the permeameter to be closer to in situ vertical conductivity values and those measured after disaggregation and repacking to be somewhat higher, lying between the true vertical and horizontal conductivities. Overall, the observed repacked conductivities were generally higher than the original conductivities, but the contrast is not great. For the ten cored wells described in McElwee and Butler (1995), the mean original permeameter conductivity is 0.35×10^{-3} m/s and the mean repacked conductivity is 0.58×10^{-3} m/s. If the mean original permeameter conductivity is taken as indicative of the average vertical conductivity of the aquifer, and the overall average result from pumping tests, about 1.5×10^{-3} m/s, is taken as the horizontal conductivity, then the results indicate a very mild vertical to horizontal anisotropy ratio, about 1:4.

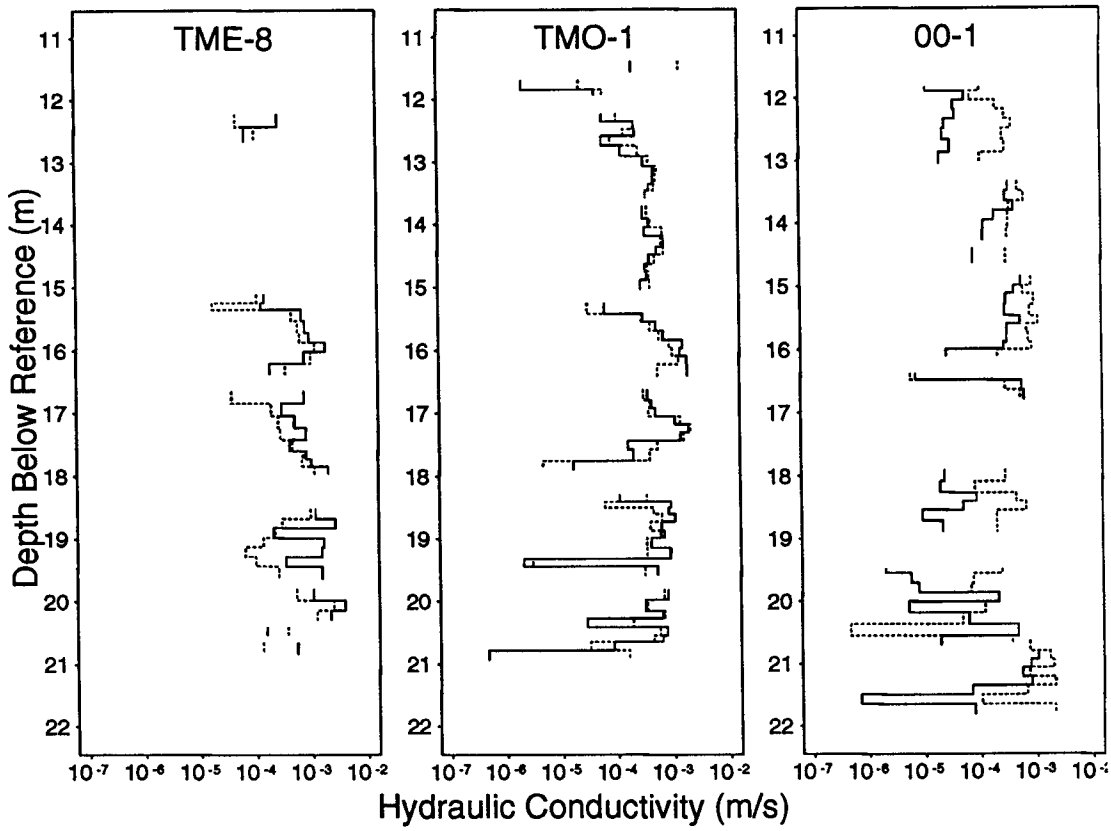

Figure 7.5. Original (solid line) and repacked (dashed line) hydraulic conductivity versus depth for three GEMS wells.

The average original and repacked conductivities for all the core samples from TME-8, TMO-1, and well 00-1 are almost identical. The original conductivities range from 4.6×10^{-7} m/s to 3.8×10^{-3} m/s with a mean of 0.51×10^{-3} m/s and the repacked conductivities range from 4.6×10^{-7} m/s to 2.4×10^{-3} m/s with a mean of 0.50×10^{-3} m/s. As shown in Figure 7.5, the original and repacked conductivities for TMO-1, in the middle of the network, are quite similar. For TME-8, the repacked conductivities are somewhat lower than the original conductivities, while the opposite is true at well 00-1. There appears to be no consistent relationship between original and repacked conductivities for these three wells.

Figure 7.6 compares the core permeameter hydraulic conductivity values for these three wells to the relative hydraulic conductivity distribution derived from GEMSTRAC1. The core sample depths have been converted to elevations above datum assuming that the reference elevation for each borehole is roughly the same as the elevation of the Corps stake (i.e., slightly above ground level). The resulting elevations are only approximate. The permeameter-measured conductivities have been converted to relative values by dividing each conductivity by $.51 \times 10^{-3}$ m/s, the overall average original core sample conductivity for all three wells.

The core permeameter analyses for TMO-1, in the middle of the sampler network, seem to reveal the two most permeable zones apparent in the results from GEMSTRAC1. Otherwise, the permeameter conductivity profiles do not correspond very well with that derived from the tracer test. However, some of the discrepancies may reveal information about lateral conductivity variations that quite possibly influenced the tracer test. For example, the core analyses for TME-8, 2.7 meters from the injection well, reveal a very strong contrast in conductivities between the upper half of the aquifer and the lower half, since the segments missing from the upper portions of TME-8 represent low-conductivity clay-rich sediments. The presence of a similar contrast at the injection well would account for the exclusion of tracer mass from the upper portion of the aquifer. Similarly, the core analyses for well 00-1, especially the repacked conductivities, seem to reveal a relatively high-conductivity zone at roughly the same elevation as port 10 in TMC-1 (5.8 meters above datum). Well 00-1 is south of the tracer network, about 5.9 meters from TMC-1 and 4.1 meters from the discharge well. If the conductivity distribution at the south end of the tracer network is similar to that at well 00-1, then the anomalous appearance of a large peak at port 10 of TMC-1 could be explained by the diversion of tracer into this relatively high-conductivity zone.

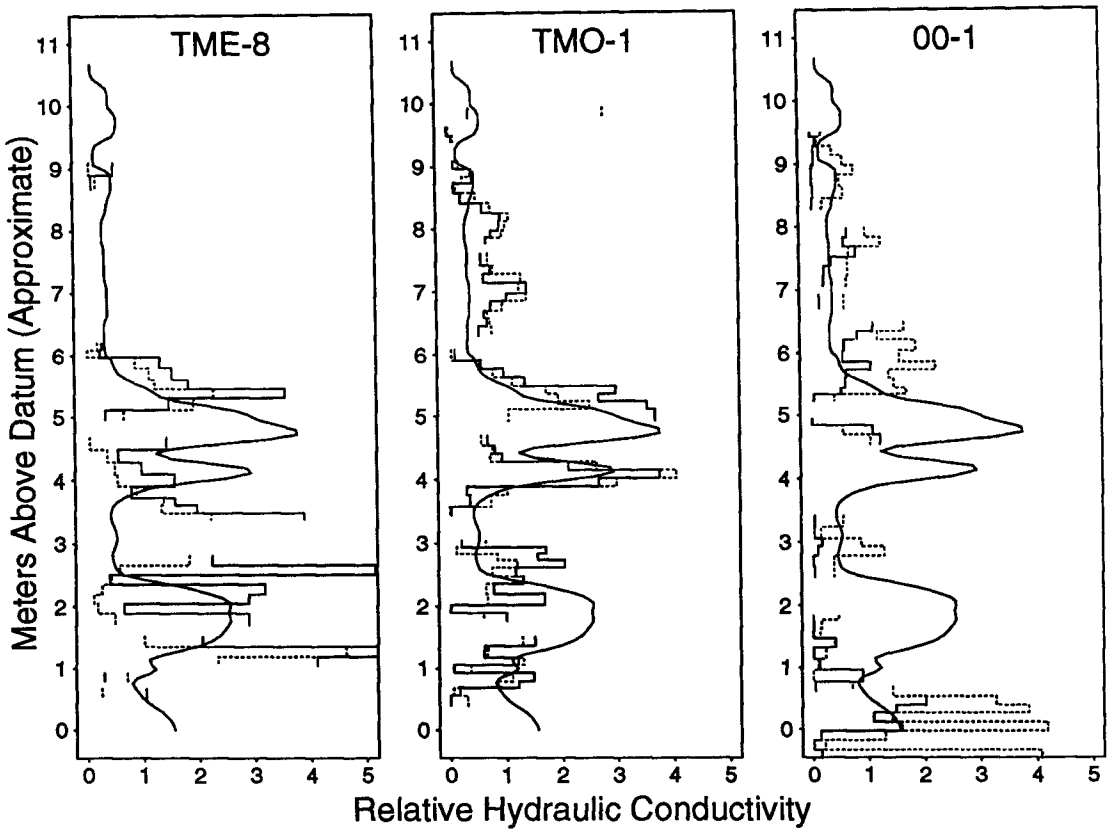

Figure 7.6. Relative original (solid line segments) and repacked (dashed line segments) hydraulic conductivities from core analyses along with relative conductivity profile from GEMSTRAC1 (continuous solid line)

Although core sampling and analysis is not likely to be a feasible technique for routine site characterization, the GEMS core analyses contribute to our overall efforts to establish an "underground laboratory" for testing of other techniques. The core analyses demonstrate most clearly the considerable heterogeneity of the sediments, at least at the core scale, with conductivity contrasts of up to two to three orders of magnitude occurring between successive core segments. Further work is required to determine how these vertically oriented, small-scale conductivity measurements relate to the larger-scale and predominantly horizontal flow processes characterizing in situ well tests and most contaminant transport problems.

VI. SINGLE-WELL DIPOLE FLOW TESTS

Zlotnik and Ledder (1996) present the theory of dipole flow tests and Zlotnik and Zurbuchen (1998) describe the design and field application of the dipole flow apparatus. Butler *et al.* (1998) describe a set of dipole flow tests performed at the GEMS site, in wells Gems4N and Gems4S, immediately to the west of the tracer test network (Figure 2.3). In a dipole flow test, a pump moves water between two separate chambers, isolated with packers, in a long-screened well, establishing a circulating flow pattern in the aquifer adjacent to the well. The steady-state head difference between the two chambers can be used to estimate the horizontal conductivity using a formula presented by Zlotnik and Ledder (1996). Although the development of this formula assumes a homogeneous aquifer (Zlotnik and Ledder, 1996), Butler *et al.* (1998) demonstrate that application of the method appears to yield reasonable conductivity estimates even in the presence of vertical heterogeneity. However, Butler *et al.* (1998) point out that care must be taken to assess the possible influence of unwanted flow along a disturbed zone near the well and more importantly to ensure that adequate well development has been performed prior to testing.

As described in Butler *et al.* (1998), advantages of the dipole flow test are that no water need be added or removed from the formation during testing and that the scale of the region of influence of the test is reasonably well known (it is approximately the same as the center-to-center distance of the dipole). Also, in high permeability aquifers the head difference between the two chambers reaches steady state quite rapidly, a matter of a few seconds at GEMS.

Figure 7.7 shows the results of the dipole flow surveys performed in Gems4N and Gems4S along with the composite conductivity distribution derived from the results of GEMSTRAC1. The chamber length employed in these surveys was 0.6 meters and the

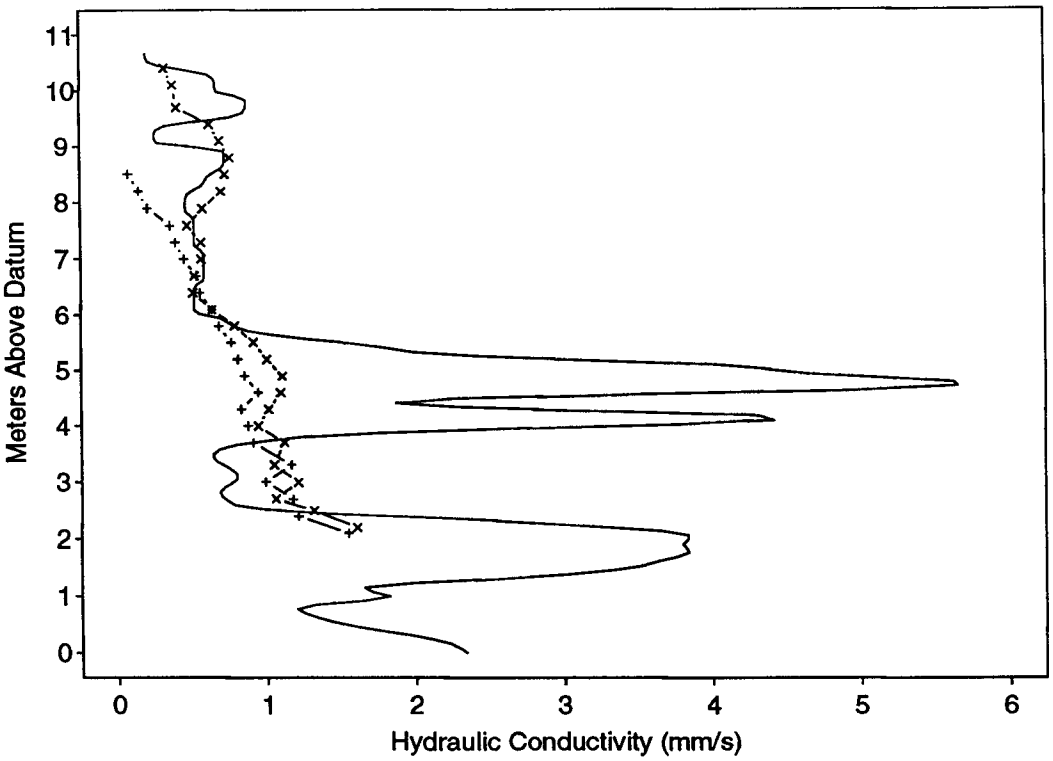

Figure 7.7. Composite conductivity distribution from GEMSTRAC1 (solid line) along with conductivities estimated from dipole flow surveys at Gems4N (+) and Gems4S (X).

chamber separation distance (center to center) was 1.2 meters. The dipole assembly was moved in 0.3-meter increments between successive tests. The conductivity values estimated from the dipole flow tests are assigned to the center depth of the dipole assembly for each test. Unfortunately, the elevations of these two wells have not yet been surveyed. The dipole center depths have been converted to elevations assuming that the measurement point elevation for each well is 21.5 meters above datum, approximately the same as that for the nearby wells 7-1 and 11-1. Both of the conductivity profiles from the dipole flow surveys reveal the generally increasing trend of conductivity with depth. One could almost view the profile from Gems4S as a smoothed version of the profile derived from GEMSTRAC1. If so, the degree of smoothing is quite high and the

method fails to reveal the magnitude of the conductivity contrasts. It is possible that use of smaller dimensions for the dipole tool would reveal greater detail in the vertical distribution of conductivity. However, the use of a shorter central packer would lead to an increased possibility of packer circumvention, which could adversely affect the test results.

VII. HYDRAULIC TOMOGRAPHY

Current work at GEMS includes an assessment of a method we have dubbed "hydraulic tomography". Although the concepts involved in hydraulic tomography are really no different from those involved in the automated inverse analysis of traditional pumping tests, hydraulic tomography is distinguished by the vertical detail in the drawdown measurements obtained in the aquifer and also in the use of a number of different stressed intervals in the pumping and/or injection wells, creating a number of different flow configurations in the aquifer. The reconstruction of the aquifer properties from the information provided by the varied flow configurations is similar in concept to the reconstruction of acoustical properties from the information provided by the crossed raypaths employed in crosshole seismic tomography.

Figure 7.8 shows a schematic diagram of two pumping tests in a series of tests in a tomographic format, with limited intervals of a long-screened well packed off and pumped in sequence. During each test, drawdown measurements are obtained at a number of measurement points in the aquifer, represented by the circles in Figure 7.8. A simultaneous inversion of the drawdown data from all the tests should allow for a reasonable reconstruction of the vertical distribution of hydraulic conductivity. However, the method depends on the ability to obtain point measurements of drawdown. Even a relatively short-screened well may provide too much vertical averaging of drawdown to be of use.

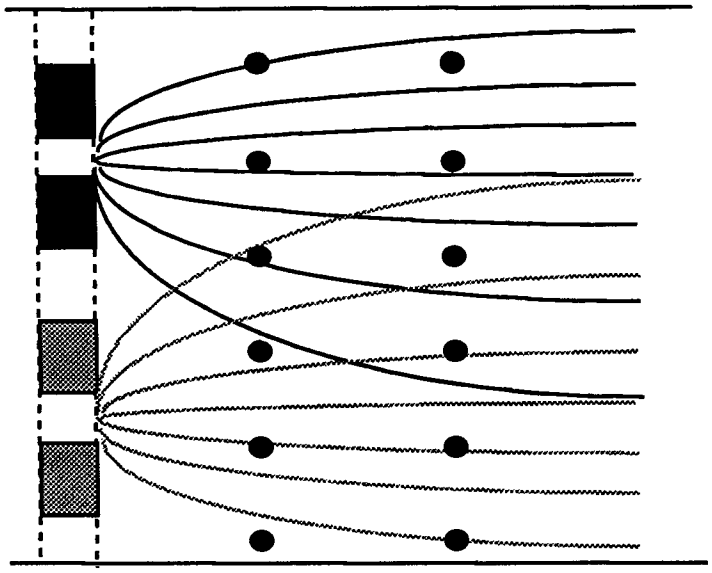

Figure 7.8. Schematic diagram of hydraulic tomography, representing two different tests in a series of tests involving pumping over limited intervals in a long-screened well; drawdown measurement points shown as circles.

Recent work at GEMS has involved exploration of the use of the multilevel samplers employed in the tracer test as sources of drawdown data, with pressure measurements in the sampling tubes providing information regarding the drawdown in the immediate vicinity of the sample port (Butler *et al.*, 1997). Because conventional pressure transducers are too large to be used in the sampling tubes, alternative pressure measurement devices must be employed. Work at the site originally involved the use of fiber optic pressure transducers. Unfortunately, these transducers have been plagued with a number of technical problems that led us to question their ultimate utility in this area. As described in Butler *et al.* (1997), a cheaper and apparently more reliable alternative is to use air pressure transducers attached to the top of each sampling tube. With a tight seal between the transducer and the sample tube, an increase in drawdown at the sample port leads to a decrease in pressure within the air column above the water in the sample tube. The sensor response to this change in air pressure can be

reliably calibrated in terms of drawdown changes in the aquifer, thus providing a means to obtain point measurements of drawdown.

During a test in August 1997, air pressure sensors attached to ports 3 and 7 of TMC-3 and TMC-7 were used to measure the response to pumping at well DW. The late-time drawdown measurements from the ports followed essentially parallel straight lines when plotted versus logarithmic time, with the common slope reflecting the overall average hydraulic conductivity of the aquifer (Butler and Liu, 1993), and the measurements also showed reliable and predictable responses to the beginning and cessation of pumping. Both of these results indicate that the drawdown measurement technique appears to be fundamentally sound. At each sampler, persistent differences in drawdown were observed between the two ports, which are separated by a vertical distance of 2.4 meters. The difference in drawdown between ports 3 and 7 of TMC-3 (4.84 meters from DW) was about 0.04 meters, while that at TMC-7 (10.86 meters from DW) was about 0.01 meters. Butler (pers. comm, 1998) reports that these differences can be attributed to three factors: vertical heterogeneity, effective partial penetration of well DW, and vertical to horizontal anisotropy in the hydraulic conductivity on the order of 0.1 to 0.01. The vertical variations in steady-state drawdown and the increase in these variations with decreasing distance from well DW indicate that this well must be effectively partially penetrating, even though the screen extends through most of the aquifer. The exact mechanism leading to this effective partial penetration is not known. Similarly, the anisotropy is unknown. As described above, the core permeameter data do not seem to indicate a very strong anisotropy, but it is quite possible that the core analyses would not be sensitive to the structures that might impart a macroscale anisotropy to the aquifer conductivity.

In order to gain more insight into the potential of hydraulic tomography, a radial-coordinate finite-difference model was used to simulate a sequence of pumping tests over limited vertical intervals in

an aquifer with characteristics similar to that at GEMS. An inverse analysis of the data generated from this forward run reveals the fundamental soundness of the estimation technique under idealized conditions. In inverse mode, the program uses a modified Levenberg-Marquardt algorithm, developed by Garbow *et al.* (1980), to estimate optimal parameters based on observed data. The simulated data were produced by running the model in forward mode using a layered conductivity distribution approximating the composite conductivity distribution derived from GEMSTRAC1, shown above. The model grid contains 35 cells in the vertical at a regular spacing of 0.30 meters (1 foot). Thus the thinnest conductivity layers in the input distribution are 0.3 meters in thickness. The input boundary conditions simulated a series of tests with pumping in successive isolated intervals of well DW. All of the pumped intervals are 0.61 meters (2 feet) thick, except for the topmost, which is 0.91 meters (3 feet) thick. The simulated data represent drawdown measurements at all 17 ports of TMC-1 (1.75 meters from DW) and TMC-3 (4.84 meters from DW). The drawdown measurements are made at five-second intervals from five seconds to 1000 seconds into the test, for a total of 200 measurements per sampling port per test and a grand total of 115600 observations over all 17 tests.

The forward model was run using an anisotropy ratio of 0.01. A smaller anisotropy ratio inhibits vertical flow and produces greater sensitivity of the data to the vertical variations in conductivity. Unfortunately, the anisotropy at GEMS is not very strong, as discussed above, so it is likely that the value of 0.01 is smaller than that of the aquifer at the site. However, for larger anisotropy ratios, the iterative solution procedure used in the finite difference model converges very slowly, leading to extremely long run times for the inverse program. Future work will explore a wider range of scenarios, possibly after the efficiency of the finite difference algorithm has been improved, allowing for more reasonable run times.

The output from the forward run was used to create three different sets of input data for the inverse runs, one with no noise, and two with zero-mean Gaussian noise added to the simulated drawdowns, one set with a standard deviation of 0.0003 meter (0.001 foot), and the other with a standard deviation of 0.003 meter (0.01 foot). The latter level of noise is significant relative to the magnitude of simulated drawdowns (see Figure 7.10), so that drawdown records obtained at only a few measurement points for a single test would certainly not allow for a unique identification of the conductivity distribution. For each set of synthetic drawdown data, the program was run in inverse mode twice, using two different conductivity zonations. The first zonation, referred to as the true zonation in the following discussion, corresponds exactly to the layering pattern used in the forward model. Such a situation is highly unrealistic, because the layering structure would never be known in advance in a real application. However, the inverse runs using the true zonation establish the fundamental soundness of the estimation algorithm. The second zonation represents a regular layering structure with each layer corresponding exactly with one of the pumping intervals. That is, there are 17 layers, all 0.61 meters (2 feet) in thickness except for the top layer, which is 0.91 meters (3 feet) thick. This will be referred to as the regular layer zonation. In both cases the correct anisotropy value (0.01) and the correct specific storage value (3.3×10^{-5} m^{-1}) were employed in the inverse run. In practice these values would not be known and would have to be estimated, along with the horizontal conductivity values. For both sets of inverse runs, the initial value of the horizontal hydraulic conductivity for all zones (layers) was 1.5×10^{-3} m/s, the overall average conductivity. It is presumed that, in advance of performing such an analysis, a reasonable estimate of average conductivity would be available from a larger-scale test.

The inverse runs employing the true zonation were able to exactly reproduce the input conductivity values for all three noise levels, demonstrating that the tomographic technique is able to

reconstruct a relatively complicated layered conductivity distribution with great precision. Figure 7.9 shows the conductivity values estimated when the regular layer zonation was employed in the inverse run, along with the actual conductivity distribution used to produce the data. The estimated conductivity distribution is about as close to the actual distribution as possible, given the discrepancy in zonation between the forward and inverse model runs. Where one of the regular layers used in the inverse run spans two or three layers of the true zonation, the estimated conductivity value for the regular layer represents an approximate average of the conductivities of the corresponding actual layers. This may seem like a rather minor accomplishment, but quite often the combination of high dimensionality of the parameter space and model error results in parameter estimates that are not even physically plausible. In this case 17 parameters are being estimated in the presence of model error resulting from the discrepancy between the true zonation and the regular layer zonation.

Figure 7.10 shows the synthetic data (with the higher noise level of 0.003 meter) from selected ports of TMC-1 for the fifth test in the sequence of 17 tests, along with the corresponding fitted responses for the regular layer inverse run. The fundamental information in these data is conveyed by the persistent differences in drawdown between ports. Port 5, at 2.78 meters above datum, is closest in elevation to the pumping interval (2.4 to 3.0 meters above datum) for this test. Accordingly, the drawdowns for this test are highest at port 5 and decrease with increasing vertical distance from the elevation of the pumped interval. The asymmetric decrease in drawdown with increasing vertical distance from the pumped interval is primarily a function of the conductivity distribution. For example, although port 4 (at 2.2 meters above datum) is closer to the pumped interval than port 6 (at 3.4 meters above datum), the drawdowns at port 4 are lower than those at port 6. This is because port 4 is in a relatively high conductivity region, with a true hydraulic conductivity of 3.8×10^{-3} m/s,

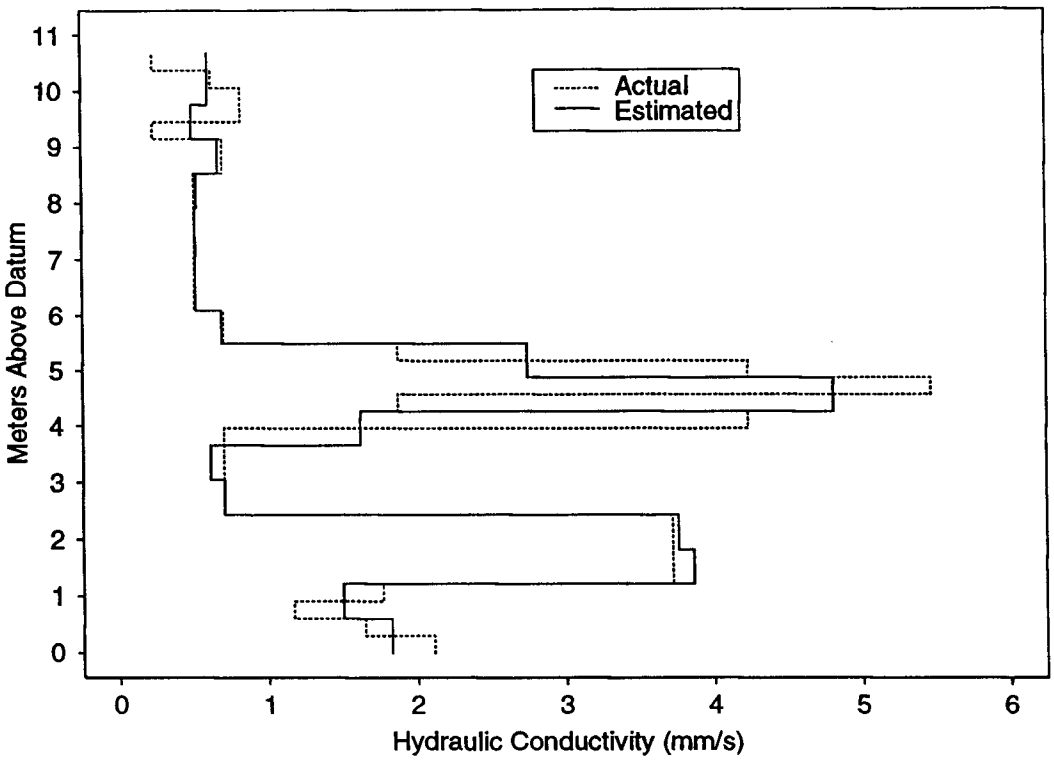

Figure 7.9. Estimated hydraulic conductivity distribution using regular layer zonation compared to the actual conductivity distribution.

while port 6 is in a relatively low conductivity region, with a conductivity of 0.72×10^{-3} m/s. The collection of drawdown data from multiple ports over multiple tests provides a considerable amount of information regarding such conductivity variations, allowing for a successful inversion.

VIII. DISCUSSION

Clearly, multilevel slug tests, single-well dipole flow tests, and hydraulic tomography all have some potential for revealing salient features of the hydraulic conductivity distribution at a site. Core sampling and analysis can also yield important information, although the discrepancy in both scale and orientation of predominant flow

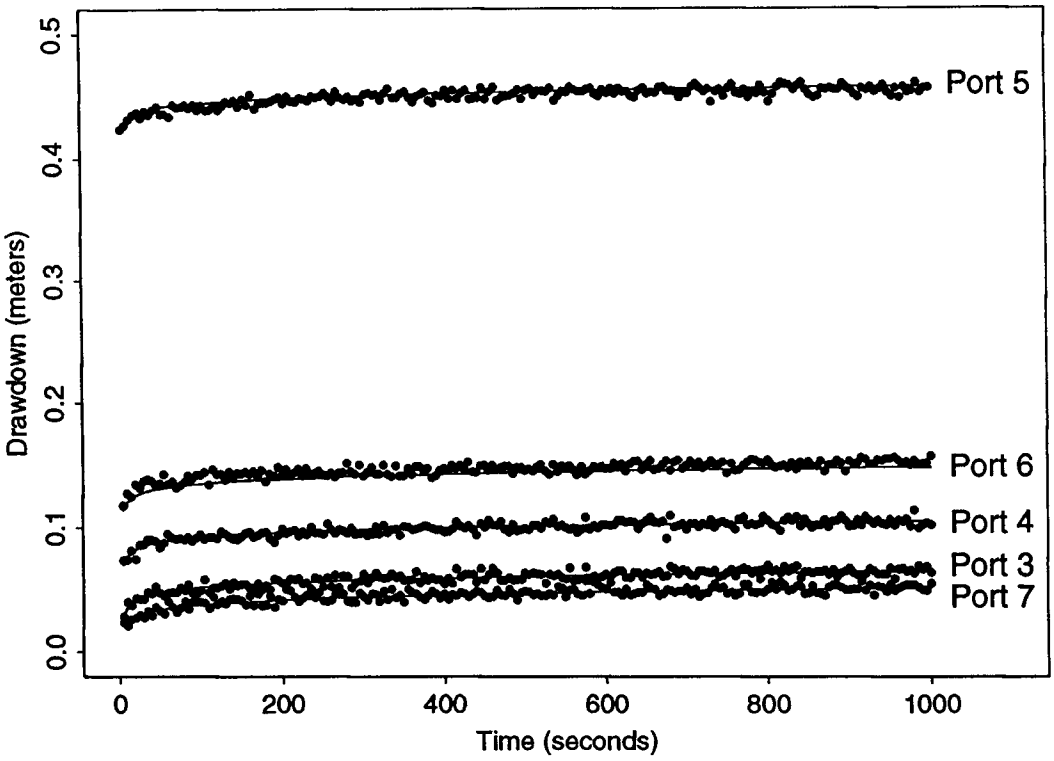

Figure 7.10. Synthetic observed data (points) and fitted responses (lines) for selected ports of TMC-1 during the fifth of 17 tests. The synthetic data shown here contains Gaussian noise with a standard deviation of 0.003 meter.

between the lab setting and the field introduce some difficulty in interpreting and applying the core analysis results.

Neither hydraulic tomography nor core sample analysis is likely to be applied on a regular basis for site characterization, due to the large amounts of time, effort, and equipment that these techniques require. Both of these methods will probably be used primarily as part of well-funded and well-staffed research projects. However, it is possible that hydraulic tomography would be a feasible option at any site which is already equipped with multilevel samplers or similar devices, allowing this method to be inexpensively "piggy-backed" on tracer tests or sampling programs.

The slug tests and dipole flow tests performed at GEMS have shown tantalizing hints that these methods might be able to provide conductivity measurements at a resolution necessary for transport modeling, although evaluation of slug tests at the site has been hampered by the complications due to high water velocities, described above, and the dipole flow test configuration employed has apparently yielded overly smoothed conductivity estimates. A primary advantage of dipole flow tests over slug tests is their lack of dependence on transient data, which is often influenced by factors such as wellbore storage and near-well disturbed zones, even in the absence of the additional factors complicating slug tests analysis at GEMS. However, it is possible that using a chamber separation distance small enough to resolve high-conductivity layers as thin as those seen at GEMS would also result in a conductivity estimate that is too strongly influenced by near-well properties, offsetting the advantage gained by the use of steady state data. Exploration of both these methods, and hydraulic tomography, will continue at GEMS.

CHAPTER 8: CONCLUSIONS

I. CONCLUSIONS

The distribution of aquifer hydraulic conductivity plays a significant role in the transport of contaminants in groundwater. The field-scale conductivity distribution, represented either by continuous trends or by the geometry of boundaries between contrasting conductivities, constitutes a first-order effect in contaminant transport, determining the primary paths and rates of transport. The smaller-scale conductivity variations that have been the focus of stochastic transport theory are second-order effects, contributing to the rate of spreading of contaminant about its predominant transport trajectory. In the past two decades, a great deal of research has been devoted to quantifying the influence of these smaller-scale variations. Meanwhile, practitioners faced with the problem of predicting plume movement or remediating a contaminated site have received relatively little guidance from the research community concerning methods for characterizing the field-scale conductivity distribution.

Although geophysical techniques can contribute greatly to such characterization efforts and geologic process models can provide insight concerning typical patterns of conductivity variation, reliable characterization of the conductivity distribution at a particular site will always be grounded in a program of hydraulic tests. The primary focus of research at GEMS has been the development and refinement of well testing techniques allowing investigators to map out the conductivity distribution at a site without requiring inordinate investments of money and time. Techniques that show the most promise in this regard involve surveys of long-screened wells using a single "tool" to successively test different vertical intervals. Techniques in this category include multilevel slug tests and single-well dipole flow tests. These methods provide estimates of the vertical distribution of hydraulic conductivity at each well location employing a minimum

amount of equipment. Correlation of the conductivity profiles at different locations would allow the investigator to build up a three-dimensional image of the conductivity distribution. Assuming that there is some correspondence between the distributions of hydraulic and geophysical parameters, surface and borehole geophysical techniques could be used to supplement the hydraulic information, helping to resolve ambiguities involved in interpolating or correlating between wells. Recent testing indicates that crosshole radar tomography could prove to be very effective in this regard at GEMS.

GEMSTRAC1, the induced gradient tracer test performed at GEMS in October, 1994, vividly demonstrated that it is necessary to delineate site-specific features in the conductivity distribution to have any hope of accurately predicting contaminant transport. As shown in the exploratory analysis of the tracer test data in Chapter 4, a great deal of tracer mass entered three principal high-conductivity zones and was transported rapidly though the tracer network. The lower zone lies between about 1 and 2.5 meters above datum and the upper two are centered at about 4.1 and 4.8 meters above datum, respectively. The latter two zones appear to be separated by a zone of relatively low conductivity, with the high-low-high alternation occurring at three successive ports in TMC-8 and TMC-6, each with a port-spacing of 0.3 meters (1 foot). The high-conductivity zone at 4.1 meters above datum is no more than 0.6 meters thick and similarly for the lower-conductivity zone above it. Thus, any site characterization method must be able to resolve features at least this narrow in order to provide reliable input to transport simulations, at least in similar sedimentological settings.

The range of flux rates fitted to the individual port breakthrough curves (Tables 6.1 through 6.8) indicate that advective travel times from the injection well to the discharge well at different levels in the aquifer could have ranged from one day to almost a month. Although the design modeling presented in Chapter 3 successfully predicted

certain aspects of the test, such as the overall duration of the test and the expected temporal width of breakthrough curves at individual ports, it failed to take into account the effects of such large contrasts in transport rates. Using a sampling strategy based on a vertically averaged transport rate, we initially focused on the samplers nearest the injection well, intending to move the sampling downgradient as the tracer moved. Thus we failed to sample along the entire length of the network early in the test and missed peak breakthroughs at a number of downgradient ports.

Another factor complicating the analysis of GEMSTRAC1 was the poor characterization of the distribution of tracer mass immediately after injection, requiring the inclusion of initial concentration and injection zone mixing factor as unknown parameters in the transport model used to fit the tracer breakthrough curves. Ideally, these factors would have been specified as known, so that only the factors relating more directly to aquifer properties, the flux rate per unit thickness and the dispersivity, would have been included as fitting parameters in the analysis. Attempting to estimate all four parameters from the tracer breakthrough data leads to some highly nonunique fits, especially for those ports at which peak breakthroughs were missed. The sensitivity analysis presented in Chapter 5 demonstrates the negative impact of delayed sampling on our ability to uniquely identify the model parameters.

Factors that potentially led to systematic deviations between the actual transport behavior and that predicted by the horizontal, radially convergent transport model include potentially significant lateral deviations from a radial flow pattern, caused either by flow towards the rural water district wells to the west or the compensator well to the east, and significant deviations from horizontal flow, caused by a lack of perfect stratification of the hydraulic conductivity and/or effective partial penetration of the discharge well. The latter mechanism is required to explain the vertical differences in drawdown observed at

different sampling ports at TMC-3 and TMC-7 during a pumping test performed in August, 1997.

Despite these complications, the analysis of the tracer transport data, presented in Chapter 6, met with some success. In particular, the profiles of reference concentration and flux rate estimated from the individual-port breakthroughs (Figures 6.9 and 6.10) show some horizontal consistency and accord reasonably well with the graphical analysis of the tracer test presented in Chapter 4. The profile of fitted reference concentrations summarizes the distribution of tracer mass throughout the test, while the fitted flux rates reflect the relative distribution of horizontal hydraulic conductivity. The spatial correlation between these two profiles indicates that the tracer mass preferentially entered high-conductivity zones, resulting in an undersampling of lower conductivity zones. The dispersivity and injection zone mixing factors are very poorly estimated in almost all cases, so that the profiles of these estimates, shown in Figures 6.11 and 6.12, should be regarded with some skepticism. There does appear to be some spatial correlation between the estimated injection zone mixing factors and the fitted flux rates. This would be the expected result if the initial injection radius was larger in higher conductivity zones. The estimated longitudinal dispersivity values appear to increase with increasing transport distance. However, this effect could very easily be the result of the transport model's neglect of other mixing processes, such as horizontal and vertical transverse dispersion, rather than an indication of a scale effect in the dispersivity.

The comparative assessment of well testing methodologies in Chapter 7 shows that, upon further refinement, both multilevel slug tests and single-well dipole flow tests may be capable of yielding conductivity profiles of the resolution necessary for transport prediction. However, further work is required to fully evaluate the effectiveness of these methods. The numerical simulations of hydraulic tomography presented in Chapter 7 show that this method is

capable of resolving a considerable amount of detail in the hydraulic conductivity distribution. The results of the August, 1997, pumping test at the site indicate that relatively inexpensive air pressure transducers can be used to obtain drawdown measurements in multilevel samplers, providing the vertical resolution necessary for successful application of hydraulic tomography.

II. SUGGESTIONS FOR FUTURE RESEARCH

Any future tracer tests performed at the site should incorporate at least two major modifications of the procedures employed during GEMSTRAC1. First of all, the injection process must be carefully controlled and monitored so that the initial distribution of tracer mass is well-characterized. One possibility would be to inject the tracer into a sequence of separately packed-off intervals in the injection well, assuring that approximately equal amounts of tracer enter each level of the aquifer. A logical extension of this would be to perform several separate tracer tests over more limited intervals of the aquifer. Secondly, sampling must begin immediately after injection at all ports of interest in the test, in order to obtain complete breakthrough curves at all levels. In fact, it would probably be reasonable to perform some less ambitious tracer tests, configured to influence a smaller portion of the aquifer and focusing more on the collection of complete breakthrough curves at a few samplers, rather than on spatial snapshots at greater time intervals. For example, a test could involve injection over the lower half of the aquifer at well TMO-1 with more time-continuous monitoring at the ports in the two detailed samplers (TMC-4 and TMC-2) lying between TMO-1 and DW. (Alternatively, discharge could occur at well IW, with monitoring at TMC-8 and TMC-6). More limited tests of this nature might help to address some of the uncertainties surrounding GEMSTRAC1 without requiring the level of effort involved in that test.

As mentioned above, work on multilevel slug tests and dipole flow tests should continue at the site, in order to more fully assess the utility of these methods, both of which show promise. A more complete campaign of multilevel slug tests should be analyzed with the recently developed slug test model accounting for the various mechanisms influencing slug tests in highly-permeable media (McElwee and Zenner, 1998) and dipole flow tests employing smaller dipole tool dimensions should be performed, in order to determine whether these can provide the necessary vertical resolution in the estimated conductivity profile. Work on hydraulic tomography should also continue. Although logistical considerations will probably keep hydraulic tomography from becoming a routine site characterization technique, its use at tracer test sites with existing networks of multilevel samplers could provide considerable additional insight regarding the influence of conductivity variations on tracer transport. Current work in this area involves the design and testing of modified multilevel samplers at GEMS. The modified samplers are intended to be more appropriate for use as drawdown measurement devices than the existing samplers at the site. Development of a multilevel sampler that can also be employed to obtain high-resolution vertical profiles of drawdown would represent a significant contribution to site characterization technology.

REFERENCES

Adams, E. E., and L. W. Gelhar, 1992, Field study of dispersion in a heterogeneous aquifer, 2. Spatial moments analysis, Water Resources Research 28(12), 3293-3307.

Amos, D. E., 1986, Algorithm 644, a portable package for Bessel functions of a complex argument and nonnegative order, ACM Transactions on Mathematical Software, 12(3), 265-273.

Beck, J. V., and K. J. Arnold, 1977, Parameter Estimation in Engineering and Science, John Wiley, New York.

Bidaux, P., and C.-F. Tsang, 1991, Fluid flow patterns around a well bore or an underground drift with complex skin effects, Water Resources Research, 27(11), 2993-3008.

Boggs, J. M., S. C. Young, L. M. Beard, L. W. Gelhar, K. R. Rehfeldt, and E. E. Adams, 1992, Field study of dispersion in a heterogeneous aquifer, 1. Overview and site description, Water Resources Research 28(12), 3281-3291.

Butler, J. J., Jr., 1990, The role of pumping tests in site characterization: Some theoretical considerations, Ground Water 28(3), 394-402.

Butler, J. J., Jr., and W. Z. Liu, 1993, Pumping tests in nonuniform aquifers: The radially asymmetric case, Water Resources Research 29(2), 259-269.

Butler, J. J., Jr., G. C. Bohling, Z. Hyder, and C. D. McElwee, 1994, The use of slug tests to describe vertical variations in hydraulic conductivity, Journal of Hydrology, 156, pp. 137-162.

Butler, J. J., Jr., and C. D. McElwee, 1996, Well-testing methodologies for characterizing heterogeneities in alluvial-aquifer systems: Final technical report, Kansas Geological Survey Open File Report 95-75, 311 p.

Butler, J. J., Jr., C. D. McElwee, and D. D. Davies, 1997, Hydraulic tracers: A new tool for characterizing subsurface variations in hydraulic conductivity, KGS Open File Report 97-70, 9 pp.

Butler, J. J., Jr., and J. M. Healey, 1998, Relationship between pumping-test and slug-test parameters: Scale effect or artifact?, Ground Water, in press.

Butler, J. J., Jr., J. M. Healey, V. A. Zlotnik, and B. R. Zurbuchen, 1998, The dipole flow test for site characterization: Some practical considerations, KGS Open File Report 98-20, 11 pp.

Chen, C.-S., 1987, Analytical solutions for radial dispersion with Cauchy boundary at injection well, Water Resources Research, 23(7), 1217-1224.

Cooper, H. H., Jr., J. D. Bredehoeft, and I. S. Papadopulos, 1967, Response of a finite diameter well to an instantaneous charge of water, Water Resources Research 3(1), 263-169.

Copty, N., and Y. Rubin, 1995, A stochastic approach to the characterization of lithofacies from surface seismic and well data, Water Resources Research 31(7), 1673-1686.

Dagan, G., 1988, Time-dependent macrodispersion for solute transport in anisotropic heterogeneous aquifers, Water Resources Research, 24(9), 1491-1500.

de Hoog, F. R., J. H. Knight, and A. N. Stokes, 1982, An improved method for numerical inversion of Laplace transforms, SIAM Journal of Scientific and Statistical Computing, 3(3), 357-366.

Denne, J. E., R. E. Miller, L. R. Hathaway, H. G. O'Connor, and W. C. Johnson, 1998, Hydrogeology and geochemistry of glacial deposits in northeastern Kansas, Kansas Geological Survey, Bulletin 229, 127 pp.

Dennis, J. E., Jr., D. M. Gay, and R. E. Welsch, 1981, An adaptive nonlinear least-squares algorithm, ACM Transactions on Mathematical Software, 7, 348-368.

Deutsch, C. V., and Journel, A. G., 1992, GSLIB: Geostatistical Software Library and User's Guide, Oxford University Press, New York, 340 p.

Deutsch, C. V., and T. A. Hewett, 1996, Challenges in reservoir forecasting, Mathematical Geology, 28(7), 829-968.

Dufford, A. E., 1958, Quaternary geology and ground-water resources of Kansas River valley between Bonner Springs and Lawrence, Kansas, Kansas Geological Survey, Bulletin 130, Part 1, 96 pp.

Fader, S. W., 1974, Ground water in the Kansas River valley, Junction City to Kansas City, Kansas, Kansas Geological Survey, Bulletin 206, Part 2, 12 pp.

Freeze, R. A., and J. A. Cherry, 1979, Groundwater, Prentice-Hall, Inc., Englewood Cliffs, N. J., 604 p.

Freyberg, D. L., 1986, A natural gradient experiment on solute transport in a sand aquifer, 2. Spatial moments and the advection and dispersion of nonreactive tracers, Water Resources Research 22(13), 2031-2046.

Garabedian, S. P., D. R. LeBlanc, L. W. Gelhar, and M. A. Celia, 1991, Large-scale natural gradient tracer test in sand and gravel, Cape Cod, Massachusetts, 2. Analysis of spatial moments for a nonreactive tracer, Water Resources Research 27(5), 911-924.

Garbow, B. S., K. E. Hillstrom, and J. J. More, 1980, The Minpack Project, Argonne National Laboratory.

Gay, D. M., 1984, A trust-region approach to linearly constrained optimization, Lecture Notes in Mathematics, 1066, 71-105.

Gelhar, L. W., and C. L. Axness, 1983, Three-dimensional analysis of macrodispersion in aquifers, Water Resources Research, 19(1), 161-180.

Guvanasen, V., and V. M. Guvanasen, 1987, An approximate semianalytical solution for tracer injection tests in a confined aquifer with a radially converging flow field and finite volume of tracer and chase fluid, Water Resources Research, 23(8), 1607-1619.

Hall, J. M., 1998, Nitrate in a confined, alluvial aquifer, Douglas County, Kansas, Master's thesis, Department of Geology, University of Kansas, 110 pp.

Hess, K. M., S. H. Wolf, and M. A. Celia, 1992, Large-scale natural gradient tracer test in sand and gravel, Cape Cod, Massacusetts, 3. Hydraulic conductivity variability and calculated macrodispersivities, Water Resources Research, 28(8), 2011-2077.

Hyndman, D. W., and S. M. Gorelick, 1996, Estimating lithologic and transport properties in three dimensions using seismic and tracer data: The Kesterson aquifer, Water Resources Research 32(9), 2659-2670.

Huettl, T. J., 1994, An evaluation of a borehole induction single-well tracer test to characterize the distribution of hydraulic properties in an alluvial aquifer: Master's Thesis, Department of Geology, University of Kansas, Lawrence, KS.

Hvorslev, M. J., 1951, Time lag and soil permeability in groundwater observations, Waterways Experimental Station Bulletin 36, U.S. Army Corps of Engineers, Vicksburg, Miss., 50 p.

Isaaks, E. H., and R. M. Srivastava, 1989, An Introduction to Applied Geostatistics, Oxford University Press, New York, 561 pp.

Jacob, C. E., 1946, Radial flow in a leaky artesian aquifer: American Geophysical Union Transactions, 27(2), 198-205.

Javandel, I., C. Doughty, and C. F. Tsang, 1984, Groundwater Transport: Handbook of Mathematical Models, Water Resources Monograph 10, American Geophysical Union, Washington, D. C., 228 p.

Jensen, K. H., K. Bitsch, and P. L. Bjerg, 1993, Large-scale dispersion experiments in a sandy aquifer in Denmark: Observed tracer movements and numerical analysis, Water Resources Research 29(3), 673-696.

Journel, A. G., and F. Alabert, 1987, Focusing on spatial connectivity of extreme-valued attributes: Stochastic indicator models of reservoir heterogeneities, SPE Technical Paper 18324.

Journel, A. G., and H. Zhu, 1990, Integrating soft seismic data: Markov-Bayes updating, an alternative to cokriging and traditional regression, in Report 3, Stanford Center for Reservoir Forecasting, Stanford, CA.

Killey, R. W. D., and G. L. Moltyaner, 1988, Twin Lake tracer tests: Setting, methodology, and hydraulic conductivity distribution, Water Resources Research 24(10), 1585-1612.

Kitanidis, P. K., 1994, The concept of dilution index, Water Resources Research 30(7), 2011-2026.

Knopman, D. S., and C. I. Voss, 1987, Behavior of sensitivities in the one-dimensional advection-dispersoin equation: Implications for parameter estimation and sampling design, Water Resources Research, 23(2), 253-272.

Koltermann, C. E., and S. M. Gorelick, 1996, Heterogeneity in sedimentary deposits: A review of structure-imitating, process-imitating, and descriptive approaches, Water Resources Research 32(9), 2617-2658.

LeBlanc, D. R., S. P. Garabedian, K. M. Hess, L. W. Gelhar, R. D. Quadri, K. G. Stollenwerk, and W. W. Wood, 1991, Large-scale natural gradient test in sand and gravel, Cape Cod, Massachusetts, 1. Experimental design and observed tracer movement, Water Resources Research 27(5), 895-910.

Li, L., D. A. Berry, P. J. Culligan-Hensley, and K. Bajracharya, 1994, Mass transfer in soils with local stratification of hydraulic conductivity, Water Resources Research 30(11), 2891-2900.

Mackay, D. M., D. L. Freyberg, P. V. Roberts, and J. A. Cherry, 1986, A Natural gradient experiment on solute transport in a sand and gravel aquifer, 1. Approach and overview of plume movement, Water Resources Research, 22(13), 2017-2029.

Mackay, D. M., G. Bianchi-Mosquera, A. A. Kopania, and H. Kianjah, 1994, A forced-gradient experiment on solute transport in the Borden aquifer, 1. Experimental methods and moment analyses of results, Water Resources Research, 30(2), 369-383.

Macpherson, G. L., and M. K. Schulmeister, 1994, Source(s), fate and residence time of nitrate at two sites in Kansas -- a comparison of carbonate and alluvial aquifers, Kansas Water Resources Research Institute Report, Contribution No.312, 81 pp.

Macpherson, G. L., C. D. McElwee, J. J. Butler, Jr., and G. C. Bohling, 1996, Water chemistry variation in an alluvial aquifer -- Multi-level samplers reveal more than screened wells, Geological Society of America, Abstracts with Programs, 28(7), p. A-460.

McElwee, C. D., 1982, Sensitivity analysis and the ground-water inverse problem, Ground Water, 20(6), 723-735.

McElwee, C. D., 1998, Multilevel nonlinear slug tests to characterize high conductivity aquifers, Kansas Geological Survey Open File Report 98-62.

McElwee, C. D., and J. J. Butler, Jr., 1995, Characterization of heterogeneities controlling transport and fate of pollutants in unconsolidated sand and gravel aquifers: Final report, Kansas Geological Survey Open File Report 95-16.

McElwee, C. D., and J. J. Butler, Jr., 1996, Experimental verification of a general model for slug tests, Kansas Geological Survey Open File Report 96-47.

McElwee, C. D., G. C. Bohling, and J. J. Butler, Jr., 1995, Sensitivity analysis of slug tests, Part 1. The slugged well, Journal of Hydrology, 164, 53-67.

McElwee, C. D., and M. A. Zenner, 1998, A nonlinear model for analysis of slug-test data, Water Resources Research 34(1), 55-66.

Melville, J. G., F. J. Molz, and O. Güven, 1989, Multilevel slug tests: Performance and analysis, *in* Molz, F. J., J. G. Melville, and O. Güven, eds., Proceedings of the Conference on New Field Techniques for Quantifying the Physical and Chemical Properties of Heterogeneous Aquifers, NWWA, Dublin, OH, p. 693-703.

Moench, A. F., 1989, Convergent radial dispersion: A Laplace transform solution for aquifer tracer testing, Water Resources Research, 25(3), 439-447.

Moench, A. F., 1991, Convergent radial dispersion: A note on evaluation of the Laplace transform solution, Water Resources Research, 27(12), 3261-3264.

Moench, A. F., 1996, Correction to "Convergent radial dispersion: A Laplace transform solution for aquifer tracer testing", Water Resources Research, 32(5), 1475.

Moltyaner, G. L., and R. W. D. Killey, 1988a, Twin Lake tracer tests: Longitudinal dispersion, Water Resources Research 24(10), 1613-1627.

Moltyaner, G. L., and R. W. D. Killey, 1988b, Twin Lake tracer tests: Transverse dispersion, Water Resources Research 24(10), 1628-1637.

Molz, F. J., O. Güven, J. G. Melville, R. D. Crocker, and K. T. Matteson, 1986, Performance, analysis, and simulation of a two-well tracer test at the Mobile Site, Water Resources Research, 22(7), 1031-1037.

Molz, F. J., O. Güven, J. G. Melville, J. S. Nohrstedt, and J. K. Overholtzer, 1988, Forced-gradient tracer tests and inferred hydraulic conductivity distributions at the Mobile Site, Ground Water, 26(5), 570-579.

Molz, F. J., and O. Güven, 1988, Comment on "A natural gradient experiment on solute transport in a sand aquifer: Spatial variability of hydraulic conductivity and its role in the dispersion process" by E. A. Sudicky, Water Resources Research, 24(7), 1209-1210.

Molz, F. J., R. H. Morin, A. E. Hess, J. G. Melville, and O. Güven, 1989, The impeller meter for measuring aquifer permeability variations: Evaluation and comparison with other tests, Water Resources Research, 25(7), 1677-1683.

O'Connor, H. G., 1992 (Revised), Geologic Map, Douglas County, Kansas, Kansas Geological Survey, Map M-26, Scale 1:50,000.

Orion Research, 1991, Model 94-35 and 94-53 halide electrodes instruction manual: Orion Research Incorporated, Form IM9435,3, 29 pp.

Parker, J. C., and M. Th. van Genuchten, Flux-averaged and volume-averaged concentrations in continuum approaches to solute transport, Water Resources Research, 20(7), 866-872, 1984.

Press, W. H., S. A. Teukolsky, W. T. Vetterling, and B. P. Flannery, 1992, Numerical Recipes in FORTRAN, The Art of Scientific Computing, Second Edition, Cambridge University Press, 963 pp.

Reed, J. E., 1980, Type curves for selected problems of flow to wells in confined aquifers, Techniques of Water-Resources Investigations of the United States Geological Survey, Book 3, Chapter 3, U.S. Government Printing Office, 106 pp.

Rehfeldt, K. R, and L. W. Gelhar, 1992, Stochastic analysis of dispersion in unsteady flow in heterogeneous aquifers, Water Resources Research, 28(8), 2085-2099.

Rehfeldt, K. R., J. M. Boggs, and L. W. Gelhar, 1992, Field study in a hetergeneous aquifer, 3. Geostatistical analysis of hydraulic conductivity, Water Resources Research 28(12), 3309-3324.

Srivastava, R. M., 1994, An overview of stochastic methods for reservoir characterization, *in* Yarus, J. M., and R. L. Chambers (eds.), Stochastic Modeling and Geostatistics: Principles, Methods, and Case Studies, AAPG Computer Applications in Geology No. 3, American Association of Petroleum Geologists, Tulsa, Oklahoma, 3-16.

Statistical Sciences, 1995, S-Plus Guide to Statistical and Mathematical Analysis, Version 3.3, StatSci, a division of MathSoft, Inc., Seattle.

Sudicky, E. A., 1986, A natural gradient experiment on solute transport in a sand aquifer: Spatial variability of hydraulic conductivity and its role in the dispersion process, Water Resources Research 22(13), 2069-2082.

Sudicky, E. A., J. A. Cherry, and E. O. Frind, 1983, Migration of contaminants in groundwater at a landfill: A case study, 4, A natural-gradient dispersion test, Journal of Hydrology 63, 81-108.

Sudicky, E. A., and P. S. Huyakorn, 1991, Contaminant migration in imperfectly known heterogeneous groundwater systems, Reviews of Geophysics, Supplement, April 1991, U. S. National Report to the International Union of Geodesy and Geophysics

1987-1990, Contributions in Hydrology, American Geophysical Union, Washington, D. C., 240-253.

Thorbjarnarson, K. W., and D. M. Mackay, 1994, A forced-gradient experiment on solute transport in the Borden aquifer, 2. Transport and dispersion of the conservative tracer, Water Resources Research, 30(2), 385-399.

Voegeli, S. L., 1991, Initial analysis of the 10/22/88 pumping test at the Geohydrologic Experimental and Monitoring Site, Advanced Special Problems Report for Master of Science, Water Resources Science, Department of Civil Engineering, University of Kansas, 30 pp.

Wang, H. F., and M. P. Anderson, 1982, Introduction to Groundwater Modeling: Finite Difference and Finite Element Methods, W. H. Freeman and Company, New York, 237 p.

Wheatcraft, S. W., and F. Winterberg, 1985, Steady state flow passing through a cylinder of permeability different from the surrounding medium, Water Resources Research, 21(12), 1923-1929.

Widdowson, M. A., F. J. Molz, and J. G. Melville, 1990, An analysis technique for multilevel and partially penetrating slug test data, Ground Water, 28(6), 937-945.

Woodbury, A. D., and E. A. Sudicky, 1991, The geostatistical characteristics of the borden aquifer, Water Resources Research 27(4), 533-546.

Yeh, T.-C. J., J. Mas-Pla, T. M. Williams, and J. F. McCarthy, 1995, Observation and three-dimensional simulation of chloride plumes in a sandy aquifer under forced-gradient conditions, Water Resources Research 31(9), 2141-2157.

Zlotnik, V. A., and G. Ledder, 1996, Theory of dipole flow in uniform anisotropic aquifers, Water Resources Research 32(4), 1119-1128.

Zlotnik, V. A., and J. D. Logan, 1996, Boundary conditions for convergent radial tracer tests and effect of well bore mixing volume, Water Resources Research, 32(7), 2323-2328.

Zlotnik, V. A., and B. R. Zurbuchen, 1998, Dipole probe: Design and field application of a single-borehole device for measurements of small-scale variations of hydraulic conductivity, Ground Water, in press.

APPENDIX A: SITE SURVEY AND PORT ELEVATION DATA

Table A.1. November 8, 1994, network survey data. Survey origin was an index rod near GEMS well 10-1.

name	MLS ID #	Direction[b]	RodHeight (meters)[c]	Distance 1 (meters)[d]	Distance 2 (meters)[d]
CS[a]	-	90° 00'	1.387	8.14	8.12
IW	-	-6° 10'	0.753	22.72	22.72
TMO-1	-	1° 50'	0.943	16.15	16.15
DW	-	18° 25'	0.904	10.10	10.10
TMC-1	11	12° 45'	1.044	11.50	11.48
TMC-2	21	8° 40'	1.021	12.69	12.67
TMW-3	31	-2° 45'	0.785	13.69	13.65
TMC-3	32	4° 55'	0.946	14.05	14.04
TME-3	33	11° 40'	1.068	14.82	14.81
TMW-4	41	-4° 20'	0.902	15.01	15.00
TMC-4	42	2° 40'	0.825	15.46	15.46
TME-4	43	8° 45'	0.954	16.19	16.19
TMWW-4.5	51	-10° 45'	1.094	15.14	15.13
TMW-5	52	-5° 30'	0.884	16.20	16.18
TMC-5	53	0° 30'	0.919	16.86	16.85
TME-5	54	6° 15'	0.991	17.40	17.40
TMEE-5	55	10° 40'	1.038	18.35	18.35
TMW-6	61	-6° 45'	1.007	17.58	17.58
TMC-6	62	-1° 30'	1.015	18.15	18.15
TME-6	63	3° 55'	0.989	18.69	18.69
TMW-7	71	-7° 45'	0.863	19.03	19.03
TMC-7	72	-3° 00'	0.613	19.62	19.61
TME-7	73	2° 50'	1.009	20.25	20.25
TMW-8	81	-8° 35'	1.048	20.49	20.48
TMC-8	82	-4° 25'	0.870	20.98	20.98
TME-8	83	0° 20'	1.149	21.70	21.71
TMC-9	91	-7° 50'	0.965	24.55	24.53

[a]Corps Stake. The top of the Corps Stake is the elevation reference point.

[b]Direction, with respect to north, from origin to well or MLS. There is actually some uncertainty regarding true north. The direction from the survey origin to the Corps Stake is taken as due east in this report.

[c]Stadium rod reading when rod set on measurement point of well or top of sampler.

[d]Distance 1 and Distance 2 are tape-measured distances from the origin to the well or sampler. Distance 2 was measured on November 10, 1994.

Table A.2. Sampler coordinates computed from survey data (Table A.1).

name	MLS ID #	Meters east of origin	Meters north of origin	Network x coord. (meters)[a]	Network y coord. (meters)[a]	Elev. (meters)[b]
IW	-	-2.44	22.59	0.00	0.00	0.634
TMO-1	-	0.52	16.14	7.09	0.15	0.444
DW	-	3.19	9.58	14.17	0.00	0.483
TMC-1	11	2.54	11.21	12.42	0.05	0.343
TMC-2	21	1.91	12.53	10.96	0.00	0.366
TMW-3	31	-0.66	13.65	8.91	-1.91	0.602
TMC-3	32	1.20	13.99	9.33	-0.07	0.441
TME-3	33	3.00	14.51	9.58	1.78	0.319
TMW-4	41	-1.13	14.97	7.51	-1.83	0.485
TMC-4	42	0.72	15.45	7.81	0.06	0.562
TME-4	43	2.46	16.00	7.99	1.88	0.433
TMWW -4.5	51	-2.82	14.87	6.93	-3.42	0.293
TMW-5	52	-1.55	16.12	6.29	-1.76	0.503
TMC-5	53	0.15	16.86	6.29	0.10	0.468
TME-5	54	1.89	17.30	6.58	1.88	0.396
TMEE-5	55	3.40	18.03	6.50	3.55	0.349
TMW-6	61	-2.07	17.46	4.86	-1.69	0.380
TMC-6	62	-0.48	18.14	4.86	0.04	0.372
TME-6	63	1.28	18.65	5.10	1.85	0.398
TMW-7	71	-2.57	18.85	3.38	-1.60	0.524
TMC-7	72	-1.03	19.59	3.31	0.11	0.774
TME-7	73	1.00	20.23	3.53	2.22	0.378
TMW-8	81	-3.06	20.26	1.89	-1.49	0.339
TMC-8	82	-1.62	20.92	1.86	0.09	0.517
TME-8	83	0.13	21.71	1.83	2.01	0.238
TMC-9	91	-3.34	24.31	-1.94	-0.15	0.422

[a]Network x coordinate is distance along the centerline from IW to DW (S23°E). Network y coordinate is distance perpendicular to the centerline, positive to the east (N67°E).

[b]Elevation of well measurement point or top of MLS above top of Corps Stake.

Table A.3. MLS port elevations, meters above datum. Datum is 21.33 meters (70 feet) below the top of the Corps Stake and corresponds roughly with the bottom of the aquifer. Most MLS have ports at 0.61-meter (2-foot) spacings, with the top port (port 17) 11.58 meters (38 feet) below the top of the MLS. TMC-2, TMC-4, TMC-6, and TMC-8 have a 0.30-meter (1-foot) port spacing with port 17 located 16.15 meters (53 feet) below the top of the MLS.

MLS name	port number								
	1	2	3	4	5	6	7	8	9
TMC-1	0.343	0.952	1.562	2.172	2.781	3.391	4.000	4.610	5.219
TMC-2	0.366	0.671	0.975	1.280	1.585	1.890	2.194	2.499	2.804
TMW-3	0.602	1.212	1.821	2.431	3.040	3.650	4.259	4.869	5.479
TMC-3	0.440	1.050	1.660	2.269	2.879	3.488	4.098	4.707	5.317
TME-3	0.319	0.928	1.538	2.147	2.757	3.366	3.976	4.585	5.195
TMW-4	0.485	1.095	1.704	2.314	2.923	3.533	4.143	4.752	5.362
TMC-4	0.561	0.866	1.171	1.476	1.781	2.085	2.390	2.695	3.000
TME-4	0.433	1.042	1.652	2.262	2.871	3.481	4.090	4.700	5.309
TMWW -4.5	0.293	0.902	1.512	2.121	2.731	3.340	3.950	4.560	5.169
TMW-5	0.503	1.112	1.722	2.332	2.941	3.551	4.160	4.770	5.379
TMC-5	0.468	1.077	1.687	2.297	2.906	3.516	4.125	4.735	5.344
TME-5	0.396	1.006	1.615	2.225	2.835	3.444	4.054	4.663	5.273
TMEE-5	0.349	0.959	1.568	2.178	2.787	3.397	4.006	4.616	5.226
TMW-6	0.380	0.990	1.599	2.209	2.818	3.428	4.037	4.647	5.257
TMC-6	0.372	0.677	0.981	1.286	1.591	1.896	2.201	2.505	2.810
TME-6	0.398	1.007	1.617	2.226	2.836	3.446	4.055	4.665	5.274
TMW-7	0.524	1.134	1.743	2.353	2.963	3.572	4.182	4.791	5.401
TMC-7	0.774	1.384	1.993	2.603	3.212	3.822	4.432	5.041	5.651
TME-7	0.378	0.988	1.597	2.207	2.816	3.426	4.035	4.645	5.254
TMW-8	0.338	0.948	1.557	2.167	2.777	3.386	3.996	4.605	5.215
TMC-8	0.517	0.821	1.126	1.431	1.736	2.041	2.345	2.650	2.955
TME-8	0.238	0.847	1.457	2.066	2.676	3.286	3.895	4.505	5.114
TMC-9	0.422	1.032	1.641	2.251	2.860	3.470	4.080	4.689	5.299

Table A.3, continued: MLS port elevations, meters above datum.

MLS name	port number 10	11	12	13	14	15	16	17
TMC-1	5.829	6.439	7.048	7.658	8.267	8.877	9.486	10.096
TMC-2	3.414	3.718	4.023	4.328	4.633	4.938	5.242	5.547
TMW-3	6.088	6.698	7.307	7.917	8.526	9.136	9.746	10.355
TMC-3	5.927	6.536	7.146	7.755	8.365	8.974	9.584	10.194
TME-3	5.805	6.414	7.024	7.633	8.243	8.852	9.462	10.072
TMW-4	5.971	6.581	7.190	7.800	8.410	9.019	9.629	10.238
TMC-4	3.609	3.914	4.219	4.524	4.828	5.133	5.438	5.743
TME-4	5.919	6.528	7.138	7.748	8.357	8.967	9.576	10.186
TMWW -4.5	5.779	6.388	6.998	7.607	8.217	8.827	9.436	10.046
TMW-5	5.989	6.599	7.208	7.818	8.427	9.037	9.646	10.256
TMC-5	5.954	6.564	7.173	7.783	8.392	9.002	9.611	10.221
TME-5	5.882	6.492	7.101	7.711	8.321	8.930	9.540	10.149
TMEE-5	5.835	6.445	7.054	7.664	8.273	8.883	9.493	10.102
TMW-6	5.866	6.476	7.085	7.695	8.304	8.914	9.524	10.133
TMC-6	3.420	3.724	4.029	4.334	4.639	4.944	5.248	5.553
TME-6	5.884	6.493	7.103	7.713	8.322	8.932	9.541	10.151
TMW-7	6.010	6.620	7.230	7.839	8.449	9.058	9.668	10.277
TMC-7	6.260	6.870	7.479	8.089	8.699	9.308	9.918	10.527
TME-7	5.864	6.474	7.083	7.693	8.302	8.912	9.521	10.131
TMW-8	5.824	6.434	7.044	7.653	8.263	8.872	9.482	10.091
TMC-8	3.564	3.869	4.174	4.479	4.784	5.088	5.393	5.698
TME-8	5.724	6.333	6.943	7.553	8.162	8.772	9.381	9.991
TMC-9	5.908	6.518	7.127	7.737	8.347	8.956	9.566	10.175

APPENDIX B: GEMSTRAC1 CONCENTRATION DATA

Table B.1 (succeeding pages). Bromide concentrations in mg/l from GEMSTRAC1 tracer test, performed October, 1994. The "Sample Time" column shows the time of day the sample was taken. The "Test Hours" column shows the elapsed time (in decimal hours) since the beginning of injection (10:13 on October 7, 1994).

Sample Date	Sample Round	Sample Time	Test Hours	MLS ID	port 1	port 2	port 3	port 4	port 5	port 6	port 7	port 8	port 9	port 10	port 11	port 12	port 13	port 14	port 15	port 16	port 17
10/7/94	1	14:04	3.85	TMC-9	1.69	8.64	79.24	0.18	0.27	0.30	0.30	0.29	0.16	0.21	0.23	0.23	0.25	0.19	0.25	0.26	0.24
10/7/94	1	14:25	4.20	TMC-8	0.16	0.49	0.47	194.51	163.45	115.54	0.27	0.22	0.22	0.33	0.26	112.08	0.18	0.34	0.31	0.20	0.23
10/7/94	1	14:40	4.45	TMW-8	0.20	0.14	6.33	53.83	0.19	0.22	0.66	0.85	0.19	0.16	0.20	0.21	0.20	0.19	0.22	0.25	0.24
10/7/94	1	14:55	4.70	TME-8	0.17	0.18	0.20	0.20	0.19	0.19	0.17	0.17	0.17	0.21	0.24	0.22	0.21	0.20	0.19	0.19	0.17
10/7/94	1	15:10	4.95	TMC-7	0.22	2.46	18.01	0.19	0.26	0.22	0.25	0.22	0.15	0.17	0.21	0.19	0.20	0.20	0.22		0.21
10/7/94	2	18:49	8.60	TMC-8	0.21	1.36	0.83	306.49	243.28	203.49	2.37	0.34	0.91	0.29	0.29	314.82	0.19	106.28	281.63	0.17	0.28
10/7/94	2	19:07	8.90	TMW-8	0.21	0.15	38.19	129.67	0.27	0.33	2.88	25.04	0.18	0.20							
10/7/94	2	19:41	9.47	TMC-7	0.15	6.83	166.26	0.15	0.17	0.19	0.23	0.67	0.14	0.15							
10/7/94	3	22:11	11.97	TMW-8	0.29	0.23	86.16	197.12	0.30	1.67	10.51	21.81	0.29	0.20	0.25	0.25	0.22	0.21	0.24	0.27	0.25
10/7/94	3	22:28	12.25	TMC-8	26.12	1.83	2.12	356.24	300.99	262.19	14.12	1.86	5.09	0.59	4.72	355.14	3.09	350.10	369.39	0.26	0.26
10/7/94	3	22:46	12.55	TME-8	0.23	3.59	3.90	0.22	0.22	0.21	0.23	0.21	0.19	0.22	0.23	0.25	0.23	0.21	0.18	0.21	0.20
10/7/94	3	23:01	12.80	TMC-7	0.19	29.26	253.85	0.20	0.19	0.20	0.22	65.16	0.17	0.16	0.21	0.20	0.25	0.22	0.20		0.22
10/7/94	3	23:18	13.08	TMC-9	0.21	0.48	5.25	0.18	0.22	0.21	0.25	0.24	0.18	0.17	0.21	0.21	0.21	0.24	0.25	0.23	0.22
10/8/94	4	6:36	20.38	TMC-7	0.97	67.53	302.97	0.21	0.34	0.23	3.01	227.77	0.14	0.19							
10/8/94	4	6:49	20.60	TME-8	0.25	65.55	9.88	0.19	0.29	0.20	0.26	0.24	0.17	0.25	0.21	0.27	0.25	0.21	0.22	0.18	0.19
10/8/94	4	7:02	20.82	TMC-8	227.27	5.52	11.61	339.20	283.12	278.65	47.21	11.93	25.26	8.34	119.56	278.92	64.95	64.36	57.54	170.03	0.44
10/8/94	4	7:13	21.00	TMW-8	1.48	0.16	149.83	207.48	3.53	10.55	6.66	6.79	9.01	0.27	0.22	0.23	0.20	0.23	0.27	0.23	0.25
10/8/94	4	7:28	21.25	TMC-9	0.15	0.13	1.52	0.18	0.21	0.20	0.20	0.22	0.17	0.18	0.17	0.19	0.19	0.21	0.23	0.19	0.21
10/8/94	5	10:21	24.13	TMC-7	4.19	114.08	306.42	0.58	0.79	0.25	12.07	246.38	0.17	0.24	0.19	0.23	0.24	0.20	0.23		0.22
10/8/94	5	10:38	24.42	TME-8	0.54	108.06	6.06	0.16	0.18												
10/8/94	5	10:53	24.67	TMC-8	263.08	12.63	40.95	281.76	235.25	246.20	71.22	31.16	40.35	16.30	175.23	172.74	96.99	32.10	17.62	372.91	9.78
10/8/94	5	11:07	24.90	TMW-8	1.58	0.17	163.19	201.56	6.66												
10/8/94	6	13:59	27.77	TMC-7	8.79	126.41	264.24	1.56	3.88	0.43	38.31	120.02	0.19	0.28							
10/8/94	6	14:13	28.00	TME-8	0.60	135.50	4.31	0.17	0.19	0.19	0.43	0.20	0.17	0.21	0.19	0.28	0.22	0.19	0.19	0.19	0.22
10/8/94	6	14:26	28.22	TMC-8	292.06	26.37	64.52	241.13	203.45	207.20	80.97	34.87	55.54	26.94	240.72	115.04	127.55	18.73	4.91	416.33	44.23
10/8/94	6	14:39	28.43	TMW-8	1.51	0.29	162.33	179.80	8.39	16.97	1.66	0.23	0.34	0.28	0.23	0.23	0.19	0.21	0.28	0.25	0.25
10/8/94	6	14:54	28.68	TMC-9	0.17	0.13	0.72	0.19	0.22	0.15	0.18	0.20	0.16	0.17	0.17	0.19	0.19	0.21	0.23	0.19	0.19
10/8/94	7	18:03	31.83	TMC-6	43.87	18.70	43.29	97.28	152.35	216.94	167.67	15.38	5.60	0.78	0.48	199.57	2.67	22.40	102.25	0.54	0.27
10/8/94	7	18:20	32.12	TMC-7	14.82	149.63	225.66	2.80	9.49	1.42	33.44	47.40	0.17	0.27							
10/8/94	7	18:37	32.40	TME-8	1.35	135.44	2.21	0.17	0.17	0.20	0.78	0.19	0.15	0.17	0.22	0.27	0.22	0.19	0.19	0.21	0.20
10/8/94	7	18:56	32.72	TMC-8	304.90	34.37	133.91	166.11	155.85	161.82	102.15	51.03	71.45	37.63	280.33	57.37	189.91	8.81	0.87	322.94	81.19
10/8/94	7	19:17	33.07	TMW-8	1.65	0.14	165.38	153.22	13.08												
10/8/94	8	22:21	36.13	TMW-8	2.23	0.17	164.72	128.63	15.93	39.51	0.64	0.23	0.22	0.31	0.23	0.21	0.20	0.20	0.30	0.25	0.25
10/8/94	8	22:41	36.47	TMC-8	293.55	35.89	162.86	122.14	123.04	126.09	96.11	57.08	81.22	52.56	267.78	32.36	192.17	4.37	0.49	97.08	52.66
10/8/94	8	22:58	36.75	TMC-7	17.82	152.06	179.76	5.30	18.20	7.18	25.01	14.48	0.19	0.28	0.21	0.24	0.23	0.20	0.22		0.20
10/8/94	8	23:16	37.05	TMC-6	49.67	15.38	46.10	131.92	176.24	201.09	178.27	22.23	7.09	0.78	0.48	217.12	6.25	8.27	40.08	2.75	0.29
10/8/94	8	23:32	37.32	TMC-5	2.33	0.60	223.12	180.90	1.08	1.52	127.08	8.94	0.19	0.24	0.19	0.23	0.20	0.26	0.28	0.19	0.19
10/9/94	9	6:19	44.10	TMC-8	301.46	49.40	233.72	71.96	75.50	86.10	74.01	44.59	97.45	83.56	226.56	21.11	213.12	1.29	0.35	2.31	8.60
10/9/94	9	6:33	44.33	TMC-7	71.20	148.51	105.81	15.08	27.02	37.63	38.42	0.91	0.98	0.28	0.18	0.22	0.22	0.29	0.23		0.20
10/9/94	9	6:48	44.58	TMC-6	27.13	16.56	23.87	132.08	107.46	126.52	134.55	16.50	5.60	0.71	1.81	154.06	32.79	1.27	4.58	50.79	0.25
10/9/94	9	7:01	44.80	TMW-8	2.96	0.24	129.88	68.78	27.14	51.17	0.40	0.22	0.19	0.27	0.21	0.18	0.16	0.18	0.23	0.23	0.22
10/9/94	9	7:31	45.30	TMW-7	0.10	0.11	4.50	4.34	0.19	0.18	0.17	0.20	0.17	0.15	0.16	0.17	0.20	0.20	0.19	0.21	0.20
10/9/94	10	10:10	47.95	TME-7	0.15	14.29	0.19	0.18	0.18	0.17	0.25	0.16	0.16	0.15	0.16	0.20	0.17	0.18	0.16	0.17	0.19

Sample Date	Sample Round	Sample Time	Test Hours	MLS ID	port 1	port 2	port 3	port 4	port 5	port 6	port 7	port 8	port 9	port 10	port 11	port 12	port 13	port 14	port 15	port 16	port 17
10/9/94	10	10:26	48.22	TMC-8	269.07	53.03	244.61	54.35	59.07	70.18	59.88	47.56	102.75	97.52	154.08	19.23	189.22	0.63	0.34	0.47	8.17
10/9/94	10	10:39	48.43	TMC-7		142.99	82.93	12.54	33.67	42.03	43.27	0.39	6.41	0.27	0.23	0.25	0.22	0.52	0.24		0.23
10/9/94	10	10:54	48.68	TMC-6	22.03	24.83	17.68	128.88	89.31	111.88	120.14	15.95	5.58	0.70	3.44	140.36	34.07	0.77	1.30	111.21	0.27
10/9/94	10	11:08	48.92	TMC-5	0.38	7.27	160.55	143.43	1.70	6.33	51.47	0.53	0.20	0.25	0.21	0.26	0.20	0.21	0.24	0.21	0.21
10/9/94	10	11:21	49.13	TMC-4	8.90	5.37	1.97	6.51	7.38	67.73	89.14	37.39	11.05	13.93	102.44	31.58	0.71	12.21	0.25	0.23	0.24
10/9/94	11	14:47	52.57	TMC-1	0.15	0.19	89.03	58.22	7.16	28.69	23.56	0.21	0.20	0.27	0.22	0.25	0.21	0.21	0.29	0.24	0.25
10/9/94	11	14:58	52.75	TMC-2	0.09	0.11	0.16	0.13	1.27	31.62	70.57	4.10	0.24	0.25	0.25	14.58	1.03	0.16	0.17	0.17	0.23
10/9/94	11	15:11	52.97	TMC-3	0.10	0.13	9.88	68.64	0.20	0.18	0.17	0.19	0.18	0.15	0.18	0.18	0.20	0.20	0.21	0.23	0.22
10/9/94	11	15:23	53.17	TMC-5	0.44	8.73	130.76	118.51	2.27	6.27	37.14	0.37	0.19	0.24	0.22	0.25	0.20	0.21	0.24	0.23	0.23
10/9/94	11	15:39	53.43	TMC-7	75.41	129.28	64.53	17.81	38.51	49.55	53.42	0.31	9.93	0.27	0.22	0.24	0.19	1.67	0.22		0.23
10/9/94	11	16:02	53.82	TMW-6	0.22	0.22	0.27	4.78	0.34	0.24	0.21	0.18	0.17	0.17	0.15	0.18	0.17	0.18	0.21	0.21	0.24
10/9/94	11	16:26	54.22	TME-6	7.26	0.85	15.82	0.17	0.19	0.45	37.48	0.64	0.14	0.17	0.19	0.25	0.21	0.17	0.18	0.20	0.25
10/9/94	12	22:16	60.05	TMC-1	0.19	0.24	85.50	62.41	5.14	21.99	15.34	0.24	0.23	0.26	0.21	0.24	0.20	0.21	0.27	0.23	0.25
10/9/94	12	22:33	60.33	TMC-3	0.10	0.13	9.57	57.56	0.18	0.15	0.16	0.20	0.20	0.14	0.14	0.16	0.19	0.21	0.20	0.20	0.20
10/9/94	12	22:51	60.63	TMC-4	7.39	4.45	1.33	2.97	3.19	33.23	52.56	27.17	9.15	19.80	92.47	13.37	0.33	2.20	0.30	0.19	0.21
10/9/94	12	23:09	60.93	TMC-5	0.91	12.05	101.20	94.62	2.60	8.33	24.17	0.31	1.80	0.25	0.22	0.23	0.18	0.27	0.25	0.22	0.22
10/9/94	12	23:26	61.22	TMC-7	76.06	122.67	45.12	18.87	52.78	43.15	59.39	0.25	3.76	0.27	0.21	0.25	0.20	3.64	0.25		0.21
10/9/94	12	23:43	61.50	TMW-7	0.15	0.12	2.14	2.21	0.20	0.17	0.17	0.18	0.16	0.15	0.13	0.14	0.16	0.16	0.19	0.18	0.19
10/10/94	13	6:08	67.92	TMC-1	0.11	0.13	65.05	55.97	3.65	9.49	9.70	0.21	0.20	0.24	0.23	0.24	0.24	0.25	0.30	0.25	0.25
10/10/94	13	6:22	68.15	TMC-3	0.12	0.15	9.86	46.03	0.20	0.19	0.18	0.20	0.19	0.16	0.18	0.18	0.19	0.21	0.22	0.24	0.23
10/10/94	13	6:33	68.33	TMC-5	1.86	23.20	65.63	69.49	3.86	9.00	15.56	0.27	20.85	0.27	0.22	0.25	0.21	0.28	0.28	0.26	0.22
10/10/94	13	6:45	68.53	TMC-6	35.08	51.55	26.22	92.03	40.51	53.00	58.64	16.83	8.09	0.89	2.92	64.69	25.77	0.24	0.32	22.28	22.75
10/10/94	13	6:57	68.73	TMC-7	62.05	104.84	32.56	22.23	66.77	36.96	51.43	0.24	0.99	0.28	0.23	0.29	0.23	10.45	0.28		0.24
10/10/94	13	7:11	68.97	TMW-8	1.75	0.17	60.23	23.50	8.30	17.29	0.29	0.20	0.16	0.24	0.22	0.18	0.17	0.17	0.23	0.23	0.24
10/10/94	14	11:07	72.90	TMC-8	110.41	44.80	146.14	17.21	29.22	29.21	41.37	72.11	111.92	149.50	70.59	11.01	96.51	0.20	0.42	0.22	83.47
10/10/94	14	11:18	73.08	TMC-7	52.40	98.77	27.20	25.11	69.55	35.99	42.91	0.24	1.10	0.26	0.21	0.25	0.25	16.85	0.40		0.30
10/10/94	14	11:29	73.27	TMC-6	23.19	43.36	10.36	76.15	24.18	36.48	47.11	12.48	5.10	1.23	4.72	41.95	26.39	0.23	0.26	3.17	2.06
10/10/94	14	11:40	73.45	TMC-5	2.43	23.91	48.17	54.24	4.20	11.21	11.67	0.24	25.04	0.25	0.20	0.22	0.20	0.25	0.25	0.25	0.20
10/10/94	14	11:51	73.63	TMC-4	2.95	2.25	0.72	1.59	1.24	24.83	30.38	13.07	6.93	33.77	52.07	9.52	0.23	0.20	0.28	0.24	0.24
10/10/94	14	12:01	73.80	TMC-3	0.14	0.22	7.98	33.10	0.30	0.20	0.19	0.21	0.20	0.19	0.19	0.18	0.21	0.21	0.22	0.25	0.21
10/10/94	14	12:12	73.98	TMC-2	0.11	0.13	0.16	0.15	1.99	21.15	37.26	3.11	0.21	0.28	0.27	0.31	0.34	0.17	0.19	0.18	0.19
10/10/94	14	12:23	74.17	TMC-1	0.13	0.16	49.07	46.04	2.83	5.47	5.53	0.25	0.22	0.27	0.23	0.25	0.24	0.25	0.31	0.25	0.26
10/10/94	15	16:06	77.88	TMC-1	0.09	0.13	46.24	42.83	3.17	3.90	3.77	0.26	0.22	0.26	0.21	0.24	0.24	0.24	0.30	0.25	0.25
10/10/94	15	16:20	78.12	TMC-3	0.19	0.28	8.20	32.57	0.31	0.21	0.22	0.24	0.23	0.19	0.17	0.20	0.23	0.23	0.25	0.23	0.25
10/10/94	15	16:33	78.33	TMC-5	1.89	27.82	40.31	51.07	4.61	13.31	11.47	0.27	11.67	0.28	0.23	0.26	0.21	0.28	0.28	0.26	0.22
10/10/94	15	16:47	78.57	TMW-6	0.13	0.12	0.20	2.49	0.26	0.63	0.19	0.18	0.19	0.16	0.20	0.17	0.21	0.21	0.21	0.21	0.23
10/10/94	15	17:00	78.78	TME-6	103.70	3.71	6.72	0.21	1.03	1.24	2.51	0.28	0.16	0.26	0.24	0.27	0.23	0.20	0.23	0.22	0.25
10/10/94	15	17:14	79.02	TME-8	9.26	29.50	0.67	0.19	0.20	0.24	0.28	0.23	0.17	0.20	0.21	0.26	0.24	0.18	0.19	0.20	0.20
10/10/94	15	17:30	79.28	TMW-8	1.35	0.24	48.21	17.71	3.82	8.16	0.35	0.26	0.21	0.27	0.24	0.20	0.19	0.21	0.28	0.25	0.24
10/10/94	15	17:43	79.50	TMC-7	44.02	95.17	21.91	29.48	74.62	37.04	31.02	0.28	5.14	0.31	0.24	0.34	0.39	25.20	0.80		0.36
10/10/94	16	22:00	83.78	TMC-7	27.63	94.88	18.61	30.42	77.86	36.22	24.69	0.26	12.43	0.31	0.24	0.38	0.75	32.56	0.45		0.25
10/10/94	16	22:15	84.03	TMC-5	3.27	31.16	37.67	49.36	5.58	11.85	12.81	0.26	1.28	0.27	0.22	0.23	0.20	0.28	0.27	0.42	0.23
10/10/94	16	22:30	84.28	TMC-3	0.13	0.16	8.46	29.58	0.21	0.21	0.20	0.22	0.19	0.17	0.20	0.20	0.23	0.25	0.26	0.30	0.29

Sample Date	Sample Round	Sample Time	Test Hours	MLS ID	port 1	port 2	port 3	port 4	port 5	port 6	port 7	port 8	port 9	port 10	port 11	port 12	port 13	port 14	port 15	port 16	port 17
10/10/94	16	22:45	84.53	TMC-1	0.13	0.16	39.77	40.52	3.23	3.56	2.76	0.27	0.24	0.26	0.23	0.24	0.27	0.28	0.33	0.28	0.27
10/11/94	17	6:24	92.18	TMC-1	0.16	0.16	28.34	32.58	3.07	1.55	1.52	0.57	0.24	0.26	0.21	0.24	0.28	0.25	0.29	0.27	0.26
10/11/94	17	6:39	92.43	TMC-3	0.12	0.15	6.81	21.68	0.22	0.18	0.18	0.21	0.19	0.16	0.18	0.18	0.21	0.22	0.20	0.25	0.23
10/11/94	17	6:56	92.72	TMC-5	3.14	30.18	26.18	37.22	5.84	11.37	10.08	0.26	0.24	0.25	0.22	0.22	0.20	0.22	0.25	0.84	0.22
10/11/94	17	7:13	93.00	TMC-7	28.40	80.12	13.63	34.34	85.23	36.57	13.75	0.24	39.10	0.41	0.28	0.46	2.82	41.80	2.17		0.18
10/11/94	18	11:21	97.13	TMC-7	18.96	74.41	11.86	35.93	91.83	38.51	15.08	0.22	57.09	0.58	0.36	0.62	5.02	47.69	0.95		0.21
10/11/94	18	11:33	97.33	TMC-8	37.30	47.45	68.46	8.27	15.70	18.54	38.62	77.80	102.63	161.93	31.21	6.07	44.63	0.20	0.28	0.21	23.45
10/11/94	18	11:44	97.52	TMC-6	6.86	21.18	5.27	52.38	8.35	18.07	27.76	10.84	10.41	9.04	7.19	8.24	32.45	0.18	0.24	0.23	0.76
10/11/94	18	11:55	97.70	TMC-5	3.18	40.49	19.02	30.47	6.51	13.27	9.38	0.23	0.19	0.24	0.19	0.20	0.18	0.20	0.23	1.55	0.20
10/11/94	18	12:05	97.87	TMC-4	1.53	0.74	0.29	0.97	0.43	11.11	12.85	4.84	8.24	40.95	11.29	7.44	0.22	0.19	0.24	0.21	0.20
10/11/94	18	12:15	98.03	TMC-3	0.11	0.13	6.05	17.61	0.17	0.18	0.16	0.18	0.16	0.13	0.18	0.16	0.21	0.20	0.19	0.23	0.21
10/11/94	18	12:25	98.20	TMC-2	0.15	0.12	0.15	0.14	1.55	11.78	17.12	2.26	0.16	0.21	0.21	0.22	0.21	0.15	0.15	0.17	0.17
10/11/94	18	12:35	98.37	TMC-1	0.11	0.13	21.69	29.49	3.65	1.37	0.88	1.96	0.36	0.23	0.19	0.20	0.24	0.22	0.23	0.24	0.23
10/11/94	19	15:51	101.63	TMC-1	0.11	0.17	18.97	28.54	4.01	1.07	0.77	1.74	0.41	0.23	0.18	0.19	0.24	0.21	0.23	0.21	0.21
10/11/94	19	16:02	101.82	TMC-3	0.10	0.12	5.44	15.05	0.16	0.16	0.16	0.20	0.17	0.14	0.16	0.16	0.20	0.19	0.19	0.20	0.20
10/11/94	19	16:13	102.00	TMC-5	1.46	37.14	17.08	28.27	6.67	12.64	8.97	0.22	0.19	0.24	0.20	0.21	0.19	0.20	0.24	8.15	0.17
10/11/94	19	16:27	102.23	TME-5	7.20	12.59	7.19	0.33	3.50	33.99	1.37	0.75	0.18	0.25	0.28	0.24	0.27	0.22	0.26	0.21	0.21
10/11/94	19	16:38	102.42	TMW-5	0.16	0.15	0.18	0.19	0.19	0.19	0.18	0.19	0.14	0.16	0.19	0.19	0.22	0.23	0.24	0.23	0.26
10/11/94	19	16:49	102.60	TMW-7	0.13	0.12	1.10	0.74	0.19	0.20	0.19	0.24	0.18	0.15	0.17	0.18	0.22	0.21	0.21	0.24	0.22
10/11/94	19	17:00	102.78	TME-7	0.87	9.31	0.22	0.19	0.18	0.23	0.25	0.20	0.18	0.16	0.21	0.22	0.23	0.20	0.17	0.23	0.25
10/11/94	19	17:11	102.97	TMC-7	22.09	55.26	9.20	34.87	77.91	37.22	9.78	0.25	65.18	1.22	0.45	0.89	7.25	59.18	3.82		0.35
10/11/94	20	22:01	107.80	TMC-7	13.83	52.66	8.62	38.68	86.20	39.34	10.29	0.23	79.53	1.53	0.65	1.07	11.57	68.34	3.26		0.25
10/11/94	20	22:13	108.00	TMC-5	2.86	42.16	16.19	28.00	8.34	13.29	8.16	0.25	0.22	0.26	0.22	0.21	0.20	0.25	0.30	9.10	0.21
10/11/94	20	22:25	108.20	TMC-3	0.12	0.13	5.23	13.10	0.20	0.19	0.17	0.21	0.19	0.15	0.18	0.18	0.22	0.23	0.23	0.27	0.24
10/11/94	20	22:35	108.37	TMC-1	0.13	0.17	17.22	30.37	5.61	1.19	0.59	1.05	0.66	0.27	0.21	0.20	0.26	0.26	0.29	0.24	0.23
10/12/94	21	5:59	115.77	TMC-1	0.09	0.12	11.48	26.32	6.07	0.82	0.41	0.33	1.17	0.33	0.20	0.21	0.24	0.26	0.28	0.22	0.22
10/12/94	21	6:11	115.97	TMC-3	0.19	0.17	3.97	10.05	0.21	0.21	0.19	0.23	0.23	0.16	0.17	0.19	0.22	0.21	0.19	0.22	0.22
10/12/94	21	6:23	116.17	TMC-5	2.18	35.70	10.93	21.84	8.94	13.81	6.31	0.24	0.23	0.30	0.21	0.25	0.19	0.22	0.30	23.55	
10/12/94	21	6:34	116.35	TMC-7	15.31	38.83	6.38	35.30	71.87	33.67	8.56	0.24	71.42	2.25	1.08	1.83	15.68	72.29	8.88		0.32
10/12/94	22	10:58	120.75	TMC-7	9.15	34.87	5.43	35.64	73.02	32.19	9.53	0.22	64.57	2.49	1.38	2.47	19.69	80.36	7.26		0.27
10/12/94	22	11:09	120.93	TMC-8	12.85	46.52	31.44	4.37	10.29	11.39	28.28	66.95	72.73	126.10	18.04	2.92	24.22	0.20	0.28	0.20	9.56
10/12/94	22	11:19	121.10	TMC-6	3.98	11.77	6.21	37.07	4.33	7.44	18.75	12.85	19.67	30.57	32.08	2.34	23.73	0.21	0.28	0.22	1.21
10/12/94	22	11:29	121.27	TMC-5	2.07	33.17	9.82	19.83	10.23	16.25	5.84	0.22	0.20	0.25	0.22	0.22	0.18	0.21	0.32	38.36	
10/12/94	22	11:39	121.43	TMC-4	0.38	0.37	0.18	0.50	0.24	4.51	5.87	1.91	8.28	30.11	1.57	3.45	0.21	0.19	0.27	0.18	0.19
10/12/94	22	11:49	121.60	TMC-3	0.12	0.14	3.72	8.27	0.20	0.19	0.18	0.20	0.18	0.16	0.18	0.17	0.20	0.20	0.21	0.21	0.20
10/12/94	22	11:59	121.77	TMC-2	0.15	0.19	0.18	0.15	0.92	6.21	8.96	1.33	0.15	0.22	0.19	0.20	0.19	0.13	0.16	0.16	0.17
10/12/94	22	12:09	121.93	TMC-1	0.10	0.14	9.13	24.66	6.84	0.72	0.31	0.44	0.90	0.30	0.20	0.19	0.25	0.26	0.28	0.23	0.22
10/12/94	23	16:15	126.03	TMC-1	0.13	0.18	8.64	23.05	6.41	0.56	0.30	0.31	0.67	0.32	0.19	0.19	0.23	0.25	0.27	0.22	0.22
10/12/94	23	16:31	126.30	TMC-3	0.09	0.12	3.21	7.16	0.22	0.17	0.16	0.23	0.23	0.16	0.15	0.16	0.21	0.21	0.21	0.21	0.23
10/12/94	23	16:43	126.50	TMC-5	1.88	30.51	8.05	18.44	10.94	15.97	5.15	0.23	0.21	0.28	0.22	0.24	0.19	0.21	0.31	26.57	
10/12/94	23	16:56	126.72	TME-4	9.94	31.83	3.98	0.43	11.35	28.09	4.67	0.23	0.19	0.28	0.28	0.26	0.22	0.19	0.25		0.17
10/12/94	23	17:08	126.92	TME-5	5.08	54.48	2.66	0.43	9.08	21.72	0.48	0.98	0.17	0.30	0.24	0.23	0.30	0.20	0.24	0.19	0.19
10/12/94	23	17:20	127.12	TME-6	86.48	71.93	0.49	0.24	7.78	7.79	0.31	0.22	0.17	0.29	0.26	0.23	0.20	0.18	0.23	0.20	0.23

Sample Date	Sample Round	Sample Time	Test Hours	MLS ID	port 1	port 2	port 3	port 4	port 5	port 6	port 7	port 8	port 9	port 10	port 11	port 12	port 13	port 14	port 15	port 16	port 17
10/12/94	23	17:33	127.33	TME-7	1.05	3.62	0.19	0.19	0.20	0.21	0.23	0.17	0.16	0.18	0.17	0.18	0.19	0.17	0.18	0.17	0.18
10/12/94	23	17:46	127.55	TMC-7	10.49	25.99	4.27	30.41	59.16	24.74	7.56	0.22	44.56	5.25	1.58	2.85	22.03	67.90	13.35		0.58
10/12/94	24	22:00	131.78	TMC-7	8.36	26.18	4.23	32.12	61.69	25.90	9.05	0.24	41.92	6.29	1.63	3.79	28.33	74.34	12.51		0.29
10/12/94	24	22:12	131.98	TMC-5	1.83	34.84	7.62	16.80	12.56	20.26	4.73	0.24	0.21	0.28	0.20	0.22	0.20	0.22	0.33	30.84	
10/12/94	24	22:22	132.15	TMC-3	0.15	0.18	3.03	6.19	0.20	0.19	0.19	0.21	0.20	0.16	0.18	0.19	0.21	0.21	0.20	0.25	0.23
10/12/94	24	22:33	132.33	TMC-1	0.11	0.13	7.19	23.97	8.90	0.98	0.34	0.22	1.25	0.28	0.21	0.20	0.23	0.26	0.27	0.23	0.22
10/13/94	25	5:55	139.70	TMC-1	0.16	0.22	5.62	21.66	9.99	0.51	0.34	0.24	1.54	0.33	0.19	0.19	0.23	0.25	0.28	0.21	0.21
10/13/94	25	6:07	139.90	TMC-3	0.10	0.13	2.56	4.97	0.22	0.17	0.17	0.21	0.19	0.16	0.16	0.19	0.21	0.21	0.22	0.20	0.22
10/13/94	25	6:17	140.07	TMC-5	2.23	26.50	6.34	15.27	15.31	22.11	3.53	0.23	0.21	0.30	0.23	0.23	0.19	0.23	0.60	38.79	
10/13/94	25	6:29	140.27	TMC-7	8.71	18.65	3.35	29.12	48.73	20.14	8.02	0.22	31.43	12.13	1.55	4.83	33.77	67.15	17.88		0.42
10/13/94	26	10:58	144.75	TMC-7	8.10	17.43	3.06	27.77	48.35	19.14	9.83	0.21	26.84	19.06	1.53	5.57	41.20	71.93	16.58		0.26
10/13/94	26	11:09	144.93	TMC-8	8.23	52.14	16.31	2.71	6.51	7.56	23.47	50.84	43.13	91.26	10.10	1.67	15.73	0.20	0.32	0.20	2.76
10/13/94	26	11:21	145.13	TMC-5	2.26	24.16	5.64	14.02	16.18	24.39	3.28	0.21	0.19	0.30	0.19	0.21	0.17	0.23	0.42	38.85	
10/13/94	26	11:31	145.30	TMC-6	3.41	6.29	5.15	17.88	2.29	3.91	13.16	15.48	32.38	45.76	43.28	0.86	13.03	0.20	0.31	0.21	0.65
10/13/94	26	11:41	145.47	TMC-4	0.36	0.36	0.31	0.41	0.35	2.34	4.25	1.58	7.71	25.58	0.77	1.85	0.20	0.18	0.28	0.17	0.20
10/13/94	26	11:51	145.63	TMC-3	0.11	0.13	2.36	4.55	0.18	0.18	0.17	0.20	0.18	0.15	0.17	0.17	0.20	0.21	0.21	0.21	0.21
10/13/94	26	12:01	145.80	TMC-2	0.11	0.13	0.15	0.14	0.53	3.22	4.80	0.92	0.16	0.24	0.20	0.21	0.18	0.14	0.16	0.16	0.17
10/13/94	26	12:11	145.97	TMC-1	0.15	0.15	4.68	21.34	10.91	0.65	0.33	0.21	1.85	0.33	0.19	0.19	0.21	0.25	0.27	0.23	0.21
10/13/94	27	15:58	149.75	TMC-1	0.11	0.12	4.00	20.61	10.31	0.40	0.31	0.21	1.66	0.29	0.16	0.17	0.20	0.23	0.23	0.23	0.19
10/13/94	27	16:11	149.97	TMC-3	0.14	0.16	1.98	3.76	0.21	0.18	0.18	0.19	0.18	0.16	0.16	0.17	0.19	0.19	0.20	0.22	0.21
10/13/94	27	16:21	150.13	TMC-5	2.23	21.88	5.32	12.95	16.93	25.15	2.77	0.21	0.19	0.28	0.20	0.21	0.18	0.23	0.37	33.73	0.07
10/13/94	27	16:31	150.30	TMW-6	0.09	0.11	0.16	0.30	0.34	2.44	0.16	0.15	0.14	0.17	0.18	0.14	0.17	0.17	0.20	0.20	0.20
10/13/94	27	16:41	150.47	TMEE-5	0.22	0.24	0.24	0.19	0.28	0.17	0.18	0.18	0.17	0.22	0.16	0.17	0.18	0.15	0.19	0.17	0.15
10/13/94	27	16:51	150.63	TME-3	2.02	8.52	7.76	0.24	1.04	2.98	0.22	0.21	0.18	0.26	0.21	0.18	0.20	0.17	0.21	0.19	0.20
10/13/94	27	17:01	150.80	TME-5	9.46	68.03	1.64	0.84	32.17	40.35	0.29	0.90	0.19	0.31	0.22	0.19	1.04	0.19	0.24	0.19	0.17
10/13/94	27	17:11	150.97	TMC-7	7.27	13.81	2.67	24.47	41.85	16.06	6.81	0.19	21.58	22.71	1.41	5.20	43.19	60.30	18.58		0.35
10/13/94	28	21:57	155.73	TMC-7	6.76	13.46	2.29	23.80	41.25	15.09	7.43	0.21	16.15	21.69	1.19	5.49	50.72	63.03	16.52		0.26
10/13/94	28	22:07	155.90	TMC-5	2.04	19.98	4.51	11.53	18.01	25.82	2.33	0.20	0.18	0.27	0.17	0.20	0.17	0.25	0.40	36.90	1.07
10/13/94	28	22:17	156.07	TMC-3	0.14	0.17	1.76	3.20	0.21	0.18	0.19	0.19	0.18	0.16	0.16	0.18	0.20	0.19	0.20	0.21	0.23
10/13/94	28	22:27	156.23	TMC-1	0.13	0.14	3.47	20.62	11.47	0.30	0.40	0.27	2.73	0.31	0.16	0.18	0.21	0.24	0.26	0.34	0.22
10/14/94	29	6:00	163.78	TMC-1	0.30	0.31	2.68	17.52	12.03	0.24	0.51	0.29	3.59	0.35	0.17	0.20	0.22	0.26	0.28	0.51	0.21
10/14/94	29	6:10	163.95	TMC-3	0.13	0.15	1.40	2.41	0.21	0.17	0.16	0.19	0.17	0.14	0.15	0.17	0.20	0.19	0.19	0.21	0.21
10/14/94	29	6:20	164.12	TMC-5	1.81	16.76	3.75	9.68	17.96	26.23	1.75	0.20	0.19	0.29	0.29	0.21	0.18	0.29	0.31	29.19	0.84
10/14/94	29	6:30	164.28	TMC-7	5.58	10.27	1.71	19.75	28.50	11.86	8.21	0.19	9.15	10.53	0.59	5.00	52.17	48.12	17.51		0.65
10/14/94	30	10:59	168.77	TMC-7	5.50	9.67	1.75	18.89	26.55	10.95	9.62	0.20	7.11	6.99	0.46	5.18	57.33	49.36	15.99		0.26
10/14/94	30	11:11	168.97	TMC-8	5.07	63.87	6.91	1.29	3.36	4.21	16.19	33.12	24.16	49.45	4.75	0.82	8.08	0.21	0.41	0.20	0.40
10/14/94	30	11:21	169.13	TMC-6	3.12	3.44	3.85	9.40	1.07	2.02	8.30	17.62	35.53	45.47	39.39	0.45	8.21	0.20	0.34	0.22	0.30
10/14/94	30	11:30	169.28	TMC-5	1.15	15.87	3.28	8.82	19.67	25.72	1.80	0.22	0.24	0.33	0.27	0.22	0.18	0.41	0.37	26.82	0.86
10/14/94	30	11:39	169.43	TMC-4	0.25	0.21	0.12	0.23	0.20	1.28	2.15	1.17	8.93	17.76	0.39	0.84	0.19	0.18	0.25	0.18	0.20
10/14/94	30	11:48	169.58	TMC-3	0.10	0.14	1.20	2.13	0.20	0.16	0.16	0.19	0.18	0.15	0.15	0.16	0.19	0.19	0.19	0.21	0.20
10/14/94	30	11:57	169.73	TMC-2	0.10	0.12	0.15	0.13	0.27	1.71	2.01	0.50	0.16	0.20	0.19	0.20	0.18	0.13	0.14	0.15	0.16
10/14/94	30	12:06	169.88	TMC-1	0.13	0.13	1.97	16.72	12.56	0.19	0.35	0.22	5.62	0.33	0.15	0.17	0.20	0.24	0.25	1.02	0.18
10/14/94	31	16:12	173.98	TMC-1	0.17	0.12	2.04	17.16	13.32	0.19	0.34	0.19	4.43	0.28	0.15	0.17	0.19	0.23	0.23	1.32	0.19

Sample Date	Sample Round	Sample Time	Test Hours	MLS ID	port 1	port 2	port 3	port 4	port 5	port 6	port 7	port 8	port 9	port 10	port 11	port 12	port 13	port 14	port 15	port 16	port 17
10/14/94	31	16:23	174.17	TMC-3	0.14	0.16	1.22	2.12	0.19	0.18	0.16	0.18	0.16	0.14	0.16	0.16	0.17	0.18	0.19	0.23	0.21
10/14/94	31	16:35	174.37	TMC-5	1.12	15.17	3.08	8.55	19.12	27.95	1.68	0.18	0.18	0.25	0.19	0.19	0.16	0.56	0.35	21.12	0.70
10/14/94	31	16:47	174.57	TME-5	19.15	61.17	0.66	1.03	27.20	50.71	0.25	0.44	0.17	0.29	0.22	0.22	3.64	0.25	0.24	0.19	0.19
10/14/94	31	16:58	174.75	TME-6	42.94	98.26	0.29	0.35	8.38	12.68	0.25	0.18	0.17	0.28	0.23	0.20	0.20	0.18	0.22	0.22	0.23
10/14/94	31	17:09	174.93	TMW-5	0.14	0.14	0.17	0.17	0.18	0.17	0.16	0.15	0.13	0.17	0.17	0.18	0.18	0.18	0.20	0.19	0.23
10/14/94	31	17:19	175.10	TMW-6	0.10	0.11	0.16	0.20	0.29	1.81	0.16	0.16	0.14	0.17	0.18	0.15	0.18	0.17	0.19	0.22	0.20
10/14/94	31	17:30	175.28	TMC-7	4.48	8.63	1.42	18.03	23.10	8.88	6.49	0.18	4.32	2.92	0.38	4.47	50.80	40.16	19.68		1.87
10/14/94	32	22:00	179.78	TMC-7	4.79	8.60	1.44	17.20	22.83	8.46	8.59	0.21	2.77	2.23	0.33	5.12	58.33	41.55	19.21		0.27
10/14/94	32	22:10	179.95	TMC-5	1.34	13.68	2.91	8.22	19.84	28.96	1.52	0.20	0.19	0.28	0.21	0.21	0.18	0.82	0.48	18.94	0.66
10/14/94	32	22:20	180.12	TMC-3	0.13	0.16	1.09	1.93	0.20	0.17	0.17	0.18	0.17	0.16	0.16	0.18	0.19	0.21	0.25	0.31	0.29
10/14/94	32	22:30	180.28	TMC-1	0.23	0.14	1.83	17.10	14.08	0.23	0.49	0.23	8.23	0.32	0.16	0.19	0.21	0.28	0.34	2.86	0.24
10/15/94	33	6:04	187.85	TMC-1	0.27	0.13	1.38	14.69	14.81	0.22	0.43	0.24	11.42	0.31	0.16	0.17	0.20	0.23	0.25	4.58	0.20
10/15/94	33	6:15	188.03	TMC-3	0.15	0.16	0.90	1.46	0.21	0.18	0.16	0.18	0.17	0.16	0.18	0.18	0.19	0.19	0.18	0.31	0.21
10/15/94	33	6:25	188.20	TMC-5	1.08	10.82	2.22	6.45	20.09	27.47	1.00	0.20	0.17	0.28	0.20	0.19	0.18	0.86	0.40	7.84	0.90
10/15/94	33	6:35	188.37	TMC-7	3.65	6.96	1.16	14.08	16.42	5.87	6.07	0.19	1.72	1.19	0.29	3.59	43.22	33.08	19.44		0.66
10/15/94	34	11:07	192.90	TMC-7	4.37	6.64	1.03	13.71	14.15	5.43	5.89	0.19	1.23	0.87	0.27	3.67	41.75	32.16	18.53		0.26
10/15/94	34	11:19	193.10	TMC-8	3.61	74.66	3.81	0.82	1.82	2.30	16.24	29.77	16.99	23.44	3.12	0.43	3.35	0.20	0.29	0.19	0.21
10/15/94	34	11:31	193.30	TMC-6	4.32	2.15	2.52	5.88	0.97	1.21	5.84	15.61	31.80	37.87	25.79	0.32	5.46	0.18	0.30	0.21	0.18
10/15/94	34	11:42	193.48	TMC-5	1.29	9.33	1.88	5.89	19.88	28.62	0.81	0.19	0.18	0.28	0.24	0.19	0.17	1.04	0.38	7.07	0.58
10/15/94	34	11:54	193.68	TMC-4	0.26	0.30	0.18	0.23	0.29	0.73	1.78	0.79	10.60	12.91	0.28	0.43	0.18	0.16	0.26	0.15	0.17
10/15/94	34	12:06	193.88	TMC-3	0.11	0.13	0.75	1.24	0.23	0.16	0.14	0.18	0.15	0.15	0.15	0.15	0.18	0.18	0.20	0.27	0.18
10/15/94	34	12:23	194.17	TMC-2	0.14	0.12	0.14	0.12	0.24	1.21	1.28	0.47	0.14	0.18	0.21	0.20	0.17	0.13	0.15	0.14	0.14
10/15/94	34	12:35	194.37	TMC-1	0.27	0.13	1.17	13.70	14.20	0.19	0.28	0.20	7.60	0.31	0.15	0.16	0.20	0.24	0.25	5.67	0.21
10/15/94	35	17:22	199.15	TMC-1	0.28	0.11	1.06	13.51	12.70	0.18	0.25	0.18	6.47	0.30	0.14	0.15	0.18	0.24	0.25	6.20	0.24
10/15/94	35	17:36	199.38	TMC-3	0.14	0.14	0.65	1.12	0.21	0.16	0.15	0.17	0.16	0.15	0.15	0.15	0.17	0.18	0.19	0.29	0.18
10/15/94	35	17:48	199.58	TMC-5	1.25	8.33	1.72	5.45	20.69	29.07	0.78	0.18	0.17	0.28	0.19	0.18	0.16	1.10	0.40	8.54	0.50
10/15/94	35	18:00	199.78	TME-4	14.27	81.10	0.64	0.41	22.50	16.20	0.35	0.19	0.16	0.32	0.20	2.58	0.22	0.15	0.22		0.19
10/15/94	35	18:12	199.98	TME-5	31.80	40.24	0.41	1.06	34.24	37.59	0.25	0.27	0.18	0.38	0.24	0.39	12.84	1.18	0.31	0.20	0.20
10/15/94	35	18:25	200.20	TME-3	7.41	36.33	4.46	0.19	3.57	3.58	0.22	0.21	0.16	0.28	0.23	0.19	0.20	0.16	0.22	0.19	0.19
10/15/94	35	18:37	200.40	TMW-5	0.14	0.13	0.15	0.15	0.18	0.16	0.15	0.15	0.12	0.18	0.16	0.18	0.16	0.16	0.19	0.18	0.21
10/15/94	35	18:49	200.60	TMC-7	3.38	6.17	0.77	12.47	11.51	4.21	5.57	0.18	0.81	0.64	0.25	3.70	33.28	29.07	21.96		0.73
10/15/94	36	21:59	203.77	TMC-7	4.40	6.50	0.76	12.69	11.44	4.04	5.36	0.18	0.70	0.64	0.25	3.73	31.68	29.88	20.46		0.33
10/15/94	36	22:10	203.95	TMC-5	1.27	8.27	1.59	5.29	21.29	29.97	0.66	0.19	0.18	0.27	0.20	0.17	0.17	1.26	0.63	6.60	0.59
10/15/94	36	22:21	204.13	TMC-3	0.15	0.14	0.65	1.11	0.23	0.17	0.15	0.18	0.17	0.17	0.16	0.15	0.18	0.21	0.28	0.59	0.35
10/15/94	36	22:32	204.32	TMC-1	0.45	0.14	0.98	13.13	16.71	0.20	0.31	0.21	9.42	0.37	0.16	0.17	0.20	0.27	0.35	9.84	0.37
10/16/94	37	12:25	218.20	TMC-1	0.43	0.13	0.69	11.10	15.63	0.18	0.23	0.18	10.38	0.30	0.15	0.15	0.19	0.26	0.24	12.53	1.17
10/16/94	37	12:37	218.40	TMC-2	0.13	0.11	0.17	0.14	0.17	0.65	0.58	0.34	0.15	0.17	0.18	0.16	0.16	0.13	0.14	0.15	0.14
10/16/94	37	12:48	218.58	TMC-3	0.11	0.12	0.50	0.85	0.20	0.15	0.14	0.17	0.17	0.16	0.15	0.15	0.18	0.19	0.19	0.40	0.18
10/16/94	37	13:00	218.78	TMC-4	0.22	0.15	0.12	0.20	0.20	0.47	1.19	0.70	12.41	9.91	0.23	0.28	0.18	0.19	0.26	0.15	0.16
10/16/94	37	13:11	218.97	TMC-5	1.06	5.71	1.16	3.86	21.60	28.56	0.49	0.20	0.18	0.27	0.20	0.18	0.17	1.03	0.53	4.89	0.53
10/16/94	37	13:23	219.17	TMC-6	4.26	0.82	1.49	4.10	0.56	0.72	3.87	14.27	25.17	24.86	14.07	0.26	3.21	0.19	0.29	0.20	0.16
10/16/94	37	13:34	219.35	TMC-8	3.70	70.79	2.35	0.86	1.04	1.19	10.03	25.60	10.22	10.15	2.06	0.32	1.62	0.20	0.27	0.20	0.19
10/16/94	37	13:46	219.55	TMC-7	2.44	5.47	0.60	10.12	8.16	2.15	3.77	0.18	0.37	0.40	0.23	2.43	23.18	26.38	21.68		0.57

Sample Date	Sample Round	Sample Time	Test Hours	MLS ID	port 1	port 2	port 3	port 4	port 5	port 6	port 7	port 8	port 9	port 10	port 11	port 12	port 13	port 14	port 15	port 16	port 17
10/16/94	38	20:58	226.75	TMC-7	2.36	5.59	0.54	9.28	6.28	1.64	2.74	0.18	0.31	0.33	0.21	1.82	19.11	24.73	18.13		0.24
10/16/94	38	21:09	226.93	TME-6	20.13	43.00	0.23	0.26	3.00	2.13	0.22	0.17	0.16	0.28	0.20	0.17	0.19	0.17	0.20	0.18	0.15
10/16/94	38	21:20	227.12	TME-5	32.33	25.55	0.27	0.78	31.28	17.75	0.22	0.23	0.18	0.31	0.23	0.53	25.04	4.45	0.22	0.19	0.19
10/16/94	38	21:31	227.30	TMC-5	0.70	5.21	0.80	3.10	21.52	28.03	0.42	0.19	0.18	0.28	0.21	0.17	0.17	0.87	0.35	2.99	0.54
10/16/94	38	21:42	227.48	TMC-3	0.14	0.16	0.37	0.63	0.26	0.15	0.14	0.18	0.17	0.15	0.15	0.14	0.18	0.18	0.19	0.46	0.18
10/16/94	38	21:53	227.67	TMC-1	0.59	0.24	0.64	8.57	16.38	0.18	0.29	0.21	13.56	0.43	0.14	0.16	0.20	0.27	0.27	13.03	1.76
10/17/94	39	10:40	240.45	TMC-1	0.55	0.13	0.51	8.31	15.32	0.19	0.18	0.20	10.33	1.24	0.14	0.13	0.19	0.28	0.34	12.48	4.91
10/17/94	39	10:49	240.60	TMC-2	0.15	0.17	0.16	0.13	0.18	0.34	0.35	0.26	0.14	0.17	0.16	0.15	0.16	0.13	0.14	0.14	0.12
10/17/94	39	10:58	240.75	TMC-3	0.10	0.11	0.28	0.45	0.16	0.14	0.12	0.17	0.15	0.13	0.14	0.12	0.17	0.17	0.16	0.37	0.16
10/17/94	39	11:07	240.90	TMC-4	0.18	0.12	0.13	0.19	0.25	0.30	0.63	0.48	12.08	7.31	0.19	0.20	0.18	0.18	0.25	0.14	0.14
10/17/94	39	11:16	241.05	TMC-5	0.77	4.17	0.71	2.82	21.42	26.73	0.32	0.19	0.19	0.29	0.19	0.15	0.16	0.69	0.36	2.56	0.48
10/17/94	39	11:25	241.20	TMC-6	3.82	0.47	0.79	3.28	0.42	0.54	2.89	11.93	19.26	13.53	7.60	0.22	2.01	0.21	0.28	0.20	0.14
10/17/94	39	11:34	241.35	TMC-8	1.83	64.65	1.23	0.35	0.45	0.73	6.46	21.91	8.63	3.59	1.12	0.26	0.99	0.20	0.25	0.19	0.15
10/17/94	39	11:43	241.50	TMC-7	1.62	5.09	0.44	8.00	5.63	0.92	3.47	0.18	0.26	0.30	0.20	1.46	14.41	24.27	19.26		0.38
10/17/94	40	21:00	250.78	TMC-7	1.81	5.69	0.41	7.01	4.07	0.78	3.66	0.17	0.23	0.25	0.19	1.58	14.71	23.31	19.55		0.25
10/17/94	40	21:11	250.97	TMC-5	0.63	3.86	0.61	2.29	20.00	25.00	0.34	0.18	0.17	0.28	0.19	0.17	0.16	0.60	0.30	2.07	0.57
10/17/94	40	21:21	251.13	TME-4	19.93	44.80	0.24	0.27	27.67	4.19	0.25	0.17	0.17	0.26	0.22	11.78	4.73	0.19	0.18		0.20
10/17/94	40	21:30	251.28	TME-3	10.65	40.61	1.20	0.16	4.66	1.86	0.25	0.20	0.15	0.25	0.19	0.52	0.26	0.14	0.18	0.17	0.20
10/17/94	40	21:40	251.45	TMC-3	0.17	0.24	0.35	0.52	0.36	0.16	0.17	0.18	0.16	0.17	0.15	0.17	0.18	0.18	0.19	0.46	0.23
10/17/94	40	21:49	251.60	TMC-1	0.59	0.15	0.39	7.38	14.91	0.18	0.20	0.19	9.39	4.24	0.12	0.16	0.18	0.29	0.31	12.16	8.49
10/18/94	41	10:19	264.10	TMC-1	0.58	0.13	0.31	6.77	14.35	0.18	0.17	0.16	9.25	12.08	0.14	0.14	0.20	0.45	0.40	11.71	13.51
10/18/94	41	10:30	264.28	TMC-2	0.13	0.13	0.15	0.13	0.14	0.24	0.26	0.24	0.14	0.14	0.15	0.15	0.14	0.12	0.12	0.14	0.13
10/18/94	41	10:40	264.45	TMC-3	0.11	0.14	0.23	0.40	0.18	0.15	0.14	0.15	0.15	0.13	0.14	0.15	0.16	0.17	0.17	0.41	0.19
10/18/94	41	10:49	264.60	TMC-4	0.18	0.15	0.10	0.17	0.17	0.27	0.78	0.41	10.61	4.70	0.18	0.21	0.18	0.18	0.21	0.14	0.15
10/18/94	41	10:58	264.75	TMC-5	0.59	3.11	0.50	1.81	16.58	21.40	0.29	0.18	0.18	0.29	0.20	0.17	0.16	0.49	0.28	1.52	0.46
10/18/94	41	11:07	264.90	TMC-6	4.29	0.37	0.71	3.01	0.37	0.40	2.13	9.99	13.86	6.25	3.84	0.23	1.43	0.18	0.23	0.19	0.16
10/18/94	41	11:17	265.07	TMC-8	1.44	41.17	0.85	0.31	0.34	0.46	10.13	18.96	6.99	1.33	0.69	0.28	0.55	0.19	0.22	0.18	0.17
10/18/94	41	11:26	265.22	TMC-7	1.13	5.66	0.31	5.90	3.89	0.41	1.55	0.17	0.21	0.26	0.17	0.99	9.97	20.87	19.88		0.36
10/18/94	42	20:52	274.65	TMC-7	1.15	5.98	0.30	5.48	3.44	0.36	1.47	0.17	0.21	0.25	0.18	1.20	11.00	20.04	19.70		0.27
10/18/94	42	21:01	274.80	TME-6	15.63	20.05	0.25	0.22	1.20	0.31	0.23	0.17	0.15	0.26	0.20	0.19	0.20	0.15	0.19	0.17	0.17
10/18/94	42	21:10	274.95	TME-5	35.26	15.80	0.33	0.54	17.68	5.70	0.23	0.19	0.17	0.31	0.21	0.48	33.19	1.45	0.20	0.19	0.19
10/18/94	42	21:19	275.10	TMC-5	0.47	2.50	0.43	1.58	14.65	18.31	0.28	0.19	0.20	0.31	0.21	0.17	0.16	0.40	0.31	1.36	0.35
10/18/94	42	21:28	275.25	TMC-3	0.15	0.15	0.22	0.33	0.21	0.16	0.14	0.16	0.16	0.15	0.15	0.15	0.17	0.17	0.18	0.34	0.19
10/18/94	42	21:37	275.40	TMC-1	0.62	0.12	0.25	6.10	12.30	0.19	0.16	0.17	8.81	22.59	0.14	0.14	0.22	0.67	0.49	10.08	17.23
10/19/94	43	9:59	287.77	TMC-1	0.77	0.21	0.27	5.62	12.74	0.21	0.19	0.18	8.82	40.65	0.17	0.16	0.29	1.08	0.54	9.09	21.52
10/19/94	43	10:08	287.92	TMC-2	0.18	0.22	0.18	0.16	0.20	0.23	0.26	0.24	0.16	0.18	0.16	0.16	0.16	0.13	0.15	0.14	0.14
10/19/94	43	10:17	288.07	TMC-3	0.12	0.12	0.20	0.27	0.16	0.15	0.14	0.16	0.15	0.13	0.15	0.15	0.18	0.17	0.17	0.30	0.18
10/19/94	43	10:26	288.22	TME-3	11.66	29.00	0.55	0.19	4.34	1.12	0.31	0.20	0.17	0.45	0.21	1.22	0.81	0.16	0.24	0.18	0.24
10/19/94	43	10:35	288.37	TME-4	21.00	18.84	0.25	0.22	19.09	1.62	0.24	0.18	0.15	0.31	0.23	10.14	8.13	0.17	0.21		0.21
10/19/94	43	10:44	288.52	TMC-4	0.12	0.09	0.13	0.13	0.15	0.20	0.36	0.51	8.65	3.01	0.17	0.18	0.19	0.19	0.29	0.14	0.14
10/19/94	43	10:53	288.67	TMC-5	0.48	2.65	0.48	1.35	13.40	14.24	0.29	0.20	0.19	0.32	0.24	0.17	0.17	0.38	0.28	1.03	0.32
10/19/94	43	11:02	288.82	TMC-6	2.66	0.25	0.46	2.55	0.26	0.36	1.57	8.39	9.83	3.26	1.62	0.21	1.04	0.20	0.29	0.20	0.16
10/19/94	43	11:11	288.97	TMC-7	0.75	5.29	0.32	4.94	3.05	0.27	1.16	0.18	0.20	0.25	0.18	0.90	8.35	18.57	20.41		0.42

Sample Date	Sample Round	Sample Time	Test Hours	MLS ID	port 1	port 2	port 3	port 4	port 5	port 6	port 7	port 8	port 9	port 10	port 11	port 12	port 13	port 14	port 15	port 16	port 17
10/19/94	43	11:20	289.12	TMC-8	1.07	31.78	0.63	0.29	0.32	0.37	4.54	18.45	5.47	0.67	0.38	0.24	0.38	0.20	0.21	0.19	0.18
10/20/94	44	10:29	312.27	TMC-1	0.58	0.14	0.24	4.62	9.51	0.22	0.15	0.16	5.76	82.60	0.16	0.14	0.29	1.84	0.74	6.77	23.09
10/20/94	44	10:38	312.42	TMC-2	0.19	0.20	0.17	0.15	0.17	0.19	0.23	0.21	0.15	0.16	0.16	0.16	0.16	0.13	0.14	0.14	0.14
10/20/94	44	10:46	312.55	TMC-3	0.16	0.19	0.20	0.28	0.28	0.17	0.17	0.17	0.15	0.18	0.15	0.16	0.17	0.17	0.19	0.25	0.18
10/20/94	44	10:55	312.70	TMC-4	0.13	0.11	0.12	0.14	0.15	0.18	0.33	0.35	7.50	2.18	0.16	0.18	0.17	0.17	0.20	0.13	0.14
10/20/94	44	11:03	312.83	TMC-5	0.29	1.84	0.33	1.00	9.38	9.02	0.25	0.18	0.18	0.29	0.20	0.16	0.16	0.33	0.27	0.89	0.25
10/20/94	44	11:11	312.97	TME-5	34.68	13.12	0.21	0.34	8.28	3.07	0.20	0.15	0.16	0.24	0.22	0.29	28.09	0.50	0.20	0.19	0.17
10/20/94	44	11:19	313.10	TME-6	12.39	10.26	0.20	0.19	0.69	0.25	0.21	0.15	0.15	0.22	0.19	0.18	0.21	0.14	0.17	0.18	0.16
10/20/94	44	11:27	313.23	TMC-6	2.53	0.17	0.40	2.37	0.21	0.30	1.17	7.53	6.52	2.07	0.65	0.21	0.74	0.19	0.24	0.18	0.15
10/20/94	44	11:35	313.37	TMC-7	0.73	4.79	0.28	4.19	2.34	0.21	0.59	0.16	0.19	0.23	0.16	0.77	7.95	17.24	20.86		3.30
10/20/94	44	11:43	313.50	TMC-8	0.86	20.70	0.44	0.26	0.28	0.31	5.59	14.69	4.76	0.35	0.28	0.25	0.30	0.19	0.18	0.16	0.17
10/21/94	45	9:50	335.62	TMC-1	0.55	0.14	0.20	3.91	7.82	0.21	0.14	0.15	2.93	100.93	0.15	0.15	0.22	2.36	1.19	5.27	19.04
10/21/94	45	9:58	335.75	TMC-2	0.18	0.22	0.20	0.16	0.27	0.18	0.21	0.22	0.15	0.15	0.16	0.15	0.14	0.13	0.12	0.14	0.14
10/21/94	45	10:06	335.88	TMC-3	0.16	0.16	0.17	0.25	0.13	0.16	0.14	0.14	0.15	0.11	0.15	0.14	0.17	0.17	0.14	0.23	0.18
10/21/94	45	10:14	336.02	TME-3	10.49	15.58	0.30	0.24	2.45	0.56	0.29	0.20	0.16	0.39	0.20	1.76	0.68	0.15	0.19	0.18	0.22
10/21/94	45	10:22	336.15	TME-4	17.43	9.89	0.18	0.20	10.00	0.69	0.20	0.14	0.14	0.23	0.21	4.30	3.83	0.17	0.16		0.20
10/21/94	45	10:30	336.28	TMC-4	0.16	0.16	0.13	0.16	0.16	0.19	0.51	0.28	6.31	1.39	0.16	0.18	0.16	0.18	0.19	0.14	0.14
10/21/94	45	10:38	336.42	TMC-5	0.22	1.64	0.27	0.71	6.04	5.66	0.22	0.16	0.17	0.22	0.20	0.15	0.15	0.29	0.22	0.78	0.26
10/21/94	45	10:46	336.55	TMC-6	1.90	0.18	0.42	2.07	0.17	0.29	0.94	5.50	6.03	1.37	0.34	0.20	0.58	0.19	0.21	0.17	0.15
10/21/94	45	10:55	336.70	TMC-7	0.56	3.92	0.24	3.39	2.03	0.20	0.35	0.16	0.19	0.21	0.16	0.62	7.10	14.56	20.93		5.81
10/21/94	45	11:03	336.83	TMC-8	0.67	14.27	0.38	0.24	0.26	0.29	4.44	11.45	4.17	0.24	0.24	0.23	0.24	0.18	0.14	0.15	0.15
10/22/94	46	10:08	359.92	TMC-1	0.49	0.13	0.18	3.49	7.51	0.22	0.15	0.15	1.65	88.61	0.15	0.13	0.20	2.21	2.58	4.30	12.83
10/22/94	46	10:09	359.93	TMC-1	0.55	0.18	0.17	3.56	7.79	0.24	0.17	0.15	1.61	90.31	0.15	0.14	0.21	2.22	2.59	4.39	12.80
10/22/94	46	10:21	360.13	TMC-2	0.19	0.17	0.18	0.16	0.20	0.19	0.18	0.21	0.15	0.19	0.16	0.15	0.16	0.14	0.17	0.16	0.14
10/22/94	46	10:32	360.32	TMC-4	0.14	0.17	0.15	0.17	0.25	0.15	0.38	0.32	4.63	1.15	0.14	0.18	0.16	0.17	0.22	0.11	0.13
10/22/94	46	10:44	360.52	TME-5	26.16	9.52	0.17	0.26	3.10	1.66	0.18	0.14	0.14	0.29	0.20	0.24	21.87	0.22	0.22	0.19	0.16
10/22/94	46	10:54	360.68	TMC-5	0.18	1.31	0.25	0.63	4.75	2.89	0.20	0.16	0.15	0.25	0.19	0.14	0.15	0.25	0.26	0.57	0.23
10/22/94	46	11:05	360.87	TMW-5	0.24	0.23	0.25	0.22	0.52	0.16	0.15	0.16	0.13	0.25	0.15	0.17	0.17	0.18	0.24	0.16	0.19
10/22/94	46	11:17	361.07	TMC-6	2.33	0.14	0.33	1.78	0.23	0.26	0.77	4.60	4.58	1.36	0.20	0.21	0.47	0.18	0.28	0.13	0.16
10/22/94	46	11:29	361.27	TMC-7	0.67	3.48	0.21	2.70	2.11	0.20	0.26	0.16	0.17	0.23	0.14	0.55	6.39	11.19	21.99		5.85
10/22/94	46	11:41	361.47	TMC-8	0.58	11.01	0.38	0.31	0.67	0.30	4.22	11.60	3.46	0.38	0.24	0.26	0.23	0.19	0.26	0.18	0.15
10/23/94	47	13:46	387.55	TMC-1	0.26	0.14	0.19	2.74	7.04	0.28	0.14	0.15	0.68	57.21	0.18	0.13	0.18	1.85	3.98	3.99	8.02
10/23/94	47	13:47	387.57	TMC-1	0.44	0.20	0.17	2.99	7.28	0.29	0.16	0.14	0.70	57.62	0.18	0.14	0.18	1.85	4.05	3.98	8.12
10/23/94	47	14:02	387.82	TMW-3	0.15	0.14		0.15	0.17	0.15	0.14	0.18	0.16	0.19	0.18	0.17	0.19	0.17	0.21	0.20	0.18
10/23/94	47	14:13	388.00	TMW-4	0.14	0.12	0.15	0.17	0.16	0.14	0.14	0.14	0.15	0.19	0.17	0.17	0.17	0.17	0.20	0.22	0.20
10/23/94	47	14:25	388.20	TME-3	9.62	9.04	0.19	0.18	1.12	0.37	0.22	0.16	0.15	0.28	0.19	0.58	0.43	0.14	0.21	0.19	0.20
10/23/94	47	14:37	388.40	TME-4	15.71	6.34	0.18	0.16	5.29	0.41	0.20	0.16	0.13	0.31	0.20	2.56	2.14	0.15	0.22		0.19
10/24/94	48	10:16	408.05	TMC-1	0.29	0.13	0.19	2.60	4.89	0.29	0.14	0.16	0.38	34.08	0.18	0.13	0.17	1.56	4.56	4.01	5.79
10/24/94	48	10:17	408.07	TMC-1	0.41	0.18	0.16	2.56	5.26	0.30	0.15	0.14	0.38	33.74	0.20	0.14	0.17	1.62	4.58	4.00	5.83
10/24/94	48	10:25	408.20	TMC-2	0.19	0.18	0.14	0.13	0.24	0.16	0.16	0.16	0.13	0.22	0.16	0.14	0.13	0.12	0.19	0.15	0.12
10/24/94	48	10:33	408.33	TMC-3	0.12	0.12	0.13	0.17	0.21	0.16	0.13	0.12	0.12	0.18	0.17	0.13	0.15	0.15	0.23	0.22	0.16
10/24/94	48	10:41	408.47	TMC-4	0.11	0.09	0.11	0.12	0.19	0.15	0.18	0.19	3.00	0.58	0.16	0.14	0.14	0.15	0.25	0.13	0.13
10/24/94	48	10:49	408.60	TMC-5	0.16	0.75	0.18	0.44	3.17	0.90	0.18	0.14	0.15	0.33	0.19	0.13	0.13	0.22	0.31	0.56	0.18

Sample Date	Sample Round	Sample Time	Test Hours	MLS ID	port 1	port 2	port 3	port 4	port 5	port 6	port 7	port 8	port 9	port 10	port 11	port 12	port 13	port 14	port 15	port 16	port 17
10/24/94	48	10:57	408.73	TMC-6	2.38	0.23	0.35	1.39	0.31	0.25	0.74	3.25	3.31	1.29	0.18	0.21	0.35	0.18	0.26	0.16	0.17
10/24/94	48	11:06	408.88	TMC-7	0.72	2.71	0.21	2.20	1.37	0.21	0.28	0.14	0.18	0.27	0.16	0.42	5.51	6.53	22.13		5.06
10/24/94	48	11:14	409.02	TMC-8	0.45	6.31	0.32	0.31	0.44	0.25	3.03	7.83	2.87	0.26	0.20	0.24	0.20	0.18	0.19	0.17	0.17
10/24/94	48	11:22	409.15	TME-5	21.28	5.32	0.17	0.23	1.14	1.05	0.22	0.15	0.14	0.30	0.25	0.24	17.78	0.18	0.24	0.21	0.16
10/25/94	49	11:07	432.90	TMC-1	0.34	0.19	0.15	2.00	4.67	0.22	0.15	0.14	0.24	17.04	0.17	0.15	0.17	1.44	4.74	3.96	4.77
10/25/94	49	11:08	432.92	TMC-1	0.36	0.18	0.15	2.18	4.78	0.20	0.14	0.13	0.25	17.45	0.17	0.14	0.16	1.45	4.79	4.07	4.95
10/25/94	49	11:13	433.00	TMC-1	0.35	0.18	0.16	1.96	4.98	0.22	0.15	0.14	0.27	17.55	0.19	0.15	0.20	1.54	4.26	3.71	4.92
10/25/94	49	11:22	433.15	TME-3	7.77	5.20	0.18	0.18	0.93	0.33	0.21	0.15	0.15	0.34	0.20	0.32	0.25	0.14	0.26	0.20	0.19
10/25/94	49	11:31	433.30	TME-4	11.47	2.89	0.17	0.15	3.19	0.34	0.21	0.15	0.13	0.33	0.23	2.26	1.52	0.15	0.26		0.19
10/25/94	49	11:39	433.43	TME-5	18.74	3.66	0.18	0.20	1.07	0.87	0.20	0.14	0.13	0.29	0.25	0.24	14.94	0.20	0.28	0.21	0.18
10/26/94	50	9:57	455.73	TMC-1	0.22	0.16	0.18	1.70	3.28	0.20	0.16	0.15	0.23	9.82	0.16	0.15	0.17	1.24	4.52	4.01	3.96
10/26/94	50	10:02	455.82	TMC-1	0.34	0.22	0.16	1.62	3.75	0.22	0.16	0.14	0.23	9.65	0.16	0.16	0.19	1.44	4.28	3.71	3.90
10/26/94	50	10:12	455.98	TMC-2	0.15	0.17	0.15	0.13	0.20	0.15	0.16	0.16	0.14	0.20	0.15	0.15	0.12	0.12	0.18	0.14	0.14
10/26/94	50	10:29	456.27	TMC-4	0.21	0.29	0.20	0.22	0.48	0.21	0.28	0.21	1.85	0.53	0.19	0.20	0.15	0.20	0.28	0.16	0.17
10/26/94	50	10:37	456.40	TMC-5	0.15	0.47	0.17	0.33	2.20	0.42	0.21	0.15	0.15	0.30	0.18	0.15	0.13	0.21	0.29	0.43	0.20
10/26/94	50	10:46	456.55	TMC-6	1.76	0.19	0.23	0.94	0.32	0.25	0.54	2.40	2.16	0.93	0.21	0.20	0.25	0.18	0.28	0.16	0.16
10/26/94	50	10:55	456.70	TMC-7	0.40	1.50	0.19	1.63	0.79	0.21	0.21	0.14	0.17	0.26	0.17	0.26	4.10	3.74	12.94		4.68
10/26/94	50	11:04	456.85	TMC-8	0.25	2.42	0.22	0.20	0.29	0.24	2.30	5.18	2.09	0.23	0.20	0.24	0.19	0.18	0.19	0.17	0.16
10/28/94	51	10:06	503.88	TMC-1	0.21	0.15	0.17	0.99	1.85	0.20	0.15	0.15	0.19	3.50	0.17	0.14	0.19	1.23	3.83	3.79	2.56
10/28/94	51	10:11	503.97	TMC-1	0.26	0.17	0.16	1.08	2.33	0.19	0.16	0.15	0.19	3.56	0.19	0.14	0.18	1.36	3.66	3.47	2.41
10/28/94	51	10:19	504.10	TME-3	6.09	2.16	0.19	0.21	0.47	0.34	0.22	0.17	0.16	0.26	0.21	0.25	0.21	0.15	0.19	0.22	0.20
10/28/94	51	10:27	504.23	TME-4	7.78	1.19	0.16	0.15	1.38	0.31	0.20	0.16	0.15	0.24	0.23	1.19	0.81	0.15	0.21		0.20
10/28/94	51	10:35	504.37	TMC-4	0.23	0.23	0.20	0.27	0.46	0.20	0.21	0.21	1.08	0.34	0.20	0.17	0.16	0.19	0.20	0.16	0.14
10/28/94	51	10:43	504.50	TMC-5	0.17	0.28	0.20	0.28	1.15	0.27	0.19	0.16	0.16	0.25	0.19	0.15	0.15	0.21	0.24	0.41	0.20
10/28/94	51	10:51	504.63	TME-5	12.92	1.82	0.17	0.18	0.45	0.45	0.21	0.15	0.14	0.23	0.24	0.22	7.60	0.17	0.19	0.20	0.17
10/28/94	51	10:59	504.77	TME-6	6.07	1.24	0.20	0.14	0.25	0.26	0.21	0.16	0.14	0.18	0.22	0.18	0.18	0.14	0.16	0.20	0.17
10/28/94	51	11:07	504.90	TMC-6	1.33	0.18	0.22	0.67	0.27	0.25	0.42	1.66	1.32	0.44	0.21	0.20	0.23	0.22	0.22	0.17	0.17
10/28/94	51	11:15	505.03	TMC-7	0.29	0.78	0.21	1.12	0.42	0.20	0.20	0.16	0.20	0.22	0.16	0.21	2.62	2.05	5.80		2.57
10/28/94	51	11:23	505.17	TMC-8	0.19	1.07	0.23	0.20	0.25	0.22	1.66	3.25	1.48	0.18	0.18	0.21	0.23	0.20	0.16	0.17	0.16
10/31/94	52	14:08	579.92	TMC-1	0.15	0.16	0.15	0.81	1.19	0.17	0.18	0.15	0.17	1.72	0.15	0.17	0.18	1.51	4.90	3.26	1.37
10/31/94	52	14:13	580.00	TMC-1	0.21	0.21	0.15	0.76	1.47	0.20	0.17	0.14	0.21	1.50	0.17	0.15	0.18	1.50	4.41	2.68	1.30
10/31/94	52	14:24	580.18	TMC-2	0.18	0.17	0.19	0.15	0.14	0.15	0.13	0.16	0.13	0.15	0.17	0.14	0.14	0.13	0.14	0.15	0.13
10/31/94	52	14:35	580.37	TMC-3	0.26	0.39	0.20	0.23	0.39	0.23	0.24	0.17	0.17	0.23	0.20	0.21	0.17	0.19	0.24	0.24	0.24
10/31/94	52	14:46	580.55	TMC-4	0.16	0.14	0.12	0.14	0.18	0.17	0.17	0.16	0.39	0.19	0.18	0.15	0.15	0.16	0.15	0.14	0.14
10/31/94	52	14:58	580.75	TME-4	5.01	0.32	0.17	0.16	0.40	0.26	0.17	0.14	0.12	0.21	0.20	0.57	0.29	0.13	0.18		0.17
10/31/94	52	15:10	580.95	TME-5	8.38	0.77	0.17	0.22	0.43	0.41	0.25	0.15	0.16	0.26	0.23	0.23	1.99	0.18	0.23	0.22	0.21
10/31/94	52	15:20	581.12	TMC-5	0.18	0.19	0.21	0.23	0.86	0.23	0.18	0.16	0.17	0.28	0.17	0.16	0.14	0.20	0.28	0.39	0.18
10/31/94	52	15:31	581.30	TMC-6	0.84	0.13	0.19	0.36	0.20	0.24	0.28	0.95	0.68	0.30	0.19	0.21	0.21	0.20	0.23	0.16	0.17
10/31/94	52	15:42	581.48	TMC-7	0.23	0.41	0.19	0.89	0.32	0.19	0.22	0.16	0.20	0.22	0.16	0.24	1.04	1.13	2.17		1.06
10/31/94	52	15:53	581.67	TMC-8	0.12	0.48	0.17	0.21	0.28	0.20	1.40	2.00	1.11	0.22	0.18	0.26	0.23	0.21	0.19	0.15	0.19
11/8/94	53	13:38	771.42	TMC-1	0.14	0.17	0.15	0.25	0.46	0.17	0.16	0.15	0.16	0.32	0.17	0.19	0.50	0.68	0.24	0.39	0.26
11/8/94	53	13:49	771.60	TMC-2	0.17	0.17	0.18	0.15	0.17	0.16	0.15	0.16	0.15	0.18	0.16	0.14	0.14	0.13	0.16	0.15	0.14
11/8/94	53	14:00	771.78	TMC-3	0.13	0.14	0.15	0.17	0.19	0.16	0.13	0.14	0.13	0.16	0.15	0.14	0.16	0.18	0.21	0.78	0.17

Sample Date	Sample Round	Sample Time	Test Hours	MLS ID	port 1	port 2	port 3	port 4	port 5	port 6	port 7	port 8	port 9	port 10	port 11	port 12	port 13	port 14	port 15	port 16	port 17
11/8/94	53	14:11	771.97	TMC-4	0.15	0.16	0.12	0.16	0.22	0.16	0.18	0.16	0.20	0.21	0.16	0.16	0.14	0.15	0.18	0.13	0.14
11/8/94	53	14:22	772.15	TME-3	1.67	0.34	0.16	0.16	0.22	0.25	0.19	0.15	0.15	0.18	0.18	0.18	0.14	0.15	0.22	0.21	0.19
11/8/94	53	14:32	772.32	TME-4	2.70	0.18	0.16	0.15	0.25	0.24	0.16	0.15	0.14	0.20	0.17	0.41	0.16	0.14	0.21		0.18
11/8/94	53	14:43	772.50	TMC-5	0.14	0.14	0.16	0.20	0.37	0.17	0.18	0.14	0.15	0.22	0.14	0.15	0.16	0.24	0.31	0.41	0.18
11/8/94	53	14:54	772.68	TMC-6	0.42	0.12	0.16	0.18	0.20	0.21	0.21	0.45	0.26	0.21	0.18	0.17	0.18	0.16	0.18	0.15	0.15
11/8/94	53	15:04	772.85	TMC-7	0.31	0.21	0.17	0.50	0.23	0.18	0.17	0.14	0.16	0.18	0.16	0.56	0.21	0.23	0.45		0.56
11/8/94	53	15:15	773.03	TMC-8	0.17	0.25	0.11	0.17	0.34	0.20	0.73	0.62	0.48	0.23	0.17	0.22	0.18	0.17	0.19	0.14	0.17